Identification of potential therapeutic targets against trypanosomatid parasite related infections ; molecular and functional characterization of components of the flagellar pocket collar

Anna Albisetti

université de BORDEAUX

THÈSE PRÉSENTÉE

POUR OBTENIR LE GRADE DE

DOCTEUR DE L'UNIVERSITÉ DE BORDEAUX

ÉCOLE DOCTORALE: Sciences de la Vie et de la Santé

SPÉCIALITÉ: Microbiologie - Immunologie

Par Anna Cristina ALBISETTI

Identification de cibles thérapeutiques potentielles contre les infections par les trypanosomatides; caractérisation moléculaire et fonctionnelle des composants du collier de la poche flagellaire

Sous la direction de: Mélanie BONHIVERS

Soutenue le 8 décembre 2016

Membres du jury:

M. TEICHMANN, Martin	Professeur	Bordeaux	Président
M. McKEAN, Paul	Senior Lecturer	Lancaster (UK)	Rapporteur
Mme. VAUGHAN, Sue	Senior Lecturer	Oxford (UK)	Rapporteur
M. SEEBECK, Thomas	Professeur	Berne (CH)	Examinateur
Mme. BONHIVERS, Mélanie	Chargée de recherche	Bordeaux	Directrice de thèse

Titre: Identification de cibles thérapeutiques potentielles contre les infections par les trypanosomatides; caractérisation moléculaire et fonctionnelle des composants du collier de la poche flagellaire.

Résumé en francais

Trypanosoma brucei, un parasite flagellé unicellulaire, est responsable de la trypanosomiase humaine africaine aussi connue comme la maladie du sommeil.

Les microtubules (MTs) sous-pelliculaires, le quartet de MTs (MTQ), le flagelle (F) et le collier de la poche flagellaire (CPF) sont les principaux composants du cytosquelette du trypanosome. À ce jour, une seule protéine du CPF, BILBO1, a été identifiée et caractérisée.

Dans cette étude, nous montrons *in vivo* que BILBO1 forme des polymères capables de construire un échafaudage qui permet l'ancrage de protéines partenaires. Ainsi, un crible en double hybride chez la levure a identifié plusieurs protéines partenaires de BILBO1, notamment une nouvelle protéine appelée FPC4. Nous démontrons que FPC4 est une protéine spécifique des kinétoplastides, localisée au CPF mais aussi au hook-complex, une structure proche du CPF. L'interaction FPC4 – BILBO1 est démontrée in vitro et in vivo, et les domaines d'interaction identifiés. En outre, nous démontrons in vivo et in vitro que FPC4 est une protéine associée aux microtubules. Nos données suggèrent fortement que FPC4 est impliquée dans le processus de séparation des CPFs au cours du cycle cellulaire. Nos résultats mettent en évidence un lien étroit entre le MtQ et le CPF et l'implication probable du hook-complex.

Enfin, nous mettons en évidence une structure analogue au hook-complex chez les Leishmanies.

L'interaction BILBO1 – FPC4 représente une nouvelle cible thérapeutique et sera caractérisée plus avant.

Mots clés: *Trypanosoma brucei*, BILBO1, cytosquelette, quartet de microtubules, collier de la poche flagellaire

Title: Identification of potential therapeutic targets against trypanosomatid parasite related infections; molecular and functional characterization of components of the flagellar pocket collar.

Abstract in English

Trypanosoma brucei, a unicellular flagellated parasite, is responsible for the human African trypanosomiasis also known as sleeping sickness.

Sub-pellicular microtubules (MT), the MT quartet (MtQ), the flagellum (F) and the Flagellar Pocket Collar (FPC) are the main components of the *T. brucei* cytoskeleton. To date, only a single FPC protein, BILBO1, has been identified and characterized.

In this study we demonstrate *in vivo* that BILBO1 forms polymers able to build a scaffold structure that anchors partner proteins. As such, a yeast-2-hybrid screen identified several BILBO1 interacting protein partners.

We demonstrate that FPC4 is a kinetoplastid-specific protein, which is localized at the FPC and at the hook complex. Its specific interaction with BILBO1 has been demonstrated *in vitro* and *in vivo*, and the interacting domains identified. Furthermore, we demonstrate that FPC4 is a microtubule binding protein. Our data strongly suggest that FPC4 is involved in the separation of the old and the newly formed FPC during the cell cycle.

Altogether, our results demonstrate a tight connection and interplay between the MtQ and the FPC and the likely involvement of an adjacent third structure, the hook complex. Finally, we highlight a structure similar to the hook-complex in Leishmania.

The BILBO1 – FPC4 interaction represents a new therapeutic target and will be characterized further.

Keywords: *Trypanosoma brucei*, BILBO1, cytoskeleton, microtubule quartet, flagellar pocket collar

Laboratoire de Microbiologie Fondamentale et Pathogenicité - UMR5234

146, Rue Leo Saignat, 33076 Bordeaux Cedex (France)

Acknowledgments

I first of all want to thank Dr. Mélanie BONHIVERS, who welcomed me in the Laboratory, who helped me with the project with useful suggestions and discussions and for being a very good supervisor. The very direct and honest way of discussing helped me also to strengthen my character for my future scientific career (and not only).

Very special thanks to Prof. Martin TEICHMANN, Dr. Paul McKEAN, Dr. Sue VAUGHAN and Prof. Thomas SEEBECK, who kindly accepted to be part of my thesis committee and took the time to read, correct and judge my thesis work.

I would like to thank the LabEx ParaFrap PhD Program for the financial support during these 3 years and for all the very useful workshops that I could follow during my thesis. Among the ParaFrap students, I could not only find good scientists, but also friends.
I would also like to thank the BASTIEN Laboratory in Montpellier, especially Lucien for the technical support and Laurianne for the scientific discussions and the hosting during our ParaFrap collaboration on *L. major*.

Thanks to Dr. Derrick R. ROBINSON, who selected me among the ParaFrap applicants and for even taking care about my eyesight, constantly asking if I needed glasses...
I want to acknowledge present and past members of the ROBINSON-BONHIVERS Team, especially Denis DACHEUX, for hiding the dead mice in the very upper drawer of the freezer, Nicolas LANDREIN, for the technical support in the lab and for the “patisserie”-preparations and Doranda PERDOMO, for the support in organizing the TGIFs. Thanks to Anne CAYREL, Benoit ROGER, Elodie BERDANCE, Marie EGGENSPIELER and Célia FLORIMOND, who contributed in different ways to my project.
Thanks to the entire MFP Laboratory, particularly the paramyc-floor, that indirectly forced me to learn French.

An additional thank to the ParaTryp organization, which assigned me the ParaTryp Travel Award 2014, giving me the chance to go to Woods Hole for the KMCBM 2015 meeting.

Finally, I want to thank all my friends for the continuous encouragement. A huge thanks to my family for the support and for visiting me in Bordeaux and Erico for his motivation and for making me always smile.

Abbreviations list

ΔB1BD		delta BILBO1 Binding Domain
A	Ala	Alanine
aa		amino acid
amp		ampicillin
APOL1		ApoLipo protein L1
ATP		Adenosine TriPhosphate
B		Blasticidin
B1BD		BILBO1 Binding Domain
BARP		brucei alanin rich protein
BB		Basal Body
BBB		Blood Brain Barrier
BD		Binding Domain
bp		base pair
BSF		bloodstream form
Ca2+		Calcium ion
CATT		The Card Agglutination Test for Trypanosomiasis
CC		Coiled-Coil
CCVs		Clathrin-Coated Vesicles
CDK		cyclin-dependent kinase
CiPo		Ciliary Pocket
CK		Cytoskeleton
CKI		CDK Inhibitor
CL		cutaneous leishmaniasis
Cl-		Chlorid ion
CM		Conditioned Medium
CNS		Central Nervous System
CRAM		Cysteine Rich Acid trans-Membrane
Da		Dalton
DAPI		4',6-Diamidino-2-Phenylindole
DEPC		diethylpyrocarbonate
DNA		Deoxyribonucleic acid
DTT		dithiothreitol
ECL		Enhanced ChemiLuminescence
EE		Early Endosomes
EGTA		Ethylene Glycol Bis(2-aminoethyl Ether)tetraacetic Acid
EM		Electron Microscopy
ER		Endoplasmic Reticulum
ESAG		Expression-Site Associated Gene
ESB		Expression-Site Body
EtOH		Ethanol
Evs		Extracellular Vesicles
F		Phleomycin
F	Phe	Phenylalanine
FAZ		Flagellar Attachment Zone
FC		Flagellar Connector
FCS		Fœtal Calf Serum
Fg		Flagellum
FL		Full Length
FP		Flagellar Pocket
FPC		Flagellar Pocket Collar
g		gravity constant
G1-Phase		Gap1-Phase
G2-Phase		Gap2-Phase
G418		Neomycin
gDNA		genomic DNA
GFP		Green Fluorescent Protein
GPI		Glycosyl-Phosphatidyl-Inositol
gRNA		guide RNA
H		Hygromycin
h		hours
HAT		Human African Trypanosomiasis
HAT		Hypoxanthin-Aminopterin-Thymidine
HC		hook complex
HGPRT		Hypoxanthine Guanine PhosphoRibosyl Transferase
His		histidine
HRP		Horse Radish Peroxidase
hygro		hygromycin
iEM		immuno-Electron Microscopy
IFT		IntraFlagellar Transport
IMDM		Iscove's modified Dulbecco's Medium
IPTG		Isopropyl β-D-1-thiogalactopyranoside
ISG		Invariable Surface Glycoprotein
K	Lys	Lysine
kana		kanamycin
kDNA	K	kinetoplast DNA
KO		Knock Out
L	Leu	leucine
L		liter
LB		Lysogeny Broth medium
LC-MS/MS		Liquid Chromatography Mass Spectrometry/Mass spectrometry
LE		Late Endosomes
Lm		Leishmania major
Lmx		Leishmania mexicana
LRRP1		Leucine Rich Repeated Protein1
LS		long slender
mA		milli Ampere

MAP		Microtubule Associated Protein
MeOH		Methanol
mg		milli gram
min		minutes
mL		millilitre
MM		Molecular Mass
MORN1		Membrane Occupation and Recognition Nexus 1
mQ-H2O		milli-Q water
MT		Microtubule
MTOC		MicroTubule Organizing Center
MtQ		Microtuble Quartett
N		nucleus
neo		neomycin
NHS		Normal Human Serum
NLS		Nuclear Localization Signal
NTD		N-terminal domain
OD		optical density
ODC		Ornitine decarboxylase
ORF		Open Reading Frame
P		Puromycin
PAGE		PolyAcrylamide Gel Electrophoresis
pBB		pro-Basal Body
PBS		Phosphate Buffer Saline
PCF		procyclic form
PCIA		phenol:chloroform:Isoamyl Alcohol
PCR		Polymerase Chain Reaction
PEG		polyethylene glycol
PFA		Para FormAldehyde
PFR		ParaFlagellar Rod
phleo		phleomycin
PLK		Polo-like kinase
puro		puromycin
rDNA		ribosomal DNA
RE		Recycling Endosomes
RNA		Ribonucleic acid
RNAi		RNA interference
rpm		rotation per minute
rRNA		ribosomal RNA
RT		room temperature
RT-PCR		Reverse Transcription PCR

S-Phase		Synthesis-Phase
SC		Synthetic Complete medium
SDM		Semi-Defined Medium
SDS		Sodium dodecyl sulfate
SDS SB		SDS sample buffer
sec		seconds
SL		Spliced Leader
spp		subspecies
SRA		Serum-Resistance associated protein
SS		short stumpy
T7 Pol		T7 RNA Polymerase
TAC		Tripartite Attachment Complex
Tb		Trypanosoma brucei
TbHpHbR		Haptoglobin Hemoglobin receptor
TEM		Transmission-Electron Microscopy
Tet		Tetracyclin
TetO		Tetracyclin Operator
TetR		Tetracyclin Repressor
TfR		Transferrin Receptor
TgsGP		T. brucei gambiense specific GlycoProtein
TLF		TrypanoLytic Factor
TMD		Trans Membrane Domain
tRNA		transfer RNA
U		units
UTRs		UnTranslated Regions
V		volt
VAT		Variable Antigen Type
VL		Visceral Leishmaniasis
VSG		Variable Surface Glycoprotein
W	Trp	tryptophan
w/o		without
H_2O		water
WC		Whole cell
WHO		World Health Organization
WT		Wild Type
Y	Tyr	Tyrosine
YFP		Yellow Fluorescent Protein
YNB		Yeast nitrogen base
YPD		yeast peptone dextrose

Summary:

1. INTRODUCTION

1. Introduction

Understanding the basic, but fascinating, biology of parasites is the primary goal of my thesis. The name parasite comes from ancient Greek word "*parásitos"* which means "person who eats at the table of another". In other words, parasitism represents a non-reciprocal symbiotic relationship between two different species, where the parasite takes benefits from the host, possibly causing host death.
During my thesis, I focused my interest on organisms which diverged early in evolution, such as Trypanosomatids.

The historian Ibn Khaldun reported in 1373, the death "by lethargy" of King Diata II, sultan of Mali, and this is considered to be one of the first written reports of human sleeping sickness (WHO). It was approximately 350 years later, that Atkins, a British naval surgeon, described the symptoms of what Winterbottom in 1803 called "negro lethargy" (Cox, 2002). During the slave trade (15-19 century) numerous cases of negro lethargy were reported (WHO).
In the middle of the 19th century, David Gruby coined the name trypanosoma, after the identification of the parasites in frogs (Gruby, 1843). However, it was not until 1881 that Griffith Evans found parasites in the blood of camels and horses affected by surra and suggested therefore the connection between the parasite and the disease (Evans 1881).
At the beginning of the 20th century, David Bruce discovered *Trypanosoma brucei* (*T. brucei*) as the aetiological agent of the disease Nagana (Steverding, 2008).

I. Kinetoplastidae

Kinetoplastidae is a class of flagellated protists. This class is divided into two orders: Trypanosomatida and Bodonida, which differ in the number of flagella, more precisely in mono- or multiflagellated parasites, respectively (Moreira et al., 2004). These parasites possess a single large mitochondrion containing the mitochondrial DNA network, called kinetoplast (kDNA) (Alexeieff, 1917).

Trypanosomatid parasites can be found in a vast repertoire of eukaryotic hosts. Plants, for examples, can be infected by phytomonas, whereas small animals like birds, fishes, rats and amphibians can be colonized by *T. avium*, *T. siniperca, T. lewisi and T. hosei*, respectively (Votýpka et al., 2002; Gu et al., 2007; Strickland, 1911; Saxena and Miyata, 1993). Other animals of larger size are not free from trypanosomatid infections; some examples are:

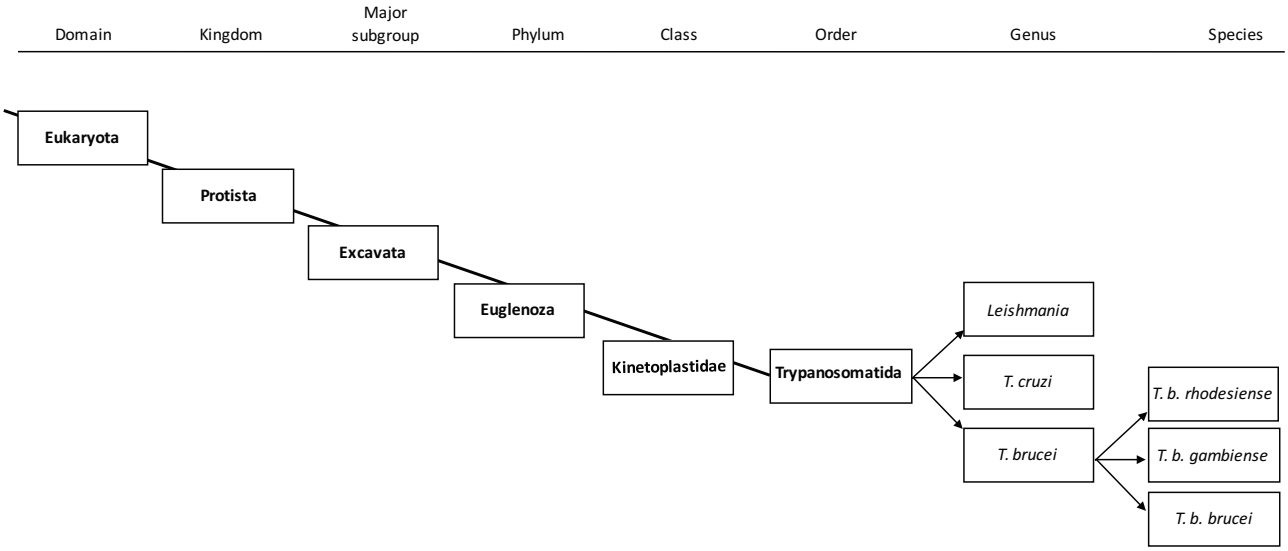

Fig. 1.1 *Phylogenetic Tree of protozoan parasites such as Trypanosomatida.* *Trypanosoma brucei*, *Trypanosoma cruzi* and *Leishmania* belong to the class of Kinetoplastidae, characterized by the presence of a kinetoplast.

koalas (*T. irwini*), badgers (*T. pestanai*) and horses (*T. equiperdum* and *T. equinum*) (McInnes et al., 2009; Yorke and Blacklock, 1912).

Within Trypanosomatids there are three species that are responsible for human neglected tropical diseases: *Leishmania*, *Trypanosoma cruzi* and *Trypanosoma brucei* (Fig.1.1), whilst *T. congolense, T. vivax and T. brucei brucei* are responsible for the disease Nagana in cattle (Morrison et al., 2016).

The genus Trypanosoma can be divided in two sections according to the mode of transmission: *Salivaria* vs *Stercoraria* (Hughes and Piontkivska, 2003). *T. brucei*, belongs to the *Salivaria* subgenus, meaning that the transmission occurs via the saliva of the vector. On the contrary, *T. cruzi* is the most important representative of the *Stercoraria* subgenus, in which transmission of parasites, and thus disease, is *via* the excrement of the insect vector (Simpson et al., 2006; Vickerman and Preston, 1976; Adl et al., 2005).

Animals and humans can act as reservoirs for these parasites, which renders parasite control difficult. This raises the interest in finding an efficient drug against these diseases, because the preventative treatment of all the potential hosts is not possible.

a) Leishmania

From a historical point of view, diseased caused by Leishmania, previously known as oriental sore, were firstly described in the 10th century in the Middle East by Arab physicians. In India, at the beginning of the 19th century, a different form of the disease, called Kala azar, now known as visceral leishmaniasis, was often confused with Malaria. Only in 1900, Leishman and Donovan discovered the parasite, and in 1911 Vianna noticed that the parasites in South America differed from those found in the Old World. A decade later, the vectors involved in the transmission were discovered by the Sergent brothers (Cox, 2002).

Leishmaniasis is caused by around 20 different *Leishmania* spp. The parasites are transmitted to humans or animals, such as dogs, horses and cats, by the bite of a female infected *Phlebotominae* in the Old World (Europe and Asia) and *by Lutzomyia* sandfly in the New World (Americas) (Killick-Kendrick, 1990; Bates and Rogers, 2004; Bates, 2007). These infected humans and animals act as reservoirs.

There are three main forms of the disease: cutaneous (caused mostly by *L. major, L. tropica, L. brasiliensis, L. mexicana*), visceral (*L. infantum*) and muco-cutaneous Leishmaniasis (*L. donovani*) (Walker et al., 2014). I will mostly focus on *Leishmania major*, since I have used this parasite during my thesis.

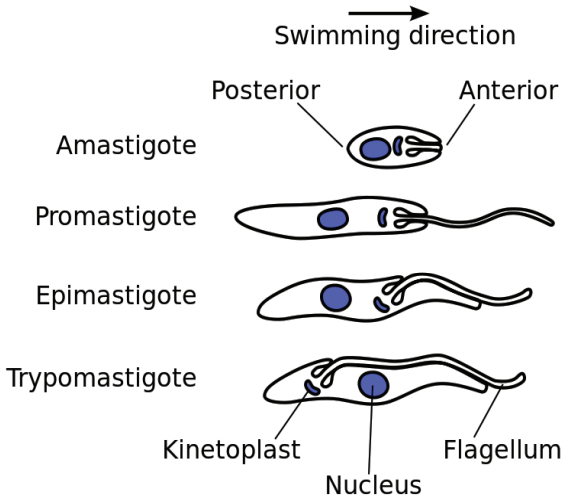

Fig. 1.2 *The different forms of Trypanosomatids parasites.*
This representation takes into account the cell-body shape, the position of the kDNA and the flagellum length. Amastigote parasites are characterized by a very short flagellum, which does not exit the cell body. Promastigotes show an elongated cell body, which a long free flagellum. Epimastigote parasites are similar to promastigotes, but have a part of the flagellum attached to the cell body. Trypomastigotes, on the contrary, possess the kDNA located in the posterior end of the cell and a flagellum which is attached upto the anterior end of the cell body. Modified from (Hoare, 1966) and Zephyris.

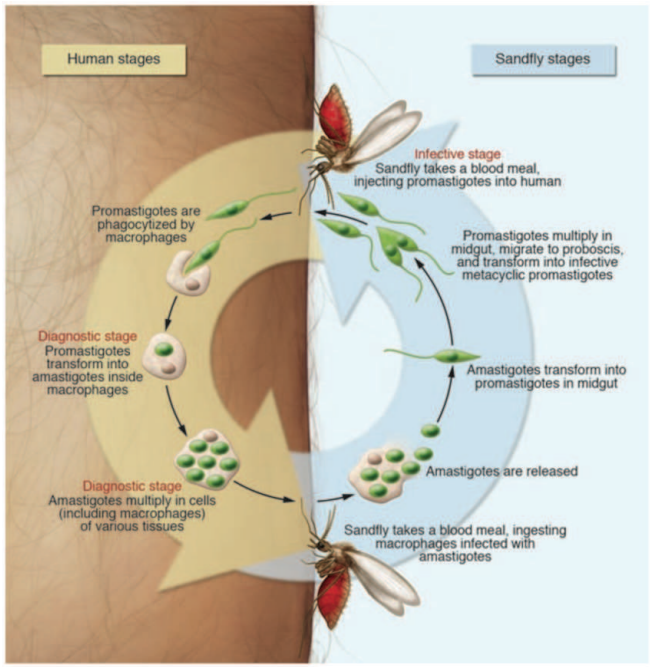

Fig. 1.3 *Life cycle of Leishmania (Stuart et al., 2008)*
Leishmania is transmitted by the bite of an infected sandfly during its blood meal. These parasites invade macrophages by receptor-mediated endocytosis - for example CR3 (complement receptor 3) and some TLR (Toll-like Receptor). (Mosser and Rosenthal, 1993; Stafford et al., 2002) and differentiate into the amastigote form that can multiply by binary fission. During a blood meal on an infected host, a sandfly takes macrophages that contain amastigotes forms that will differentiate into the promastigote form in the midgut and become afterwards infective.

The life cycle of *Leishmania,* as well as for *T. cruzi*, and other *Trypanosomes*, is divided into two stages, one in a mammalian host and the other in the vector. *L. major* is found as an obligate intracellular amastigote (Fig.1.2) in monocytes and macrophages (mononuclear phagocyte system) of the host, and as the promastigote parasite in the vector (Fig.1.2) (Walker et al., 2014).

After the bite of the infected sandfly, promastigotes are phagocytized by macrophages. Once in the macrophages, they differentiate into amastigote parasites that can massively replicate. The sandfly, during its blood meal, can take up infected macrophages. The amastigote parasites are then released in the midgut and differentiate into promastigote parasites, which can then multiply and differentiate into infective metacyclic promastigotes. This infective form is injected into the mammalian host during subsequent sandfly blood meals (Fig.1.3) (Stuart et al., 2008).

Cutaneous Leishmaniasis is spread in South America, on the Mediterranean coast and in the Middle East (see Fig.1.4). CL is currently treated with intralesional injections of pentavalent antimonials (den Boer et al., 2011). Visceral Leishmaniasis, present on the Brazilian Coast, the Mediterranean area, Sub-Saharan Africa and India (see Fig.1.5), is nowadays treated with Amphotericin B®, Miltefosine and Paromomycin (den Boer et al., 2011; Singh et al., 2012).

Leishmania is an organism which shows a partially aneuploid genome (Ravel et al., 1998). It possesses 36 chromosomes, mostly diploids. The genome contains approximately 8200 protein-coding genes; among them 900 genes have no orthologues in *T. brucei* or *T. cruzi* (Ivens et al., 2005; Berriman et al., 2005; El-Sayed et al., 2005). Around 30% of these genes are involved in key metabolic differences between *Leishmania* and *Trypanosomes*, whereas the remaining 70% of these *Leishmania*-specific genes have unknown functions (Ivens et al., 2005).

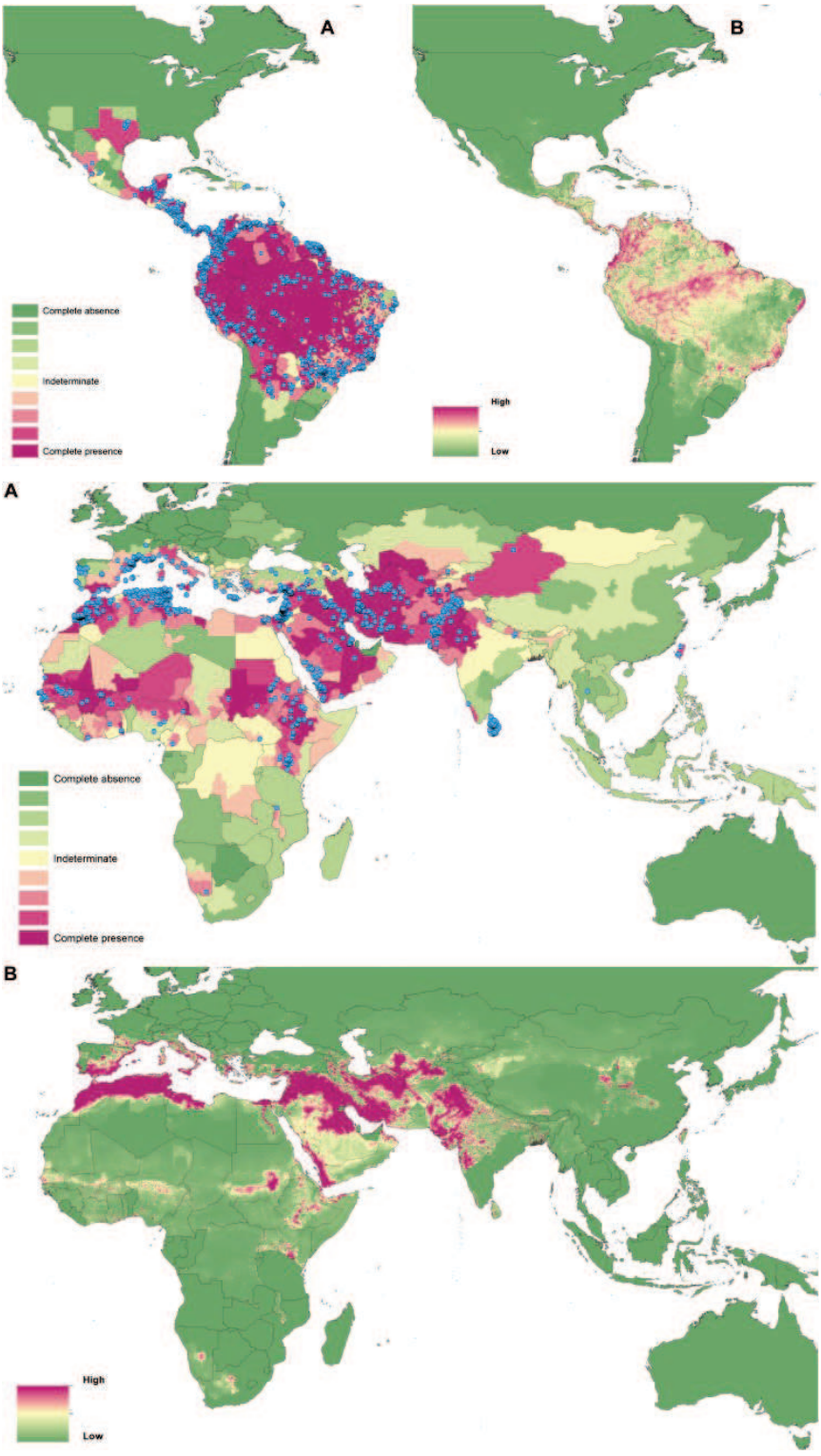

Fig. 1.4 *Cutaneous Leishmaniasis (CL) distribution (Pigott et al., 2014)*
Reported (A) and predicted (B) distribution of CL in the New World (first panel) and Old World (second panel). In (A) blue spots show important occurrence points of the disease, whereas in (B) the probability of infection is represented in red and green (high and low probability, respectively). CL risk is higher in South America as well as on the Mediterranean coast and Middle East.

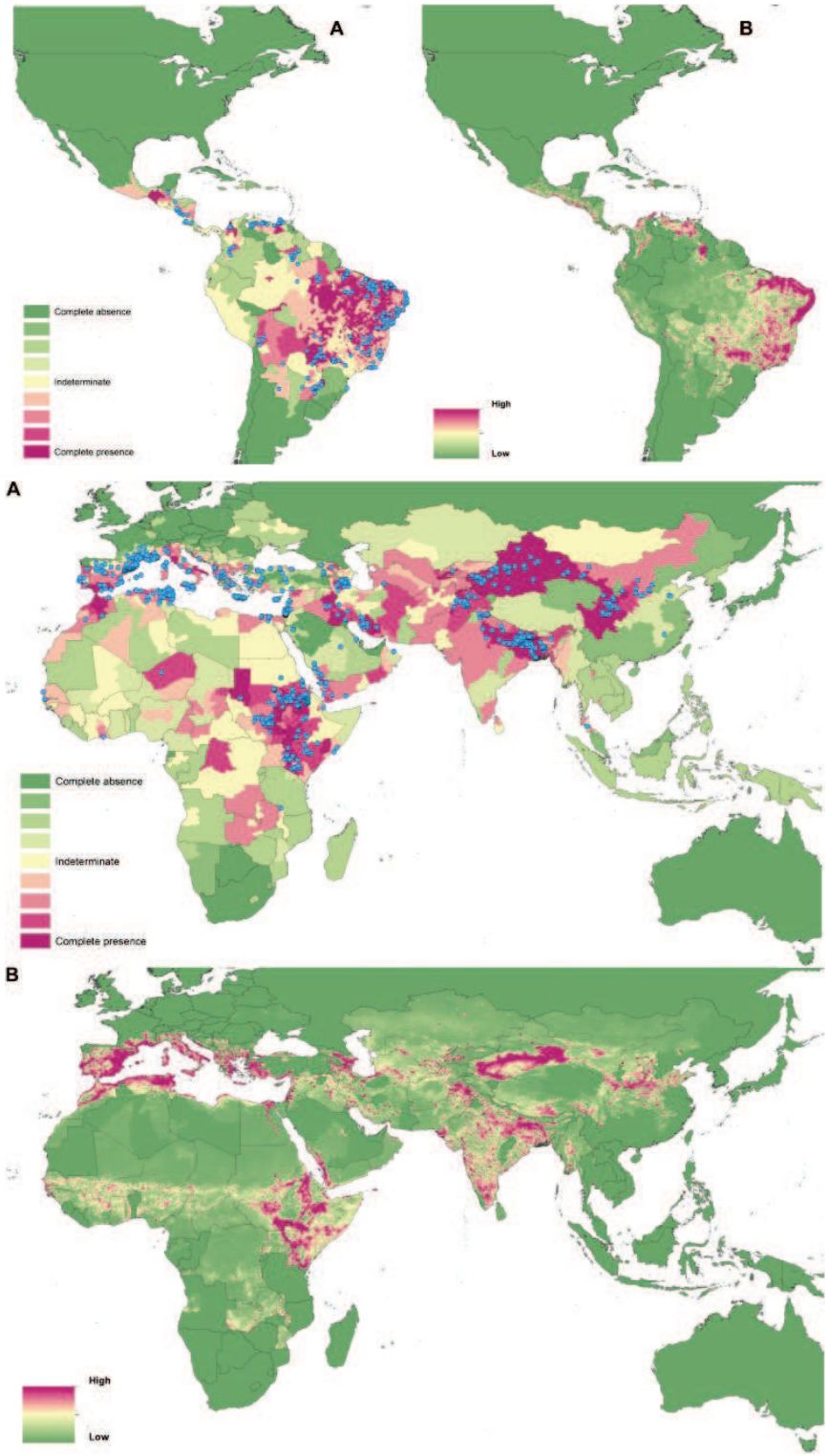

Fig. 1.5 *Visceral Leishmaniasis (VL) distribution (Pigott et al., 2014)*
The maps represent the reported (A) and predicted (B) distribution of VL in the New World (first panel) and Old World (second panel). In (A) blue spots represent the principal occurrence points of the disease. In (B) high (red) and low (green) level of probability of infection are represented. VL risk is higher on the Brazilian east coast, on the Mediterranean coast, part of Sub-Saharan Africa and India.

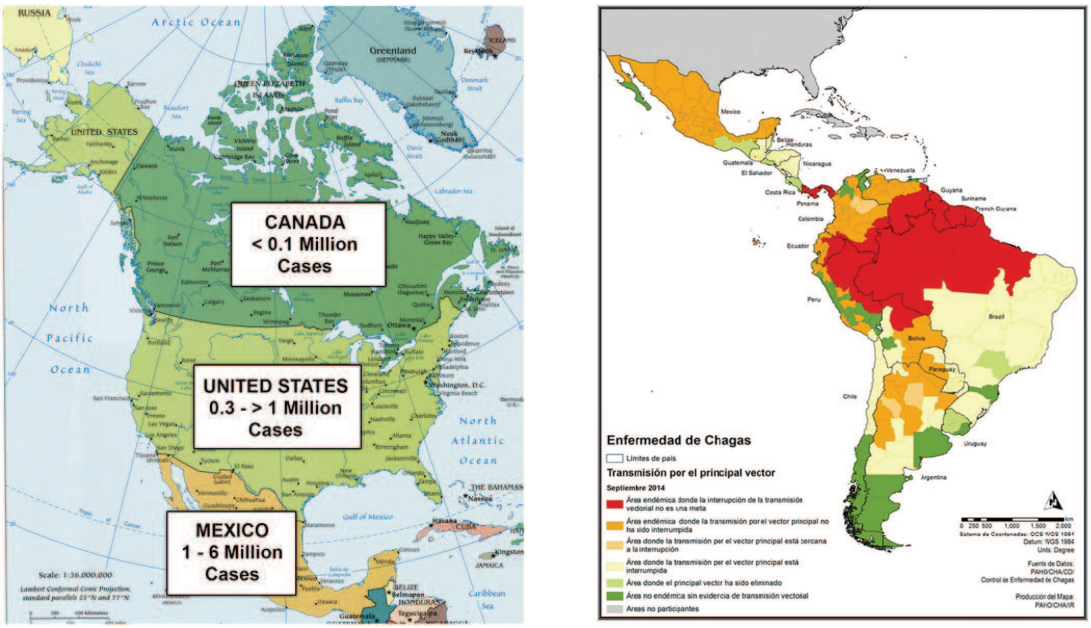

Fig. 1.6 *Distribution of Chagas disease (Hotez et al., 2013; WHO 2014).*
Chagas disease is spread, mostly, in Central and South America, but also in North America. Left panel shows the incidence in North and Central America. On the right map, red and orange represent endemic areas in Central and South America, yellow shows areas where the transmission by the vector has been blocked, whereas green represent non-endemic areas or areas where the vector has been eliminated.

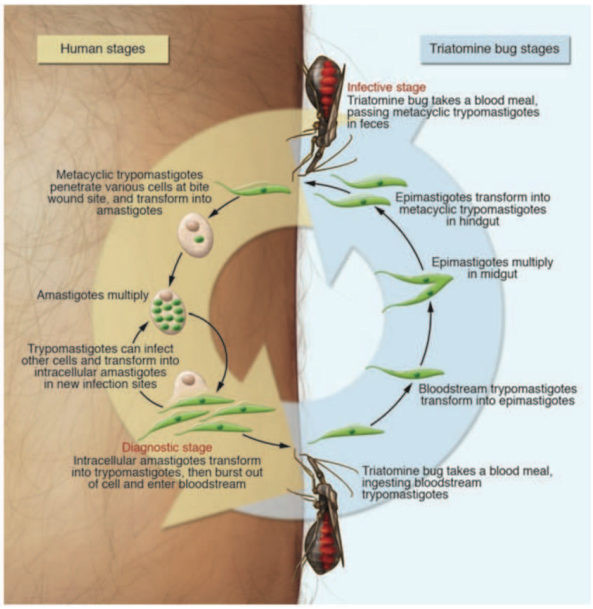

Fig. 1.7 *Life cycle of T. cruzi (Stuart et al., 2008).*
During the blood meal the Triatomine bug deposits its parasite-containing faeces on the host. The parasites are able to penetrate primarily, but not exclusively, epithelial cells at the biting site and develop into the amastigote form. Amastigotes can differentiate into trypomastigotes and are released in the bloodstream, where an insect takes them up during a blood meal. Within the insect, the parasite differentiates, firstly into epimastigote form, and then into infective metacyclic trypomastigotes.

b) *Trypanosoma cruzi*

The first observations of the devastation caused by this disease were seen in spontaneously mummified humans. At the beginning of the 20th century, Chagas and Cruz discovered the parasite (*T. cruzi*) responsible for Chagas disease. Years later, a French parasitologist, Brumpt, discovered the transmission route *via* the faeces of the infected vector (Cox, 2002).

Trypanosoma cruzi is the aetiological agent of American trypanosomiasis, also known as Chagas disease and can infect humans and more than 150 species of domestic animals, such as dogs, cats, horses, cattle and pigs (Fujita et al., 1994; Rassi et al., 2010), in more than 20 Central and South American states (WHO) (Fig.1.6).

The transmission of the parasites occurs primarily *via* the faeces of the hematophagous *Triatomine* bug (also known as the kissing bug (Zeledón and Rabinovich, 1981) but also *via* blood transfusion, organ transplants, vertical mother-to-daughter transmission, or contaminated food. The disease is therefore not only limited to endemic regions, but can easily be spread all over the world. In contrast to the transmission of *Leishmania* or *T. brucei*, both female and male *Triatomine* bugs can carry and transmit the parasites. Three main vectors are responsible for the transmission to humans: *Triatoma infestans*, *Rhodnius prolixus* and *Triatoma dimidiata* (Zeledón and Rabinovich, 1981).

In the insect, the parasites taken up in the blood meal, are in the trypomastigote form and can differentiate into the epimastigote form in the midgut. The epimastigote form is characterized by the position of the kDNA anterior to the nucleus. Epimastigote parasites can multiply and differentiate into infective non-dividing metacyclic trypomastigotes (Fig.1.2) in the posterior gut. The Triatomine bug takes a blood meal and passes the infective *T. cruzi* in the faeces. In the human host, at the wound site, metacyclic trypomastigotes can invade cells and transform into the intracellular amastigote form (in nucleated cells or when phagocytized by macrophages) that can replicate and invade new cells. Amastigotes can also be released into the bloodstream and differentiate into the trypomastigote form, which will be taken up by the insect in the blood meal (Fig.1.7) (Nagajyothi et al., 2012; Stuart et al., 2008).

Chagas disease is characterized by an initial acute phase (weeks to a couple of months), and progresses into a chronic phase, most of the time asymptomatic, that lasts for the entire host's lifetime (Nagajyothi et al., 2012). The symptoms observed in the acute phase are fever, enlargement of lymph nodes, spleen and liver and general malaise. The chronic phase can lead to cardiac and/or gastrointestinal disease and death (Rassi et al., 2010).

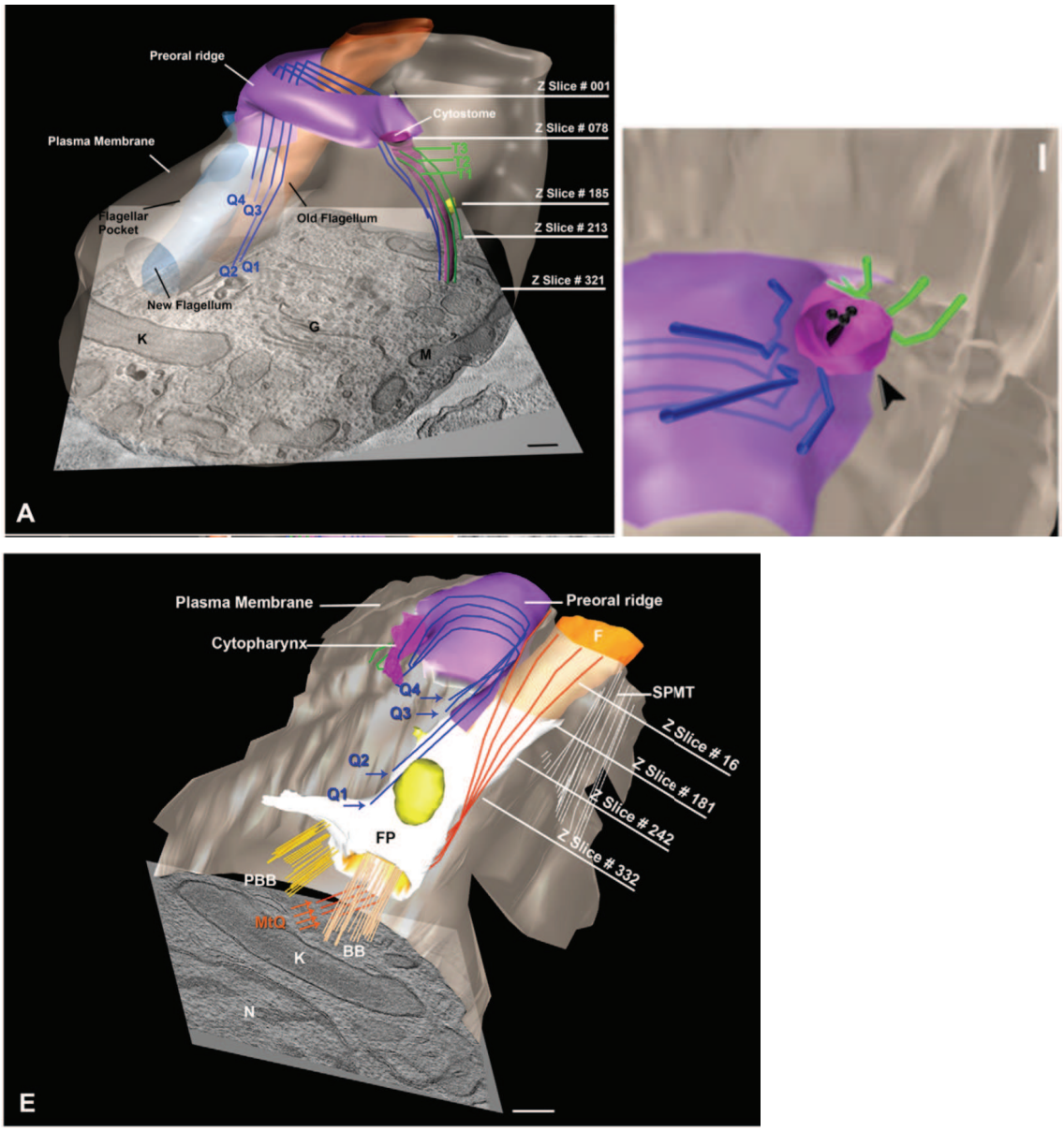

Fig. 1.8 *Microtubules organization along the Cytostome in T. cruzi (Alcantara et al., 2014)*
3-D model obtained by tomography of the FP area of *T. cruzi* (A, E). Two sets of MTs are found associated with the cytostome (pink with arrow-head) of *T. cruzi*. A triplet of MTs (green) and a quartet of MT (blue) give mechanical support to the cytostome (A, I, E). Additional to these two sets of MTs, the MtQ, as in *T. brucei*, is represented in orange (E).

At the moment, treatment is only available for the acute phase. Nifurtimox and Benznidazole are two relatively safe and effective molecules but there is always a need for more effective trypanocidal drugs that can be efficient also in the chronic phase (de Andrade et al., 1996; Rassi et al., 2010).

T. cruzi has a predominantly diploid genome, which contains around 12,000 protein-coding genes and approximately 2000 of them are *T. cruzi* specific (El-Sayed et al., 2005; Agüero et al., 2000). Fifty percent of the genome consists of repetitive sequences (El-Sayed et al., 2005). *T. cruzi* has maintained the CapZ F-actin capping complex, which is absent in *T. brucei* and *Leishmania*. This difference in the actin-myosin system can be linked to the cytostome-cytopharynx complex, which is only present in *T. cruzi* (El-Sayed et al., 2005).
In *Trypanosomatids,* endo- and exocytosis events occur at a specific site called the Flagellar Pocket (FP) (an invagination of the cytoplasmic membrane) that is the only region of the cell devoid of sub-pellicular microtubules allowing vesicle fusion with the flagellar pocket membrane. *T. cruzi* possesses an additional invagination of the cell membrane used as the main site of endocytosis for macromolecules in the epimastigote form, the so-called cytostome-cytopharynx complex (Milder and Deane, 1969; Alcantara et al., 2014; Alcantara et al., 2016). The opening at the cell surface, called the cytostome, and a deep tube-shaped invagination, called the cytopharynx, define this dynamic cytoskeletal structure. The cytostome-cytopharynx complex disappears in G2 phase, when the cells exhibit two kinetoplasts and two FPs (Milder and Deane, 1969).

Two sets of microtubules (MT) are associated with this complex: a triplet of MT originates underneath the cytostome membrane and runs along the cytopharynx, and a quartet of MTs which originates underneath the flagellar-pocket membrane, follows the preoral ridge (the plasma membrane domain in between the cytostome and the FP) and ends in close proximity to the cytopharynx (Fig.1.8). Both MT sets appear to give mechanical support to the complex, leaving, however, a MT-free side on the cytopharynx membrane for vesicles budding and fusion (Alcantara et al., 2014; Alcantara et al., 2016).
In *T. brucei* a MT quartet (MtQ), associated with the FP, has been described (Sherwin and Gull, 1989a). In *T. cruzi* this MtQ is also present, but it is a distinct quartet to the one supporting the cytopharynx (Fig.1.8 E). It originates close to the Basal Body (BB), surrounds the FP and is inserted in the MT cortex, close to the FP opening (Alcantara et al., 2014).

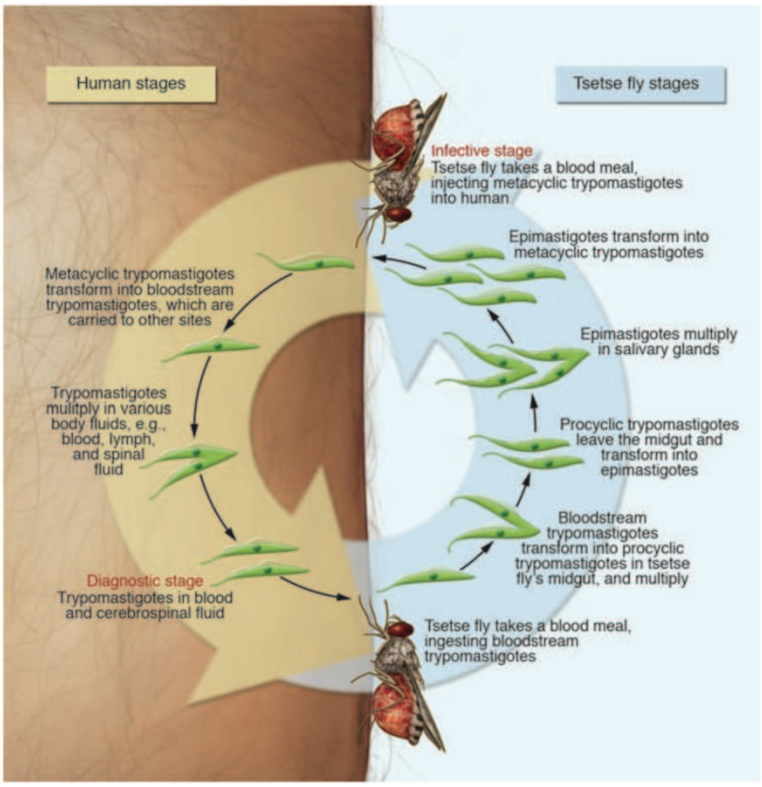

Fig. 1.9 *Life cycle of T. brucei (Stuart et al., 2008)*

When a tsetse fly takes a blood meal from an infected human (or animal), it ingests bloodstream parasites, which undergo several differentiation stages within the fly and become infective metacyclic trypomastigotes. This infective form is then injected into the bloodstream of the host during the next blood meal of the tsetse fly. From the bloodstream the parasite can spread and invade principally the central nervous system (CNS).

Tab. 1.1 *Anti-trypanosome treatment for first- and second-stage human African trypanosomiasis (Malvy and Chappuis, 2011)*

TABLE I. Anti-trypanosomal treatment for first- and second-stage human African trypanosomiasis

Disease and stage	First-line treatment	Dosing	Other treatment(s)
Trypanosoma brucei gambiense HAT			
First-stage	Pentamidine isethionate	4 mg/kg/day IM or IV (diluted in saline and given in 2-h infusions) x 7 days	
Second-stage	NECT: Eflornithine + Nifurtimox	Eflornithine: 400 mg/kg/day IV in 2 (1-h) infusions x 7 days Nifurtimox: 15 mg/kg/day PO in 3 doses x 10 days	Eflornithine: 400 mg/kg/day IV in 4 infusions x 14 days Second line (e.g. treatment of relapse): Melarsoprol 2.2 mg/kg/day IV x 10 days
Trypanosoma brucei rhodesiense HAT			
First-stage	Suramin	Test dose of 4–5 mg/kg IV (day 1), then 20 mg/kg IV weekly x 5 weeks (maximal dose/injection: 1 g)	
Second-stage	Melarsoprol	2.2 mg/kg/day IV x 10 days	Three series of 3.6 mg/kg/day IV x 3 days spaced by intervals of 7 days

HAT, human African trypanosomiasis; IM, intramuscular; IV, intravenous; NECT, Nifurtimox–eflornithine combination therapy; PO, *per os*.

c) *Trypanosoma brucei*

As previously introduced, the Scottish microbiologist David Bruce identified, in 1895, *Trypanosoma brucei* parasites as the causative agent of the disease Nagana, and suggested the transmission *via* the tsetse fly vector. It was later, in 1909, that the German Friedrich Karl Kleine, showed the cyclical transmission of *T. brucei* mediated by the tsetse fly (Steverding, 2008).

The World Health Organization (WHO) has been actively involved in the eradication of this disease for many years. In the last 20 years, the number of new infections has dropped significantly; reporting, in 2014, a record low, with fewer than 4000 new reported human cases. The objectives of the WHO programme include supporting the field activities for diagnosis and prevention, monitoring treatments and drug resistance, and the control of the vector, the reservoirs and the disease (WHO).

Human African Trypanosomiasis (HAT), also known as sleeping sickness, is an endemic disease present in 36 countries in Sub-Saharan Africa, with a great socio-economic effect in rural areas (Malvy and Chappuis, 2011). The parasite responsible is *T. brucei*, which is transmitted, almost in 100% of cases, by the bite of a female infected tsetse fly (genus *Glossina*). To date, fewer than 15 cases of human mother-daughter transmission have been reported (De Kyvon et al., 2016).

When the fly has a blood meal from an infected host (animal or human), trypomastigote trypanosomes differentiate into the procyclic form in the midgut of the vector. Procyclic trypanosomes can proliferate and leave the midgut to reach the salivary gland, where they differentiate into the replicative epimastigote form. Epimastigotes are then able to differentiate into the infective metacyclic trypomastigote form, which will infect the next host during the next fly's blood meal. Trypanosomes in the metacyclic form are a pre-adapted form for the host's environment. In the host, trypomastigote trypanosomes can multiply in the bloodstream and be taken up in the feed of another fly (Fig.1.9) (Stuart et al., 2008).

Two subspecies of *T. brucei* are responsible for the human disease: *T. brucei rhodesiense* and *T. brucei gambiense*. A third *T. brucei* sup-species, *T. brucei brucei* is responsible for the disease Nagana in cattle. Infected animals can unfortunately serve as a reservoir for the human parasite. The parasites live exclusively in an extracellular form, fully exposed to the host immune system.

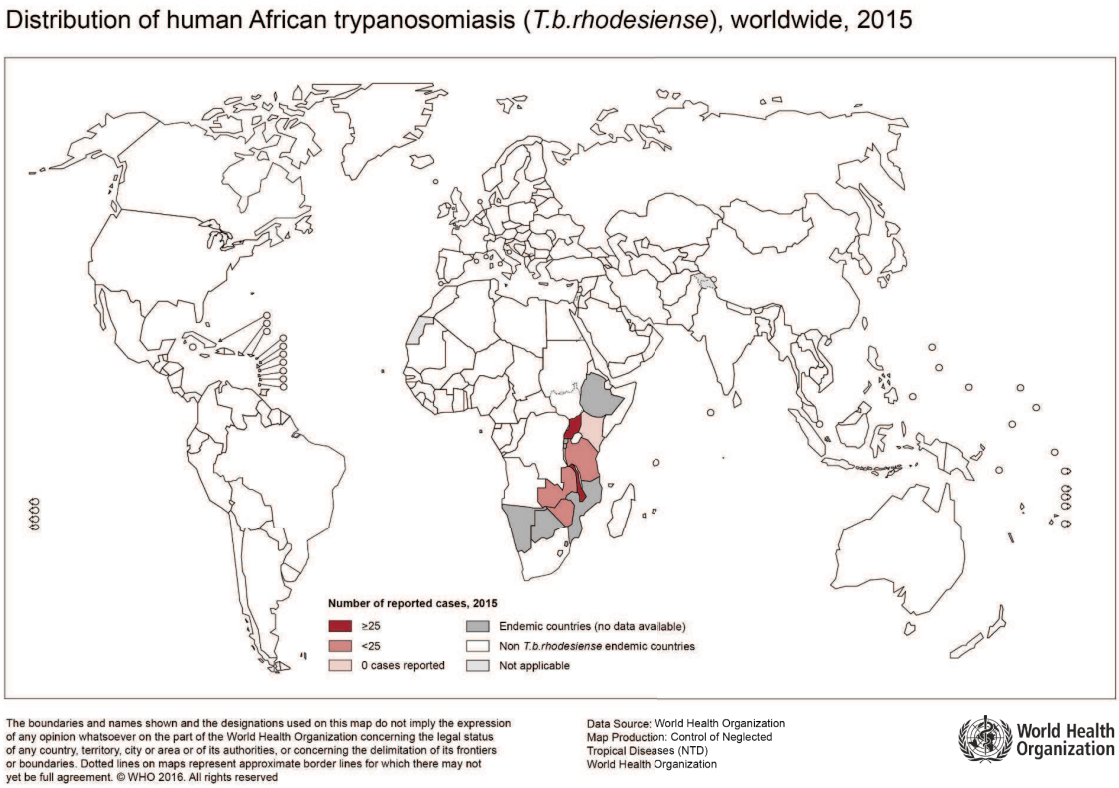

Fig. 1.10 *Distribution of T. b. rhodesiense (WHO, 2015).*
T. b. rhodesiense is found predominantly in Eastern and Southern Africa.

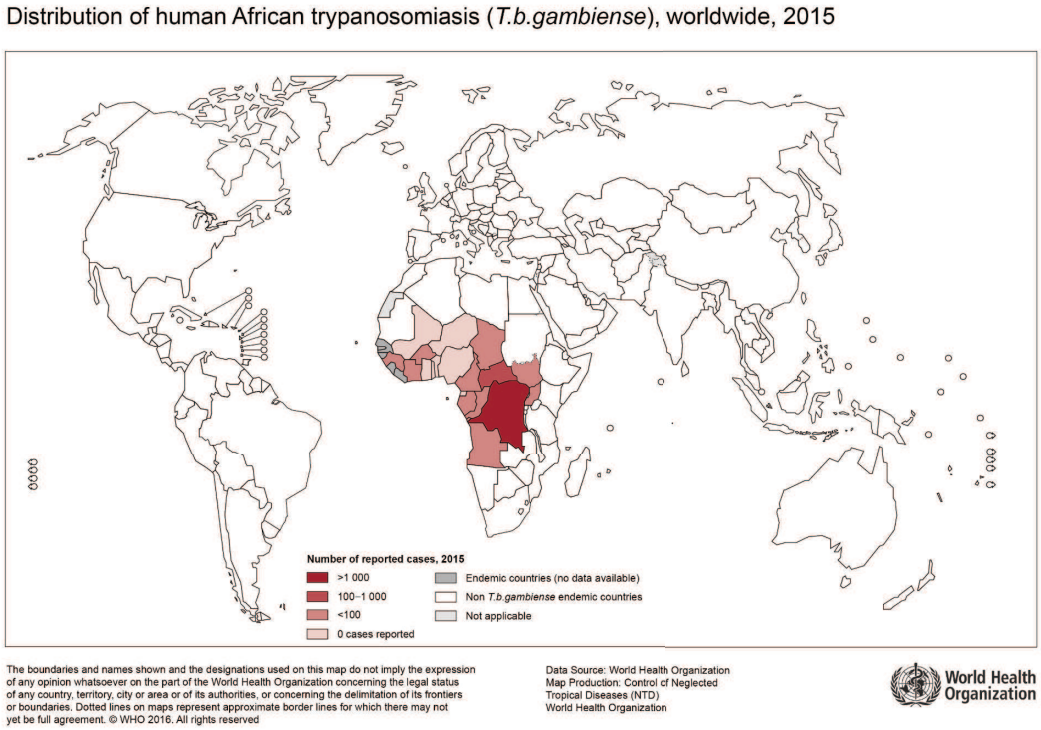

Fig. 1.11 *Distribution of T. b. gambiense (WHO, 2015).*
Repartition of T. b. gambiense, predominantly found in Western and Central Africa.

The disease, if left untreated, leads to coma and death. Currently, no vaccines are available and are not conceivable due to the antigenic variation that the parasites undergo within the mammalian host bloodstream to evade the immune system (Jacobs et al., 2011a; Jacobs et al., 2011b). Recently, a promising proteasome inhibitor (GNF6702) has been tested on mice infected by *T. brucei*, *T. cruzi* or *L. donovani* and seemed to be effective as a general drug for the treatment of these three diseases (Khare et al., 2016).

The disease, for all the three subspecies, is characterized by two phases: during the first phase, the parasites are found in the blood, in the lymphatic system and in subcutaneous tissues (haemolymphatic stage). This leads to fever, headache and articular pains (WHO). Recently, it has been shown that the parasites can also be found in adipose tissue (Trindade et al., 2016). In the second stage, the so-called meningo-encephalitic or neurological phase, the parasites cross the BBB (blood brain barrier) and invade the CNS. This results in changes in behaviour, problems in coordination and sleep disorders (Steverding, 2008); these last symptoms give the name to this disease.

c1) *T. brucei rhodesiense*

T. b. rhodesiense (Stephens and Fantham, 1910) is transmitted by *G. morsitans* and is involved in 2% of the sleeping sickness affected patients (WHO). It is responsible for the acute form of the disease in Eastern and Southern Africa (Malvy and Chappuis, 2011) (Fig. 1.10). The first symptoms can appear within weeks post infection and can lead to death within months (Steverding, 2008).

T. b. rhodesiense expresses a mRNA that codes for the serum-resistance-associated protein (SRA) (De Greef and Hamers, 1994; Gibson et al., 2002), which confers resistance to *T. b. rhodesiense* against normal human serum (NHS). This protein is not present in *T. b. brucei* and *T. b. gambiense*.
NHS contains two TrypanoLytic Factors (TLF-1 and TLF-2) (Wheeler, 2010; Namangala, 2011). These two TLFs are both associated with APOL1. They enter the cells, binding to the *Tb*HpHbReceptor (Haptoglobin Hemoglobin receptor) in a competitive and non-competitive way, respectively, but lyse the cells in the same way. APOL1 enters the parasite (associated with TLF1 or TLF2) by endocytosis and remains in the endosomal pathway. At low pH conditions, typical of the endosomal pathway, APOL1 undergoes a conformational change that enables the protein to insert into the lysosomal membrane. Once inserted into the membrane, a pore-forming domain of APOL1 creates pores in the membrane and leads to

an influx of chloride ions (Cl^-) and the consequent lysosome swelling, which leads to parasite death (Pérez-Morga et al., 2005).
In the case of *T. b. rhodesiense*, SRA is able to interact with Apolipoprotein L1 and this interaction blocks APOL1 activity and therefore inhibits the pore formation in the lysosomal membrane. This consequently prevents parasite death (Hager and Hajduk, 1997; Oli et al., 2006). The fact that SRA can confer resistance to human serum has been shown by adding one copy of the SRA gene into *T. b. brucei* genome and observing their ability to survive in human serum (Xong et al., 1998).

The treatments currently available to treat acute trypanosomiasis are shown in Tab.1.1.
For the first stage of the disease, intravenous Suramine injections are recommended. The mechanism of action of Suramine is still unknown, but its trypanocidal activity can be due to the inhibition of enzymes acting in respiratory or glycolysis processes (Drug Bank - Bayer). Unfortunately, Suramine is toxic and not efficient in the second stage.
Melarsoprol (Sanofi-Aventis), an arsenic derivative, is able to cross the BBB, and is used in the second stage of the disease. However, its high toxicity is responsible for 5-10% of treatment-related patients' deaths (Jacobs et al., 2011b). Melarsoprol is metabolized to Melarsen oxide (Mel Ox), which is able to interact with trypanothione (Fairlamb et al., 1992) and block trypanothione-reductase, inducing parasite death.

c2) *T. brucei gambiense*

T. b. gambiense derives its name from The Gambia, the state where the parasites were observed for the first time, in the early 1900s by Forde and Dutton (WHO).

T. b. gambiense is transmitted by *G. palpalis* and is responsible for the chronic form of the disease in Western and Central Africa (Fig.1.11). This sub-species contributes to the vast majority (98%) of sleeping sickness cases. The disease symptoms are the same as for *T. b. rhodesiense* but they differ in their severity, frequency and kinetics of disease progression (Franco et al., 2014). *T. b. gambiense* induced disease can take months before the first appearance of symptoms and potentially years before reaching the CNS, leading to death if untreated (Jacobs et al., 2011a; Checchi et al., 2008).
T. b. gambiense, differs from *T. b. rhodesiense*, in that it does not possess the SRA-gene, and therefore has developed another way to resist normal human serum (NHS) and allow the disease to develop.
This parasite possesses a specific GlycoProtein (*Tgs*GP), which localizes in the endocytic compartment together with APOL1, internalized into the parasite within the TLFs. *Tgs*GP

interacts with lipids *via* a beta-sheet, inducing membrane stiffening and preventing APOL1 activity and therefore parasite death (Capewell et al., 2013; Uzureau et al., 2013). In *Tgs*GP knock-out parasites, NHS leads to membrane swelling and consequent cell death (Uzureau et al., 2013).

In order to treat patients in the first stage of disease, Pentamidine intramuscular injections are given. The mechanism of action of Pentamidine is not fully understood, but it might interfere with the nuclear activity, such as DNA and RNA synthesis and consequently phospholipids and protein synthesis (drug bank). For treatment of the second stage, Eflornithine alone or combined therapies of Nifurtimox/Eflornithine are administered (Tab.1.1) (Malvy and Chappuis, 2011; Priotto et al., 2008). Eflornithine is described as a "suicide" inhibitor, since it irreversibly binds to Ornitine decarboxylase (ODC), an enzyme involved in the first step of polyamines synthesis; polyamines are known to be required for cell growth (Willert and Phillips, 2008).

For *T. b. gambiense* detection, a cheap and quick test can be used: The Card Agglutination Test for Trypanosomiasis (CATT) (Magnus et al., 1978). It is a direct agglutination test, which detects antibodies in blood, serum or plasma of patients infected by *T. b. gambiense*. It is based on recognition of variable antigen type (VAT) present on the variable part of VSG. In the case of a positive test, additional techniques, like microscopic analysis, are used to confirm the presence of the parasite (Chappuis et al., 2004).

c3) *T. brucei brucei*

T. b. brucei contributes, together with *T. congolense*, *T. vivax* and *T. evansi,* to the animal trypanosomiasis, also known as Nagana disease. It mostly affects cattle and sheep and has a huge impact on the population in terms of economic loss (Ilemobade, 2009). These parasites, in general, are not pathogenic for humans, since they are sensitive to normal human serum, as described previously.

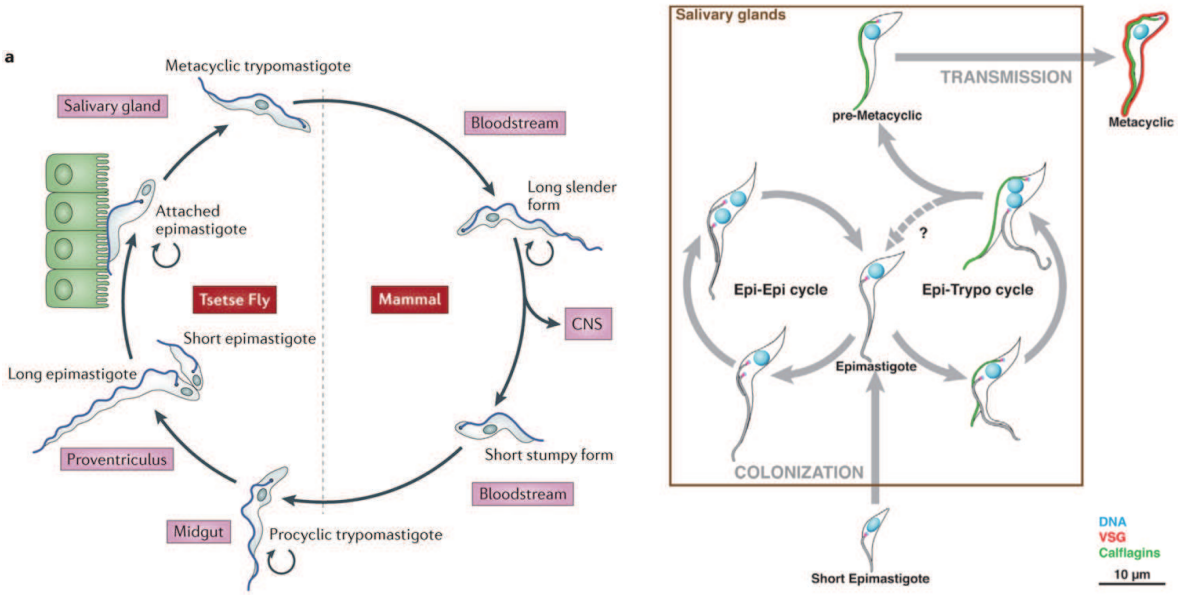

Fig. 1.12 *Life cycle of Trypanosoma brucei (Langousis and Hill, 2014), (Rotureau et al., 2014).*

(Left panel) This simplified life cycle shows the replicative long slender BSF in the mammalian host and the Procyclic trypomastigote (which we cultivate in the laboratory) in the vector. It also shows the different position of the kinetoplast during the cell cycle and different cell length in the distinct developmental stages. The right panel represents the insect salivary glands, where epimastigote parasites can divide and produce either epimastigote cells or metacyclic infective trypanosomes.

II. *T. brucei brucei* – the model organism

In 2005 the entire *T. brucei* genome was sequenced (Berriman et al., 2005), facilitating the study of trypanosome genes and enabling the identification of parasite-specific genes that can be used as therapeutic targets.
T. brucei brucei is a very good model organism, because 1) it is genetically similar to the other two *T. brucei* species, *T. b. gambiense* and *T. b. rhodesiense,* sharing parasite-specific genes that can be used as drug targets for the three species, 2) it is not pathogenic for humans, and 3) its cultivation, in both, insect and mammalian stages, does not require other cells, since it is not an intracellular parasite.

a) Life cycle

a1) Vector – Host Interaction

In this more simplified life cycle of *T. brucei* (Fig.1.12 left) (Langousis and Hill, 2014), the parasites are in the replicative procyclic form (PCF) in the mid-gut of the tsetse fly. They differentiate into an asymmetrically dividing epimastigote form, characterized by the repositioning of the kDNA anterior to the nucleus. In the salivary gland, the replicative epimastigote form remains attached to the endothelium, and differentiates then to the metacyclic infective form (Fig1.12 right). The latter is transmitted to humans by the bite of an infected tsetse fly. Metacyclic trypanosomes will differentiate into a replicative long slender (LS) bloodstream form (BSF). They can cross the Blood Brain Barrier (BBB) and colonize the brain. Those remaining in the bloodstream can then differentiate into a short stumpy form (SS), which is a non-replicative form. This SS form is pre-adapted for the fly, and is taken up during a blood meal by the tsetse fly. Once in the fly, it differentiates into replicative PCF. Trypanosomes can divide by binary fission, called cytokinesis, and both replicative BSF and PCF can be cultivated in the laboratory.

One of the main differences between BSF and PCF parasites, except for their host, is their metabolism. BSF mostly (or completely) rely on ATP production from the glycosomes (peroxisome-like organelles) which contains most of the enzymes involved in glycolysis (Michels, 1989; Haanstra et al., 2016). On the other hand, PCF in absence of glucose can perform oxidative phosphorylation within the mitochondria to produce energy. Oxidative phosphorylation consists of the catabolism of amino acids (proline and threonine predominantly) to produce ATP (Besteiro et al., 2005; Hellemond et al., 2005). In BSF, the single mitochondrion, lacking most of the respiratory chain components and the capacity for

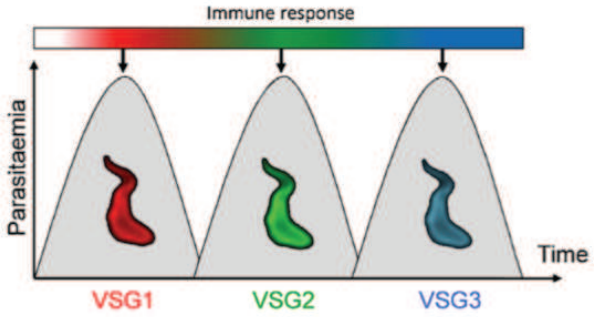

Fig. 1.13 *VSG expression and switching* ***-*** *Antigenic Variation*
The mechanism of antigenic variation allows the parasites to escape the host immune system by switching its coat from one VSG to another (Horn, 2014).

oxidative phosphorylation, is not required for energy production but it is not dispensable, because it consumes ATP to generate mitochondrial membrane potential (Schnaufer et al., 2005).
Other main differences between PCF and BSF, such as kDNA positioning and the surface coat, will be discussed later.

a2) VSG/procyclin

The parasites possess a surface coat consisting of procyclins and VSGs (Variable Surface Glycoproteins), which are GPI-anchored (Glycosyl-Phosphatidyl-Inositol) glycoproteins, present on the vector PCF/epimastigote and on the mammalian BSF parasites, respectively.

- Procyclins:

There are two forms of procyclins: one with a dipeptide composed of glutamic acid and proline (EP), and the other with a penta-peptide composed of glycine – proline – two glutamic acids and one threonine (GPEET) (Bütikofer et al., 1997). Six genes code for EP and two for GPEET (Ruepp et al., 1997); these genes are all transcribed by the RNA polymerase I (Pol I) (Günzl et al., 2003). The two types of procyclin are co-expressed on the cell surface (Ruepp et al., 1997) and anchored to the membrane *via* GPI-anchors (Ferguson, 1999). The procyclin coat serves to protect the parasites from the digestive enzymes of the tsetse fly (Acosta-Serrano et al., 2001).
On the surface of epimastigote parasites, in the salivary gland of the fly, BARPs (*brucei* Alanin-rich protein) are the major GPI-anchored proteins exposed (Urwyler et al., 2007).

- Variable Surface Glycoproteins (VSG):

VSG are found as homodimers on the surface of BSF parasites and build the so-called VSG coat. At any given time, on the cell surface, there are approximately 5-10x10^6 VSGs per cell (Jackson et al., 1985). These molecules are very immunogenic (Rudenko, 2011); they can easily provoke an immune response in the mammalian host. Similar to procyclins, VSGs are attached to the membranes (plasma and flagellar) *via* C-terminal GPI-anchors. The N-terminus of a VSG is the variable part, and it is against this part that the host produces antibodies. The size of a VSG is approximately 500 amino acids long (55-60 kDa) (Vanhamme et al., 2001). The entire VSG coat varies periodically (Taylor and Rudenko, 2006) rendering an efficient antibody response almost impossible and allowing the consequent escape from the host immune system. This process is called antigenic variation (see Fig.1.13). Individual cells switch the VSG being produced on the surface at low frequency and while the host immune system is occupied fighting against the major population of VSG, these minority cells will start proliferating, maintaining the infection (reviewed in Schwede et al., 2015).

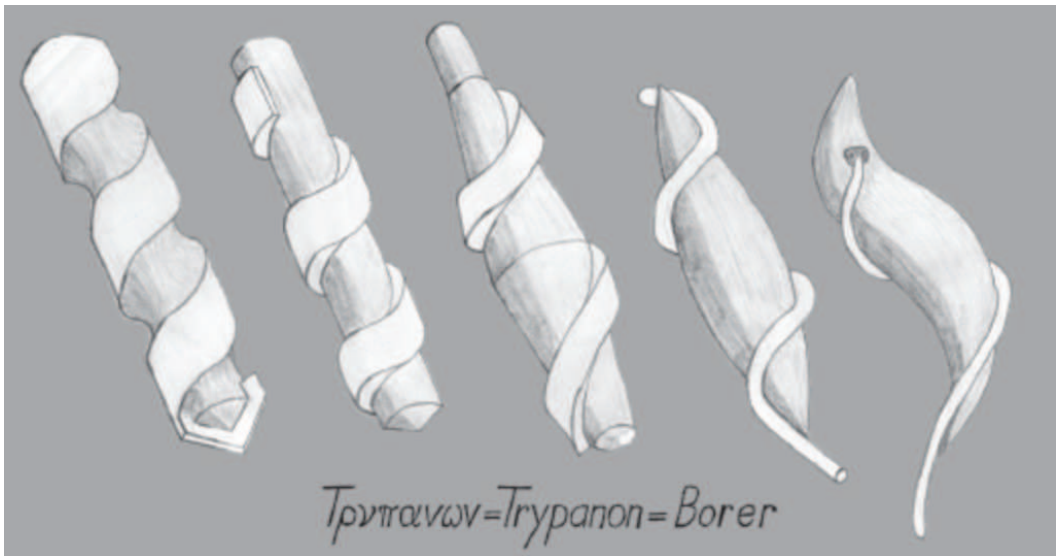

Fig. 1.14 *The origin of the name Trypanosoma (Schneider – cover Trends in Parasitology 2011 Vol.27, nr.10)*

Trypanon = borer and soma = body. Because of its shape, Trypanosoma means borer body.

The *T. brucei* genome contains around 2,000 VSG or VSG-related genes (Gadelha et al., 2011; Cross et al., 2014), but only one is expressed at a time. This mono-allelic transcription occurs at Expression-Site Body (ESB), an extra-nucleolar structure present in BSF only, where there is an accumulation of RNA Pol I (Navarro and Gull, 2001; Horn, 2014). As for procyclins, RNA Pol I ensures glycoprotein transcription (Günzl et al., 2003). The VSG transcription occurs at an extremely high rate to ensure coverage of the entire cell surface (Günzl et al., 2015).
The distribution of VSG on the cell body surface is organized so that they are distant enough to allow small molecules to rapidly diffuse through the cell membrane, but they are sufficiently tightly packed to prevent antibodies inserting into the coat (Borst and Fairlamb, 1998).

The surface coat also contains invariant surface glycoproteins (ISG), which are TMD proteins, similar in size and structurally related to VSG (Ziegelbauer et al., 1992; Ziegelbauer and Overath, 1992; Schwede et al., 2015). It has been estimated that there is 1 ISG molecule for every 50 VSGs. The mechanism by which these proteins are not recognized by the host immune system remains unknown (Schwede et al., 2015).

a3) Cell morphology (related to cytoskeleton)

The name Trypanosoma derives from ancient Greek words *Trypanon* = borer and *soma* = body, because of the movement it makes to progress (Fig.1.14). The PCF parasites measure approximately 20-25 µm in length and 3-5 µm in diameter, whereas BSF are shorter, around 15 µm in length and 2 µm in diameter (Morga and Bastin, 2013). The anterior end of the cell corresponds to the part where the flagellum is free and also determines the direction of progression/movement. The cell shape is maintained/determined by a corset of highly polarized microtubules (MTs) (sub-pellicular microtubules corset), which make up the majority of the cytoskeleton.

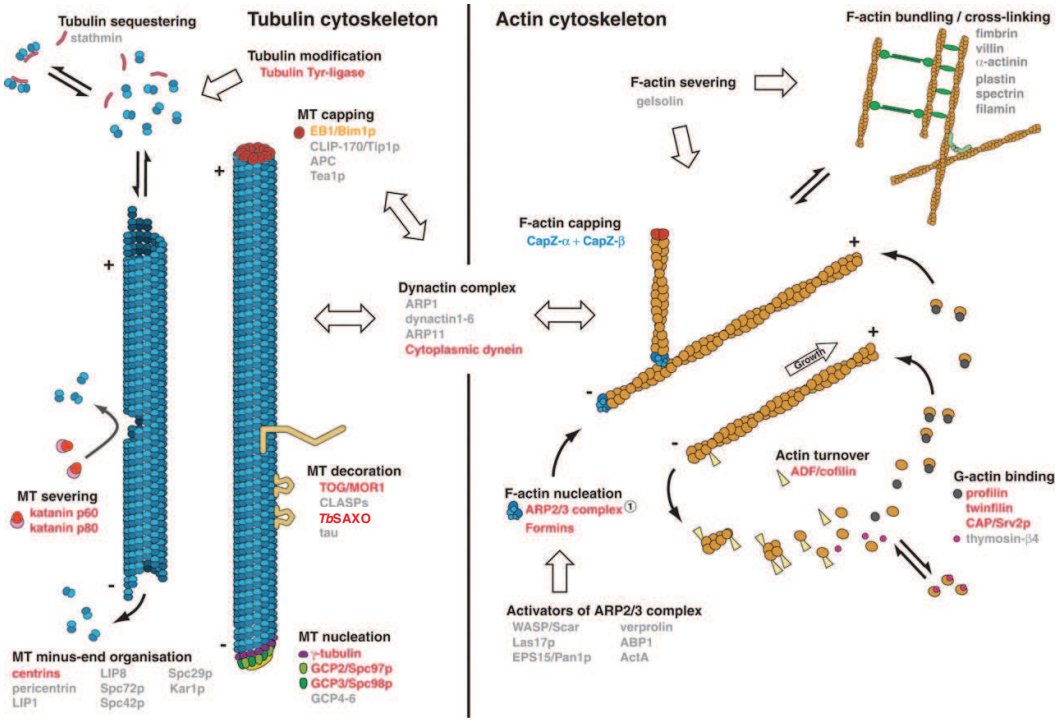

Fig. 1.15 *Core cytoskeletal components in T. brucei, T. cruzi and Leishmania (from Berriman et al., 2005)*

A schematic representation of tubulin-based (left) and actin-based (right) cytoskeleton. Tubulin hetero-dimers (blue and light blue circles) are the main component of MTs, whereas actin monomers (orange) are the principal component of actin filaments. Black text indicates processes involved in cytoskeleton organization. Red text represents components present in one or more homologues in the TriTryp genomes, and in grey, components absent in all of them. CapZ genes are present in *T. cruzi* only, whereas orange components are present in *T. brucei* and *T. cruzi*. The ARP2/3 complex is divergent in *Leishmania*.

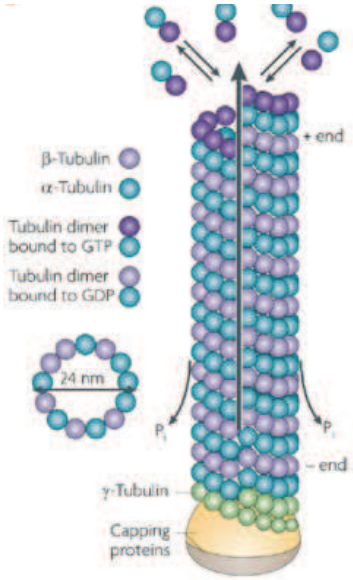

Fig. 1.16 *Structure of a single Microtubule* (Conde and Cáceres, 2009)

MTs are composed of heterodimers of α- and β-tubulin. They possess a very dynamic plus-end, the extremity, where the rate of polymerization is higher than the rate of depolymerization, allowing MT growth.

b) Cell architecture

b1) Cytoskeleton

The biogenesis of the cytoskeleton in trypanosomes is of major interest to our laboratory, because it is the main actor involved in the parasite morphology. The cell body shape, in fact, is constituted and maintained by a sub-pellicular MT array. The cell shape is adapted during the cell cycle to fit the different forms seen in the insect vector and the mammalian host. Furthermore, the cytoskeleton plays an important role in organelle positioning and in flagellum biogenesis. Cytoskeletal elements are therefore promising therapeutic targets.

The cytoskeleton of *T. brucei* is distinct genomically, because genes encoding tubulins and actin are present, but not those for intermediate filaments. Despite the presence of its gene, no actin filaments have yet been observed. Compared to other eukaryotes, the TriTryp genomes appear to be less depend on an actin-myosin network, whereas they rely on an organized MT-based cytoskeleton (Fig.1.15) (Berriman et al., 2005).

i) Sub-pellicular corset of microtubules

The cell body shape of *T. brucei* is maintained by a highly organized corset of sub-pellicular MTs cross-linked to each other and to the plasma membrane (Sherwin and Gull, 1989a; Seebeck et al., 1988). The sub-pellicular MTs are composed in a helical arrangement along the longitudinal axis of the cell (Hemphill et al., 1991). Differently to other eukaryotes, the genome of *T. brucei* codes for tubulins and actin but there are no genes coding for intermediate filaments. Despite the presence of actin genes and ARP2/3 complex genes, no actin filament has been observed so far (Fig.1.15) (Berriman et al., 2005; Ben Amar et al., 1988; Gull, 1999). In BSF, actin is localized in the endocytic pathway and is essential for vesicles formation and trafficking originating from the flagellar pocket. In PCF, actin is distributed throughout the entire cell. Actin down-regulation in PCF affects the Golgi apparatus and leads to the production of a heterogeneous population of vesicles, without, however, killing the parasites. On the contrary, actin RNAi in BSF rapidly arrests cell growth, producing cells with an enlarged flagellar pocket, leading ultimately to cell death. Moreover, the down regulation of actin impairs endocytosis, thus demonstrating that it is essential for vesicle formation and trafficking from the FP (García-Salcedo et al., 2004).

MTs are composed of 13-18 protofilaments of alpha and beta tubulin heterodimers, assembled in a cylinder shape and measure 24 nm in diameter (Conde and Cáceres, 2009; Seebeck et al., 1983; Kohl and Gull, 1998).

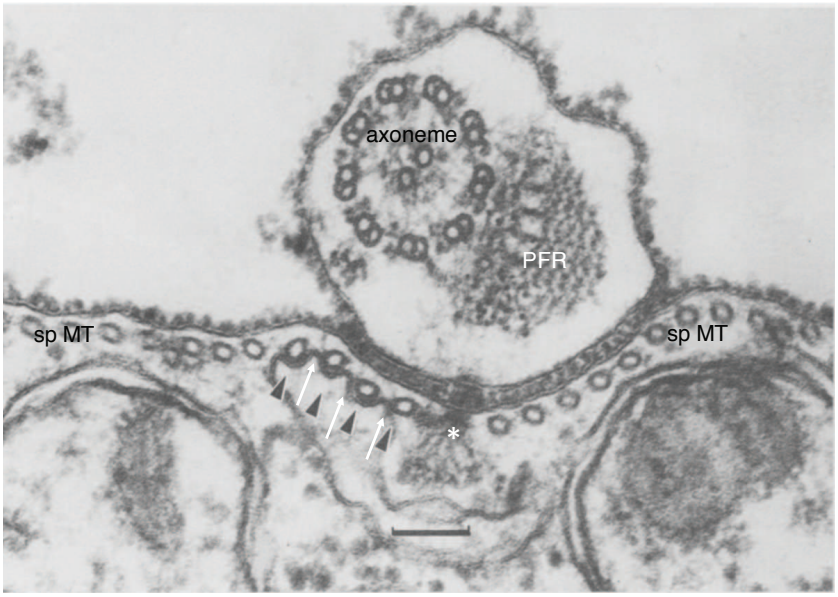

Fig. 1.17 *Thin section showing the MtQ, a specialized subset of MTs in T. brucei (Sherwin and Gull, 1989a)*
The MtQ (arrowheads) is associated with the ER membrane (white arrows). The FAZ filament (asterisk) is located close to the MtQ in between the sub-pellicular MT (sp MT).

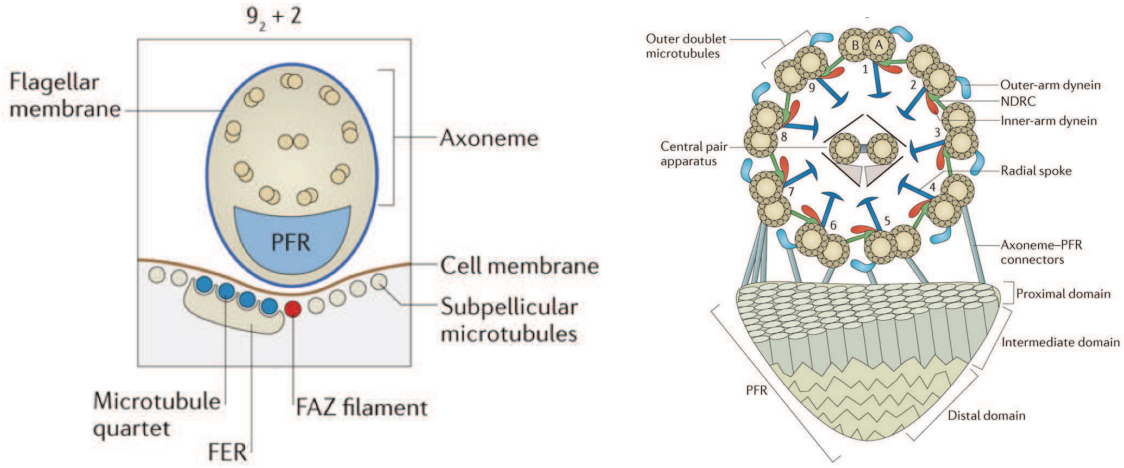

Fig. 1.18 *Flagellar section (Langousis and Hill, 2014)*
Left panel: The flagellum contains the typical axonemal 9+2 MT organization and the PFR. The flagellum is attached to the cell body *via* the FAZ. The MtQ is positioned along the FAZ, associated with the ER (FER in the image). Right panel: Enumeration of the 9 doublets making up the axoneme and the different sections of the PFR.

MT can have a very dynamic plus-end, where new tubulin heterodimers can be added allowing the MT to grow (Kohl and Gull, 1998) (Fig.1.15, Fig.1.16). Studies on the polarity of the sub-pellicular MTs showed that they have their plus-end at the posterior end of the cell, and their minus-ends at the anterior of the cells (Robinson et al., 1995). Reversible post-translational modifications (PTM) of tubulin normally act as stability markers for MT. Tyrosinated α-tubulin is a marker for dynamic assembly of new MT. On the contrary, stable MTs are normally detyrosinated and acetylated (Schneider et al., 1987; Sherwin and Gull, 1989a). During the cell cycle new MTs are inserted in between pre-existing MTs, leading to a semi-conservative corset division during cytokinesis (Sherwin and Gull, 1989a).

T. brucei possess the gene for γ-tubulin. An antibody against γ-tubulin shows some labelling at the BB (Scott et al., 1997; McKean, 2003) considered to be the MT organizing centre (MTOC), from which the flagellar axoneme originates. γ-tubulin is also found associated to the anterior end of the cells where minus-ends of MT are located, on a small specific subset of sub-pellicular MTs and one dot is visible in the nucleus of G1 cells. This dot duplicates and changes its shape to develop the mitotic spindle during mitosis (Scott et al., 1997). RNAi ablation of γ-tubulin does not impair the formation of the new flagellum but renders it immotile, since the central pair of MT is missing (McKean, 2003).

ii) The microtubule quartet

A set of four specialized MTs, called the MT quartet (MtQ), originates between the basal body and the pro-BB and make a half turn around the FP to reach the flagellar pocket collar (FPC) and runs up to the anterior end of the cell body. The MtQ shows inverted polarity compared to the sub-pellicular MTs. Interestingly, the MtQ is closely associated with the endoplasmic reticulum (ER) and runs together with the FAZ filament (Flagellar Attachment Zone) all along the cell body (See Fig.1.17, Fig.1.18 left panel) (Sherwin and Gull, 1989a). In 1969 (Taylor and Godfrey, 1969), for the first time, this special subset of four MTs was seen by EM and was named “subpellicular organelle”. Years later, a monoclonal antibody, 1B41, was produced that was specific for β-tubulin. Its localization, however, was not on all the sub-pellicular MTs, but showed a punctuate staining along the flagellum on the cytoplasmic side. 1B41 was therefore described as the first MtQ marker (Gallo et al., 1988), even though its definitive proof was not shown (such as immuno-gold labelling). To date, only two proteins, SpefI and *Tb*PLK (Polo-like kinase), have been localized associated with the MtQ.

SpefI is a microtubule associated protein (MAP) located in a specific region of the MtQ, between the BB and the FPC (Gheiratmand et al., 2013). This protein has been identified *via* an immuno-isolation of the bi-lobe complex, with YFP-tagged LRRP1 and the results showed it to be essential in PCF. Its down-regulation by RNAi did not affect BB, kDNA and flagellum duplication, but affected their segregation and led to defects in cellular motility, biogenesis of the FPC, the bi-lobe and the FAZ (Gheiratmand et al., 2013). The morphological phenotypes observed upon SpefI RNAi included mostly generation of multinucleated cells, 1K2N cells, where the kDNA was duplicated but not segregated, and 2K2N cells with an incorrect positioning of the kDNA (NKKN or KKNN). The assembly of a new MtQ was inhibited, and this could explain the inhibited biogenesis of the FPC, the bi-lobe and the FAZ (Gheiratmand et al., 2013). This suggests an important role of the MtQ in the overall cytoskeleton organization.
SpefI (also known as CLAMP) is a component of motile flagella, which is associated with MT and plays a role in MT stabilization (Dougherty et al., 2005). For example, in mice, SpefI is located in the sperm tail around the axoneme, and appears to be involved in flagellar biogenesis (Chan et al., 2005). In *Xenopus laevis* embryos, the MAP SpefI/CLAMP homologue plays a role in stabilizing MT during radial intercalation, a cell motility process by which cells move from an inner layer to an outer layer orthogonal to the plane of tissue. SpefI collaborates with the Par complex components to achieve this movement (Werner et al., 2014).

In early stages of the cell cycle, *Tb*PLK localizes close to the kDNA and the BB, and up to the FPC on the MtQ (Ikeda and de Graffenried, 2012). At later cell stages, *Tb*PLK is associated with the bi-lobe/hook complex and to the flagellar tip (de Graffenried et al., 2008). This protein has been associated with different functions like the biogenesis of the hook-complex, BB segregation and cytokinesis. More details about *Tb*PLK will be described in the Bi-lobe/hook complex section.

iii) Microtubule associated proteins
Proteins associated with microtubules are called MAPs (Microtubules Associated Proteins) and they often show repeated basic motifs involved in MT binding. These proteins can have distinct roles such as MT stabilization during polymerization, capping functions and linkers between MTs and other structures. Only a handful of MAPs have been characterized in *T. brucei* and they differ in their localization and roles:
Gb4 is a cytoskeletal protein located at the posterior end of the microtubule array that form the cytoskeleton and serves as cap protein at the + end of the MTs (Rindisbacher et al., 1993).

CAP15 and CAP17 are two low molecular mass MAPs, which localize at the anterior part of the sub-pellicular corset, but not in the flagellum or the mitotic spindle. They are located at the less dynamic part of the MT corset; they might therefore play a role is the stabilization of the MT. Their over-expression impaired correct cytokinesis, resulting in cells with 1K2N, zoids and mispositioned kDNA and nuclei (Vedrenne et al., 2002).

MARP-1 and MARP-2 are composed of a short N-terminus, a long tandem of repeated sequences and a C-terminal MT-binding domain, and localize on the MT corset (Affolter et al., 1994; Affolter et al., 1994)

WCB (the name comes from the antibody “whole cell body 1”) localizes between the sup-pellicular MT and the plasma membrane; its down-regulation creates, mainly, defects in cytokinesis (Baines and Gull, 2008).

The protein p60 is a MAP that can also interact with membranes, and might cross-link MT and membrane vesicles (Seebeck et al., 1988). MARP (p320), with more than 50 repeats of 38 amino acids, localizes on the entire length of the sub-pellicular MT, but not on the flagellar axoneme (Schneider et al., 1988). I/6 and p52 localize on the sub-pellicular MTs and might be involved in cross-linking of MTs (Detmer et al., 1997; Balaban et al., 1995; Balaban et al., 1989). p15A contains 16 tandem repeats and co-localizes specifically with sup-pellicular MT and cross-links the MT to the membrane through its hydrophobic regions (Rasooly and Balaban, 2002).

So far, only *Tb*SAXO has been described as a flagellum-specific MAP, and is a MAP6-related protein involved in MT stabilisation. *Tb*SAXO may play a role in flagellum motility (Dacheux et al., 2012).

Another class of MAPs are the so-called motile MAPs. It contains the superfamilies of motor proteins like kinesins and dyneins, which can move on MTs *via* ATP hydrolysis and can transport cargo (Marx et al., 2006).

b2) The flagellum, structure and roles in the cell cycle and morphology

In kinetoplastid parasites, the flagellum is of major importance for their motility, but also for signalling, pathogenicity and cell division (Fridberg et al., 2007; Vaughan and Gull, 2003; Hill, 2010; Vaughan, 2010).

The flagellum movement is driven by bi-helical, left- and right-handed waves along its long axis (Rodríguez et al., 2009). It is an essential organelle in both BSF and PCF parasites. The flagellum functions as a sensory organelle and can transfer proteins *via* the fusion of the flagellar membrane of two flagella (Imhof et al., 2016).

Assembly of a new flagellum is directed by the old one (Moreira-Leite et al., 2001) and is involved in correct cell division, which occurs by binary fission in between the old and the new flagellum.
The flagellum exits the parasite from the flagellar pocket (FP) and follows a defined left-handed helical path, remaining attached throughout the entire length of the cell body *via* the FAZ, and with a small part being free to beat (Rodríguez et al., 2009). Unlike in axenic amastigote Leishmania that have a very short flagellum, *T. brucei* flagellum remains at least as long as the cell body throughout the entire life cycle.

The flagellum can be described as four main structures or compartments: the axoneme, the Paraflagellar rod (PFR), the flagellar matrix, and the flagellar membrane. These structures and compartments are described below.

i) The basal bodies and the axoneme
Flagella and cilia share some morphological and structural characteristics (compared in section III. of this chapter) that also render *T. brucei* a good model organism to study ciliopathies.

In G1 cells, a mature basal body (BB) and an associated pro-basal (pBB) body are located beneath the base of the FP, where the flagellum will originate from the BB. The BB is composed of a proximal zone containing 9 triplets of microtubules without a central pair. The triplets are composed of a complete A-tubule and incomplete B- and C-tubules. A transition zone with 9 doublets without a central pair (9 + 0) follows the proximal zone. At the distal end of the transition zone is the basal plate that contains the minus-end of the microtubule central pair of the axoneme that will extend from there (McKean, 2003). The pBB is located close to the BB and is composed of the proximal zone (9 + 0) only (Lacomble et al., 2010; Vaughan and Gull, 2016). During cell cycle progression, in the G1/S transition, the pBB matures and extends the transition zone within the FP to, later, build a new flagellum, and two new pBBs are created. The new BB and pBB rotate then anticlockwise around the old flagellum, and the new flagellum continues its elongation (Lacomble et al., 2010).

The axoneme originates from the basal plate of the mature BB and shows the classical 9 + 2 organization of motile cilia (9 doublets and a central pair of MTs). Each of the 9 doublets is composed of a complete A-microtubule consisting of 13 protofilaments, and a B-microtubule of 11 protofilaments connected by nexin bridges (green arrows in Fig.1.18 right panel). The axonemal MTs display an inverted polarity compared with the sub-pellicular MTs but the same polarity as of the MtQ (Robinson et al., 1995). Finally, radial spokes connect the 9 doublets to the central pair of MT (Fig.1.18 right panel with MT numbers).

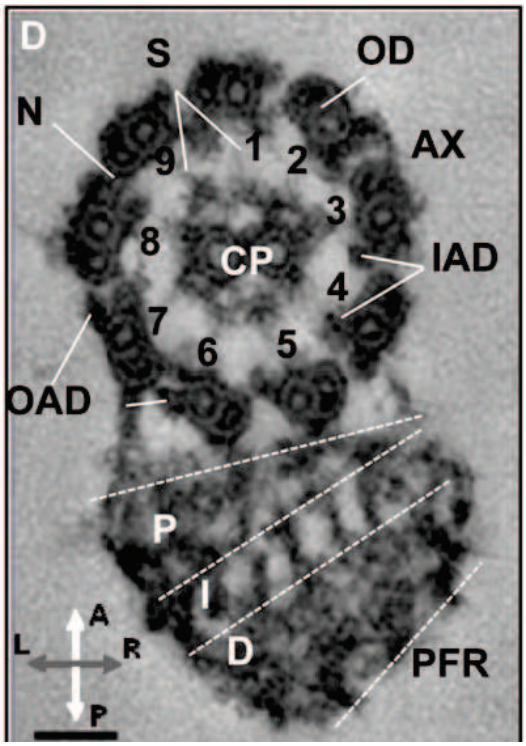

Fig. 1.19 *Axoneme and PFR of T. brucei* (Hughes et al., 2012)
The organization of the flagellum of *T. brucei* is represented in this picture. The axoneme is composed of 9 doublets of MT (numbers) and a central pair (CP). The PFR lies along the axoneme and is divided into three sections: proximal (P), intermediate (I) and distal (D).

The machinery responsible for flagellum assembly is called Intra Flagellar Transport (IFT). Its first description was in 1993 in *Chlamydomonas* (Kozminski et al., 1993).
Two families of proteins are involved in this transport machinery: kinesins and dyneins. The anterograde transport, from the BB to the tip of the flagellum, is fulfilled by kinesins. They move along the MTs and can bring cargo to the distal tip of the flagellum. Dyneins, on the other hand, are responsible for the retrograde transport and bring cargo from the tip of the flagellum back to the BB. In *T. brucei* the MT doublets 3 to 4 and 7 to 8 are used for IFT (Morga and Bastin, 2013), and recently it has been demonstrated that the ITF in *Chlamydomonas* can occur on the same doublet, with the anterograde transport on B-microtubules, whereas the retrograde transport on the A-microtubules (Stepanek and Pigino, 2016).
Two complexes of IFT proteins can be distinguished: 1) ITF-A complex contains at least five proteins involved in retrograde transport (IF-144, 140, 139, 122, 43) and 2) ITF-B complex: 11 proteins carrying out the anterograde transport (for example: kinesin-2, IFT-20, 27, 52, 57/55, 80, 88, 172) (Morga and Bastin, 2013; Taschner et al., 2012).

ii) The ParaFlagellar Rod

Discovered by Keith Vickerman in 1962 (Vickerman, 1962), the paraflagellar rod (PFR) is a lattice-like structure contained within the flagellar membrane, which elongates close to the axoneme once the flagellum has exited the FP (Kohl and Gull, 1998). The PFR can be divided in three sub-domains: proximal, intermediate and distal domains, corresponding to their position relative to the axoneme. The proximal domain is always found on the side of doublets 4 to 7 of the axoneme, whereas the distal part is linked to the FAZ (Fig.1.18 right panel, Fig.1.19). Direct connections between the PFR and axonemal dyneins have been observed, suggesting a mechanism by which mechano-chemical signals may be transmitted from the PFR to axonemal dyneins (Hughes et al., 2012). The authors also proposed that the PFR could function as a biomechanical spring, able to store and transmit energy derived from axonemal beating.
The PFR is a very resistant structure, which is maintained during flagellar isolation. The main protein components of this structure are PFR-A and PFR-C (Kohl et al., 1999), whilst at least 20 other PFR proteins have been identified (Portman et al., 2009). A yeast-two-hybrid approach demonstrated the protein-protein interaction network within the PFR structure (Lacomble et al., 2009). Importantly, the PFR structure is essential for flagellar motility and cell motility in PCF and BSF (Broadhead et al., 2006), as shown in the *snl-1* mutant strain (Bastin et al., 1998). Cell growth appeared normal but the cells sedimented to the bottom of the wells, appearing to be paralysed, because of the drastic decrease in flagellum beating.

Thin sections analysed by EM revealed the absence of the intermediate and distal part of the PFR in *snl-1* mutants (Bastin et al., 1998).

iii) The flagellar matrix

The flagellar matrix is the luminal compartment of the flagellum. In 2011 a flagellar proteome was published. This proteome made a distinction between surface proteins (membrane) from matrix proteins (soluble). The matrix proteome included 666 proteins, many of them were annotated with putative functions related to cell signalling, one of the roles played by the flagellum (Oberholzer et al., 2011). The list of the identified matrix proteins included many putative kinases. However, more than half of the identified proteins had no predicted functions, thereby revealing the large amount of work that still needs to be done to understand the biology of *T. brucei*.

iv) The flagellar membrane

The flagellar surface proteome was published in 2011 (Oberholzer et al., 2011) and included 158 proteins, more than half of them without predicted functions. These proteins were enriched for predicted TMD and most of the known flagellar membrane proteins were present within this list. Moreover, this flagellar surface proteome was depleted from IFT (intra-flagellar transport) proteins, proving its quality and reliability. The proteins showing predicted functions included mostly transporter-related activities (Oberholzer et al., 2011).
Recently, it has been shown that the fusion of the flagellar membranes is a mechanism for protein exchange between trypanosomes (Imhof et al., 2016).

v) The Flagella connector

The new flagellum is always positioned posterior to the old one and its distal tip is connected, during its entire elongation in PCF, to the old flagellum *via* the Flagella Connector (FC), a dynamic and mobile transmembrane complex (Moreira-Leite et al., 2001; Höög et al., 2016). Only two components of the FC are known to date: *Tb*PLK (a polo-like kinase) (Ikeda and de Graffenried, 2012), and FC1 (McAllaster et al., 2015). Thanks to AB1, the only antibody recognizing the FC, the Gull laboratory demonstrated that when the FC reaches a specific point on the old flagellum the complex is disassembled and stops migrating, but the flagellum continues its growth (Briggs et al., 2004).

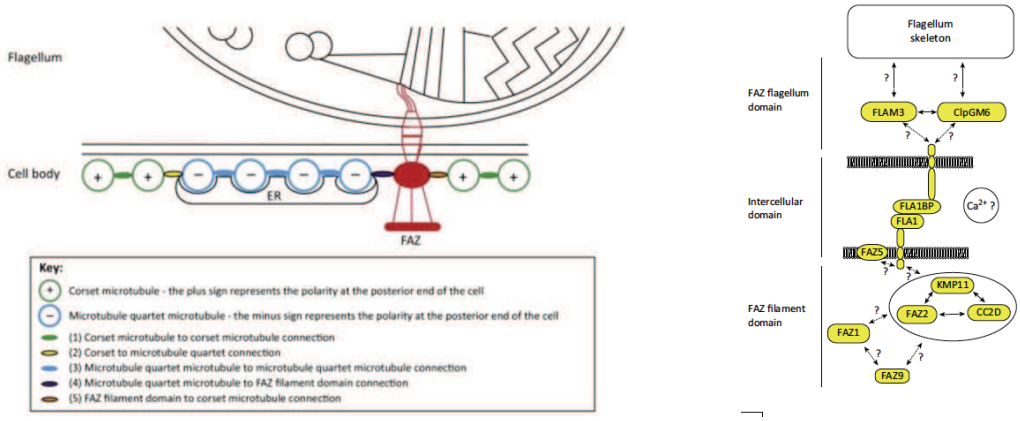

Fig. 1.20 *FAZ organization* (Sunter and Gull, 2016)

The FAZ is the physical link between the FAZ filament within the cell body, the plasma membrane and the flagellar membrane. The FAZ originates above the FP and runs along the MtQ up to the anterior end of the cell body (left). On the right, a schematic representation of the known proteins of the FAZ and their localization.

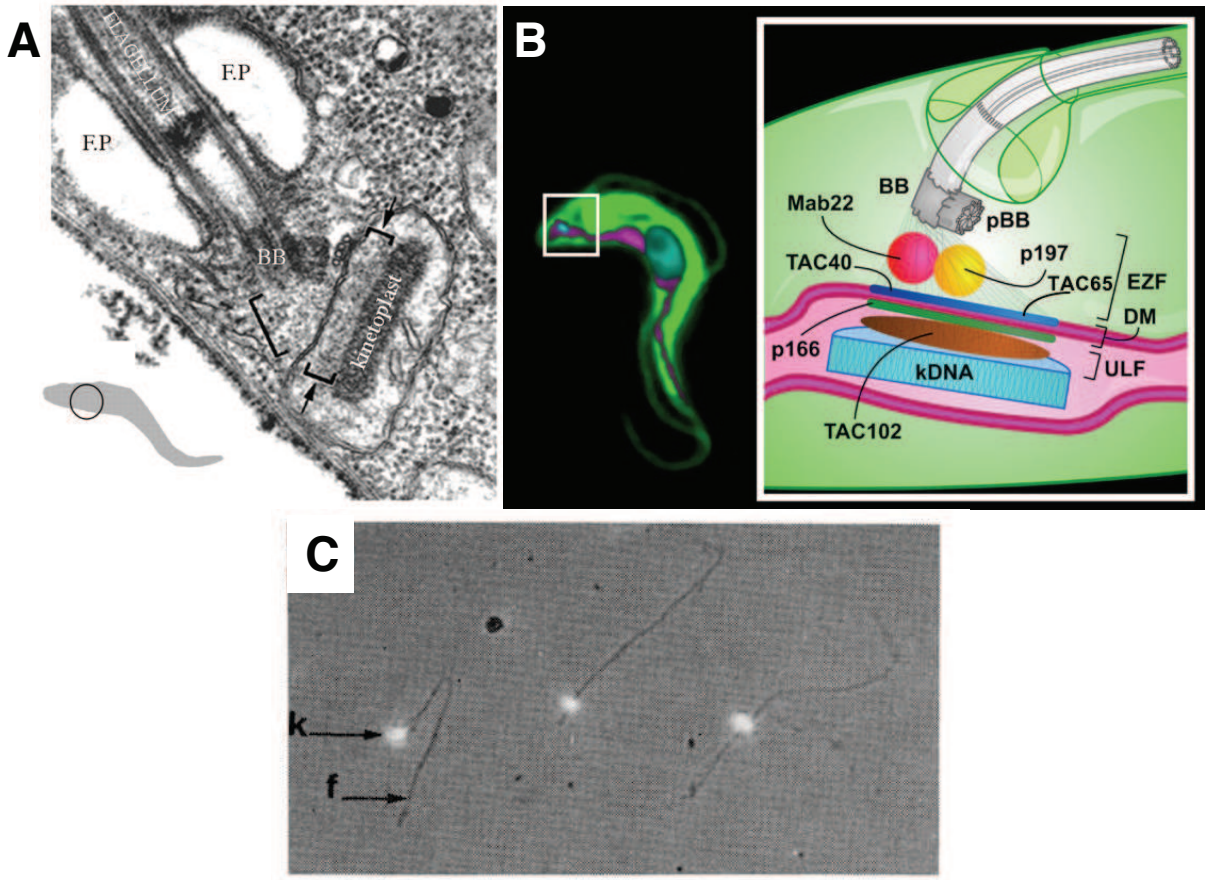

Fig. 1.21 *The Tripartite Attachment Complex of T. brucei (Matthews, 2005; modified Hoffmann et al., 2016, Robinson and Gull, 1991)*

The TAC represents a physical link between the kDNA and the BB (in brackets in A, B). The proteins identified in this region are represented in the cartoon in (B). (C) The proof that the kDNA was physically attached to the BB was provided by the isolation of flagella carrying the mitochondrial DNA.

In the BSF there is no FC *per se*, but the flagellar tip, during flagellum elongation, is located in a small invagination of the plasma membrane called the groove. The authors hypothesize that this groove, closely associated to the MtQ, plays the same role as the FC (Hughes et al., 2013).

b3) The Flagellum Attachment Zone

The Flagellar Attachment Zone (FAZ) is a complex structure that runs all along the cell body of trypanosomes with the task of maintaining the flagellum attached to the cell body (Kohl et al., 1999; Woods et al., 1989; Sunter and Gull, 2016). FAZ was first reported in 1976 when Hogan and colleagues described it as miniatura maculae adherentes (Hogan and Patton, 1976). The FAZ creates a physical link between the cell body and the flagellum with three main domains (the FAZ flagellum domain, the intercellular domain, and the FAZ filament domain) (Fig.1.20 left panel). The FAZ-filament originates above the FP and runs parallel to the MtQ up to the anterior end of the cell body.
Some examples of FAZ components are listed here: FAZ1, CC2D and FLA1 are associated with the FAZ filament (Fig.1.20 right panel) (Kohl et al., 1999; Vaughan et al., 2008; Zhou et al., 2011; LaCount et al., 2002; Rotureau et al., 2014). FLA1BP connects the plasma membrane with the flagellar membrane (Sun et al., 2013). FLAM3 and ClpGM6 are located inside the flagellum (Rotureau et al., 2014; Hayes et al., 2014) (Fig.1.20 right panel).

The FAZ complex is essential, firstly to maintain the flagellum attached to the cell body, but also to play a role in organelle positioning, and defining the positioning of the cleavage furrow during cytokinesis, which starts from the anterior end of the cell (Sherwin and Gull, 1989a). Binary fission occurs in between the two flagella and is dictated by the FAZ positioning (Robinson et al., 1995).

Many components of the FAZ are essential for parasite survival or for proper cytokinesis. It has been shown that cells with a shorter FAZ can still divide but not in a proper way, and cells in which the flagellum is detached and the FAZ is absent show impaired cytokinesis (Kohl et al., 2003).

b4) The Tripartite Attachment Complex

A highly ordered trans-membranous structure called the Tripartite Attachment Complex (TAC) allows the connection between the mitochondrial DNA (kDNA) and the BB. The physical attachment between the kDNA and the BB was shown for the first time in 1991 (Robinson and Gull, 1991) (Fig.1.21C); the name TAC came some years later, in 2003 (Ogbadoyi et al., 2003). This complex is composed by three sub-domains 1) the exclusion zone, 2) a differentiated mitochondrial membrane, and 3) the unilateral filaments (Fig.1.21A, B). The exclusion zone links the BB to the differentiated mitochondrial membrane and does not contain cytoplasmic ribosomes (for this reason it has the name exclusion zone). The differentiated mitochondrial inner membrane (IMM) does not show any cristae and looks more parallel to the outer membrane (OMM) than the rest of the mitochondrial membrane. The unilateral filaments connect the kDNA with this differentiated mitochondrial membrane. The TAC is present throughout the whole cell cycle and this explains why the kDNA is always found close to the BB, at the base of the flagellum, and why the kDNA can be isolated together with flagella (Robinson and Gull, 1991; Ogbadoyi et al., 2003).

Currently, five proteins have been identified as part of the TAC. The protein p197 (Gheiratmand et al., 2013) is found in the exclusion zone. A monoclonal antibody, mAb22, also labels the exclusion zone, but so far the target protein has not been identified (Bonhivers et al., 2008a). TAC40 and TAC65 are found in the OMM (Schnarwiler et al., 2014; Käser et al., 2016; Niemann et al., 2013), whereas p166 is localized in the IMM (Zhao et al., 2008). Recently, TAC 102 has been found on the unilateral filaments area (Trikin et al., 2016; Hoffmann et al., 2016) (see Fig.1.21B).

Since one of the essential roles of the flagellum is parasite movement, several flagellar proteomes have been performed in order to identify proteins that can serve as novel drug targets. In 2006, the first flagellar proteome, starting with the flagellar axoneme, PFR and BB allowed the identification of more than 500 proteins (Broadhead et al., 2006). More recently, two proteomic analyses allowed the identification of flagellar surface and matrix proteins (Oberholzer et al., 2011; Subota et al., 2014).
In the first proteome, 331 proteins were identified and 208 of them were trypanosomatid-specific. Oberholzer and colleagues made a distinction between flagellar surface proteins and flagellar matrix proteins; they identified 158 and 666 proteins respectively. In the most recent proteome, 751 flagellar proteins have been identified and among them, 212 non-previously associated with flagella. This shows that a lot of work should still be done to better characterize this important trypanosome organelle.

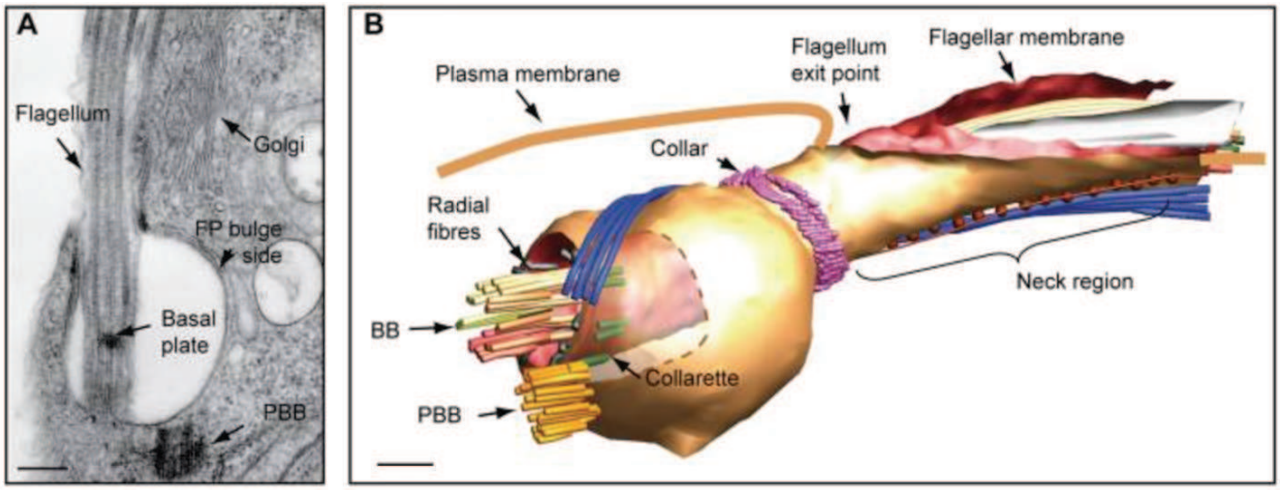

Fig. 1.22 *Electron Microscopy and Tomography analysis of the FP region of T. brucei (Lacomble et al., 2009).*
A) Thin section of *T. brucei* showing the asymmetrical shape of the FP, and the Golgi apparatus positioned on the larger side, symmetrical to the pBB. B) Tomographic reconstruction of the FP area with the major membranes and cytoskeletal regions.

b5) The Flagellar Pocket

The flagellum exits the cell body from a MT-free zone, corresponding to a small invagination of the plasma membrane. This invagination is called the Flagellar Pocket (FP). The FP membrane represents around 5% of the total cell surface area (Overath and Engstler, 2004; Engstler et al., 2004) (Fig.1.22).

The FP is the only site where endocytosis and exocytosis processes occur, and is therefore essential for parasite survival. In BSF, host-produced antibodies against, and attached to, the VSGs are eliminated from the surface of the parasite and internalized into the FP by hydrodynamic forces produced by the forward motion of trypanosomes. The immunoglobulins are then separated from the VSGs and degraded, whereas VSGs are recycled back to the surface (Webster et al., 1990; Engstler et al., 2004). This process is extremely rapid, with the entire VSG coat being recycled in approximately 12.5 minutes (Overath and Engstler, 2004). The endo- / exocytotic activity in BSF is higher than in PCF, because of the high rate of VSG recycling, to escape the host immune system (Engstler et al., 2004).

Endocytosis is restricted to the FP area located at the posterior end of the cell (Fig.1.23 A). In BSF, actin is involved in vesicle formation and trafficking (García-Salcedo et al., 2004). In the endocytotic pathway, once material has bound to a receptor on the FP membrane, it is endocytosed in a clathrin coated-vesicles class I (CCV I) and reaches the early endosomes (EE) characterized by the presence of the RAB5 GTPase. These vesicles can then migrate to the late endosomes (LE – characterized by the presence of RAB7) and reach finally the lysosomes for degradation. Lysosomes are identified by the present of p67 (see Fig.1.23 B). The EE can also be recycled into recycling endosomes (RE – containing the protein RAB11) returning to the FP to be exocytosed. A protein of the endocytic pathway, *Tb*MBAP1, has been found in all the three compartments: EE, LE and RE, but absent in lysosomes (Engstler et al., 2005).
Moreover, EE and RE can produce smaller vesicles (CCV class II), which collect fluid phase material and can, perhaps, directly reach the lysosomes (Overath and Engstler, 2004).
It has been demonstrated that the endocytic activity of the FP is regulated by a phosphatidylinositol phosphate kinase present at the neck of the pocket (Demmel et al., 2014).

Since the endocytic process in *T. brucei* exclusively occurs in a clathrin-mediated fashion, an interactome of Clathrin has been performed in order to provide insight in the endocytic

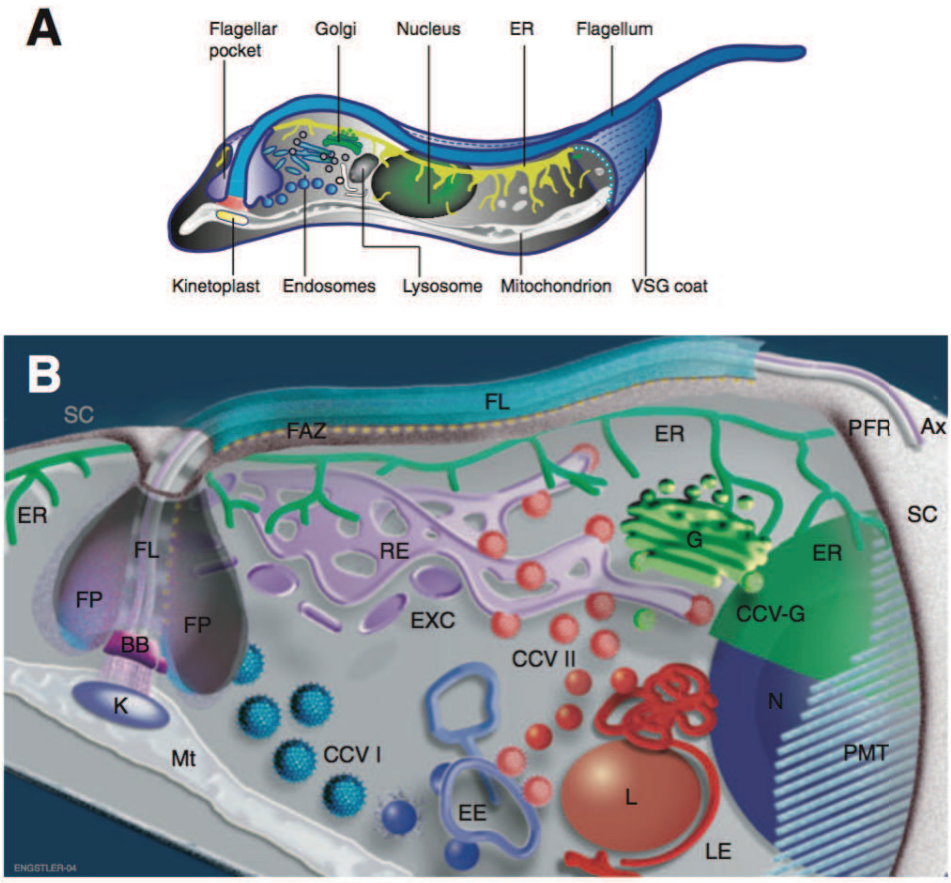

Fig. 1.23 *Endo- and Exocytosis processes within T. brucei (Overath and Engstler, 2004)* Clathrin-mediated endocytosis enables the internalization of material into the cell through the FP. Clathrin-coated Vesicles type I (CCV I) migrates from early endosomes (EE) to late endosomes (LE) and finally to lysosomes (L). From early and late endosomes, the vesicles can also be recycled, reaching firstly the recycling endosome (RE) and then being exocytosed.

system (Field et al., 2012); from this study a list of Clathrin Associated Proteins (CAPs) candidates has been made. *Tb*CAP100, *Tb*CAP161 and *Tb*Hsc70 have been further characterized and localized in the endocytic pathways, and the interaction with Clathrin is clearly supported by experimental data (Field et al., 2012).
Very few FP proteins have been identified and characterized. Among them, for example, the CRAM (Cysteine Rich Acid trans-Membrane) protein has been identified and serves as a lipoprotein receptor (Lee et al., 1990; Zheng et al., 1999), and the hetero-dimer transferrin receptor (TfR), encoded by ESAG6 and ESAG7 (Salmon et al., 1994), serves to internalize Fe^{3+}-Transferrin complex (Steverding et al., 1995). Recently, Gadelha and colleagues published a surface proteome of the FP in BSF (Gadelha et al., 2015). They detected more than 200 proteins that are, with high confidence, located at the FP surface. To validate the proteome, 23 proteins, without predicted functions, were tested for their localization and 12 of them localized at the FP, 6 at the endosomes, and 5 elsewhere.

In addition to exocytosis through the FP, the secretomes of *T. b. brucei* and *T. b. gambiense* have been published (Atyame Nten et al., 2010; Geiger et al., 2010). The secreted proteins (also called ESP = expressed/secreted proteins) could be divided into functional groups, suggesting a role of defence by these proteins against the host, or at least a protein exchange mechanism between parasites (Geiger et al., 2010). By EM analysis it was clearly shown that the parasites were able to secrete micro-vesicles (50-100 nm) from the coated plasma membrane and the flagellum. These micro-vesicles excreted cytosolic and plasma membrane proteins, whereas proteins of intracellular organelles were not detected (Geiger et al., 2010). Moreover, it has been demonstrated that cell-cell communication occurs *via* membranous nano-tube like structures, connecting two cells, and by the release of extra-cellular vesicles (EVs), a sort of exosome. These EVs are endocytosed at the FP through a receptor-independent process. This enables an efficient transfer of virulence factors, such as SRA of *T. b. rhodesiense* to *T. b. brucei*, rendering the latter resistant to human serum (Szempruch et al., 2016).

The new FP originates from the existing FP, in a highly coordinated fashion with BB duplication and segregation (Vaughan and Gull, 2016).

In the FP region, four sub-domains of the same membrane, with different structural and biochemical properties, are in close proximity: flagellar, FP, neck, and plasma membrane (Lacomble et al., 2009; Borst and Fairlamb, 1998). They differ in the density of intramembrane particles (IMP), such as integral membrane proteins (Gadelha et al., 2009).

The FP appears uniformly involved in endocytosis, but, when this process is blocked, markers for fluid-phase and receptor-mediated endocytosis accumulate in a specific region of the pocket, associated with the MtQ. This region connects the flagellar pocket lumen to the extracellular space and is called the neck channel. In this membranous region, no clathrin-coated vesicles are formed to be endocytosed (Gadelha et al., 2009).
The neck region has a cylindrical shape slightly bigger in diameter than the flagellum and represents the connection between the internal FP membrane and the external plasma membrane (Lacomble et al., 2009). As for the FP, the sub-pellicular MTs do not invade the neck region.

Recently, 3D reconstructions of the FP from whole cell tomography analysis allowed fine localisation of several cytoskeletal structures located at and close to the FP (Lacomble et al., 2009).
The FP, also defined as an asymmetric balloon, is associated with two different cytoskeletal structures: the collarette and the Flagellar Pocket Collar (FPC). The collarette is an annulus-shaped region composed of transitional fibres that links the flagellar membrane to the FP membrane at the base of the FP (Lacomble et al., 2009). (Fig.1.22 B) On the opposite site, at the flagellum exit point, is the FPC, which encloses the plasma membrane around the flagellum (Fig.1.24) (Sherwin and Gull, 1989a; Bonhivers et al., 2008b, Lacomble et al., 2009). Distal to the FPC is the neck region, which is associated with the beginning of the FAZ and the Golgi apparatus (Lacomble et al., 2009; Henley et al., 1978) and where the MtQ joins the sub-pellicular MT array. A single MT is present at the neck region and extends shortly along the FAZ, on the opposite site of the MtQ (Fig.1.24 A) (Lacomble et al., 2009). It is located between the beginning of the FAZ and before the beginning of the PFR, but its function is unknown.

Note: Epimastigote *T. cruzi* parasites possess, additionally to the FP, the cytostome and the cytopharynx that serve as endocytotic organelles. A mechanism of vesicle release from the plasma membrane has also been observed (Bayer-Santos et al., 2013). As in the other Trypanosomatids, *Leishmania* parasites possess a FP. Despite that the knowledge of the presence of this structure for many years, the 3D organization of the pocket is not well known. Recent tomography analysis in *L. mexicana* brought some insights into the FP organization. The cytoskeletal structures are very similar to those of *T. brucei* although some rearrangements of FAZ proteins occur in *L. mexicana* amastigotes (Wheeler et al., 2016).

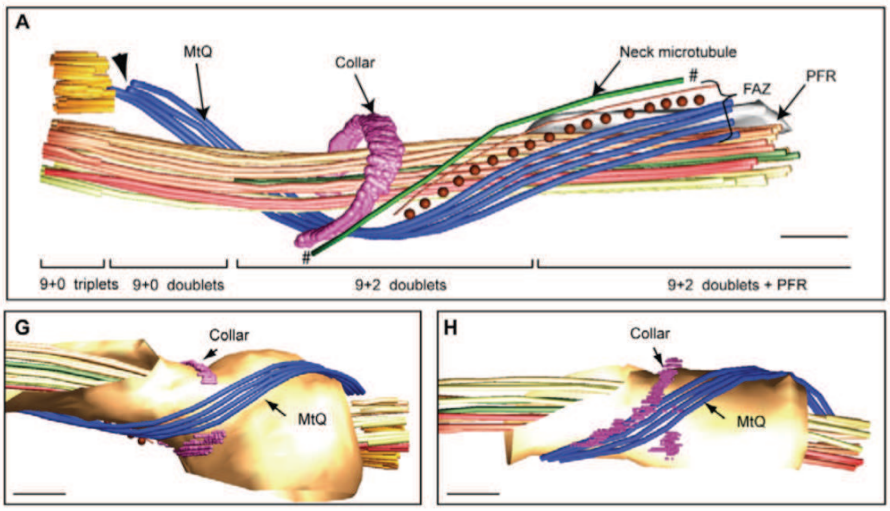

Fig. 1.24 *Tomography of the FP region in T. brucei (Lacomble et al., 2009)*
(A) Membranes were excluded to visualize only the cytoskeletal elements in the FP area. The MtQ (blue) originates from the BB region, crosses the FPC (pink) and elongates along the FAZ filament (red dot). The neck MT (green) follows the FAZ from the FPC up to the beginning of the PFR. In (G) The FP region is visualized with the FP membrane, showing the MtQ wrapping around the FP and crossing the FPC and (G), rotated 180°, shows the FPC as an open-ring traversed by the MtQ.

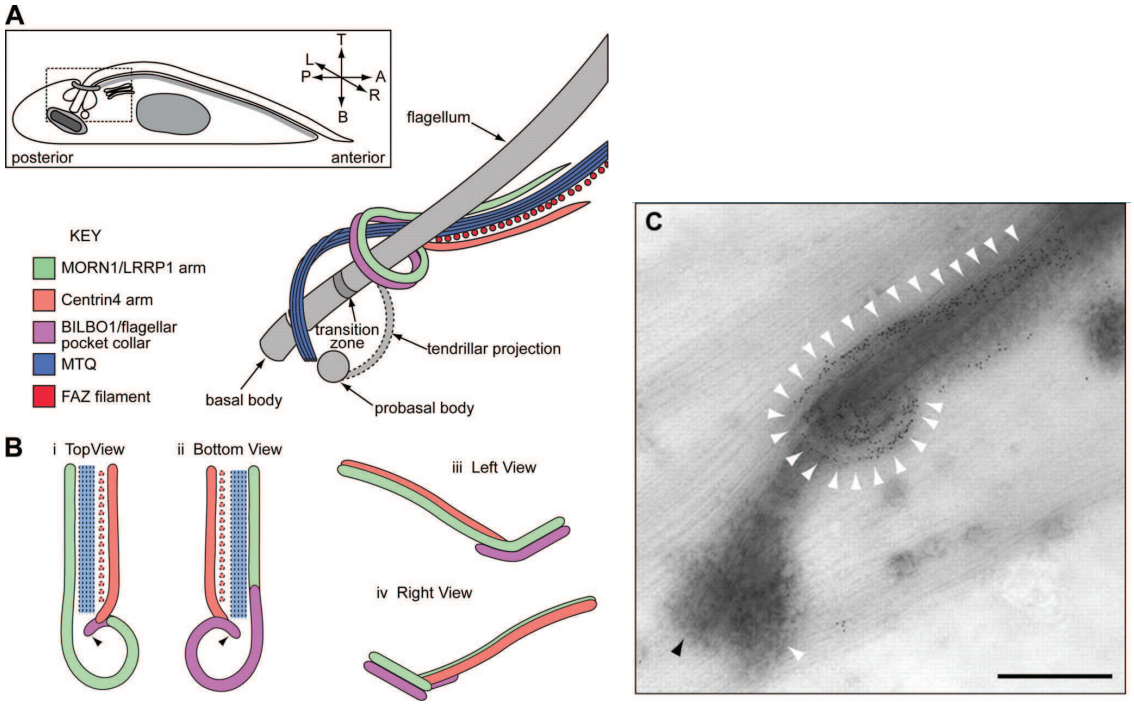

Fig. 1.25 *The hook complex in T. brucei (Esson et al., 2012)*
(A) Scheme representing the hook-complex with MORN1/LRRP1 in green and Centrin 4 in orange, which sits on FPC (BILBO1 in pink). The MORN1/LRRP1 tail runs along the MtQ (blue) and Centrin 4 runs along the FAZ (red dots). (B) The view of the hook complex from the top (i), the bottom (ii), the left (iii), and the right (iv). (C)YFP-MORN1 assumes a hook-shaped structure, which sits on the FPC and elongates along the flagellum.

b6) The Bi-lobe or Hook complex

The bi-lobe is a cytoskeletal structure (cytoskeletal in the meaning that it remains associated with the cytoskeleton after detergent extraction), first described in 2005 (He et al., 2005), with the localization of Centrin2, a protein required for Golgi duplication. Centrin4 was found, in addition to the bi-lobe localization, at the basal body, together with Centrin2 (Shi et al., 2008). Both Centrins were found to be essential for parasite survival. Down-regulation of Centrin-2 impairs Golgi duplication, whereas RNAi of Centrin-4 leads to rapid accumulation of multinucleated cells, zoids and 1K2N cells (He et al., 2005), (Shi et al., 2008).

The bi-lobe structure measures approximately 2 μm in length and, interestingly, is not visible after negative staining of cells, whilst the FPC appears as an electron dense structure (Sherwin and Gull, 1989b; Morriswood and Schmidt, 2015; Esson et al., 2012) (Fig.1.25).

The name bi-lobe originates from the shape of this structure, which is composed by two arms or lobes. One arm shows shape similarities to a fish-hook, which, recently, influenced Morriswood to re-name the structure: the Hook complex (Morriswood, 2015). Two of the most characterized proteins, which localize uniquely at the hook-complex, are MORN1 and LRRP1. Additional seven MORN1 neighbours or partners have been identified, as, and localize within the hook-complex (Esson et al., 2012).

MORN1 (Membrane Occupation and Recognition Nexus) has a highly repetitive primary sequence. It assumes a hook-shaped structure that sits on top of the FPC (Fig.1.25). Its anterior end is elongated and runs parallel to the FAZ filament on the MtQ side, whereas the hook part partially co-localizes with BILBO1 at the base of the FP neck (Esson et al., 2012; Gheiratmand et al., 2013). In PCF, MORN1 knock-down only leads to a mild growth defect, without particularly affecting cell morphology (Morriswood et al., 2009). However, in BSF, MORN1 is an essential protein, which, upon depletion, rapidly leads to cell death (Morriswood and Schmidt, 2015). Morphologically, MORN1 RNAi induces the so called “big eye” phenotype, where the FP becomes enlarged, typically associated with a failure in endocytosis. Dextran was tested as a fluid-phase endocytosis marker and resulted in its accumulation in the FP. Concanavalin A, used as a receptor-mediated endocytosis marker, accumulated in a specific spot on the cell surface. Interestingly, this accumulation spot coincided with the localization of MORN1 and the neck channel (Gadelha et al., 2009).

It was thus suggested that MORN1 could be responsible for holding the neck channel open (Morriswood, 2015) and the neck channel could be responsible for a size-exclusion mechanism (Gadelha et al., 2009).
MORN1 has not yet been characterized in other Trypanosomatids.

LRRP1 (Leucine Rich Repeated Protein1), another component of the hook complex, has been identified *via* a proteome analysis (Zhou et al., 2010) in which flagellar associated structures, like the BBs, the FPC and the hook complex were isolated and analysed by mass spectrometry. LRRP1 is essential in PCF and is required for hook-complex duplication and cell division. Moreover, LRRP1 down regulation is inhibiting the duplication of the Golgi apparatus and of the FAZ, resulting in flagellum detachment. LRRP1 RNAi also seems to have an effect on FPC segregation (Zhou et al., 2010). Furthermore, LRRP1 is able to interact with the small GTPase Ran and a Ran-binding protein like (RanBPL) forming a complex involved in the regulation of Ran-GTP hydrolysis. Interestingly, the three proteins interact *in vivo*, but the complex could not be observed by IF with endogenous level of protein in the parasite. However, their interaction was confirmed by Y2H and pull-down assays (Brasseur et al., 2014).

A list of novel hook-complex candidates has been recently obtained *via* a proximity-dependent biotin identification (BioID) approach (Roux et al., 2012). In this technique, the protein of interest, MORN1, was tagged with a mutated version of the bacterial biotin ligase (BirA*). Cells expressing BirA*-MORN1 were incubated with an excess of biotin, a soluble B-vitamin, and the reaction between the enzyme and biotin allowed the indiscriminate biotinylation (the covalently addition of biotin) of neighbours or interacting partners of MORN1. The biotinylated proteins were then affinity-purified with streptavidin-coated beads and analysed by mass spectrometry. This method allowed the identification of at least 7 proteins localizing at the hook-complex (Morriswood et al., 2013). Moreover, this work provided a valid *T. brucei*-adapted version of the BioID technique that can surely be used to identify interaction or neighbour partners of other proteins.

An additional protein has been found to be transiently associated with the hook-complex: a polo-like kinase (PLK). An affinity–purified antibody raised again *Tb*PLK localizes it at the tip of the new FAZ. In early cell stages, the protein is found in a structure close to the kDNA and on the MtQ up to the FPC. During cell cycle progression, the elongation of the new flagellum allows *Tb*PLK to move with the flagellum tip toward the anterior end of the cell (de Graffenried et al., 2008). *Tb*PLK has been shown to be the responsible for Centrin2 phosphorylation on serine 54. This phosphorylation occurs when *Tb*PLK is located at the

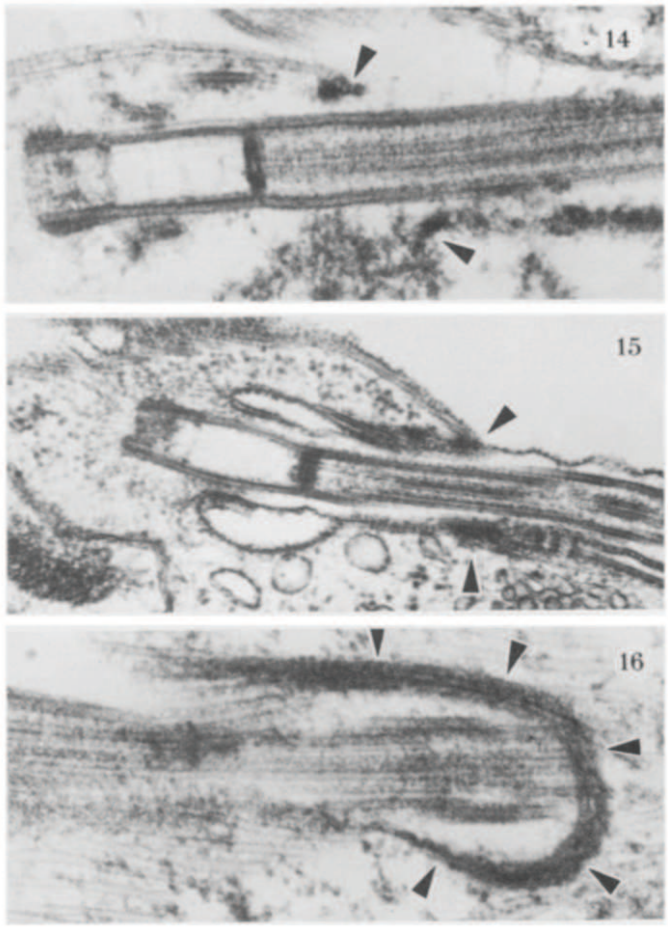

Fig. 1.26 *The Flagellar Pocket Collar seen as electron-dense material (Sherwin and Gull, 1989a).*
The FPC is indicated (arrow-head) as an electron dense structure, located around the FP neck, enclosing the FP membrane at the flagellum exit site.

hook-complex, and it is essential for the correct hook-complex-duplication (de Graffenried et al., 2013). The down-regulation of *Tb*PLK *via* RNAi induced defects in cytokinesis, kinetoplast mispositioning, accumulation of multi-nucleated cells and detachment of the flagellum (de Graffenried et al., 2008). The lack of *Tb*PLK also resulted in a perturbation of the hook-complex structure (elongated, non-divided hook structure or short unorganized hook-complex).

b7) The Flagellar Pocket Collar

Located at the neck of the FP on the cytoplasmic side, there is a cytoskeletal structure called the Flagellar Pocket Collar (FPC), which maintains the FP membrane enclosed around the flagellum. This structure is visible by electron-microscopy as electron-dense material (Fig.1.26) (Henley et al., 1978; Sherwin and Gull, 1989b).

The FPC measures around 500 nm in diameter and makes the link between the FP, the flagellar and the plasma membranes. The MtQ, which wraps around the FP and elongates along the FAZ, traverses the FPC (see Fig.1.24) at the base of the FP neck. The hook-complex, not visible as electron-dense material by EM, sits on the FPC (Fig.1.25).
The FPC can be described as a structure which maintains the flagellar and FP neck membranes in close contact.

The FPC remained an enigmatic structure in its composition and function, until the identification of BILBO1, a scaffold protein necessary for the FPC and for FP biogenesis (Bonhivers et al., 2008b). I will present BILBO1 in more details below.

c) BILBO1: identification and characterisation

The Robinson laboratory, in an attempt to identify minor, but essential, flagellar proteins of *T. brucei,* decided to immunize mice with an extract of flagellar proteins previously separated by SDS-PAGE, and to produce subsequent monoclonal antibodies. One monoclonal antibody (Mab22) recognized the TAC, but also a structure at the neck of the FP (Bonhivers et al., 2008a) (Fig.1.21 Fig.1.27).
Immuno-blot analysis using Mab22 showed multiple bands (Fig.1.27), and mass spectrometry allowed the laboratory to identify several proteins (p99, p67.5 and BILBO1 corresponding to Tb927.11.10540, Tb927.8.6660 (now known as PFC1 - Portman et al., 2009), and Tb927.11.12150, respectively) (Fig.1.27). Their respective ORF were cloned and the proteins were individually expressed in bacteria and

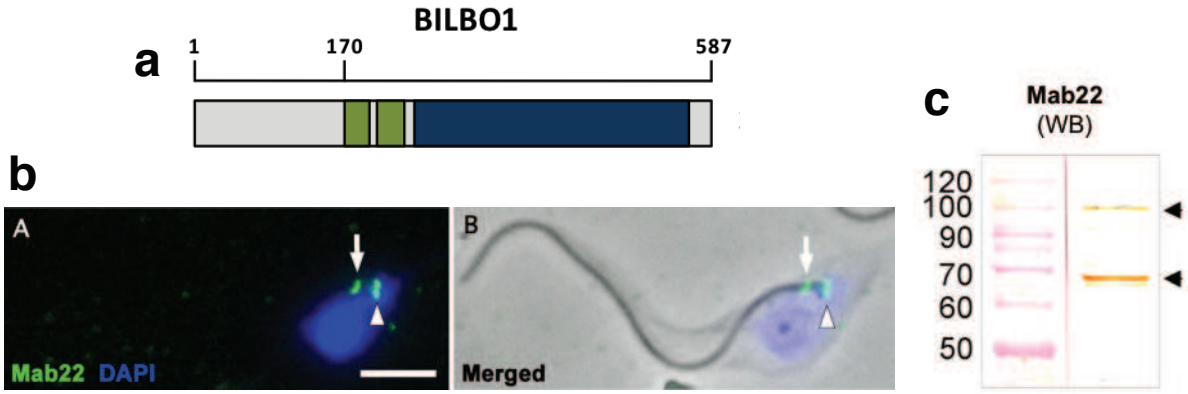

Fig. 1.27 *The discovery of BILBO1 in T. brucei*
(a) Schematic view of BILBO1. EF-Hand domains are highlighted in green, whereas the CC-domain is marked in blue. (b) Immunofluorescence analysis with the monoclonal antibody Mab22 showed two signals: one located at the TAC region (arrowhead), between the kDNA and the BB, and the second signal was located at the FPC (arrow). (c) The Immunoblot analysis of Mab22 revealed multiple bands, which were analysed by Mass Spectrometry and allowed the identification of three proteins.

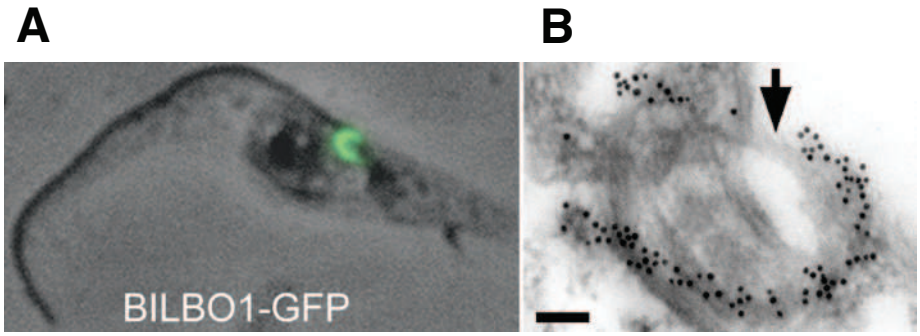

Fig. 1.28 *BILBO1 localization in T. brucei (Bonhivers et al., 2008b)*
(A) Immunofluorescence analysis of BILBO1-GFP localizes it as an open ring/horseshoe at the FPC. (B) Immuno-EM on Wild Type cells with an anti-BILBO1 antibody, localizes it at the FPC, in an open ring shape. An unstained region is marked with an arrow.

purified to produce specific antibodies in mice (Bonhivers et al., 2008a). One of these proteins was named BILBO1 because of the ring-shape of the structure labelled by immunofluorescence and immuno-electron microscopy using the monoclonal antibody (5F2B3) directed against the protein (Bonhivers et al., 2008a). Overexpression of a GFP-tagged version of BILBO1 labelling and immuno-gold EM showed a nice FPC (Fig.1.28) (Bonhivers et al., 2008b).

BILBO1 is a protein of 564 amino acids long (67.3 kDa) with a pI of 5.63. Since its discovery, more data have been obtained concerning its molecular structure and function. These data will be presented in detail in chapter “3. Results” and will be discussed together with the data obtained by the group of Gang Dong (MPFL, Austria) (Vidilaseris et al., 2014a; Vidilaseris et al., 2014b). Briefly, bioinformatics analysis identified a N-terminal domain (NTD - aa1-110) of unknown function, two EF-hand calcium-binding domains (EFHs - aa183-249), a long coiled-coil domain (CC - aa263-566), and a Leucine Zipper domain (LZ - aa534-578) (Fig.1.27 a). This gene is specific to Trypanosomatids and orthologues have been found in other kinetoplastids such as *L. major*, *T. cruzi* and *T. b. gambiense*.

In 2008, the first functional characterization of BILBO1 revealed its essentiality in both PCF and BSF (Bonhivers et al., 2008b). Additionally, a high-throughput RNAi screening of the entire *T. brucei* genome, carried out in 2011, confirmed its essentialness for proper cell survival (Alsford et al., 2011).

Efficient BILBO1 down-regulation by RNAi in PCF leads to previously un-observed morphological and lethal phenotypes: the cells were blocked at the 2K2N stage and their posterior ends were elongated and associated with a new flagellum that was not attached along the cell body (Fig.1.29 a, b) (Bonhivers et al., 2008b). Surprisingly, the new flagellum was not associated with a new FP, and cytoskeletal structures such as the new FPC and the new FAZ were not observed (Fig.1.29 d, e). The new Golgi apparatus did not co-localize with the new flagellum suggesting that the Golgi-Hook-complex-Flagellum connections were also affected. However, the kinetoplast remained close to the basal body suggesting that the TAC structure was not affected (Fig.1.29 b, d, e). Additionally, no distinct MtQ microtubules were observed adjacent to the new BB, but a cytoplasmic MT was occasionally observed. Overall, BILBO1 RNAi blocked the biogenesis of a new FPC and FP, together with other cytoskeletal structures (MtQ, FAZ), but did not affect flagellum biogenesis, as the flagellum appeared normal in structure (presence of the PFR) and function (the new flagellum was motile) (Fig.1.29 b, c, e) (Bonhivers et al., 2008b).

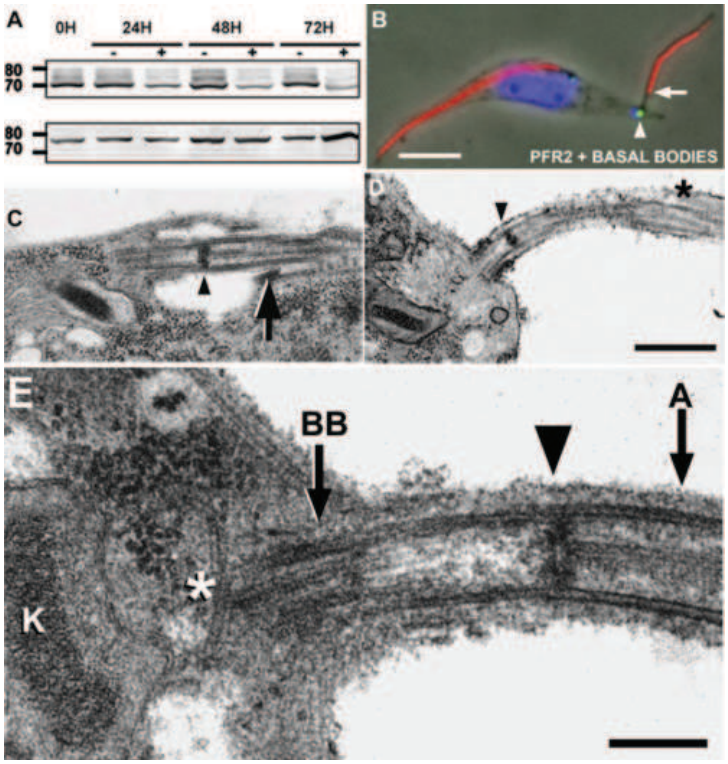

Fig. 1.29 *BILBO1 RNAi in PCF leads to peculiar phenotypes (Bonhivers et al., 2008b)*
(A) The efficiency of the RNAi system was determined by WB. Upon induction (+), BILBO1 synthesis resulted decreased (upper blot); (lower blot) anti-PFR (L8C4) as a loading control. (B) The unusual phenotype observed upon BILBO1 RNAi, consists of cells with an elongated posterior end and a detached flagellum, lacking the FP. (C) A thin section of un-induced cells shows an electron dense material representing the collar (arrow), and the transition zone inside the pocket (arrowhead). (D, E) The new flagellum of cells induced 48h shows the transition zone outside the cell body and the absence of the FPC.

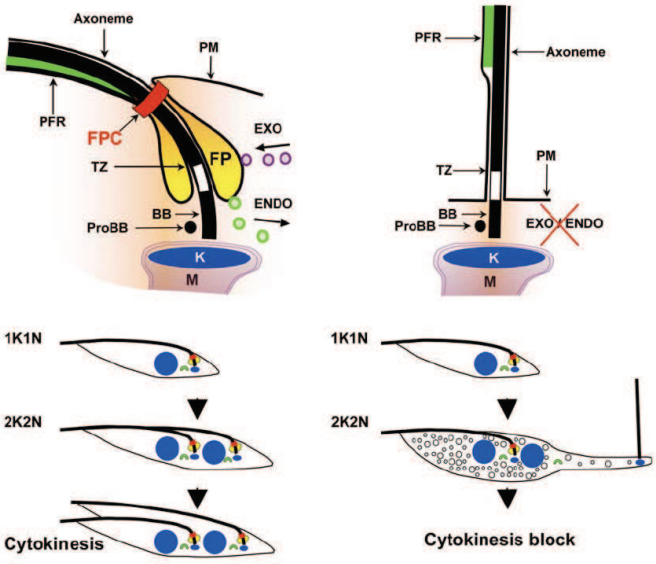

Fig. 1.30 *PCF WT cells vs BILBO1 RNAi (Bonhivers et al., 2008b)*
On the left side, the normal conformation of the FP and FPC and the correct cell cycle of WT cells. On the right side, the cells upon BILBO1 RNAi induction: the new flagellum is detached and located at the very elongated posterior end of the cells. The new FP and FPC are not constructed and there is an accumulation of vesicles, caused by an impaired endo-exocytosis system.

BILBO1 was identified in the first *T. brucei* flagellar proteome (Broadhead et al., 2006) and more recently in a proteomic analysis of the hook-complex complex (Zhou et al., 2010). This confirms the close proximity between the hook complex and the FPC.

The fact that a new FP was not formed upon BILBO1 RNAi induction in PCF, whilst the cell was duplicating (stage 2K2N), created problems in the endo- and exocytosis system resulting in an accumulation of vesicles in the cytoplasm. Finally, the BILBO1 RNAi analysis showed that the FPC has control over cell-cycle progression (Fig.1.30).

In BSF parasites, BILBO1 down-regulation was also lethal, but with different morphological phenotypes: the cells 12h post-induction started rounding up, cell division was blocked and cells died. This rapid lethal phenotype might be related to the higher endocytosis activity of the FP in BSF compared with PCF (Natesan et al., 2007).

Taken together all these results highlight the importance of BILBO1 as a cytoskeletal protein and its requirement for a proper FPC/FP biogenesis. The fact of being an essential component for parasite survival and replication renders BILBO1, and its connected cytoskeletal structures, an interesting to study and a valid drug target.

c1) BILBO1, a multi-partner protein?

Since BILBO1 is a very promising drug target, the Robinson laboratory decided to identify BILBO1 protein partners using two strategies. The first one consisted in a yeast-two-Hybrid (Y2H) screen against a genomic library of *T. brucei*, with BILBO1 as bait (this screen was performed by the Hybrigenics company). The second strategy consisted in purifying FPC structures (associated with other cytoskeletal structures) using the DHC1b RNAi mutant that is able to form a new FP/FPC but not a new axoneme (Kohl et al., 2003). The samples were analysed by LC-MS/MS generating what was call an “FPC-proteome” (unpublished data generated in the Robinson lab).
Before my arrival in the laboratory, the protein candidates from the Y2H screen and the FPC-proteome were crossed and some proteins were considered as FPC-candidates, and among them are: FPC4 and FPC5.

FPC5 is a putative kinesin, which interact with BILBO1 (Florimond et al., 2015b), and that is the purpose of a post-doctoral project.
FPC4 is a protein of interest was determined by the fact that it was a real challenge! Unlike some other putative FPC-BILBO1 partner proteins, FPC4 did not show any known or

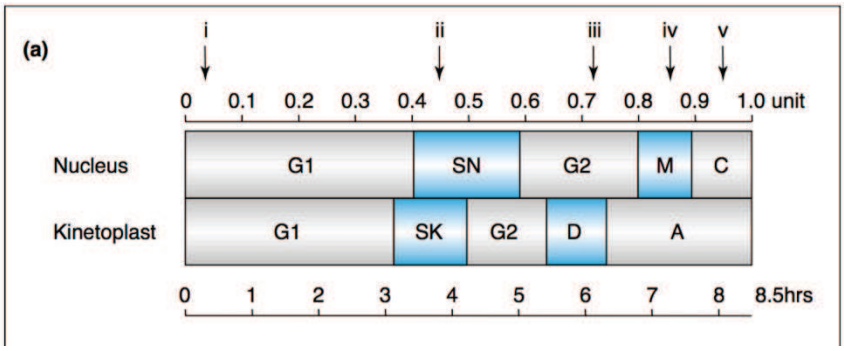

Fig. 1.31 *Major morphological events during PCF T. brucei cell cycle (McKean, 2003) based on (Sherwin and Gull, 1989b) and (Woodward and Gull, 1990).*
Duplication and segregation of kDNA and nuclear genomes do not occur simultaneously, but in a very coordinated way.
(a) The trypanosome cell cycle is separated into nuclear and kinetoplast components. Kinetoplast replication (S) initiates before the nuclear S phase, but it is shorter and thus kinetoplast segregation (D) occurs before the onset of nuclear mitosis (M). (A) represents the phase during which BBs continue to move apart.

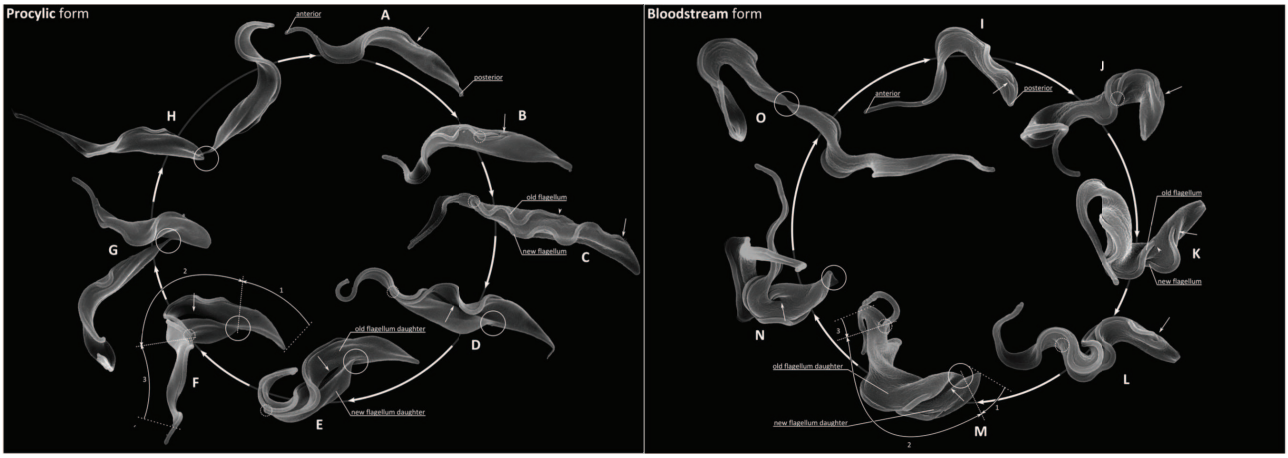

Fig. 1.32 *Comparison between PCF and BSF cell cycle (Wheeler et al., 2013)*
PCF (A-H) and BSF (I-O) stages, respectively, during the cell cycle:
(A, I) G1 cell with a single attached flagellum. The exit point of the flagellum from the FP is marked with an arrow.
(B, J) A new flagellum starts growing and extends from the FP (arrow). In PCF, the new flagellum is attached to the old one *via* the Flagellar Connector (FC), whereas in BSF it is embedded in the groove.
(C, K-L) The FP of the new flagellum (arrow) is positioned posterior to the old FP (arrowhead).
(D, M) Along the long axis a division fold is evident (arrow). In PCF the two flagella are still connected *via* the FC (D), but have grown free in BSF (M).
(E-F, N) A division cleft has opened up between the two daughter cells. In PCF (E-F) the two flagella are still connected *via* the FC.
(G-H, O): Pre-abscission stage. In PCF (G-H) the two daughter cells are attached by the posterior end of the old flagellum and the side of the new flagellum daughter *via* a connection bridge (circle). In BSF (O) the two parasites are connected posterior-to-posterior (circle).

predicted function from bioinformatics analysis. However, FPC4 remained an interesting protein because at the time I started my thesis it was not present in any flagellar proteome. Moreover, FPC4 is a kinetoplastid-specific protein and, as such, a potential drug target.

d) Cell cycle – cell division

d1) Organelles replication

One of the features of this unicellular organism is that it possesses mostly single copy organelles. In the G1 phase, trypanosomes have one nucleus, one kDNA, one flagellum, one single large mitochondrion, and one Golgi apparatus. The duplication and segregation of these organelles is highly coordinated in order to obtain two identical daughter cells. It has been shown that mitochondrial and nuclear genomes do not replicate and segregate simultaneously, but in a coordinate way (Woodward and Gull, 1990). The first event of the cell cycle is the elongation of the pro-BB, followed by the elongation of the new flagellum. The kDNA replication starts before nuclear synthesis, and is noticeably shorter. The segregation of the two kDNAs occurs before nuclear mitosis. Almost simultaneously to the start of the nuclear mitosis, the formation of the pro-BBs occurs. The last step of the cell cycle is cytokinesis (Fig. 1.31 Fig. 1.32 Fig.1.33) (Woodward and Gull, 1990; McKean, 2003).

It should be mentioned that trypanosomes, unlike higher eukaryotes, undergo a closed mitosis, meaning that the nuclear envelop does not disassemble during mitosis (Ogbadoyi et al., 2000; Zhou et al., 2014). Proteins and other molecules required during mitosis are transported in and out of the nucleus through the nuclear pores. *T. brucei* does not possess centrioles used in higher eukaryotes as mitotic poles. In *T. brucei,* the mitotic spindle is created within the nucleus and the two poles of the spindle are located at opposite sides in the nucleus. Two proteins have been associated with these two “spindle poles” and these are *Tb*TLK1 (a kinase) and *Tb*Nup92 (a nuclear pore component) (Li et al., 2007; DeGrasse et al., 2009). *Tb*TLK1 is more likely involved in the spindle formation, since its down regulation impairs spindle assembly. The function of *Tb*Nup92 remains elusive. In higher eukaryotes, the progression of the cell cycle is highly controlled by regulatory proteins such as cyclins, cyclin-dependent kinases (CDKs) and CDK inhibitors (CKI), acting as check points. In trypanosomes, 8 cyclins homologs and 6 CDKs have been identified. The down-regulation of 2 cyclins results in defects in cell cycle progression (Li and Wang, 2003; Hammarton et al., 2003). However, it has been shown that no checkpoint is present to prevent cytokinesis in case of errors in genome duplication or segregation, proven by chemical inhibition of nuclear S-phase or mitosis with rhizoxin (Ploubidou et al., 1999), which led to multinucleated and multiflagellated cells.

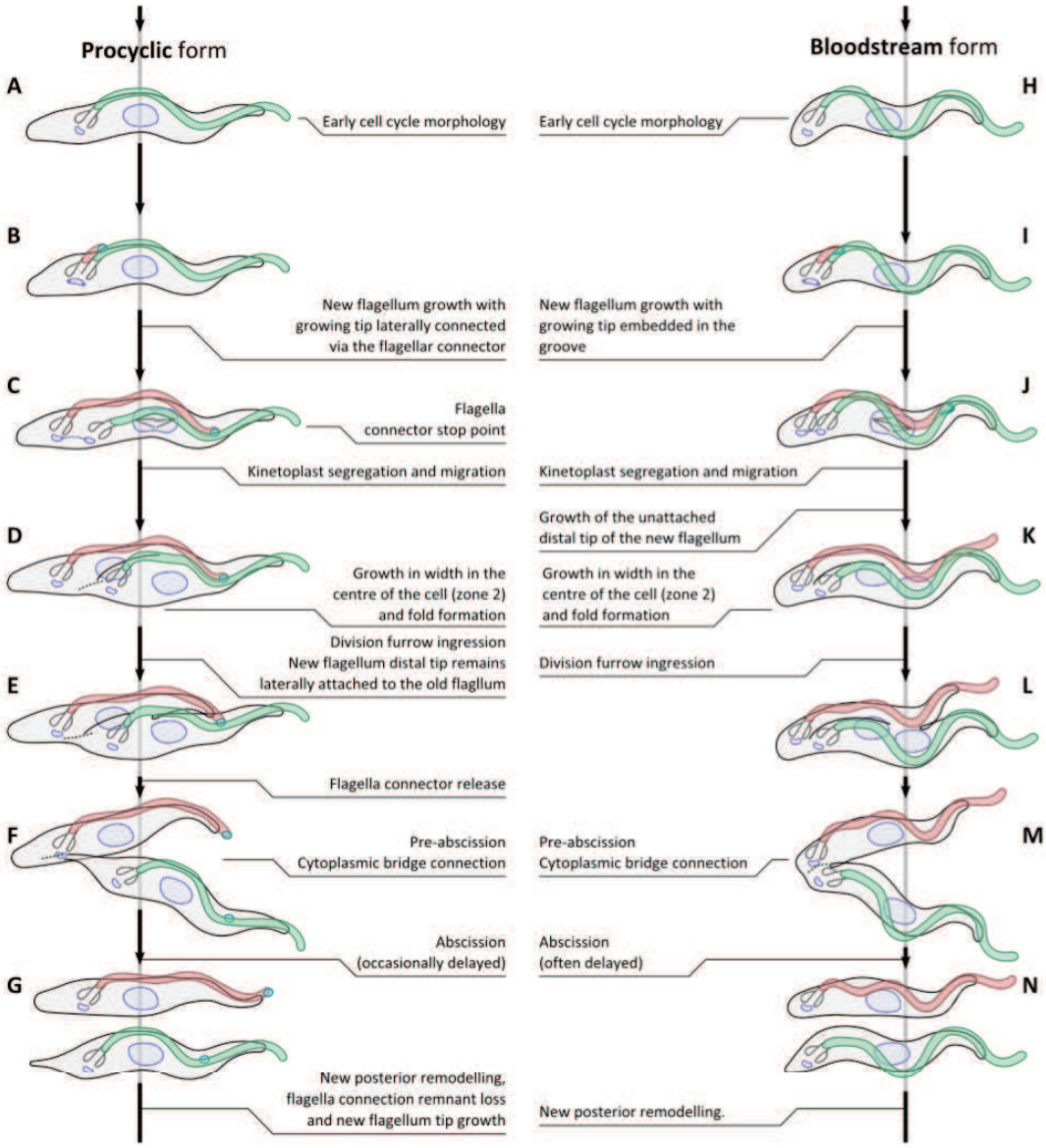

Fig. 1.33 *Comparison between PCF and BSF cell cycle and division (Wheeler et al., 2013)* Major morphologic events are shown alongside cartoon representations of the associated cell morphologies. PCF on the left and BSF on the right.

The last step of the cell cycle is cytokinesis, which occurs with the insertion of a cleavage furrow in between the two flagella, following the FAZ, from the anterior to the posterior end of the cell (Wheeler et al., 2013; Hammarton et al., 2007b) (Fig.1.32 Fig.1.33). Recently it has been published that in case of down-regulation or over-expression of CIF2 (cytokinesis initiation factor2, localized at the new FAZ tip together with CIF1), an alternative cytokinesis pathway can take place (Zhou et al., 2016): from the posterior to the anterior end of the cells. This might be a back-up mechanism in case of defective cytokinesis. Given that the FAZ does not extend up to the posterior end, it might be difficult for the parasites to target the FAZ tip-localized cytokinesis machinery to the posterior end of the cell and from there start cytokinesis (Zhou et al., 2016).

c2) Genome organization

The 26 Mb genome of *T. brucei* is composed of 11 chromosome pairs (diploid organism), containing 9068 protein-coding genes and approximately 900 pseudogenes (Berriman et al., 2005).

One of the peculiar features of Kinetoplastids is the organization of the mitochondrial genome, called the kinetoplast or kDNA (Shapiro and Englund, 1995). The kDNA consists of two concatenated different types of DNA molecules: several thousands of copies of mini circles (0.5-2.5 kb) and approximately 50 copies of maxi circles (20-40kb) (Ersfeld et al., 1999; Van der Ploeg et al., 1984). Mini circles code for guide RNAs (gRNAs) involved in RNA editing (Stuart and Panigrahi, 2002; Stuart et al., 2005). This editing consists of the post-transcriptional addition or deletion of Uridine residues in the primary RNA transcripts leading to the production of mature edited translatable mRNAs of cryptogenes (Simpson et al., 2003). Maxi circles mostly code for ribosomal subunits rRNA and proteins of the respiratory chain complex (Ersfeld, 2011).

T. brucei adopts a polycistronic organization for the genes. Polycistronic units contain between 10 and 100 genes, which are transcribed on the same mRNA (by the RNA Polymerase II). They are then processed into monocistronic mature mRNAs with a 5' Spliced Leader (39 nucleotides) and a 3' PolyA tail. This process is called *trans*-splicing (Agabian, 1990; Preußer et al., 2012).

Polycistronic organization implies that all the genes present on the unit are transcribed at the same rate. Interestingly, polycistronic units contain genes with unrelated functions and therefore gene expression is mostly controlled by post-transcriptional events (De Gaudenzi et al., 2011).

The RNA Polymerase I is responsible for transcription of VSG and procyclins, and also for ribosomal subunits RNA transcription (Zomerdijk et al., 1991). The RNA Polymerase III transcribes ribosomal subunits and tRNAs (Fantoni et al., 1994; Das et al., 2008). In general, trypanosome genes do not contain introns, however two exceptions have been described. Tyrosine tRNA gene (Schneider et al., 1993) and PAP gene (Poly-A Polymerase) (Mair et al., 2000) each contain one intron. *Cis*-splicing is therefore very exceptional, whereas *trans*-splicing events are commonplace. During *Cis*-splicing, a single molecule is processed, whereas in *trans*-splicing, two different transcripts (spliced leader and gene transcript) are ligated to create a mature mRNA (Liang et al., 2003).

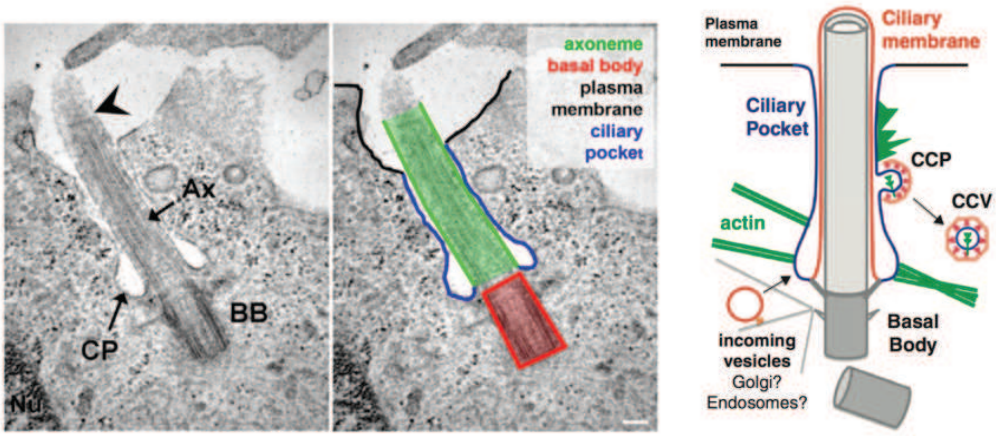

Fig. 1.34 *Cilia architecture shows similarities to flagella*
The ciliary pocket (CP), shown in the TEM pictures on the left (Molla-Herman et al., 2010), shares some common features with the FP in Trypanosomatids. No FPC has been identified in cilia, but interestingly the pocket-shape is maintained by actin-filaments (scheme on the right—(Benmerah, 2013)

III. The flagellar pocket and associated cytoskeletal structures: Analogies and differences with other organisms.

Flagella and cilia share some morphological and structural characteristics. Both are composed of a MT-based axoneme, which originates from a BB.

The axoneme consists of “9 + 2” (nine doublets of microtubules and a central pair of MTs) or “9 + 0” arrangement of MTs. In most cases 9 + 0 axonemes are described as non-motile sensory cilia, whereas 9 + 2 refers to motile cilia or flagella. Sensory cilia control key signalling pathways through sensing mechanical stresses or molecules present within the extracellular milieu (for a review see (Ghossoub et al., 2011).

At the base of most primary cilia there is a specific membrane domain, continuum to the plasma membrane, which is involved in vesicular tracking and more likely endocytosis. This membrane domain, which is smaller but resembles the flagellar pocket, is called the ciliary pocket (CiPo) (Fig.1.34) (Benmerah, 2013). Distal to the BB, the CiPo membrane gets closer to the cilium, at the docking site for actin-cables (Fig.1.34 right). Perturbations of actin polymerization modify the CiPo shape, causing the loss of interaction between the ciliary and pocket membranes, resulting in a sort of open pocket (Rattner et al., 2010).

At the base of the CiPo there are transition fibres which connect the transition zone to the plasma/CiPo membrane and function as a diffusion barrier (for a review see Benmerah, 2013). This structure might resemble the collarette of *T. brucei*. Distal to the BB, however, cilia do not possess a structure similar to the FPC (Ghossoub et al., 2011). The highly active endo- and exocytosis traffic in *T. brucei* might require the FPC as a sort of diffusion barrier.

In other eukaryotes, but also prokaryotes, similar to the FPC, other ring-structures have been observed. For example, in sperm cells, a septin ring is found at the annulus between the middle and the principal part of the sperm tail, where it plays a role of a diffusion barrier. Moreover, in spermatids a structure similar to the FP has been observed during the elongation of the sperm cell. This structure, called the flagellar canal, is only transient and is reabsorbed in the later stages of the spermiogenesis (Fawcett et al., 1971) but is role remains unclear.
In yeast, the septin ring plays a role in cell division and as a diffusion barrier (Hu and Nelson, 2011). Disruption of the septin-ring leads to a failure in cytokinesis.

Although a morphological similar structure is visible in *T. brucei*, no septin genes have been identified in the *T. brucei* genome (Berriman et al., 2005). Absence of similar proteins in trypanosomes leaves open many questions related to the composition of the FPC.

MORN1 genes have been found in other organisms, but currently, the only *Toxoplasma gondii* MORN1 has been characterized. In this apicomplexan parasite, the two daughter cells are preformed within the mother cell, and MORN1 is located within a ring-shaped complex at the apical part of the inner membrane complex (IMC). The IMC is a membranous layer under the plasma membrane, which is coupled to the cytoskeletal network (Gubbels et al., 2006). Moreover, MORN1 localizes in a discrete area within the nucleus (Gubbels et al., 2006). MORN1 is an essential protein involved in cellular replication during early cell cycle stages and in nuclear division (Lorestani et al., 2010). It has been proposed that MORN1 can be a sort of linker between the IMC and the parasites' cytoskeleton (Gubbels et al., 2006).

IV. Aims

Human African trypanosomiasis is a neglected tropical disease, which affects people in the Sub-Saharan Africa year after year. The aetiological agent is a unicellular parasite called *Trypanosoma brucei*, which efficiently escapes the host immune system by changing its surface coat to escape the mammalian host's immune system. In 2008, the Robinson laboratory discovered and characterized the first protein in the flagellar pocket collar region: BILBO1 (Bonhivers et al., 2008b). BILBO1 is a kinetoplastid-specific protein and is essential for parasite survival and for biogenesis of the new FP and FPC. Its essential nature renders BILBO1 a valid drug target, since no vaccines are presently available. A Yeast-two-hybrid screen against the *T. brucei* genomic DNA with BILBO1 as bait has been performed to identify potential BILBO1 partners. Among the candidates, FPC4 (Tb927.8.6370) has been selected for further characterization. Understanding mechanistically how the FPC and the FP are build up can give essential information to move forward in drug discovery.

No functional domains have been identified in FPC4, but the C-terminal part might be involved in BILBO1 binding.

During my thesis, I mostly focused my attention on FPC4 characterization and on its interaction with BILBO1. Knowing that BILBO1 is a potential drug target, the interaction with a partner can also be the target of drug discovery, in the sense of blocking or dissociating their interaction.

BILBO1, on the other hand, has only been partially characterized. Part of my thesis also helped to understand more particular features of this essential protein.

Currently, no evidence has been shown of a bi-lobe / Hook complex in *L. major*, therefore we started a collaboration with the Bastien Lab in Montpellier, within the ParaFrap network, with the aim of localizing some Hook complex and FPC orthologues in this parasite.

I started the characterization of proteins of the FPC/hook-complex region of *T. brucei*, to see whether the complexes are conserved in *Leishmania major* and to see if they localize at the same place as in *L. mexicana*. I was interested in orthologues of *Tb*BILBO1 (*Lm*BILBO1 = *LmjF*.09.0100), *Tb*MORN1 (*Lm*MORN1 = *LmjF*.30.3310) and *Tb*FPC4 (*Lm*FPC4 = *LmjF.*24.1860).

2. MATERIAL AND METHODS

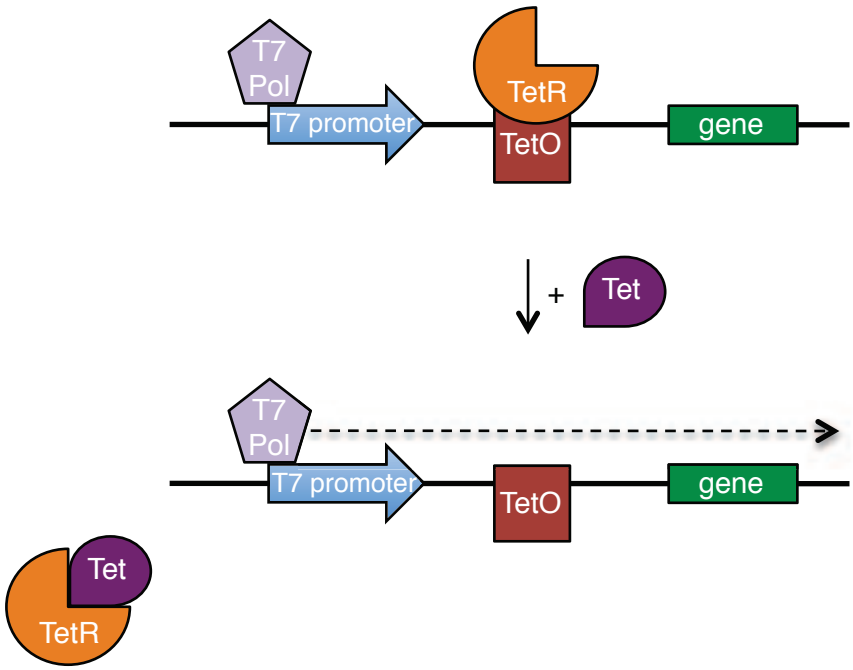

Fig. 2.1 *Principle of the inducible cell lines in T. brucei.*
In a cell line constitutively co-expressing the Tetracycline Repressor (TetR) and the T7 RNA Polymerase (T7 Pol), the addition of Tetracycline (Tet) leads to the removal of the TetR from the Tet operator (TetO) and allows the gene transcription by the T7 Pol.

2. Material and Methods

I. Material

a) Organisms, cell lines and cultures

- During my PhD I used two monomorphic strains of *Trypanosoma brucei brucei* (genotype: Lister 427). Lister 427 probably originates from Shinyanga III isolated from cattle in 1956 in Tanganyika as G. Cross (Rockefeller Center) tried to follow up. The procyclic form (PCF) *T. brucei* 29-13 and the bloodstream form (BSF) MiTat1.2 (Molteno Institute Trypanozoon antigenic type 1.2) 90-13 cell-lines have been genetically modified to constitutively co-express the bacteriophage T7 RNA polymerase (T7 Pol) and the Tetracycline repressor (TetR). This system allows the inducible ectopic expression of genes under the control of T7 promoter via the addition of tetracycline (Fig.2.1).

- For the collaboration project with the Bastien Laboratory in Montpellier, I used promastigote *Leishmania major*, strain Friedlin 3171.

- Two haploid strains of the Yeast *Saccharomyces cerevisiae* have been used for the yeast-two-hybrid experiment: Y187 (MAT α) and Y2HGold (MATa). Both strains are auxotrophic for Adenine, Histidine, Leucine, and Tryptophan and are sexually compatible to create diploid strains. They do not possess the GAL4 transcription factor. The strain Y2H Gold, derived from PJ69-4A possesses four integrated reporter genes under the control of three distinct GAL4-responsible promoters:

- ADE2 and HIS3: involved in the biosynthesis of the essential amino acids Adenine and Histidine respectively. It is only when bait and prey proteins interact that the yeasts can grow on minimal medium lacking Histidine and/or Adenine.
- AUR1-C: resistance gene for Aureobasidin A, an antifungal antibiotic.
- MEL1: gene encoding for the α-galactosidase. GAL4 activation leads to the hydrolysis of the chromogenic substrate X-α-Gal, which causes the yeast colonies to develop a blue colour allowing a white/blue screening of the colonies.

In order to perform the Y2H experiments, the Y187 strain has been transfected with the pGADT7 plasmid, which contains an auxotrophy Leucine marker for yeast selection, whereas the Y2HGold strain has been transfected with pGBKT7 that carries an auxotrophy Tryptophan selection marker.

Tab.2.1 *Antibiotics concentrations for T. brucei and L. major cultures.*

		***T. brucei* PCF**	***T. brucei* BSF**	***L. major***
		µg/mL	µg/mL	µg/mL
antibiotics	Blasticidin (B)	10	10	20
	Hygromycin (H)	25	5	30
	Neomycin (N)	10	2,5	10
	Phleomycin (F)	5	2,5	5
	Puromycin (P)	1	0,1	30

- The *E. coli* bacterial strains XL1-blue and Stellar (HST08), lacking the machinery to degrade foreign DNA, were used for molecular biology. XL1-blue cells can methylate DNA, whereas stellar lack this enzyme. The strain BL21 (*DE3*), which contains a λ-phage carrying the T7 Polymerase, was used for inducible protein expression with Isopropyl β-D-1-thiogalactopyranoside (IPTG).

- U-2 OS adherent cells (human bone Osteosarcoma-epithelial cells) ATCC Number HTB-96 were used as heterologous system, in which trypanosome proteins were expressed in order to investigate/discover their intrinsic properties.

- P3U1 myeloma cells derive from P3X63Ag8—Kearney line. It is a non-secretor cell line, HGPRT negative (Hypoxanthine Guanine PhosphoRibosyltTransferase) and HAT sensitive (Hypoxanthine-Aminopterin-Thymidine). It is useful for fusion with antibody-producing B-cells to generate hybridomas or for hybridisation studies with other myelomas or lymphomas (Köhler and Milstein, 1975) for the production of monoclonal antibodies. These non-adherent cells are grown in RPMI 1640 medium supplemented with 10% Foetal Calf Serum (FCS).

- Female BALB/c mice (Charles Rivers) were used for the production of a monoclonal antibody directed against FPC4 (Les et al., 2016).

b) Cultivation media

- PCF *T. brucei cells* were cultivated at 27 °C in SDM-79 medium (PAA company G3113,3005) (Brun and Schönenberger, 1979), containing 3.5 g/L Hemin (an iron-containing porphyrin) and supplemented with 10% FCS, and routinely kept in culture between $1x10^6$-$1x10^7$ cells/mL. The *T. brucei* 29-13 cell-line was cultivated in SDM-79 containing the antibiotics Hygromycin and Neomycin (Tab.2.1 for concentration).

- BSF *T. brucei* 427 90-13 parasites were cultivated at 37 °C + 5% CO_2 in IMDM (Gibco 10184932) medium (Iscove's modified Dulbecco's Medium) with 3.024 g/L Sodium Bicarbonate, 0.136g/L Hypoxanthine, 0.11 g/L Sodium Pyruvate, 0.039 g/L Thymidine, 0.028 g/L Bathocuprone, 0.25 mM β-Mercaptoethanol, 1.875 mM L-Cysteine, 62.5 µg/mL Kanamycine and 10% FCS, and Hygromycin and Neomycin (Tab.2.1 for concentrations) and kept in culture at a concentration between $1x10^5$-$1x10^6$ cells/mL.

- Promastigote *L. major* cells were cultivated at 26 °C in RPMI—Glutamax (Gibco 11554526) with 20% FCS, supplemented with antibiotics when required (Tab.2.1 for concentrations), and kept in culture between $3x10^5$ and $2x10^7$ cells/mL.

The antibiotics concentrations are summarized in Tab.2.1.

Parasites were counted using Quick-Read™ Precision Cell (Globe Scientific). After a 1/10 dilution into 3.7% Formaldehyde in PBS (for PCF) or a 1/2 dilution in vPBS (for BSF: 8 g/L NaCl, 0.22 g/L KCl, 2.27 g/L Na_2HPO_4, 0.41 g/L KH_2PO_4, 15.7 g/L Sucrose and 1.8 g/L Glucose), 10 µl of the mixture are deposited in the Quick-read™ chamber and the number of parasites in 9 circles is counted, and the cell concentration (cells/mL) is determined as follows: number of counted parasites x dilution factor x 5 x 10^3.

- Mammalian cells (U-2 OS) were cultivated in D-MEM Glutamax (Gibco) supplemented with 10% FCS and 100 units/mL Penicillin and 100 µg/mL Streptomycin (Fisher life technologies ref E3470H) at 37 °C and 5% CO_2.

- In order to transform a plasmid into a yeast strain, cells were collected from a solid culture with an inoculating loop and resuspended by vortexing in 1 mL of sterile H_2O. Cells were then spun for 30 sec at 16,000 g and the supernatant was removed. To the pellet were added in this order and without pipetting: 240 µL polyethylene glycol—(PEG) 350 (50% w/v), 36 µL 1 M LiAc, 50 µL boiled Salmon sperm carrier DNA (2 mg/mL) and 1–5 µg plasmid DNA in 34 µL. The tube was vortexed and incubated then for 2–3 h at 42 °C in a water bath. After incubation, the cells were centrifuged for 30 sec at 16,000 g, the supernatant was removed and the cells resuspended in 200 µL sterile H_2O. Two different volumes (20 µL and 180 µL) were plated on solid SC medium (Synthetic Complete composed of 1.7 g/L Yeast Nitrogen Base, 5 g/L Ammonium Sulfate, 20 g/L Dextrose and 0.59 g/L Complete Supplement Mixture, with addition of 40 g/L Adenine, 20 mg/L Histidine and 20 mg/L Uracil). The SC medium was without Leucine (SC-L) or without Tryptophan (SC-W) for pGADT7 or pGBKT7 plasmids, respectively. The plates were then incubated for 3–4 days at 30 °C.

  Y187 and Y2HGold haploid strains were cultivated at 30 °C on solid YPD medium (10 g/L Yeast extract, 10 g/L bactoPeptone and 20 g/L Dextrose) with the addition of 40 mg/L of Adenine. To obtain diploid strains, previously transformed MATa (Y2HGold) and MATα (Y187) were cultivated together in liquid YPDA medium (40 g/L Yeast extract, 40 g/L bactoPeptone, 80 g/L Dextrose and 80 mg/L Adenine) at 30 °C,

Tab.2.2: *Cloning vectors used in different organisms.*
Resistance antibiotics used for bacteria: kana = kanamycin; amp = ampicillin; and for eukaryotic cells: neo = neomycin; bla = blasticidin; puro = puromycin; phleo = phleomycin.

	plasmid name	resistance	bp	details	source reference
bacteria	pET28a	kana	5368	N-ter 6-His tag cloning vector for protein expression in bacteria	Novagen
yeast	pGADT7	amp	7988	GAL4 activation domain (AD) as N-terminal tag in yeast for Y2H tests. It contains a NLS	Clontech - Chien et al.1991
	pGBKT7	kana	7304	GAL4 DNA binding domain (BD) as N-terminal tag in yeast for Y2H tests	Clontech - Louret et al. 1997
U-2 OS	pcDNA3	amp, neo	5446	cloning vector for protein expression in mammalian cells	Invitrogen
	pcDNA3.1 CT-TOPO GFP	amp, neo	6157	"five min cloning" vector for expression of C-terminal GFP tagged proteins in mammalian cells. It contains a covalently bound topo-isomerase	Termofischer - Invitrogen
T. brucei	pHD1336	amp, bla	5071	cloning vector for RNAi in Trypanosomes	C. Clayton, Heidelberg
	pJM-1	amp, puro	5735	pLew-based cloning vector for N-ter 3x myc tag protein over-expression in *T. brucei*	A.Schneider, Bern
	pLew100-GFP-X	amp, phleo	7250	pLew-based cloning vector for N-ter GFP tag protein over-expression in *T. brucei*	modified from Alibu et al. 2005
	pLew100-X-myc	amp, phleo	5735	pLew-based cloning vector for C-ter 3x myc tag protein over-expression in *T. brucei*	modified from Alibu et al. 2005
	pMOTag23M	amp, puro	4150	pMOTag2-based vector for C-ter 3x myc endogenous tag in *T. brucei*	Oberholzer et al. 2006
	p2T7-177	amp, phleo		cloning vector with double promoter for dsDNA production and RNAi in *T. brucei*	Wickstead et al. 2002

250 rpm shaking and selected on solid SC medium. This medium does not contain Leucine and Tryptophan and is therefore called SC-L-W. It allows the selection of diploid yeasts carrying both plasmids pGADT7 and pGBKT7 (Tab.2.2).

c) Plasmids

The cloning vectors used during my thesis and their characteristics have been summarized in Tab.2.2.

The pET28a(+) plasmid (Novagen) has been used for the expression of recombinant protein in bacteria, with the possibility to add an N—and/or a C- terminal 6-Histine tags. The protein expression is inducible with the addition of IPTG.

The pGADT7 and pGABKT7 plasmids, used for the Y2H experiments, contain as N-terminal tag the GAL4 activation domain and the GAL4 DNA binding domain, respectively. The plasmid pGADT7 also contains the Leu2 gene, for Leucine synthesis, and a NLS (nuclear localizing signal). The pGBKT7 plasmid carries the Trp1 gene for Tryptophan synthesis.

To express trypanosome proteins in a heterologous system (U-2 OS cells) two plasmids have been used: pcDNA3 (expression of the protein of interested without a tag), and pcDNA3.1 (expression of the protein of interested with a C-terminal GFP tag). Both plasmids have the same background: they contain an ampicillin resistance gene (for bacterial selection) and an aminoglycoside-3'-phosphotransferase (APH 3') resistance gene (Neomycin) for stable transfection in human cells. The gene of interest is placed under the control of a CMV (CytoMegaloVirus) promoter. For our purpose, we only made transient transfections.

In trypanosomes different plasmids have been used, but interestingly three of them are based on the pLEW plasmid (Wirtz et al., 1994). In fact, for over-expression and RNAi, the same pLEW-backbone can be used. This plasmid, upstream and downstream of the NotI restriction site, possesses homolog sequences to the rRNA spacer, which allow the homolog recombination of the plasmid into this region. The different pLEW-based plasmids carry different resistance genes for *T. brucei*, for example puromycine-N-acetyl transferase (PAC) for Puromycin, or bleomycin resistance gene (ble) for Phleomycin, and can therefore be transfected in the same cell line and be induced at the same time.

Tab.2.3: *Overview of the produced cell lines*

	construct name	backbone, resistance	tag	aa	bp	predicted MM	pI	comments
over-expression	N-ter myc tag 1-217 FPC4	pJM-2, amp + puro	N-ter 3x myc	1-217	6341 bp	34 kDa	10.4	N-terminal domain, targeted to the FPC
	N-ter myc tag 1-252 FPC4	pJM-2, amp + puro	N-ter 3x myc	1-252	6446 bp	38 kDa	9.9	N-terminal domain including CC, targeted to the FPC
	N-ter myc tag 1-356 FPC4	pJM-2, amp + puro	N-ter 3x myc	1-356	6761 bp	44 kDa	10.4	ΔB1BD, targeted to the FPC
	N-ter myc tag 1-444 FPC4	pJM-2, amp + puro	N-ter 3x myc	1-444	7025 bp	54 kDa	10.1	FL, targeted to the FPC
	N-ter myc tag 218-356 FPC4	pJM-2, amp + puro	N-ter 3x myc	218-444	6110 bp	25 kDa	5.7	central part: soluble
	N-ter myc tag 357-444 FPC4	pJM-2, amp + puro	N-ter 3x myc	357-444	5960 bp	15 kDa	4.7	B1BD: soluble
	C-ter myc tag 1-356 FPC4	pLew X-myc, amp + phleo	C-ter 3x myc	1-356	6754 bp	44 kDa	10.1	ΔB1BD, tag cleaved
	C-ter myc tag 1-444 FPC4	pLew X-myc, amp + phleo	C-ter 3x myc	1-444	7018 bp	54 kDa	9.9	FL, tag cleaved
	C-ter myc tag 357-444 FPC4	pLew X-myc, amp + phleo	C-ter 3x myc	357-444	5953 bp	15 kDa	4.9	B1BD, tag cleaved
	N-ter GFP tag 1-444 FPC4	pLew GFP-X, amp + phleo	N-ter GFP	1-444	7631 bp	76 kDa	9.3	FL, targeted to the FPC
RNAi	pHD1336-SLBILBO4	pHD1336, amp + blast	-	target: 164-754 bp	6418 bp	-	-	RNAi in BSF
	pSLBILBO4	pLew100, amp + phleo	-	target: 164-754 bp	6789 bp	-	-	RNAi in PCF
expression in U2Os	pcDNA-FPC4 aa 1-79	pcDNA3.1 CT-GFP topo, amp	C-ter GFP	1-79	6405 bp	-	8.87	soluble in U-2 OS
	pcDNA-FPC4 aa 1-105	pcDNA3.1 CT-GFP topo, amp	C-ter GFP	1-105	6456 bp	-	9.04	soluble in U-2 OS
	pcDNA-FPC4 aa 1-151	pcDNA3.1 CT-GFP topo, amp	C-ter GFP	1-151	6621 bp	-	9.13	not clear
	pcDNA-FPC4 aa 1-217	pcDNA3.1 CT-GFP topo, amp	C-ter GFP	1-217	6819 bp	-	9.38	MT localization
	pcDNA-FPC4 aa shuffled 1-217	pcDNA3.1 CT-GFP topo, amp	C-ter GFP	1-217	6819 bp	-	9.38	soluble in U-2 OS
	pcDNA-FPC4 aa 1-356	pcDNA3.1 CT-GFP topo, amp	C-ter GFP	1-356	7236 bp	-	9.41	MT localization
	pcDNA-FPC4 aa 80-105	pcDNA3.1 CT-GFP topo, amp	C-ter GFP	80-105	6222 bp	-	5.94	soluble in U-2 OS
	pcDNA-FPC4 aa 80-151	pcDNA3.1 CT-GFP topo, amp	C-ter GFP	80-151	6386 bp	-	6.29	soluble in U-2 OS
	pcDNA-FPC4 aa 1-252	pcDNA3.1 CT-GFP topo, amp	C-ter GFP	1-252	6924 bp	-	9.17	MT localization
	pcDNA-FPC4 aa 1-444	pcDNA3.1 CT-GFP topo, amp	C-ter GFP	1-444	7487 bp	-	9.31	MT localization
	pcDNA-FPC4 aa 1-444 deltaCC	pcDNA3.1 CT-GFP topo, amp	C-ter GFP	1-444 w/o 218-252	7395 bp	-	9.47	MT localization
	pcDNA-FPC4 aa 218-444	pcDNA3.1 CT-GFP topo, amp	C-ter GFP	218-444	6852 bp	-	6.35	soluble in U-2 OS
	pcDNA-FPC4 aa 218-252	pcDNA3.1 CT-GFP topo, amp	C-ter GFP	218-252	6277 bp	-	5.31	soluble in U-2 OS
	pcDNA-FPC4 aa 218-356	pcDNA3.1 CT-GFP topo, amp	C-ter GFP	218-356	6588 bp	-	6.34	soluble in U-2 OS
	pcDNA-FPC4 aa 253-444	pcDNA3.1 CT-GFP topo, amp	C-ter GFP	253-444	6748 bp	-	6.95	soluble in U-2 OS
	pcDNA-FPC4 aa 253-356	pcDNA3.1 CT-GFP topo, amp	C-ter GFP	253-356	6483 bp	-	6.21	soluble in U-2 OS
	pcDNA-FPC4 aa 357-444	pcDNA3.1 CT-GFP topo, amp	C-ter GFP	357-444	6435 bp	-	5.72	soluble in U-2 OS
Y2H screen	pGAD-1-356 FPC4	pGADT7 AD, amp	N-ter AD	1-356	9025 bp	-	-	-
	pGAD-1-444 FPC4	pGADT7 AD, amp	N-ter AD	1-444	9292 bp	-	-	-
	pGAD-206-444 FPC4	pGADT7 AD, amp	N-ter AD	206-444	8740 bp	-	-	-
	pGAD-266-444 FPC4	pGADT7 AD, amp	N-ter AD	266-444	8575 bp	-	-	-
	pGAD-357-444 FPC4	pGADT7 AD, amp	N-ter AD	357-444	8227 bp	-	-	-
	pGBD-BILBO1-FL	pGBKT7 BD, kana	N-ter BD	1-587	9069 bp	-	-	-
	pGBD-BILBO1-T1	pGBKT7 BD, kana	N-ter BD	1-170	7810 bp	-	-	-
	pGBD-BILBO1-T3	pGBKT7 BD, kana	N-ter BD	171-587	8557 bp	-	-	-
	pGBD-MORN1-FL	pGBKT7 BD, kana	N-ter BD	1-358	8362 bp	-	-	-

The plasmid pHD1336 has also been used for RNAi in *T. brucei* and, as the pLEW plasmids, it integrates into the spacer rRNA region. It contains the blastidicine-S-deaminase resistance gene (bsd) for selection in *T. brucei* with Blasticidine.

The plasmid pMOTag22M has been modified in the laboratory to generate pMOTag23M and serves as a template for PCR with long primers. The recombination in *T. brucei* occurs *in situ* between the 3'-end of the ORF of the gene of interest and its 3' UTR. The long primers allow the addition in the PCR product of around 80 bp overhangs complementary to the recombination zone. From the plasmid a triple myc tag and a puromycin (PAC) resistance gene are amplified. The PCR product, after purification, can be directly transfected in *T. brucei.*

The p2T7-177 plasmid used for RNAi contains double opposite T7 promoters for the production of a dsRNA. The plasmid integrates in the mini chromosomal 177 bp repeat locus (Wickstead et al., 2002; Sloof et al., 1983; LaCount et al., 2000).

Bacteria, yeasts, mammalian cells, *Trypanosomes* or *Leishmania* were transformed or transfected with several plasmids. These strains are listed in Tab.2.3.

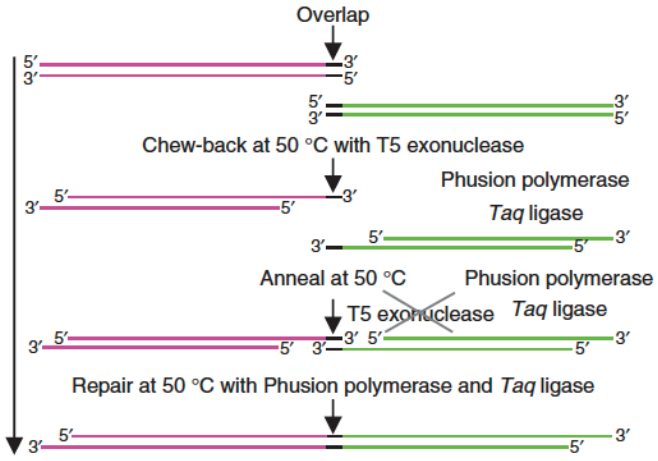

Fig. 2.2 *Schematic mechanism of in-Fusion® (Clontech) according to (Gibson et al., 2009).*
A 5'-exonuclease can remove nucleotides from the 5' of the dsDNA, the 15 bp homolog region between the PCR product and the digested plasmid will anneal and a Taq polymerase will fill the gaps. The plasmid will be closed by a ligase.

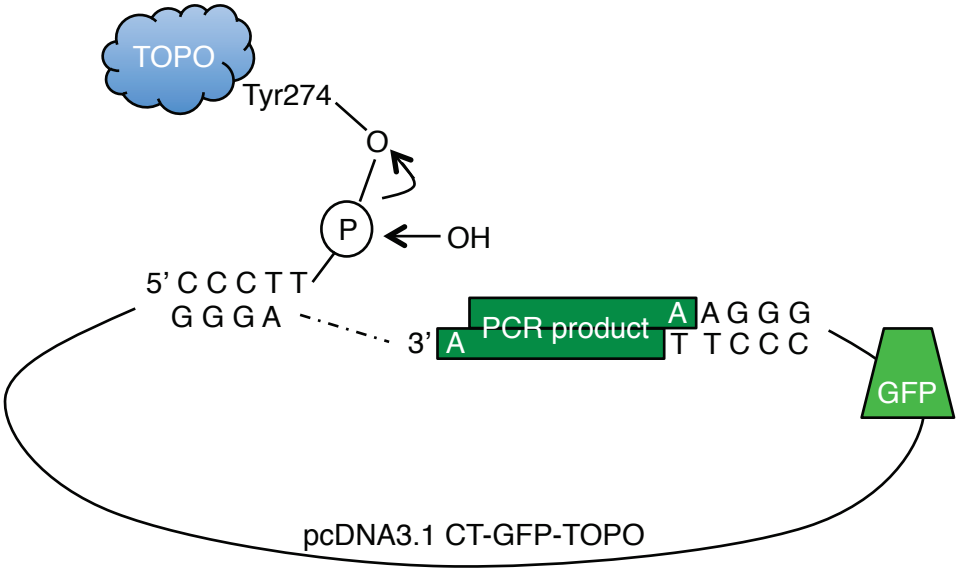

Fig. 2.3 *Schematic mechanism of TOPO®-Cloning (Invitrogen).*
A PCR product is ligated into a vector, thanks to a Topoisomerase linked to it.

II. Methods

a) Molecular biology

a1) Molecular cloning and sequencing

Three main techniques were used to clone the sequences of interest.
In vitro recombination using the In-Fusion® HD Cloning technique (Clontech): The DNA sequence of interest was amplified by PCR using primers with 15 bp overhangs complementary to the vector ends (that has been linearized with restriction enzymes) and a high-fidelity polymerase. In this technique the digested plasmid is mixed in a 1:3 ratio with the PCR-amplified insert and 1x of In-Fusion® Enzyme Premix, and incubated for 15 min at 50 °C. How exactly the technique works and what are the components of the Enzyme Premix are not explained, but more likely it works as in (Gibson et al., 2009). A 5'-exonuclease removes nucleotides from the 5' strand of a dsDNA, a Taq polymerase fills the gap and a ligase seals the gaps (see Fig.2.2). One major advantage of this technique is the rapidity and the possibility to clone the insert into basically any vector.

The second technique was called TOPO® Cloning (Invitrogen).
Also in this case the gene of interest was firstly amplified by PCR, using a high-fidelity Taq polymerase, which adds 3'-A overhangs to the PCR product. The vector used for the cloning possesses 3'-T overhangs, and a Topoisomerase I (from Vacciniavirus) is covalently bound to it. The Topoisomerase I can bind to dsDNA at specific sites and can cleave the phosphodiester backbone after a 5'-CCCTT sequence, leading to a Topoisomerase-mediated site-specific recombination (Shuman, 1991) (Fig.2.3). The energy produced by the break of the backbone is conserved by the formation of a covalent bond between the 3' Phosphate of the cleaved strand and the Tyrosyl residue (Tyr-274) of the Topoisomerase I. This bond can then be attacked by the 5'-OH of the original cleaved strand, reversing the reaction and releasing the Topoisomerase I (Shuman, 1994). The resulting vector is directly transformed in competent *E. coli* One Shot® TOP 10. One major advantage of this technique is the rapid ligation reaction (5 min at RT).

The third technique is the classical way based on the restriction enzymes. A PCR product is digested with the same restrictions enzyme used to digest the recipient plasmid, then the two fragments are incubated with the bacteriophage T4 Ligase overnight at 16 °C and the mix is transformed into XL1-blue bacteria.

To control that the PCR did not induce any mutation that could result in point mutation, absence of start or stop codon or frame shift, and that the ligation or recombination occurred correctly, all plasmids were sequenced. Briefly, 15 µl of plasmid (100 ng/mL) were mixed with 2 µL of one primer (10 µM) for the sequencing reaction in the Mix2Seq kit (Eurofins). The cycle sequencing reaction, based on Sanger sequencing, was performed by Eurofins and the obtained sequences were analysed with the Autoassembler program.

a2) DNA/RNA isolation

Genomic DNA isolation:

For a rapid genomic DNA (gDNA) isolation from *T. brucei*, 1 x 10^8 cells were harvested for 10 min at 1,200g. The pellet was gently resuspended in 150 µL of lysis buffer (TELT buffer: 50 mM Tris-HCl pH8, 62.5 mM EDTA pH9, 2.5M LiCl, 4% [v/v] Triton X-100), mixed by inversions 3–5 times without vortexing and incubated 5 min at RT. 150 µL of Phenol:Chloroform:Isoamyl Alcohol (PCIA) 25:24:1 were added to the suspension and mixed by inversion. Phenol:Chloroform mixture is used to separate proteins (that will be found in the organic phase and interphase) from the aqueous phase, which will contain the nucleic acids, whereas iso amyl alcohol is used to prevent foam formation. This mixture was centrifuged for 5 min at 13,000 g. The upper aqueous phase (containing the DNA) was moved to another tube and 300 µL100% Ethanol (EtOH) were added to precipitate DNA by gently inverting the tube for 15 sec DNA became then visible. The DNA was pelleted by 10 min centrifugation at 13,000 g. The pellet was air-dried to eliminate residual EtOH and resuspended in deionized water (dH_2O) (Medina-Acosta and Cross, 1993).

Total RNA isolation:

In order to isolate total RNA form *T. brucei*, 1 x 10^8 cells were harvested for 10 min at 1,800g and washed once in 1x PBS (8 g/L NaCl, 0.2 g/L KCl, 1.44 g/L Na_2HPO_4, 0.24 g/L KH_2PO_4 pH 7). The pellet was resuspended in 500 µl TRIzol ® (Invitrogen) (Chomczynski and Sacchi, 1987). TRIzol is a mixture of guanidine isothiocyanate and phenol. Guanidine isothiocyanate is a chaotropic agent that can denature proteins including DNases and RNases. After 5 min incubation at RT, 100 µL of Chloroform were added and the tube was vigorously vortexed for 15 sec. The mixture was spun down at 4 °C during 20 min at 12,000 g. In acidic conditions (TRIzol is at pH 4–6) the upper aqueous phase contains RNA only. The aqueous phase was moved to a new tube and the RNA was precipitated by adding 250 µL of Isopropyl Alcohol and gently mixed. After 1 h incubation at -80 °C, the RNA is pelleted at 4 °C for 10 min at 16,000 g. 500 µL of 100% Isopropanol were added to the RNA pellet. RNA can be long-term

stored at -20 °C. Just before use, the RNA is pelleted at 4 °C for 5 min at 7,500 g and resuspended in DEPC treated H_2O (DiEthylPyroCarbonate) that inhibits RNAses.

DNA and RNA concentration were evaluated by measuring the absorbance at 260 nm using a spectrophotometer (FluoStar Omega—BMG Labtech) considering that, at A260 nm, an absorbance of 1 corresponds to 50 µg/mL of dsDNA and of 40 µg/mL of ssRNA.
Their purity was determined by measuring the absorbance at 280 nm to evaluate protein contamination and by calculating the A260/280 ratio. A ratio of approximately 1.8 means pure DNA, whereas a ratio around 2 is accepted as “pure” RNA.

a3) Semi-quantitative RT-PCR (Reverse Transcription Polymerase Chain Reaction)

To control the efficiency of mRNA degradation during an RNAi induction, a semi-quantitative RT-PCR can be performed. Prior to the RT-PCR, the RNA was treated with 2 U of DNAse-TURBO (Ambion) during 30 min at 37 °C, in order to digest residual DNA contamination. The Superscript ® III One-Step RT-PCR System with Platinum ® Taq DNA Polymerase kit (Invitrogen) allows a one-step procedure in which the mRNAs are retro-transcribed into cDNA thanks to the Reverse Transcriptase (RT), a RNA-dependent DNA Polymerase, at 55 °C during 30 min. After cDNA synthesis, simultaneously the RT is inactivated, the DNA Polymerase is reactivated and the cDNA/RNA hybrid is denatured at 94 °C for 2 min. The cDNA is then amplified by PCR in the same tube (94 °C for 2 min; 25x cycles: 94 °C 15 sec [denaturing], 60 °C 30 sec [annealing], 68 °C 4 min [extending]; and as closing step 68 °C for 5 min).
As positive control, we used specific primers to amplify the small ribosomal subunit (18S) (Brenndörfer and Boshart, 2010). As negative control to prove that the RNA was not contaminated with DNA, the reaction was performed with isolated RNA and a DNA-dependent DNA Polymerase instead of the Superscript-reaction mix. No PCR products are expected, since the Taq DNA Polymerase can amplify products only starting from DNA and not RNA.
Primers specific to FPC4, amplifying from bp 660 to 1332:
(nr. 224) 5’ CCAAACTCAACCAACAGATG 3’ and
(nr. 419) 5’ TTTTATGAGTAACTCATCGG 3’.
The gene Tb927.7.6881—rRNA small subunit (18S) was used as loading control:
(nr. 476) 5’ ACGGAATGGCACCACAAGAC 3’ and
(nr. 477) 5’ GTCCGTTGACGGAATCAACC 3’ (Brenndörfer and Boshart, 2010).

b) Cell biology

b1) Parasites transfection (*T. brucei* and *L. major*) and cell line long term storage

The method to introduce purified DNA into eukaryotic cells is called transfection.
The plasmids used for stable transfection in *T. brucei* will integrate into the genome *via* homologous recombination. The integration occurs in untranslated regions of the genome, such as the intergenic region of rRNA (rRNA spacers) for pLEW-based plasmids. Prior to transfection, pLEW-based plasmids are linearized with *Not*I, which creates two free ends containing homologous regions to the rRNA spacer locus and allows the homologous recombination in this region. In *L. major*, plasmids can remain episomal (they will be amplified during the parasite cell cycle and transmitted to the daughter cells) or can also be integrated if linearized before transfection.

- *T. brucei* procyclic forms: Approximately 3 x 10^7 *T. brucei* 427 29-13 (PCF) parasites (in exponential phase 5–9 x 10^6 cells/mL) were harvested for 10 min at 700 g. The supernatant was filtered and kept as conditioned medium (CM). Cells were washed once in 1x PBS and then resuspended in 150 µL ice-cold transfection buffer (90 mM $NaPO_4$ pH 7.3, 5 mM KCl, 50 mM HEPES pH 7.3, 0.15 mM $CaCl_2$— (Schumann Burkard et al., 2011). 10 µg of purified and linearized plasmid DNA were gently mixed with the cells and placed in a 2 mm electroporation cuvette (Molecular BioProducts®). The electroporation was performed with an AMAXA® Nucleofector ® electroporator using the X-001 program. After electroporation the cells were placed in 10 mL of pre-warmed complete SDM-79 medium. Two dilutions (1:5 and 1:25) were prepared in cloning media (39.5 mL SDM-79, 7.5 mL Conditioned Medium [CM], 3 mL FCS) and aliquoted in 24-well plates (1 mL/well). Plates were placed overnight into a humid incubator at 27 °C. 18–24h post-transfection 0.5 mL of selection medium (19 mL SDM-79, 3.9 mL CM, 2.1 mL FCS, 3x selection antibiotics) were added to each well and plates were incubated for approximately two weeks.
- *T. brucei* bloodstream forms: 1 x 10^7 cells were spun for 10 min at 800 g and resuspended in 100 µL transfection buffer (as above). 10 µg of purified and linearized plasmid DNA were gently added to the cells that were then transferred into a 2 mm cuvette (Molecular BioProducts®). The electroporation was performed with an AMAXA® Nucleofector ® electroporation using the Z-001 program. After electroporation the cells were placed in 25 mL of pre-warmed IMDM medium (10% FCS). Three dilutions (1:5, 1:25, 1:100) were aliquoted (1 mL/well) in 24-well plates and incubated overnight at

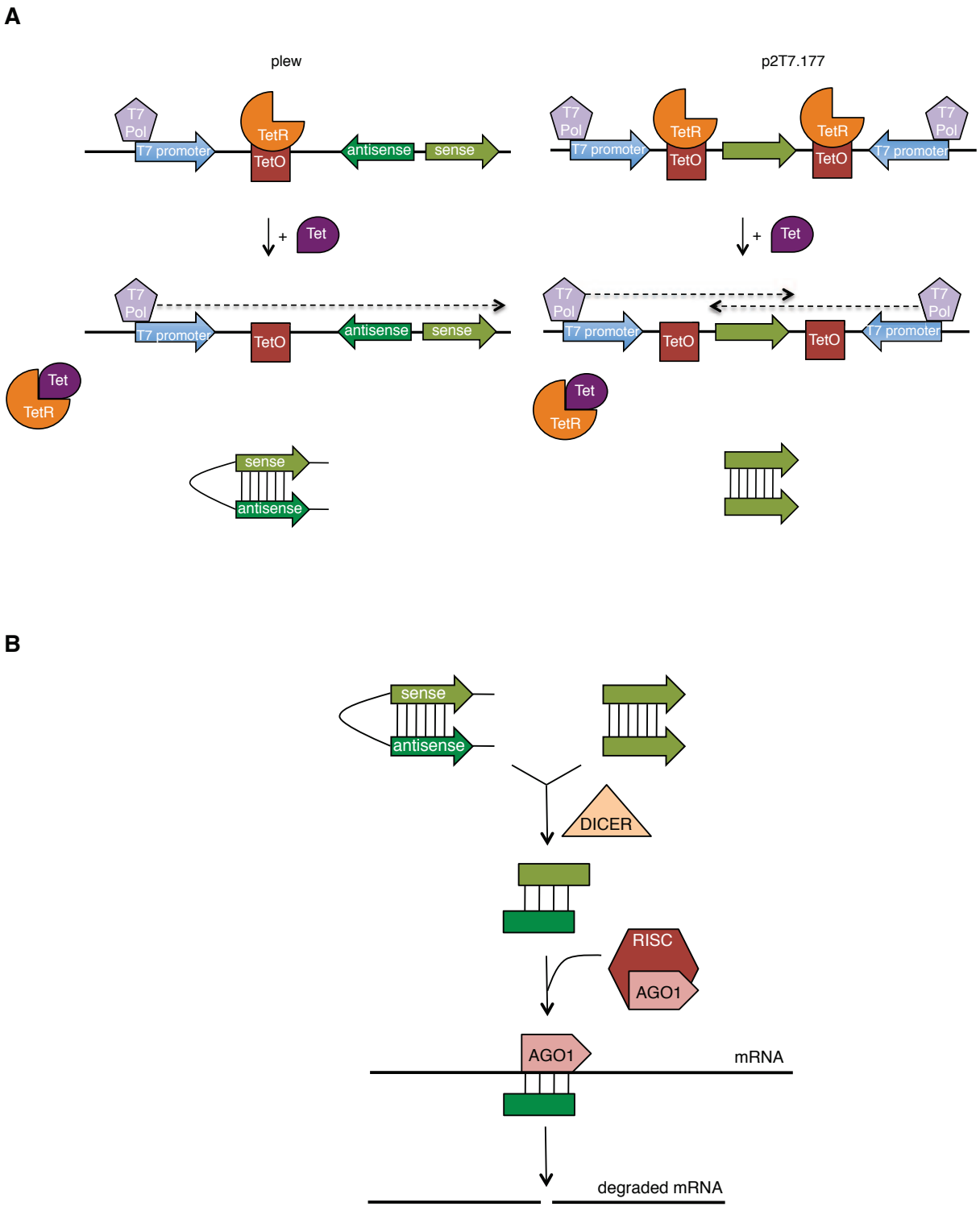

Fig. 2.4 *Gene knock-down by RNAi in T. brucei.*
(A) The addition of tetracycline (Tet) leads to the removal of the TetR from the Tet operator (TetO) and allows the gene transcription by the T7 Pol. In case of pLew-based plasmids (A - left) the product will be a stem loop composed by sense and antisense strands, whereas in p2T7 plasmids (A - right) a dsRNA will be produced by the transcription of opposite promoters.
(B) In an initial step dsRNAs are processed into approximately 21 bp-long fragments by the DICER enzyme and are then integrated as ssRNA in the RNA induced silencing complex (RISC). SsRNA will target the RISC to the complementary mRNA, which will be cleaved by the catalytic component of the RISC, the AGO1 protein, knocking down the gene expression of the target gene

- 37 °C and 5% CO_2. The next day, 0.5 mL of IMDM medium containing 3x concentrated selection antibiotics were added to each well, and plates were incubated for approximately one week.

Promastigote *L. major*: approximately 5 x 10^7 cells in exponential phase (6–8 x 10^6 cells/mL) were collected by centrifugation for 10 min at 4 °C 1,800 g. Cells were washed once in Cytomix Buffer (Hoff et al., 1992) (120 mM KCl, 0.15 mM $CaCl_2$, 10 mM K_2HPO_4, 25 mM HEPES pH 7.6, 2 mM EDTA, 5 mM $MgCl_2$) and resuspended in Cytomix Buffer to obtain a concentration of 1 x 10^8 cells/mL. 500 µL of cells were mixed with 80 µg of plasmid DNA (in 50 µL), and incubated in a 4 mm cuvette (Molecular BioProducts®) for 10 min on ice. The electroporation was performed with Biorad Electroporator (GenePulserXcell), 2 pulses of 0.5 ms at 1,500 V, with a 10 sec break in between. After electroporation the cells were incubated for 10 min on ice then transferred to 6 mL pre-warmed RPMI medium completed with Hemin (7.58 µg/mL) and incubated overnight at 26 °C. The next day, selection antibiotics were added. Resistant cells start growing approximately 8–12 days post-transfection.

Aliquots of PCF and BSF *T. brucei* and of *L. major* parasites can be frozen and stored in liquid nitrogen for long-term storage. Cells were pelleted for 10 min at 800 g and resuspended in 1/10 of the initial volume in SDM-79 +7% glycerol or IMDM +7% glycerol for *T. brucei* PCF and BSF respectively, and 1/3 of the initial volume in RPMI + 20% FCS + 10% DMSO for *L. major*. Aliquots in cryo-tubes Nunc® were cooled-down overnight in Nalgene® Mr. Frosty box at -80 °C prior liquid nitrogen long-term storage.

b2) RNA Interference (RNAi) in *T. brucei*

RNAi (also known as gene knock-down) consists in the gene silencing due to mRNA degradation triggered by gene-specific dsRNA. In *T. brucei* (Ngô et al., 1998), dsRNA is processed in 21–25 bp long dsRNA fragments by the Dicer complex—a ribonuclease type III (Bernstein et al., 2001). These short interfering RNAs (siRNA) are then integrated in the RNA-induced silencing complex (RISC) as single strand RNA. The anti-sense strand incorporated in the RISC will guide the RISC complex to the corresponding mRNA (Elbashir et al., 2001) that will be degraded by the argonaute AGO1 protein (Durand-Dubief and Bastin, 2003). In *T. brucei Tb*DCL1 (a cytoplasmic protein) and *Tb*DCL2 (a nuclear enzyme) have been identified as Dicer-like enzymes (Patrick et al., 2009; Tschudi et al., 2012). Recently two other proteins involved in RNAi have been identified: *Tb*RIF4 and *Tb*RIF5 (RNA

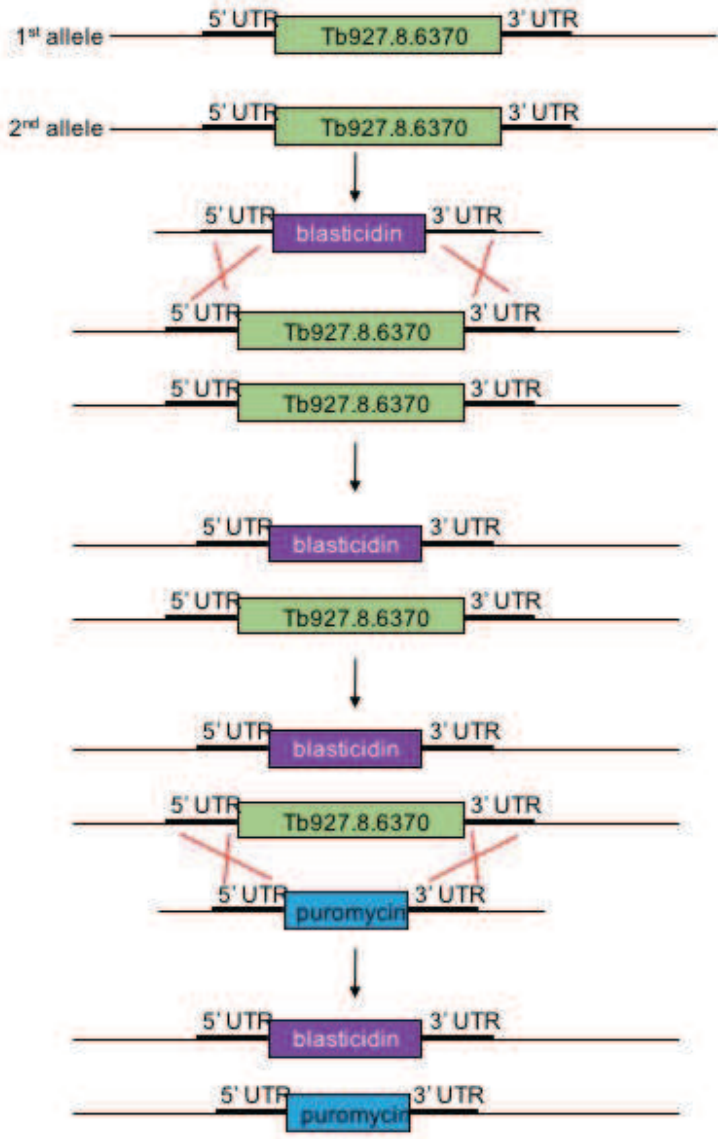

Fig. 2.5 *Two-step Knock-out cell line.*
In a first step, one allele of the gene of interest is substituted by homologous recombination with a resistance gene and, in the following step, the second allele of the gene is replaced by a different resistance gene.

Interference Factors 4 and 5) (Barnes et al., 2012). RIF4 is a 3'—5' exonuclease implicated in the conversion of siRNA from double-stranded to single stranded, allowing its integration into the RISC complex—creating the AGO1-siRNA complex. RIF5 is essential for the cytoplasmic RNAi mechanisms, and seems to be a DCL1 cofactor.
Genome analysis on other kinetoplastids like *T. cruzi*, *L. major* and *L. donovani* revealed that these 3 species do not possess all the genes required for a functional RNAi machinery (DaRocha et al., 2004, Robinson and Beverley, 2003), whereas *L. brasiliensis* does (Lye et al., 2010).

In order to produce dsRNA and induce the RNAi mechanism in *T. brucei*, we used two plasmids. Both are inducible by addition of Tetracycline, and therefore usable in *T. brucei* 29-13 (PCF) and *T. brucei* 90-13 (BSF) cell lines (Wirtz et al., 1999). In the pLEW-based plasmids —Wirtz 1999 (Fig.2.4 A left), a sense and an anti-sense sequences of about 500 bp, corresponding either to the ORF or the 3'-UTR of the gene of interest, separated by approximately 50 bp, are under control of the T7 promoter regulated by the Tet operator. The addition of tetracycline (that binds to the Tet repressor) leads to the production of a stem loop or hairpin dsRNA that will be processed by the DICER complex leading downstream to the degradation of the mRNA of the gene of interest (Fig.2.4 B). The second plasmid system (p2T7.177) (Alibu et al., 2005) (Fig.2.4 A right) is based on double promoters. A complementary sequence of the targeted gene is placed in between two opposite promoters. The addition of tetracycline leads to the transcription of two complementary transcripts that anneal thus creating a dsRNA undergoing the RNAi machinery (Fig.2.4 B).

For the knock-down of the FPC4 gene, the targeted region was bp 164 to bp 754, and the primers used to clone into the pLEW plasmid were:
(286 as) 5' GTGCggatccGGCAGTAGCAGCAACAAC 3' ,
(287 as) 5' GTGCggatccGGCAGTAGCAGCAACAAC 3',
(285 s) 5' GTCCctcgagGCAATGTTTAGAGCATCG 3',
(263 s) 5' GCGGaagcttGGCAGTAGCAGCAACAACAA 3'

b3) Gene Knock-Out in *T. brucei*

Another technique to prove the essentiality of a gene (and its corresponding protein) is the gene knock-out (KO). This technique implies the replacement of the gene of interest on both alleles (*T. brucei* is diploid), by two different resistance genes in order to carry out the selection of the KO cells.

Tab.2.4 *Primary and secondary antibodies used for western-blot and Immunofluorescence analysis.*

	Antigen	made in	dilution for WB	dilution for IF	source	accession number	MM (kDa)	comments
primary antibody	c-myc	mouse IgG1	1:100	1:20	K. Ersfeld	-	-	
	c-myc	rabbit	1:1000	1:500	Santa Cruz sc-789	-	-	
	PFR A (L8C4)	mouse IgG1	1:1000	neat	K. Gull	Tb927.8.4970	70	Kohl et al. 1999
	Ty1 (BB2)	mouse IgG1	1:50	1:10	P. Bastin	-	-	Brookman et al. 1995
	FAZ1 (L3B2)	mouse IgG1	-	neat	L. Kohl	Tb927.4.3740	192	Kohl et al. 1999
	MtQ (1B41)	mouse IgM	-	neat	L. Kohl	unknwon antigen	-	Gallo et al. 1988
	Living Colors® Full-Length (for GFP)	rabbit	1:10000	1:1000	Clontech 632460	-	-	full-length Aequorea victoria green fluorescent protein (rGFP). This antibody recognizes native and denatured forms of recombinant EGFP, as well as EGFP, EYFP, ECFP, and AcGFP fusion proteins
	Tb LRRP1	mouse	1:1000	1:4000	C. He	Tb11.01.0868	79	Zhou Q et al. 2010
	Tb SAXO (mAb25)	mouse Ig2a	1:1000	1:10	D. Robinson	Tb927.8.6240	30	Dacheux et al. 2012
	Tb BILBO1 (5F2B3-C8)	mouse IgM	1:10	1:5	D. Robinson	Tb927.11.12150	67	Bonhivers et al. 2008
	Tb BILBO1 1-110 (aa 1-110)	rabbit	1:1000	1:4000	D. Robinson	Tb927.11.12150	67	
	Tb FPC4 ser294	rat	1:500	1:250	D. Robinson	Tb927.8.6370	50	by WB, ser294 works on over-expression only
	Tb FPC4 3B10 (aa 357-440)	mouse IgG1	1:5	1:2	D. Robinson	Tb927.8.6370	50	by WB, 3B10 works on over-expression only
	Tb MORN1 (1340)	rabbit	1:20000	1:4000	B. Morriswood	Tb927.6.4670	40	B. Morriswood et al. 2013
	HA	mouse IgG2a	-	1:100	Santa Cruz sc-7392	-	-	specific to epitope mapping within an internal region of the influenza hemagglutinin (HA) protein
	α-tubulin (DM1a)	mouse IgG1	-	1:500	Sigma T9026	-	-	chicken embryo brain tubulin
	α-tubulin (TAT1)	mouse IgG2a/b	1:1000	1:100	K. Gull	-	-	Woods et al. 1989
secondary antibody for WB	anti-mouse HRP	sheep	1:10000	-	Jackson 515-035-062	-	-	
	anti-mouse HRP	goat	1:10000	-	Jackson 115-035-044	-	-	
	anti-rabbit HRP	goat	1:10000	-	Sigma A-9169	-	-	
	anti-rat HRP	goat	1:10000	-	Jackson 112-035-003	-	-	
secondary antibody for IF	anti-mouse FITC	goat	-	1:100	Sigma F-2012	-	-	
	anti-mouse AF594	chicken	-	1:100	Mol. Probes A-21201	-	-	
	anti-rabbit FITC	goat	-	1:100	Sigma F-9887	-	-	
	anti-rabbit AF594	goat	-	1:100	Mol. Probes A-11012	-	-	
	anti-rabbit AF647	donkey	-	1:100	Mol. Probes A-31573	-	-	
	anti-rat FITC	goat	-	1:100	Sigma F-6258	-	-	
	anti-rat AF488	chicken	-	1:100	Mol. Probes A-21470	-	-	
	anti-rat AF594	chicken	-	1:100	Mol. Probes A-211471	-	-	

For an efficient substitution at the locus of the gene of interest, the recombination should occur by homolog recombination on the 5' and 3'-UTRs of the ORF (Fig.2.5).

b4) Over-expression in *T. brucei*

In order to over-express a gene in *T. brucei*, and its corresponding protein with a tag, we used pLEW-based plasmids (described in tab2.2 and 2.3). The gene under the control of the TetO will be over-expressed by the addition of tetracycline. The integration of the linearized plasmid into the genome occurs at the rRNA spacer locus, an un-transcribed region.
This technique can be used to 1) overexpress a protein, 2) overexpress a modified protein such as tagged or truncated, 3) assess dominant negative phenotypes.

b5) U-2 OS Lipotransfection

The plasmid DNA is incubated with Lipofectamine 2000 to form DNA/lipid complexes where the negatively charged DNA is trapped into cationic liposomes. These liposomes can fuse with membranes and release the DNA.
The day prior to the transfection, 5 x 10^4 U-2 OS cells are incubated on glass cover slip in a 24-wells plate. The day of the transfection 2 µL of Lipofectamine™ 2000 (Invitrogen) are mixed with 0.5-1 µg of plasmid containing the gene of interest in a total volume of 100 µL OPTI-MEM® (Invitrogen) and incubated for 30 min at RT. This mixture is then deposed drop by drop at the surface. After incubation of 2 h at 37 °C and 5% CO_2, the medium is replaced by 500 µL of culture medium. The cells are again incubated at 37 °C and 5% CO_2 for 24 h to 48 h and analysed by immunofluorescence.

c) Biochemistry

c1) SDS-PAGE

Sodium Dodecyl Sulfate (SDS)—PolyAcrylamide Gel Electrophoresis (PAGE) is a technique to separate proteins according to their molecular mass (MM). The samples (whole cell lysate or cytoskeleton extracted cells) were resuspended in a denaturing sample buffer (SB), modified from Laemmli Buffer (Laemmli 1970 Nature) (10% glycerol, 2% SDS, 50 mM Tris pH 6.8, 100 mM DTT, a pinch of bromophenol blue. Benzonase (2 U for 10^8 cells) was added to digest genomic DNA that disturbs the migration and after a 5 min incubation at RT, the samples are denatured 8 min at 99 °C. SDS is an anionic detergent that breaks hydrogen

bonds leading to the loss of tertiary and secondary structure of the proteins and confers negative charges to them. These charges allow the protein to migrate during the electrophoresis. DTT [Dithiothreitol] is a disulfide bond reducing agent. The samples were then loaded on a SDS-polyacrylamide gel composed by a stacking gel [upper part] and a separating gel [lower part]. The stacking gel [5% Acrylamide/Bisacrylamide] allows the proteins to concentrate at the top of the separating gel, and the separating gel (10–15% Acrylamide/Bisacrylamide for my experiments, depending on the MM range of the proteins) allows their separation according to their MM.
The polyacrylamide gels can be stained with Coomassie blue R250 (10% acetic acid, 50% EtOH and 2.5 g/L Coomassie blue) and destained in 10% acetic acid and 25% EtOH to visualize the proteins.
The gels can also be used to transfer the proteins onto a membrane to be immuno-detected by Western Blot.

c2) Western Blot

Western Blot is a technique to transfer proteins onto a polyvinylidene fluoride (PVDF) or nitrocellulose membrane in order to detect them with specific antibodies.
The transfer occurs using a semi-dry blot apparatus (Biorad) applying a constant potential of 25V for 45 min. To control the efficient transfer, the membrane can be stained with Ponceau red for 1 min and destained with water. The membrane is then blocked for 1 h in 5% Milk in PBS - 0.2% and Tween-20 (Milk-PBS-T). The incubation with the primary antibody diluted in Milk-PBS-T occurs overnight at 4 °C. The membrane is washed 3 times in Milk-PBS-T, eventually with the addition of NaCl (to a final concentration of 1 M) to reduce unspecific binding. The incubation with the secondary antibody (HRP-coupled) occurs at RT for 1 h in Milk-PBS-T. After three washes in Milk-PBS-T, and three washes in PBS, the membrane is then incubated for 5 min in the revelation buffer Immobilon Western Chemiluminescent HRP substrate (Millipore), and observed with ImageQuant LAS 4000 (GE Healthcare). This revelation technique is called Enhanced ChemiLuminescence (ECL) as a luminescent component is produced when the revelation buffer (substrate) reacts with the peroxidase (HRP) coupled to the secondary antibody.

The primary and secondary antibodies details are summarized in the Tab.2.4.

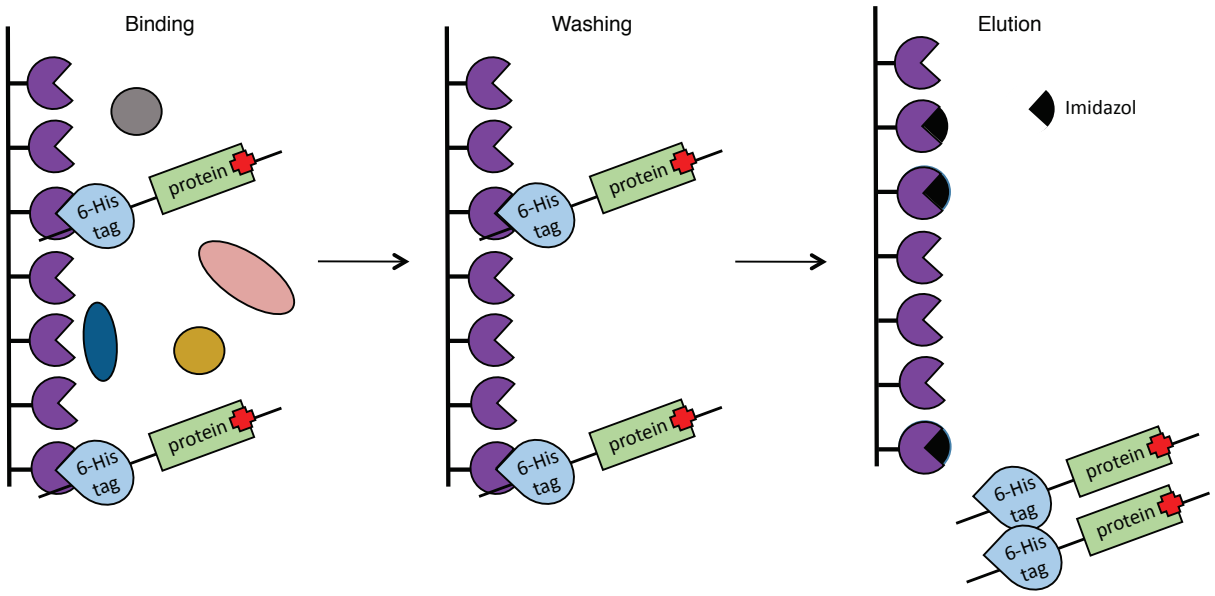

Fig. 2.6 *Affinity purification Scheme*
His-tagged proteins bind to the His-Trap column (Nickel-column), whereas proteins without the tag are washed away. To collect the His-tagged proteins, the proteins are eluted with imidazole, which has higher affinity to nickel than the His-tag and allows the release of the tagged proteins.

c3) Protein purification for *in vitro* studies and antibody production

In order to obtain purified proteins for downstream applications, recombinant proteins can be expressed in *E. coli* BL21 (*DE3*) strain. The DNA sequence coding for the truncation aa 1–260 FPC4 has been cloned into the pET28a (+) vector (Novagen) between the *Nco*I and *Hind*III restriction sites, resulting in the expression of the first 260 aa of FPC4 with a C-terminal 6-Histidine tag (Fig.2.6). The DNA sequence coding for the FPC4 truncation aa 357–440 (with the addition of a stop codon) was cloned between the *Nde*I and *Xho*I, restriction sites resulting in the expression of an N-terminal 6-Histidine tagged protein. Nicolas Landrein has carried out the purification, but briefly the protocol was as follows. The day before the purification, a pre-culture of 10 mL LB (Lysogeny Broth) medium with Kanamycin 50 µg/mL was prepared. The day of the purification the culture was diluted to an OD_{600nm}= 0.05 in 250 mL and incubated at 37 °C under constant shaking (200 rpm). At OD 0.5-0.6, target protein expression was induced with 1 mM IPTG for 3 h. The culture was centrifuged for 20 min at 4,000 g and the pellet resuspended in 25 mL Buffer A (20 mM Tris-HCl pH 7.4, 200 mM NaCl, 1 mM $MgCl_2$ and 1 mM DTT—and 1:10,000 protease inhibitor cocktail set III Calbiochem 539134) with lysozyme 0.1 mg/mL. The cells were then lysed by sonication (on ice: 20 pulses and 30 sec break, repeated for 20 times, Branson Sonifier 250) and centrifuged for 30 min at 10,000 g at 4 °C. The supernatant, which contains the soluble proteins, was loaded onto a Buffer A equilibrated HisTrap FF column (1 mL, GE Healthcare) at 0.5 mL/min using an AKTA purifying system. The column was then washed with 15 mL of Buffer A. The His-tagged protein bound to the Nickel column was eluted in 0.5 mL fractions with Buffer B (Buffer A + 300 mM imidazole, which has a higher affinity to nickel than histidine).

An aliquot of each fraction was analysed by SDS-PAGE to assess purity and quantities of the protein. Selected fractions were pooled and dialyzed in Buffer A. After determination of the protein concentration using the Pierce 660nm Protein Assay kit (11881315) (a colorimetric method for total protein quantification based on the comparison of an absorbance curve as standard, with known protein concentrations, with the absorbance of the purified samples), aliquots were stored at -20°C with 10% glycerol before use.

c4) Microtubule co-sedimentation assay

This technique allows determining the ability of a protein to interact directly with microtubules and has been previously used for the characterization of *Tb*SAXO, an axonemal protein in *T. brucei* (Dacheux et al., 2015). Marie Eggenspieler has carried out this assay.

Taxol-stabilized microtubules (MTs) (5 mg/mL) were prepared as follows based on a method published previously (Campbell and Slep, 2011). Purified bovine tubulin (99% pure, Cytoskeleton Inc.) was resuspended in cold G-PEM (80 mM PIPES pH 6.8, 1 mM EGTA, 0.5 mM $MgCl_2$, 1 mM GTP) and centrifuged at 4 °C for 10 min at 16,000 g to remove aggregated protein. Taxol (Paclitaxel, CalbiochemH) was added stepwise (addition of 1/10 of the final volume of 5 mM, 50 mM and 500 mM taxol in DMSO, with a 10 min incubation at 37 °C after each addition) to reach a final concentration of 5 mg/mL tubulin MT preparation. For co-sedimentation assays, 4 µL of MTs were mixed with different amounts of the protein of interest. Volumes were adjusted to 50 µL with PEMD (100 mM PIPES pH 6.8, 1 mM EGTA, 1 mM $MgCl_2$, 1 mM DTT) to a final concentration of 7.2 µM tubulin. Samples were then incubated for 1 h at 22 °C and centrifuged for 15 min at 16,000 g at 22 °C. Supernatants and pellets were separated and brought to equal volumes in SDS sample buffer and analysed by SDS-PAGE. Gels were stained using Instant BlueTM (Expedeon). The microtubules are in the pellet; the protein is detected in the pellet if it binds to microtubules. A control experiment consists in centrifugation of the protein without microtubules to test the absence of precipitation.

d) Imaging

d1) Sample preparation for fluorescence microscopy

- *Trypanosoma brucei* whole cells (WC)

  - PCF: Cells were centrifuged for 5 min at 1,000 g, washed once in PBS and deposed on poly-lysine coated glass slides for 5–10 min. Cells were fixed for 4 min with 3% PFA or in -20 °C Methanol (MeOH) for at least 30 min. In order to neutralize the PFA, two washes in 100 mM glycine were performed for 10 min. Cells were then permeabilized for 10 min with 0.2% Triton X-100.

  - BSF: Cells were washed once in vPBS, resuspended in 1% PFA in PBS and incubated for 2 min on ice. Cells were spun (5 min at 2000 g), resuspended in PBS and deposed on glass slides. After one wash in PBS, cells were permeabilized in -20 °C MeOH for 30 min.

- *Trypanosoma brucei* cytoskeleton extracted cells (CK)

  - PCF: Cells were washed in PBS and loaded on poly-lysine coated slides for 5–10 min. Cells were then extracted for 5 min with 0.25-1% NP40 (Igepal CA-630—Sigma i3021) in PIPES buffer (100mM PIPES pH6.9, 1 mM $MgCl_2$). After two washes

in PIPES buffer, cytoskeletons were fixed in -20 °C-cold MeOH for at least 30 min or in 3% paraformaldehyde (PFA) in PBS for 4 min. After PFA neutralization with 100 mM glycine, CK were washed twice in PBS.

- BSF: Cells were washed once in vPBS, resuspended in 0.5% NP40 (Igepal CA-630—Sigma i3021) in PIPES buffer and deposed on slide. Cytoskeletons were washed twice in PIPES buffer and once in PBS. Slides were incubated for 30 min in -20 °C-cold MeOH.

- *Trypanosoma brucei* flagella (Fg)

Cells were collected and were washed once in PBS. In a first step, the cells were extracted with 1% NP40 in PIPES buffer containing Benzonase (1:10,000 dilution, Sigma C-8263) and protease inhibitors (1:10,000 dilution Protease Inhibitor Cocktail Set III Calbiochem) for 5 min at RT. Cytoskeletons were spun for 10 min at 5,000 g at 4 °C. To extract flagella, cytoskeletons were incubated for 15 min on ice with 1% NP40 in PIPES buffer containing 1 M KCl. After centrifugation for 5 min at 5,000 g at 4 °C, flagella were washed twice in PIPES buffer and deposed on poly-lysine coated slide and let adhere for 5–10 min. The flagella were fixed at -20 °C in MeOH or in 3% PFA as described above.

d2) Immunolabelling and observation

The second part of the protocol was common for all the preparations: three washes in PBS buffer were performed and the samples (WC, CK or Fg) were incubated with the primary antibody for 1 hour in a wet chamber.

After three PBS washes, the slides were incubated with the secondary antibody for 1 hour protected from light (see Tab.2.4 for antibodies characteristics and dilutions). The slides were washed twice in PBS before staining the nuclei and the kinetoplast DNA for 5 min with DAPI (10 µg/mL in PBS)—The DNA staining step is skipped in case of flagella, since kDNA is degraded due to the benzonase treatment. Two additional PBS washes were performed before mounting with SlowFade Gold (Molecular probes S-36936).

- For U-2 OS

All solutions were pre-warmed at 37 °C including the fixation step to preserve the interphase microtubules from cold-induced depolymerization. Cells were briefly extracted for 2 min in EMT Buffer (60 mM PIPES pH 6.9, 25 mM HEPES, 10 mM EGTA, 10 mM $MgCl_2$), 0.5% Triton X-100, 10% glycerol, then fixed in PFA 3% at 37 °C for 15 min. PFA was neutralized 10 min in glycine (100 mM in PBS). After two washes in PBS, cells were incubated in PBS,

10% foetal calf serum, and 0.01% saponin for 10 minutes and incubated with the primary antibodies for 1 hour in a dark moist chamber. After two PBS washes, cells were incubated for 1 hour with the secondary antibodies (see Tab.2.4 for antibodies characteristics and dilutions). The nuclei were stained with DAPI (0.2 mg/mL in PBS for 5 minutes) and cells were washed in PBS and mounted with Prolong mounting medium (molecular probes P-36930) and observed 24h later.

d3) Fluorescence Microscopy

Images were acquired on a Zeiss Imager Z1 microscope, using a Photometrics Coolsnap HQ2 camera, using a 100x or 63x (NA 1.4) objective and with Metamorph software (Molecular Devices). Images were processed with ImageJ (Schneider et al., 2012).

d4) Electron microscopy

Derrick Robinson has performed the electron microscopy part of the work.

- Immuno-electron microscopy on flagella. Flagella were prepared as previously described for the immuno-fluorescence and loaded on grids. Briefly, 5 mL of mid-log phase parasites were collected by centrifugation for 5 min at 1,000 g, washed once in PBS and resuspended in 500 µL PBS. A droplet of cells was loaded on parafilm, and Formvar/Butvar covered, charged, carbon coated nickel grids were gently deposited at the surface of the droplet and incubated for 10–15 min to let the cells adhere. The grids were then moved to a 250 µL droplet of 1% NP40, PEME (100 mM PIPES pH 6.9, 1 mM $MgCl_2$, and 1:10,000 complete protease inhibitor cocktail (Calbiochem)) and incubated for 5 min. This extraction step was used to make cytoskeleton and was repeated once on a fresh droplet. The grids were then moved to a fresh droplet containing in addition 1 M KCl, for 30 min on ice, in order to depolimerize sub-pellicular MT and obtain flagella. The extraction was regularly controlled under the microscope. After four washes in PEME buffer with protease inhibitors, the flagella were fixed on 100 µL 3% PFA in a PEME droplet for 5 min. PFA was then neutralized with four incubations on 100 µL droplets of 100 mM glycine in PEME. The grids were then transferred through five blocking droplets for 5 min each (0.1% BSA, 0.1% Tween-20 in PBS) then to droplets containing the primary antibodies. As primary antibody anti-myc (mouse monoclonal 9E10—a kind gift from K. Ersfeld) 1:20 and anti-BILBO1 1–110 (rabbit — Robinson) 1:400 or anti-myc (mouse — Erstfeld) 1:20

and anti-MORN1 (rabbit — Morriswood) 1:400 were incubated for 2h at RT in PBS 0.01% BSA and 0.1% Tween-20. The grids were washed four times in PBS 0.01% BSA and 0.1% Tween-20 and incubated then with gold-conjugated secondary antibodies (see Tab.4 for antibodies characteristics and dilutions). EM GAR10 1:20 (anti-rabbit, 10 nm), and EM GAM15 1:50 (anti-mouse, 15 nm) in PBS 0.01% BSA and 0.1% Tween-20 for 2h at RT. The grids were then washed twice in blocking buffer, twice in PBS and then fixed for 5 min in 2.5% glutaraldehyde in PBS. After two washes in milliQ H_2O, the grids were negatively stained in 0.5% Nanovan for 5–10 sec.

- Whole cells embedding and section preparation:
  In order to make trypanosomes ultra-thin sections (70-90 nm), a mid-log phase culture was fixed for 2h in medium with 2.5% glutaraldehyde, and consequently fixed in 2.5% glutaraldehyde in 0.1 M Sorensens's Sodium Phosphate buffer pH 7.2. The cells were rinsed twice in milliQ H_2O and incubated for 1 h in 1% OsO_4 in milliQ H_2O pH 7.2. After three washes in milliQ H_2O, the cells were stained and fixed in 2% Uranyl-acetate (milliQ H_2O) at 4 °C overnight. After three washes of 10 min in milliQ H_2O, the cells were dehydrated in EtOH, starting from 30% EtOH, then 50%, 70% and 90% for 2h each and left in 90% EtOH overnight. The following day the cells were incubated three times up to 1h in 100% EtOH at RT. The cells were then incubated for 3h each with 30%, 50%, 70% and 90% EtOH:Spurs resin and as final incubation three times for 1h with 100% Spurs resin at RT, and then overnight in 100% Spurs (Low viscosity embedding kit, EMS 14300) at RT. The resin was embedded in size "OO" BEEM capsules (EMS) and let polymerize overnight at 60 °C.
  Thin sections were cut with Ultramicrotome LEICA EM-UCT at a thickness of approximately 70-90 nm. The sections were deposed on grids and stained with aqueous saturated uranyl acetate for 15-30 min. The grids were washes three times in boiled cooled water for 5 min each and then air dried. An additional wash with 0.1 N NaOH for 30 sec and three washes in boiled cooled water for 5 min.

Samples were visualized on a FEI Tecnai 12 electron microscope, camera ORIUS 1000 11MPixel (resolution 3-5 nm). Images were acquired with Digitalmicrograph and processed with ImageJ.

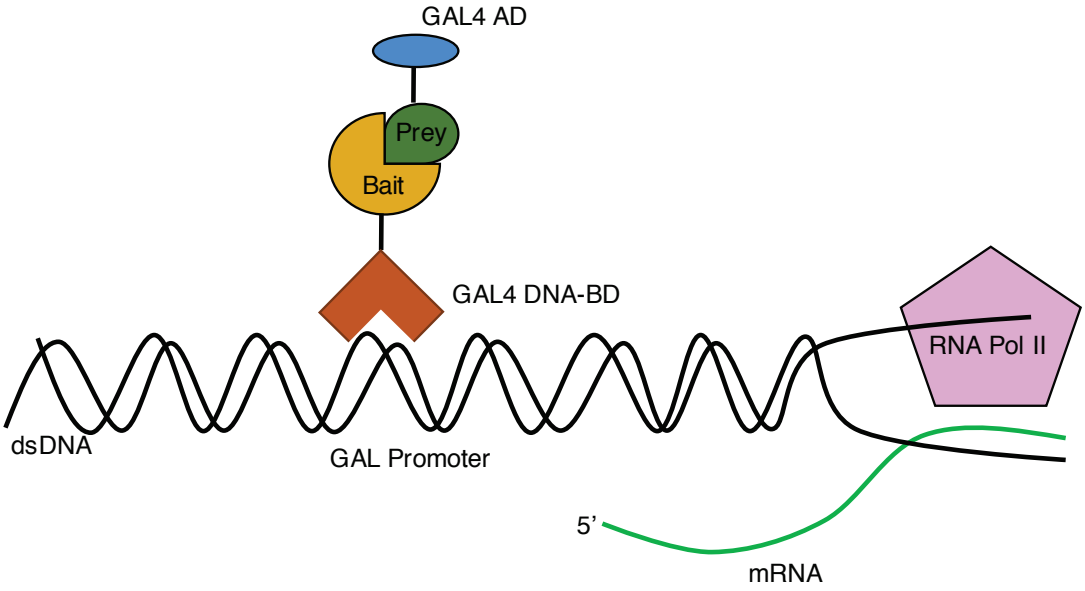

Fig. 2.7 *Yeast two-hybrid principle*
The interaction between two proteins fused to the Binding Domain (BD) or the Activation Domain (AD) of GAL4 reconstitutes the transcription factor and leads to the transcription of a reporter gene. The growth of the yeasts on selective media confirms the interaction between the two tested proteins.

e) Yeast Two-Hybrid interaction test

The Yeast two-hybrid technique is used to identify or confirm protein interaction partners. For our experiments, we used the Matchmaker™ Gold Yeast Two-Hybrid System (Clontech), which is based on the reconstitution of the transcription factor GAL4 (Fig.2.7). A prey protein is fused to the Activation Domain (AD) of GAL4, in the pGADT7 plasmid. A second protein is fused to the DNA Binding Domain (BD) of GAL4, in the pGBKT7 plasmid, which acts as Bait. These plasmids are transformed in haploid yeast strains, and after mating both plasmids are in a same diploid yeast allowing the expression of prey and bait proteins. When the two proteins interact, the complex, thanks to a nuclear localization sequence (NLS) present upstream the prey protein, is carried to the nucleus, where the reconstituted transcription factor GAL4 can bind to DNA and activate the transcription of the reporter gene which is under the control of a promoter controlled by GAL4. For our experiments, the interactions were tested by a drop test (10^6 to 10^1 cells/drop) on a solid selective medium depleted of histidine (SC-L-W-His) and on a loading control medium (SC-L-W) to test the growth of the yeast. The transcription of the reporter gene allows the diploids to grow on selective medium and confirms therefore the protein-protein interaction (Fig.2.7).
Each sequence of interest was cloned in both plasmids (pGADT7 and pGBKT7) to test the interaction on both “directions”. Toxicity and auto-activation tests were performed prior to the interaction test.

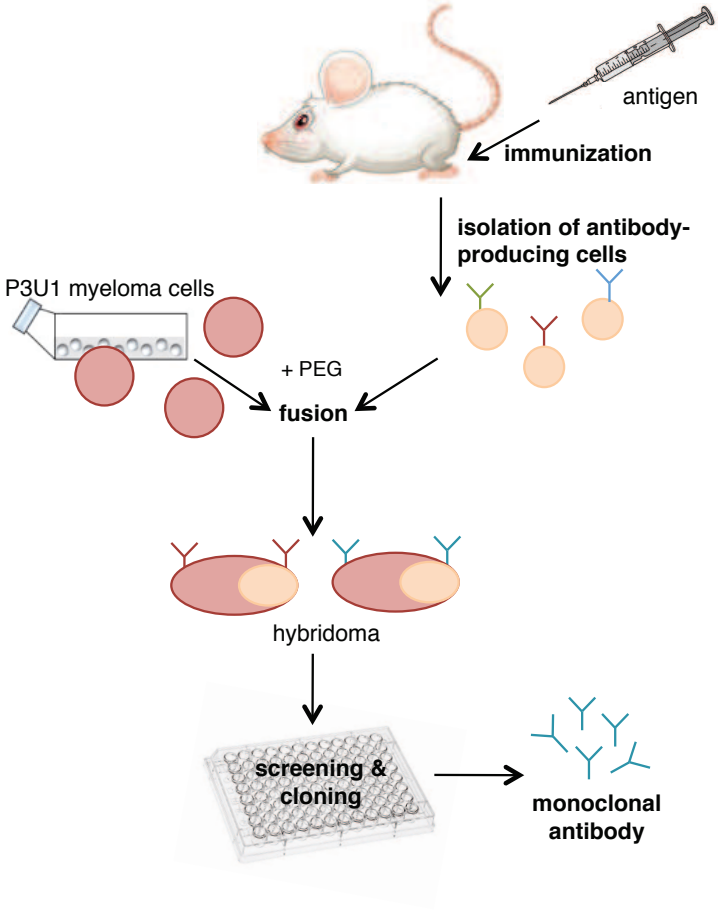

Fig. 2.8: *Principle of a monoclonal antibody production*
After 15 days post-immunisation, popliteal lymph nodes were collected to isolate antibody-producing B-cell. These cells were fused with P3U1 myeloma cells and the hybridomas obtained were tested by immunofluorescence. If positive, they were further cloned, tested again, stored in liquid nitrogen as well as kept in culture to regularly collect the supernatant containing the secreted monoclonal antibody.

f) Monoclonal antibody production

The general procedure to produce monoclonal antibodies has been described in Fig.2.8.

Five days before the mice immunisation, pre-immune serum was obtained from blood collected from the tail tip of the mice with heparinised capillary tubes, in order to retard blood coagulation. At day 0, approximately 15 µg of purified 6-His-357-440aa FPC4 in 40 µL volume emulsion 50/50 with Freund's complete adjuvant (Sigma F-5881) were injected in the footpad of three-9-week-old BALB/c female mice. Freund's adjuvant is an immuno-potentiator, composed of inactivated and dried mycobacteria in mineral oil, used to create an emulsion with the purified protein to boost the immune system to produce antibodies. At day 12, two mice were boosted with 15 µg of purified protein in incomplete Freund adjuvant and one with the complete adjuvant. At day 15, mice were sacrificed to collect the popliteal lymph nodes (PLN), located in the backside of the knee. The PLN were smashed with a plastic syringe piston in a Petri dish containing 5 mL of pre-warmed RPMI medium. The mixture was collected and cell debris sedimented for a couple of min. The supernatant was diluted with RPMI to 15 mL total volume and the lymphocytes were counted with a Quick-read^{TM} precision cell in trypan blue (that acts as an indicator for living cells) and washed in RPMI by centrifugation at 600 g rpm for 5 min. The same number of myeloma P3U1 cells were collected and washed twice in RPMI by centrifugation at 600 g rpm for 5 min. The two pellets were gently resuspended together in 10 mL RPMI and diluted to 50 mL. The cells were then collected by centrifugation at 600 g rpm for 5 min, and the pellet was incubated at 37 °C. Within 1 min, four times 250 µL PEG-150 (783641 Roche) were deposed on the cells and mixed with the pipette tip to induce cell fusion. The cells were mixed for two additional min, and then 4 mL of RPMI were deposed on the cells during 5 min (200 µL every 15 sec), always mixing with the pipette tip. To this mixture of cells were added 67 mL of HAT RPMI complete (RPMI, 8% FCS, 0.05 mM β-Mercaptoethanol, 2 mM sodium pyruvate, 1x non-essential amino acids [Gibco 11140] and 1x HAT [Sigma H0262]. Finally, the total volume was distributed [100 µL/well] in 96-well plates containing macrophages that were prepared the day before [100 µL/well]. Only the 60 central wells were used, the external wells contained only sterile PBS. After 7 days post fusion, 100 µL were removed and substituted with fresh HAT RMPI complete medium. Approximately 15 days after the fusion, colonies of hybridomas could be observed. As soon as the cells were growing, the supernatants were tested by IF analysis on WT cells and, in case of positive staining, the hybridomas were cloned with 0.3–1—and 3 cells/well. The positive hybridomas were maintained at an ideal cell density of $5x10^5$ cells/mL, then amplified and frozen (in IMDM complete, 25% FCS and 10% DMSO – stored in liquid nitrogen). It was very important to avoid passing $1x10^6$

because a rapid cell death could occur. We could isolate a positive monoclonal antibody anti-FPC4, called 3B10.

The antibody isotype was determined with the IsoStrip^{TM} Monoclonal Antibody Isotyping kit (Santa Cruz—sc-24958).

3. RESULTS

3. Results

I. BILBO1 is a scaffold protein for the Flagellar Pocket Collar

a) Introduction

As described in the introduction, a ring-shaped structure is present at the flagellum exit point and it is called the FPC for Flagellar Pocket Collar. BILBO1 is the first characterized cytoskeletal protein present within this structure and, currently, it is not clear how the FPC is made (Bonhivers et al., 2008b; Vidilaseris et al., 2014a; Vidilaseris et al., 2014b). BILBO1 is a modular protein composed of an N-terminal domain showing an ubiquitin-like fold, two EF-Hand domains (EF-Hands) able to bind calcium and a long C-terminal coiled-coil domain (CC) with a leucine zipper (LZ) (Bonhivers et al., 2008b; Vidilaseris et al., 2014a; Vidilaseris et al., 2014b).

We carried out an analysis of the roles of the different domains of BILBO1 in the structure and function of the FPC. To do so we used yeast-two-hybrid interaction tests, a mammalian cell heterologous system and *T. brucei* expression of recombinant BILBO1 and BILBO1 domains. The collaboration with the group of Dr. Gang Dong (MPFL, Vienna) allowed an Isothermal Titration Calorimetry (ITC) analysis of calcium binding.

We showed that BILBO1 has intrinsic polymerization properties via its CC and that calcium plays a role in the shape of the polymers. Furthermore, we showed that the N-terminal domain is not required either for FPC targeting or for polymerization.

We propose that BILBO1 forms a scaffold structure upon which other proteins can anchor to in order to form the FPC and connect with other cytoskeletal structures. Additionally, we propose that calcium could play a role in the function or the dynamics of the FPC by modulating the conformation of BILBO1 and thus the polymer properties, or the interaction with other proteins.

b) Results – 1st part

"Florimond *et al*. (2015), BILBO1 is a scaffold protein of the Flagellar Pocket Collar in the pathogen *Trypanosoma brucei*, PLoS Pathog 11(3)"

PLOS | PATHOGENS

RESEARCH ARTICLE

BILBO1 Is a Scaffold Protein of the Flagellar Pocket Collar in the Pathogen *Trypanosoma brucei*

Célia Florimond[1,2¤a], Annelise Sahin[1,2¤b], Keni Vidilaseris[3], Gang Dong[2,3], Nicolas Landrein[1,2], Denis Dacheux[1,2,4], Anna Albisetti[1,2], Edward H. Byard[1,2¤c], Mélanie Bonhivers[1,2‡], Derrick R. Robinson[1,2‡*]

1 University Bordeaux, Microbiologie Fondamentale et Pathogenicité, Bordeaux, France, **2** CNRS, Microbiologie Fondamentale et Pathogénicité, UMR 5234, Bordeaux, France, **3** Max F. Perutz Laboratories, Medical University of Vienna, Vienna, Austria, **4** Institut Polytechnique de Bordeaux, Microbiologie Fondamentale et Pathogénicité, UMR-CNRS 5234, Bordeaux, France

¤a Current address: Department of Microbiology and Immunology, University at Buffalo School of Medicine, Buffalo, New York, United States of America
¤b Current address: CBMN-UMR 5248 Chimie et Biologie des Membranes et des Nanoobjets, Equipe Architecture de Complexes Membranaires et Processus Cellulaires, Pessac, France
¤c Current address: Department of Biology, University of Winnipeg, Winnipeg, Canada
‡ These authors contributed equally to this work.
* derrick-roy.robinson@u-bordeaux.fr

OPEN ACCESS

Citation: Florimond C, Sahin A, Vidilaseris K, Dong G, Landrein N, Dacheux D, et al. (2015) BILBO1 Is a Scaffold Protein of the Flagellar Pocket Collar in the Pathogen *Trypanosoma brucei*. PLoS Pathog 11(3): e1004654. doi:10.1371/journal.ppat.1004654

Editor: Kent L. Hill, University of California, Los Angeles, UNITED STATES

Received: April 4, 2014

Accepted: January 4, 2015

Published: March 30, 2015

Data Availability Statement: All relevant data are within the paper and its Supporting Information files.

Funding: This work was funded by the Centre National de la Recherche Scientifique (CNRS), Aquitaine Regional Council Grant - 20111301014, (ANR-09-BLAN-0074), Preciput-ANR grant from the University of Bordeaux and a Labex - "ParaFrap" - Alliance Française Contre les Maladies Parasitaires. CF was a recipient of the Région Martinique Ph.D. fellowship. The funders had no role in study design, data collection and analysis, decision to publish, or preparation of the manuscript.

Abstract

The flagellar pocket (FP) of the pathogen *Trypanosoma brucei* is an important single copy structure that is formed by the invagination of the pellicular membrane. It is the unique site of endo- and exocytosis and is required for parasite pathogenicity. The FP consists of distinct structural sub-domains with the least explored being the annulus/horseshoe shaped flagellar pocket collar (FPC). To date the only known component of the FPC is the protein BILBO1, a cytoskeleton protein that has a N-terminus that contains an ubiquitin-like fold, two EF-hand domains, plus a large C-terminal coiled-coil domain. BILBO1 has been shown to bind calcium, but in this work we demonstrate that mutating either or both calcium-binding domains prevents calcium binding. The expression of deletion or mutated forms of BILBO1 in trypanosomes and mammalian cells demonstrate that the coiled-coil domain is necessary and sufficient for the formation of BILBO1 polymers. This is supported by Yeast two-hybrid analysis. Expression of full-length BILBO1 in mammalian cells induces the formation of linear polymers with comma and globular shaped termini, whereas mutation of the canonical calcium-binding domain resulted in the formation of helical polymers and mutation in both EF-hand domains prevented the formation of linear polymers. We also demonstrate that in *T. brucei* the coiled-coil domain is able to target BILBO1 to the FPC and to form polymers whilst the EF-hand domains influence polymers shape. This data indicates that BILBO1 has intrinsic polymer forming properties and that binding calcium can modulate the form of these polymers. We discuss whether these properties can influence the formation of the FPC.

Competing Interests: The authors have declared that no competing interests exist.

Author Summary

Trypanosoma brucei avoids destruction by, in part, changing its surface glycoprotein coat, which is trafficked onto the cell surface *via* an invagination of the cell surface called the flagellar pocket. The pocket is essential for pathogenicity. The distal membrane of the pocket is anchored to a cytoskeleton structure called the flagellar pocket collar (FPC). The FPC is a ring/horseshoe shaped structure, which itself is attached to the single copy flagellum of the parasite. How the "ring" shape of the collar is formed is not understood. Moreover, the only known protein component of the FPC is the protein BILBO1. BILBO1 is modular and has a distinct N-terminal domain, two EF-hand calcium-binding domains and a large C-terminal coiled-coil domain. Here we demonstrate that mutating the EF hand domains prevent calcium binding and that the coiled-coil domain is not only sufficient to target to the collar, but can also form polymers in mammalian cells. Mutating either or both calcium-binding domains of BILBO1 influences polymer formation and type when expressed in mammalian and trypanosome cells. Our premise is that BILBO1 has intrinsic polymer forming properties that are essential for the flagellar pocket collar making the pocket a target for intervention.

Introduction

Trypanosoma brucei is an important parasitic protozoan that is the etiological agent of sleeping sickness in sub-Saharan Africa. Related parasites are responsible for Chagas disease and Leishmaniasis in South America and many tropical countries [1,2,3]. At the G1 stage of the *T. brucei* cell cycle a single flagellum exits the cell through the flagellar pocket (FP), a structure that is located in the posterior end of the cell. The FP functions as the exclusive site for endo- and exocytosis, and has been shown to be an essential component of membrane trafficking and recycling [4,5,6]. In these roles the FP is essential for parasite virulence, because *T. brucei* must survive within both the gut and salivary glands of the tsetse fly as well as in the bloodstream of the mammalian host. Thus the FP is also most likely a functional design to sequester important parasite surface receptors away from detection by the host's innate immune system [5,7].

The tight coupling between the FP, the flagellum, and the cytoplasmic membranes has been well established in recent studies where work on the *T. brucei* FP and associated cytoskeleton suggest that new FP biogenesis is precisely timed to coordinate with flagellum duplication and segregation [6,8]. Electron microscopic imaging and tomography clearly illustrate that a cytoskeletal structure called the flagellar pocket collar (FPC), a horse-shoe/annular structure, of approximately 500–800 nm in diameter, in *T. brucei*, is present at the exit point of the flagellum [4,6,9]. The FPC surrounds the flagellum and is also attached to the sub-pellicular microtubule cytoskeleton [6,8], but it is not known how it is attached, nor is it apparent how the FPC always forms its characteristic shape around a newly formed flagellum. Recently, an important structure called the bilobe has been identified as being closely associated with the FPC. The bilobe is considered to be a Golgi-linked structure that contains Centrin 2, and numerous other proteins [9,10,11]. The intimate relationship between the FP-flagellum, the bilobe and Golgi [12] suggests that at least some of these structures are physically linked [11].

As we demonstrated previously, BILBO1 is syntenic and essential for biogenesis of the FPC [8]. RNAi knockdown of BILBO1 in *T. brucei* disrupts the formation of the FPC, inhibits the biogenesis of important cytoskeleton structures, induces severe perturbation of the endo-membrane system, cell cycle arrest, and is ultimately lethal. BILBO1 is the first, and to date the only,

FPC molecular component identified that is required for FPC and FP biogenesis, which makes it a potentially important target for intervention against kinetoplastids [8].

Recently, the three-dimensional structure of BILBO1 N-terminal domain was solved and revealed that it contains an unexpected ubiquitin-like fold with a conserved surface patch [13,14]. Mutation of the patch was lethal when expressed in *T. brucei* procyclic forms suggesting that there are important interactions between the patch and other BILBO1 protein partners [13,14]. Using electron microscopy Vidilaseris *et al.*, demonstrated that the EF-hand domains of BILBO1 change their conformation upon calcium binding, and the coiled-coil domain can form anti-parallel dimers, which can then form linear polymers *via* the C-terminal leucine zipper. Further, they demonstrated that these filaments can condense into fibers through lateral interactions [15].

In this study, we turn to an analysis of BILBO1 protein as an essential candidate of the FPC scaffold. Our overall objective was to identify the molecular role of BILBO1 in FPC formation. The primary and secondary structures of BILBO1 do not predict a specific function, and the protein does not appear to have any obvious membrane-targeting domains, but it does possess two predicted EF-hand calcium-binding domains (aa 185–213 and aa 221–249). It also has a large coiled-coil (CC) domain (aa 263–566), which is involved in protein-protein interactions [15]. Based on our hypothesis that BILBO1 is the FPC scaffold, we decided to determine 1) if BILBO1 can form polymers *in vivo*, 2) what domain(s) of the protein is(are) involved in polymer formation. We approached these questions with the following experiments; 1) Identification of functional domains involved in BILBO1-BILBO1 interaction by yeast-two hybrid analysis 2), test for intrinsic polymer formation properties of BILBO1 using a heterologous mammalian expression system and 3), characterization of these properties in the parasite.

We demonstrate in this work that BILBO1 can form polymers *in vivo* and propose that these may have important implications for the formation of the annulus/horseshoe of the FPC. The results we report here point to a substantial role for BILBO1 in forming the structural scaffold for FPC biogenesis and maintenance.

Results

BILBO1-BILBO1 interaction is *via* the coiled-coil domain

Yeast-Two-Hybrid (Y2H) analysis has been used to test interactions between soluble proteins, but also between polymer forming proteins [16,17,18]. We used this technique to test if BILBO1 could form homo-polymers and, if yes, identify the domains that are involved in this interaction. For this study several BILBO1 truncations were constructed and were named as follows; T1 for the N-terminal domain (aa 1–170), T2 for the N-terminal domain including both EF-hand calcium-binding domains (aa 1–250), T3 for the CC domain including the two EF-hand domains up to the C-terminus (aa 171–587), and T4 for the CC domain up to the C-terminus (aa 251–587) (Fig. 1A). BILBO1 and its truncations tested negative for toxicity and auto-activation in these Y2H experiments.

Interactions were visualised using two auxotrophic assays with similar results (minus Adenine is shown in Fig. 1B). As yeast growth was observed when full-length BILBO1 construct was tested (Fig. 1B), our assays show that there is a BILBO1 x BILBO1 interaction (full-length x full-length). Further, they show that the coiled-coil domain is required for the interaction (full-length x T3, or full-length x T4), and that neither the N-terminal domain (T1 and T2) nor the EF-hand domains 1 and 2 are required in this interaction *per se* (Fig. 1B).

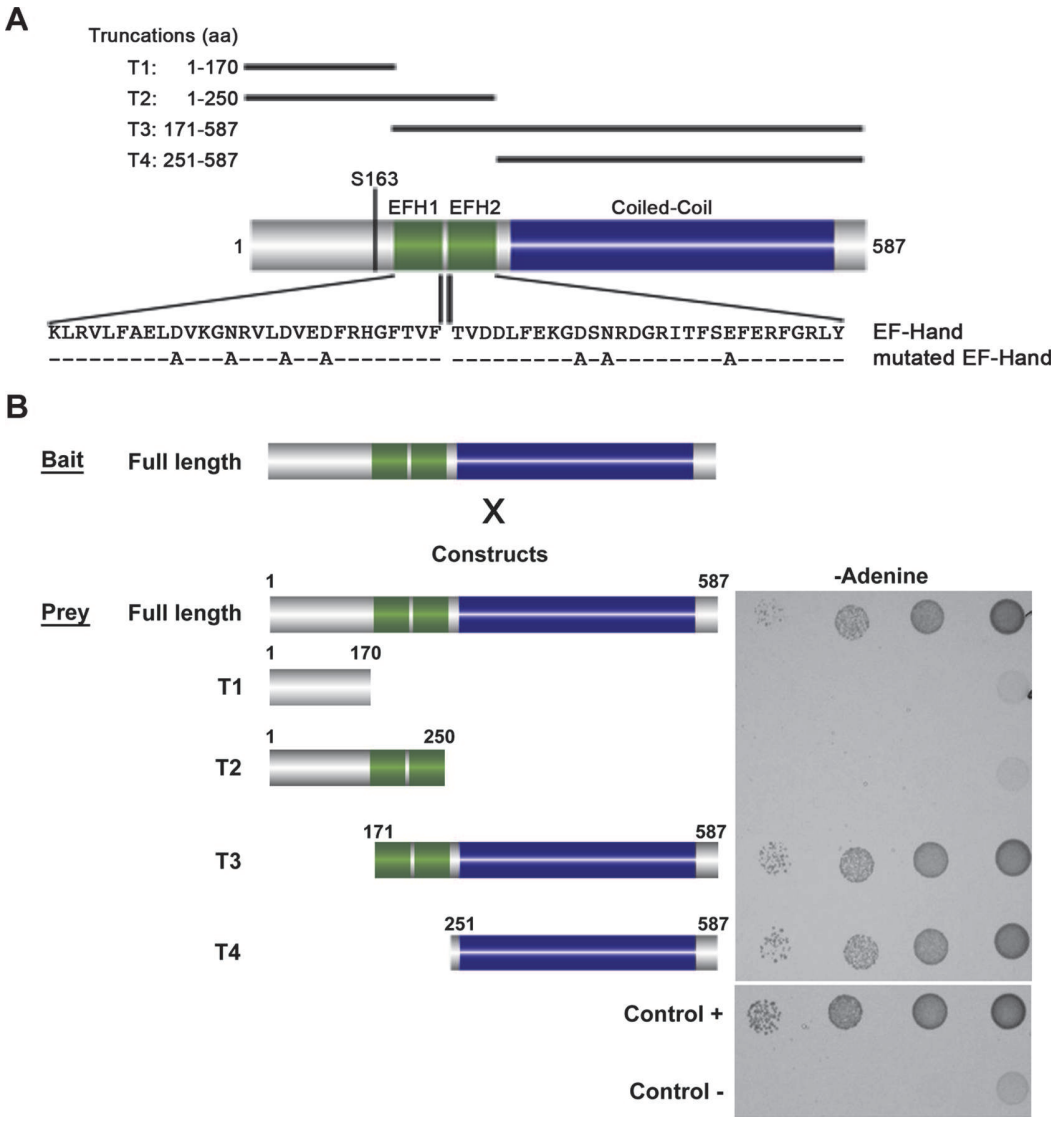

Fig 1. Schematic diagram of BILBO1 primary structure and yeast two-hybrid identification of its interaction domains. (A) BILBO1 has two predicted EF-hand calcium-binding domain EFH1 and EFH2, from amino acids Lysine 185 to Tyrosine 249, and a long domain predicted as coiled-coil. Serine 163 is phosphorylated *in vivo*. The main truncations used in this study are shown schematically and labelled as T1-T4. The mutations in the EF-hand calcium binding domains are indicated below the wild-type amino acid sequence. (B) Bait (BILBO1 full-length) and prey interactions were tested by drop tests on adenine-free selective medium. Full-length BILBO1 interacts with full-length BILBO1, whilst truncations T1 and T2 do not interact with full-length BILBO1. T3 and T4 truncations interactions were positive, demonstrating that the coiled-coil domain is required for BILBO1-BILBO1 interaction.

doi:10.1371/journal.ppat.1004654.g001

Both BILBO1 EF-hand domains bind calcium

BILBO1 has two putative calcium-binding EF-hand domains that are located between the N-terminus and the coiled-coil domain. *In silico* analysis of these EF-hand domains indicate that domain1 is non-canonical (12-residue loop—aa 194–205, but contains a lysine at position +Y, whereas this is typically aspartic acid or asparagine), but domain 2 is canonical (12-residue loop—aa 230–241) [19,20,21]. The 3D structure of the N-terminus of BILBO1 has been solved, but the domain analyzed does not contain the EF-hands [14].

To characterize further the EF-hand domains, we tested the wild-type and mutated forms for calcium binding properties using isothermal calorimetry (ITC) [22]. The DNA sequence encoding the EF-hand domains (amino acid residues 177–250) of wild-type BILBO1 were cloned to incorporate a N-terminal maltose-binding tag plus a 10 × histidine tag (MBP-His_{10}). This construct was used as a template to make the mutated forms of the EF-hand domains. For the mutant forms the following amino acid substitutions were created: Mutated EF-hand 1 (mEFH1: D194A, N198A, D202A, and D205A), and mutated EF-hand 2 (mEFH2: D230A, N232A, and E241A), or both mutated EF-hands (mEFH1+2). The amino acids selected for mutation were based on published analysis of EF-hand function by Gifford *et al.*,[19].

A schematic of BILBO1 is shown in Fig. 2A, whilst Fig. 2B shows the purified proteins on an SDS-PAGE with Coomassie blue staining. The minor bands present under the 50kDa main bands are degradation products. Fig. 2C illustrates a superimposition of BILBO1-EF-hand domains onto the modeling template of the human calmodulin-like protein hCLP (1ggz.pdb) [23]. The two proteins share 30% identity and 47% similarity in their primary sequences, which gave rise a very similar conformation with a root-mean-square deviation (r.m.s.d) of 0.82 Å over 70 aligned residues of the two structures. A ribbon diagram of the BILBO1-EF-hand domains derived from homology-based modeling, together with the two bound calcium ions from the template structure (1ggz.pdb), is shown in Fig. 2D. ITC demonstrated that the wild-type BILBO1 EF-hand domains do bind 2 calcium ions (Fig. 2E, N = 2.11, Kd = 3.46 μM), whereas mutation of either or both EF-hand domains caused loss of calcium binding (Fig. 2F-H). As a negative control, no calcium binding was observed for the MBP fusion tag alone (Fig. 2 I).

BILBO1 has polymers forming properties *in vivo*

To explore the possibility that BILBO1 can form polymers, it was expressed in an *in vivo* heterologous system in the absence of any other parasite-specific proteins. Since BILBO1 has no known mammalian orthologues, we can investigate the polymers formed in U-2 OS cells in detail albeit out of context of the FPC. By transient transfection of U-2 OS cells, we expressed full-length, untagged BILBO1 protein or BILBO1:GFP and analyzed the polymers formed. We acknowledge that there may be other proteins interacting with BILBO1 when expressed in these cells and these can contribute to polymer formation. Nevertheless, direct GFP fluorescence, immuno-labelling of untagged BILBO1 with the anti-BILBO1 monoclonal antibody 5F2B3 or electron microscopy illustrated that expression from six to 24 hours resulted in the formation of long fibrous polymers (Fig. 3A—D also refer to S1 Fig.). Thus, confirming our hypothesis that BILBO1 can indeed form polymers *in vivo*. We noticed the formation of numerous isolated annular structures when BILBO1:GFP was expressed in U-2 OS cells, but since this appears to be a GFP-tag induced artefact, these structures were not analyzed further (Fig. 3A and 3G, and S2 Fig.).

Polymers that started or terminated with globular, or annular/comma, shaped structures, were observed when untagged BILBO1 was expressed (Fig. 3B-F). When viewed by transmission electron microscopy these polymers had transversal striations that were observed after negative staining to have a mean periodicity of 46.9 nm (n = 1067, SE± 0.4nm) indicating the formation of highly ordered polymers, (Fig. 3C-F). Interestingly, this is similar to the inter N-termini distance of anti-parallel BILBO1 proteins (40–45nm) observed by Vidilaseris *et al.*, 2014 [15], suggesting a similar assembly arrangement of polymers. A similar periodicity was also observed with the BILBO:GFP construct, but since GFP induces artefacts these striations were not analyzed in detail (Fig. 3G). We have categorized the linear polymers observed by immunofluorescence as "simple"' or "complex". Simple polymers have no distinguishable features at their ends, whereas complex polymers have comma or globular structures at one or both ends. To facilitate nomenclature, these structures, from here onwards, will be referred to

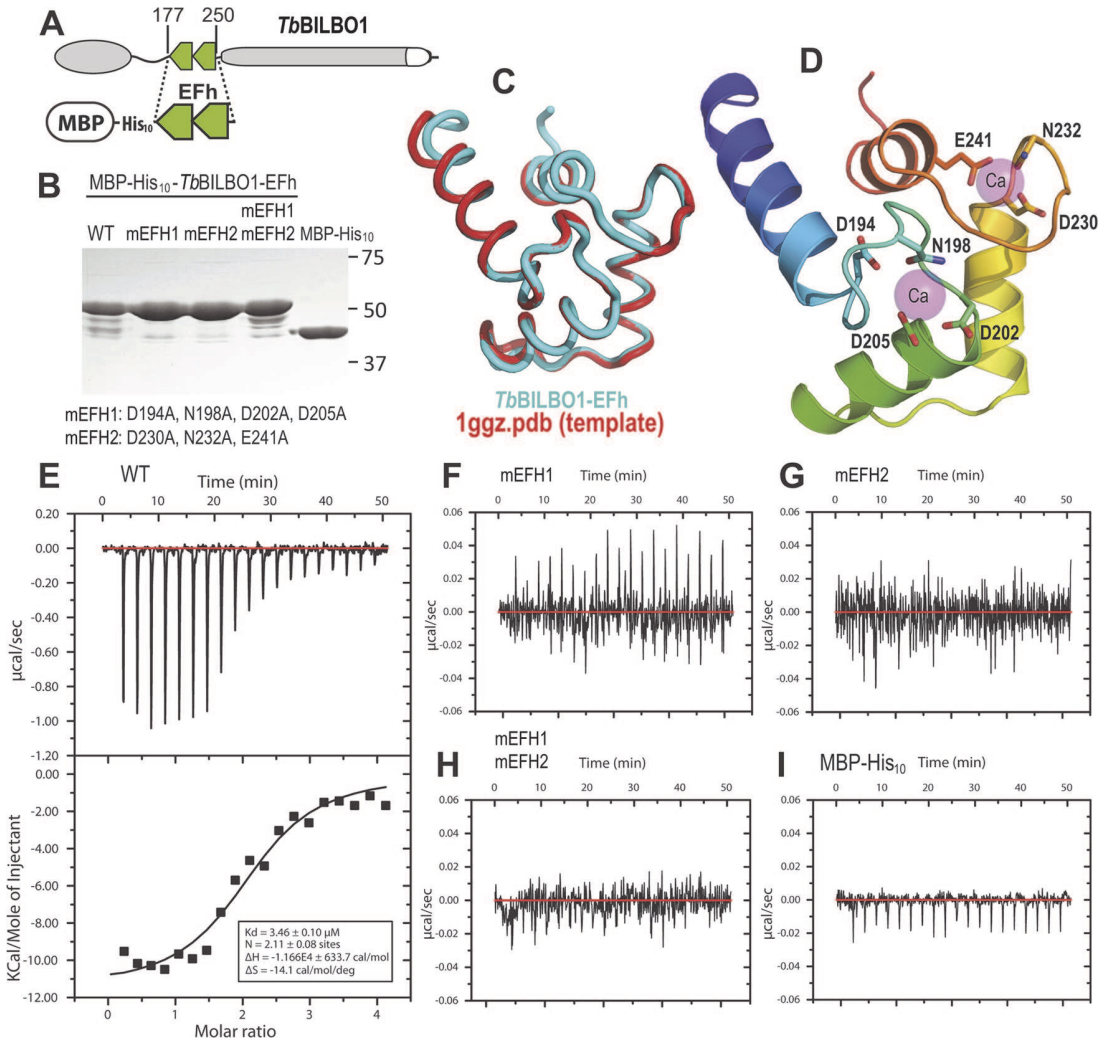

Fig 2. The conserved residues in the loops of the EF-hand domains are required for calcium binding. (A) Schematic depicting the *Tb*BILBO1-EFh (residues 177–250) expression construct used in the *in vitro* calcium-binding experiments. The protein was expressed with an N-terminal tag containing maltose-binding protein (MBP) together with a 10 × histine linker. (B) Purified proteins of wild-type (WT) and three mutants of MBP-His_{10}-TbBILBO1-EFh were analyzed by SDS-PAGE and stained using Coomassie blue. The minor bands are degradation products. The last lane shows purified MBP-His_{10} alone. (C) Superimposition of the *Tb*BILBO1-EFh model onto the modeling template 1ggz.pdb, (a human epithelial cell calmodulin-like protein). The two proteins share 30% identities and 47% similarities in their primary sequences. (D) Ribbon diagram of the *Tb*BILBO1-EFh derived from homology-based modeling shown in (C). The structure is color-ramped from blue at the N-terminus to red at the C-terminus. Conserved D/E/N residues in the loops, which are predicted to coordinate calcium binding, are shown as sticks. The two calcium sites from the modeling template (1ggz.pdb) are shown as semi-transparent magenta spheres. (E) ITC titration and fit curve for the wild-type *Tb*BILBO1-EF-hand domains. N, which represents the molar ratio between Ca^{2+} and the protein, was determined to be approximately 2, suggesting that both EF-hand domains of *Tb*BILBO1 bind calcium. (F-H) ITC titration results for mEFH1, mEFH2, and mEFH1+2. None of the three mutants were able to bind calcium. (I) ITC titration result for the MBP-His_{10} tag. The fusion tag by itself did not bind calcium.

doi:10.1371/journal.ppat.1004654.g002

collectively as "termini". Fig. 3C-F illustrates termini when visualised by electron microscopy and show that the shapes of these termini are varied. Termini that looked like "spheres" using immunofluorescence are actually dense globular structures when viewed by electron microscopy (Fig. 3E). Formation of these globules maybe due to non-specific aggregation but it is not apparent how comma/annuli are formed, but they appear to be shaped when termini curl back upon themselves.

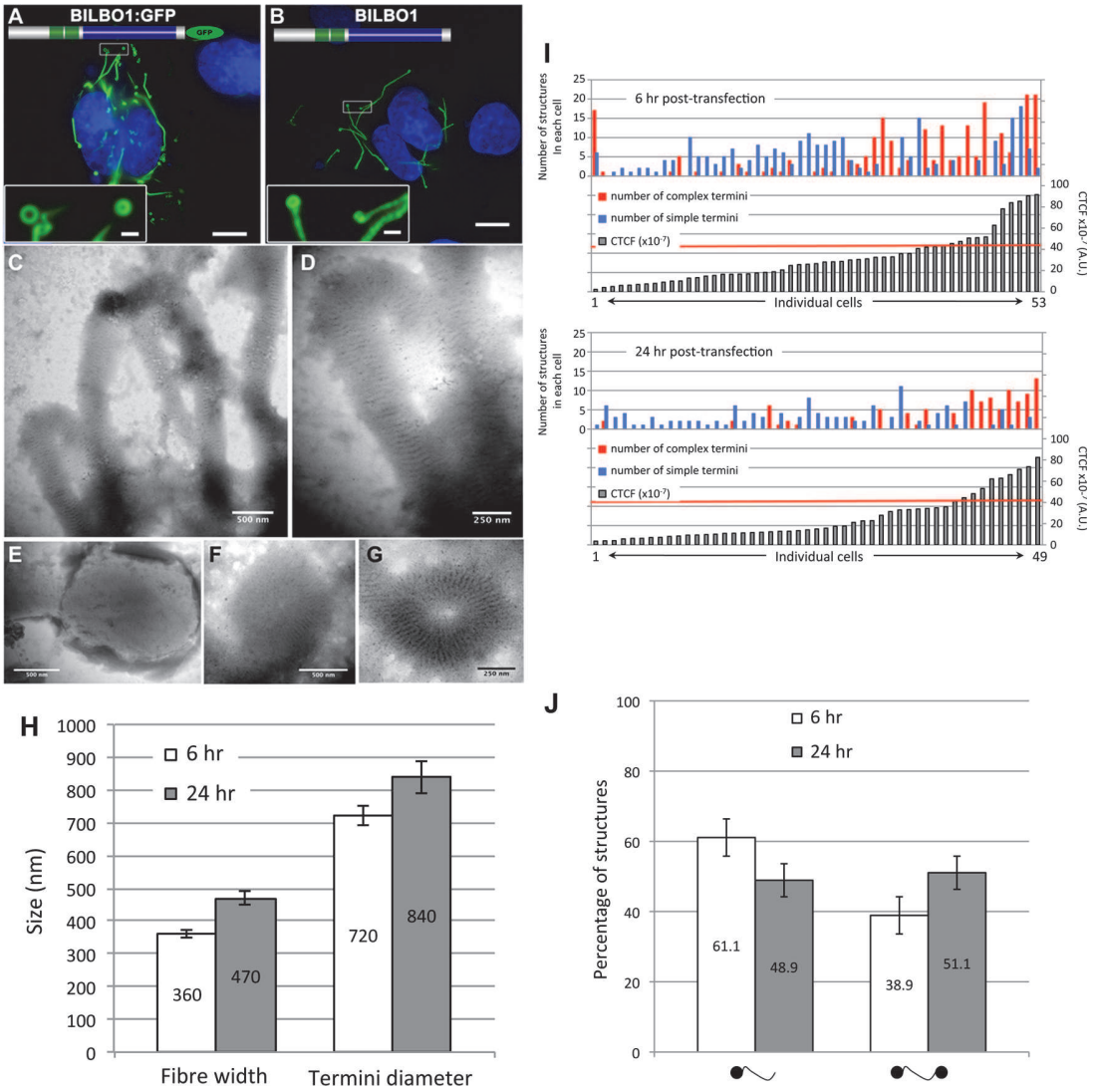

Fig 3. BILBO1 forms polymers in a heterologous system and the coiled-coil domain is required for polymerization. Heterologous expression of BILBO1:GFP (A), or un-tagged BILBO1 (B) in mammalian U-2 OS cells demonstrate that BILBO1 has self-polymerizing properties. After 6 hours post-transfection of BILBO1:GFP the polymers formed were observed by direct GFP fluorescence. After 6 hours post-transfection of un-tagged BILBO1, extracted cells were immuno-labelled with anti-BILBO1 monoclonal antibody. (C-F) Electron micrograph of extracted and negative stained U-2 OS cells after six hours of BILBO1 expression. (G) Electron micrograph of extracted and negative stained U-2 OS cells after six hours of BILBO1:GFP expression. (H) Measurements of fibre width and diameter of termini in U-2 OS cells expressing BILBO1 after six or 24 hours post-transfection and immunolabelled with anti-NTD. (I) Measurements of total fluorescence emitted per cell, as arbitrary units, after a fixed time of acquisition on anti-NTD immunolabelled BILBO1 expressing U-2 OS cells, and number of complex or simple termini in each corresponding cell. The red line indicates the 50% of maximum fluorescence intensity limit. (J) Determination of the percentage of complex polymers with termini at one end (left) or at both ends (right) in BILBO1 U-2 OS expressing cells after six or 24 hours transfection. Scale bars represent 10 μm in A and B, 1 μm in insets, 500 nm in C, E, F, and 250nm in D, G.

doi:10.1371/journal.ppat.1004654.g003

Polymers could be observed by immunofluorescence microscopy whereas the cell extraction procedure required for electron microscopy removed most of the polymers making them difficult to observe, despite numerous attempts to do so. We therefore measured the width of the BILBO1 fibres and the diameter of the termini using immunofluorescence microscopy. Globules and commas were sometimes difficult to distinguish by immunofluorescence and were therefore grouped together and counted as termini. We also counted the number and type of polymers

Table 1. Mean termini diameter, fibre width, and termini formation of untagged BILBO1 after expression in U-2 OS cells.

Post transfection time	Fibre width	Termini diameter	Polymers with complex termini / cell
6h	**360 nm** (SE± 10) *n* = 100	**720 nm** (SE± 30) *n* = 110	**61.1%** termini at one end (SE± 5.3) *n* = 23 **38.9%** Termini at both ends (SE± 5.3) *n* = 23
12h	**470 nm** (SE± 20) *n* = 94	**840 nm** (SE± 50) *n* = 109	-
24h	-	-	**48.9%** termini at one end (SE± 4.7) *n* = 61 **51.1%** Termini at both ends (SE± 4.7) *n* = 61

- indicates not done.

doi:10.1371/journal.ppat.1004654.t001

with complex termini per cell after six and 24 hours of untagged BILBO1 post transfection, (please refer to Table 1 and Fig 3H and 3J).

Measurements of BILBO1 fibre width and termini diameter was done using immunofluorescence microscopy. Measurements were made after six and 12 hours, whereas complex termini were measured after six and 24 hours. Fibre width and the number of fibres with termini at both ends increased over time.

From this data and the electron microscopy results we conclude that BILBO1 has the intrinsic capacity to polymerize into organized high order polymers in mammalian cells (in the absence of any other parasite-specific proteins) and these polymers have a tendency to form complex termini at their extremities. Reiterating the results from Fig. 3I this data suggests that the polymerization state of BILBO1 is likely to be highly dependent on the expression level of the protein or local protein concentration.

In addition to these measurements we measured the total fluorescence emitted per cell, as arbitrary units, after a fixed time of acquisition. We used the fluorescence intensity produced by each cell as a marker for protein concentration per cell. We then divided the population into two groups—cells producing less than 50% of the maximum fluorescence recorded, and cells producing more than 50% of the maximum fluorescence recorded.

After six hours of expression of untagged BILBO1 81% of cells produced 50% or **less** of the maximum fluorescence recorded/cell, and 37.2% of these cells contained polymers with only simple termini, whilst 11.6% contained polymers with complex termini and 51.2% contained both types of polymer. 19% of cells produced **more** than 50% of the maximum fluorescence recorded/cell, and 20% of these cells contained polymers with simple termini, whilst 30% contained complex polymers and 50% contained both types of polymer (Fig. 3I).

After 24 hours of expression of untagged BILBO1, 81.7% of cells produced 50% or **less** of the maximum fluorescence recorded/cell and 70% these cells contained polymers with simple termini, whilst 10% contained polymers with complex termini and 20% contained both types of polymer. 18.3% of cells produced **more** than 50% of the maximum fluorescence recorded/cell and 11.1% these cells contained polymers with only simple termini, whilst 44.4% contained polymers with only complex termini and 44.5% contained both types of polymer (Fig. 3I, 24 hours post-transfection). Taken together this data reiterates the hypothesis that the polymerization state of BILBO is likely to be highly dependent on the expression level of the protein.

To investigate whether the BILBO1 polymers were associated with pre-existing or newly formed cytoskeleton structures, U-2 OS cells expressing BILBO1:GFP were additionally labelled for F-actin (phalloidin), intermediate filaments (anti-vimentin), microtubules (anti-tubulin), endoplasmic reticulum Golgi (anti-giantin) and (anti-calnexin). The results presented in S2 Fig. demonstrate that BILBO1:GFP does not co-localize with any of these structures. We

conclude that the polymers formed by BILBO1 are not promoted by the interaction with the ER, Golgi or the cytoskeletal structures tested.

The coiled-coil domain is required for polymer formation *in vivo*

Phosphorylation or dephosphorylation can induce conformational or interaction changes in proteins. Our LC-MS/MS analysis on procyclic form (PCF) whole cell extracts identified one phosphorylated residue (S163) as already described in *T. cruzi* bloodstream forms and *T. brucei* procyclic forms BILBO1 [24,25]. We postulated that phosphorylation and/or dephosphorylation of serine 163 could induce a conformational change leading to polymer shape changes. Mutation of BILBO1 serine 163 to non-phosphorylatable alanine, or to phosphomimetic aspartic acid, did not influence the type of polymers formed when expressed in U-2 OS cells suggesting that the phosphorylation of serine 163 is not regulating the conformation of BILBO1 or at least polymer formation.

Since phosphorylation of serine 163 did not influence polymer formation we interrogated BILBO1 in detail to identify the domain(s) that permit polymer formation. Thus, we expressed truncated forms of untagged BILBO1 in U-2 OS cells and localized the truncations using immunofluorescence with the monoclonal antibody specific to the CC domain (anti-BILBO1, 5F2B3) [8], or a polyclonal antibody specific to the N-terminal domain of BILBO1 (amino acids 1–110, anti-NTD) [9].

The truncation T1 did not produce polymers, and was uniformly distributed throughout the cytoplasm (Fig. 4A). Additionally, T1 labelling could be extracted by mild detergent treatment and is found in the soluble fraction (S) by western-blot (WB) whilst full-length BILBO1 is found in the insoluble fraction (P) (Fig. 4E). T2 was also extracted with detergent treatment, and

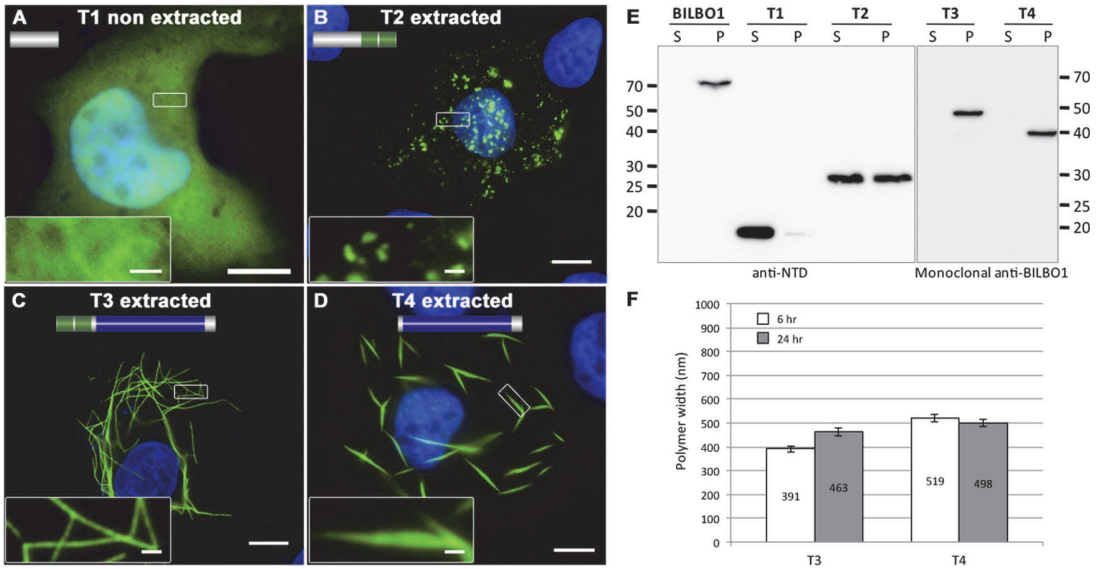

Fig 4. BILBO1 has self-polymerizing properties via its coiled-coil domain. (A-D) Immunofluorescence panels. Heterologous expression of T1 (A), T2 (B), T3 (C), and T4 truncations (D) in U-2 OS cells demonstrate that BILBO1 has self-polymerizing properties *via* its coiled-coil domain. After 6 hours post-transfection, cells expressing the different constructs were immunolabelled using anti-NTD (T1, T2) or 5F2B3 (T3, T4). The inserts in the bottom left of panels represent higher magnifications of structures observed in these panels. Scale bars represent 10 μm, and 1 μm in magnified insets. (E) Western blots probed with anti-NTD (BILBO1, T1, T2) or 5F2B3 (T3, T4) against proteins samples collected from U-2 OS cells after six hours of expression. Samples were collected from pellet and supernatant of detergent extracted cells. BILBO1, T3 and T4 are insoluble. T1 is primarily soluble and T2 is partially soluble. Predicted relative molecular masses (using ExPASy compute pI/Mw) of truncations are T1 = 19kDa, T2 = 25.25kDa, T3 = 48.3kDa, T4 = 39kDa. (F) Measurements of structure width in polymers formed by T3 and T4 truncation at six and 24 hr post-transfection.

doi:10.1371/journal.ppat.1004654.g004

Table 2. Mean T3 and T4 width after expression in U-2 OS cells.

Post transfection time	T3 mean width	T4 mean width
6h	**391 nm** (SE± 13) *n* = 193	**519 nm** (SE± 16) *n* = 102
24h	**463 nm** (SE± 18) *n* = 155	**498 nm** (SE± 15) *n* = 119

Measurements of the mean T3 and T4 width was done at six and 24 hours of expression in U-2 OS cells. Mean T3 width increased over time whereas T4 did not.

doi:10.1371/journal.ppat.1004654.t002

indicates that T2 is soluble, but can form small, insoluble, punctate aggregates (Fig. 4B, and 4E). The data also suggests that aggregation is likely to be highly dependent on expression level of the protein.

Confirming the Y2H interaction results described earlier, T3 and T4 formed linear polymers (T3) and spindle shaped polymers (T4), but no termini were observed on these fibres (Fig. 4C-D). Similar to full-length BILBO1 these polymers are insoluble and were only found in the pellet fraction by WB (Fig. 4E). Taken together, these results demonstrate that neither the N-terminal domain (corresponding to T1 and T2) nor the EF-hands form linear polymers, but they can influence the type of polymer formed by the CC domain.

We then turned to T3 and T4 and measured the width of induced polymers after six and 24 hours post transfection, (please refer to Table 2 and Fig. 4F). From these measurements we noted an increase in T3 polymer width over time compared to T4, which suggests easier lateral binding of T4 to polymers, and/or may reflect differences in protein expression levels.

The EF-hand domains influence BILBO1 polymer formation *in vivo*

Since we have established that both BILBO1 EF-hand domains bind calcium and that BILBO1 can form polymers *in vivo*, we wanted to test the potential role of the EF-hand domains in modulating polymers formed in U-2 OS cells. We therefore expressed mutated forms of EF-hand domain 1 (mEFH1), EF-hand domain 2 (mEFH2), or both mutated EF-hand domains (mEFH1+2) in U-2 OS cells (Fig. 5). Mutation of EF-hand domain 1 had a substantial effect on polymerization because the formation of long polymers was abolished, and only small insoluble punctate aggregates were observed (Fig. 5A). Similar aggregates were observed when both EF-hand domains 1 and 2 were mutated (mEFH1+2) (Fig. 5C).

Surprisingly, six-hour expression of mEFH2 resulted in the formation of insoluble helical-like, comma and annular polymers (Fig. 5B, D). Attempts to visualize these by electron microscopy failed due possibly to loss of sample upon cell extraction and/or poor visualization because of the presence of cell debris. Nevertheless, using immunofluorescence we classified them and measured their dimensions six hours post transfection, (please refer to Table 3 and Fig. 5E). The results of these data suggest that EF-hand 2 can radically influence the type of polymer formed, but it also illustrates that these structures have similar diameters even though they can be a helix, comma or annulus in shape (Fig. 5E). Interestingly, the FPC diameter in wild-type *T. brucei* cells is 842 nm, which is a diameter comparable to those of the mEFH2-induced structures (please refer to Table 3).

Western blots of untagged and mutated BILBO1 proteins, that were expressed in U-2 OS cells, were probed with anti-NTD, and show that all proteins were present in the pellet fraction of extracted cells (~ 70 kDa band) and that anti-NTD recognises the full-length proteins (Fig. 5F upper panel). The mouse monoclonal 5F2B3 recognizes the C-terminus of the CC domain of these proteins and also recognises the full-length proteins, whereas anti-NTD recognises full-length proteins and the N-terminus. 5F2B3 labelling also revealed a lower band

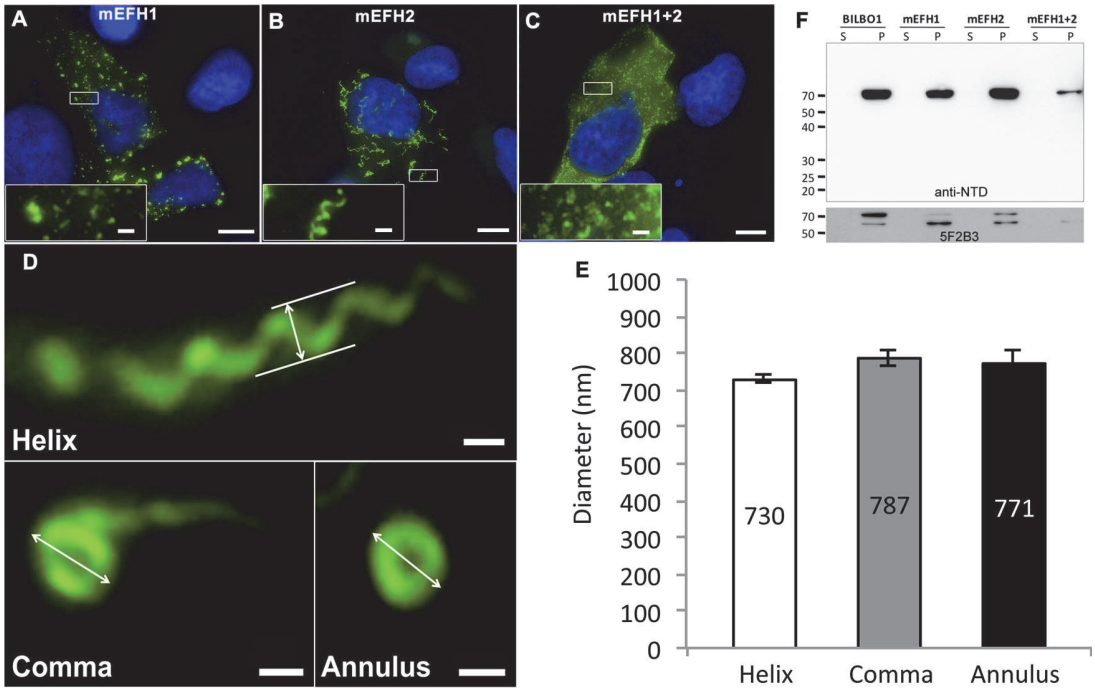

Fig 5. The EF-hand domains modulate the morphology of polymers formed by BILBO1. (A-D) Immunofluorescence panels. EH-Hand motif 1, EF-hand motif 2 and both motifs were mutated by site-directed mutagenesis (see Fig. 1). The resulting mutant proteins mEFH1 (A), mEFH2 (B), and mEFH1+2 (C) were expressed for six hours in U-2 OS cells, and the resulting polymers were immuno-localized using the anti-NTD antibody. The inserts in the bottom left of panels represent higher magnifications of structures observed in these panels. Scale bars represent 10 μm, and scale bars in magnified insets represent 1 μm. (D) Enlarged views of the helix, comma and annulus shaped polymers formed by mEFH2 in U-2 OS cells 24 hours post-transfection. Scale bar represents 500 nm. (E) Helix, comma and annulus shaped polymers have comparable dimensions as shown by the measurements of their respective diameters. (F). A western blot probed with anti-NTD (upper panel) against protein samples collected from U-2 OS cells after six hours of expression of BILBO1, mEFH1, mEFH2 or mEFH1+2 proteins. Samples were collected from pellets and supernatants of detergent extracted cells. BILBO1, mEFH1, mEFH2 and mEFH1+2 were insoluble and subject to degradation as shown with the anti-BILBO1 5F2B3 monoclonal antibody labelling (lower panel) that recognizes the coiled-coil domain.

doi:10.1371/journal.ppat.1004654.g005

of ~ 60kDa indicating probable N-terminal degradation (Fig. 5F lower panel). This data led us to question the stability of mEFH1+2 and we therefore analyzed cells after 24 hours expression followed by a six-hour treatment with the proteosome inhibitor MG132 [26]. Cells were then probed with anti-NTD (S3A Fig.) and counted for positive mEFH1+2 signal (S3B Fig.). We also tested mEFH1+2 levels by western blotting using 5F2B3 (S3C Fig.).

The counts illustrated that 3.9% (n = 633, SE± 0.29%) of the population were positive for mEFH1+2 signal in the absence of MG132 treatment, whereas 23.3% (n = 559, SE± 3.5%) were positive after MG132 treatment (S3A, B Fig.). Quantification of western blots of mEFH1+2 probed with 5F2B3, and normalization with anti-tubulin loading control, indicate that there is 1.5 x fold more mEFH1+2 protein in cells after MG132 treatment (S3C Fig.). Oddly, we did

Table 3. Mean mEFH2-induced helix, coma and annuli diameter after expression in U-2 OS cells and mean FPC diameter.

Post transfection time	mEFH2			*T. brucei* Wild-type FPC diameter
	Helix diameter	Comma diameter	Annuli diameter	
6h	**730 nm** (SE± 10) n = 95	**787 nm** (SE± 20) n = 60	**771 nm** (SE± 40) n = 20	**842 nm** (SE± 20) n = 71

The mEFH2 helix diameter, comma diameter and annuli diameter were measured after six hours post-transfection. Helix, comma, annuli and FPC diameters all have similar diameters. FPC diameter was measured on wild-type *T. brucei* procyclic cells.

doi:10.1371/journal.ppat.1004654.t003

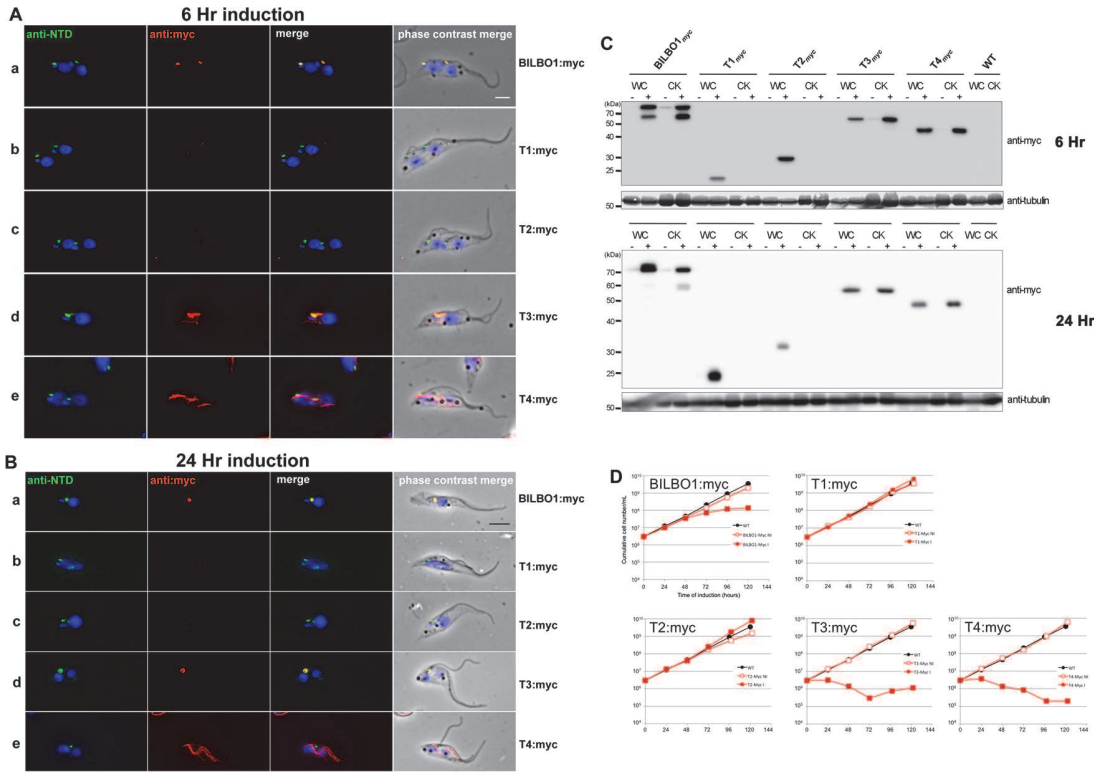

Fig 6. The coiled-domain is required for polymer formation in *T. brucei*. (A) Immunofluorescence labelling of cytoskeletons from cells expressing BILBO1:myc, T1:myc, T2:myc, T3:myc and T4:myc using anti-NTD (green) and anti-myc (red) after six hours of induction. (B) Immunofluorescence labelling of cytoskeletons expressing BILBO1:myc, T1:myc, T2:myc, T3:myc and T4:myc using anti-NTD (green) and anti-myc (red) after 24 hours of induction. (C) Western-blot of corresponding cells. 2.10^6 non-induced (-) or induced (+) for six hours from whole cells (WC) or cytoskeletons (CK) were loaded on a 12% SDS-PAGE, transferred and immuno-probed with anti-myc, or anti-tubulin (tubulin is a loading control). WT is the non-transfected parental cell line. (D) Growth curves of the parental cell line (WT, black circles) compared to the cell lines non-induced (NI, red open squares) or induced (I, red closed squares) for the expression of BILBO1, T1, T2, T3, T4 myc-tagged truncations. Scale bars in A and B represent 5μm.

doi:10.1371/journal.ppat.1004654.g006

not observe the ~ 60kDa band noted previously in Fig. 5F in these untreated cells and are uncertain why, but it may signify that degradation of mEFH1+2 is not consistent and that degradation rates and origin on mEFH1+2 can vary.

Importantly, this data indicates that there is up to 40% degradation of mEFH1+2 when expressed in U-2OS cells, but more significantly no linear, helical or annular polymers were detected in cells in the absence or presence of MG132 treatment.

BILBO1 truncations form polymers in trypanosomes

Our previous work has shown that a brief ectopic expression of a full-length tagged version of BILBO1 protein (GFP-BILBO1) in trypanosomes results in targeting and assembly into the FPC [8]. We accept the caveat that the expression of truncated, mutated or full-length forms of BILBO1 in trypanosomes will clearly involve the binding and/or interaction of other FPC proteins, which may influence the structures produced. However, we wanted to observe whether ectopic expression of these proteins would indeed form polymers in a trypanosome context. To avoid potential steric hindrance due to GFP and to discriminate between the endogenous BILBO1, we created C-terminus myc-tagged forms of the protein that are identical to those expressed in U-2 OS cells (for clarity, described here as T1:myc—T4:myc) and expressed them in procyclic *T. brucei* cells (Fig. 6), using the previously described tetracycline inducible

expression system [8,27]. *T. brucei* cells expressing different truncations were detergent extracted to make cytoskeletons (CK) and simultaneously probed with the following antibodies anti-NTD (which labels the endogenous BILBO1 and BILBO1:myc, T1:myc, T2:myc, but not T3:myc or T4:myc truncations, in which case 5F2B3 was used), and anti-myc, which labels only myc tagged ectopic proteins.

After six hours of induction we observed BILBO1:myc at the FPC thus demonstrating that the myc tag does not affect the localization of the protein (Fig. 6A a). By western blotting we noted an additional band present under the main band (Fig. 6C) after six or 24 hours of expression and suggest that this is a degradation product. It is weaker after 24 hour expression compared to six hours suggesting more complete degradation to small peptides, much less degradation or degradation during or after sample preparation (for example when making cytoskeletons) (Fig. 6C).

T1:myc or T2:myc truncations were observed in the cytoplasm by WB (Fig. 6C), but no signal was present in detergent extracted cytoskeletons by immunofluorescence or WB (Fig. 6A b-c, 6B b-c, 6C). The solubility of T1:myc and T2:myc truncations is in agreement with the soluble forms observed when expressed in U-2 OS cells and, with respect to trypanosomes, it indicates that neither the N-terminus nor the EF-hand domains are sufficient for targeting or binding to the FPC. Extensive expression of T1:myc or T2:myc truncations (>24 hours) did not dramatically affect cell morphology or cell growth (Fig. 6B, and D) indicating that neither of these domains induce dominant negative effects. When probed with anti-NTD antibody endogenous BILBO1 localization at the FPC was not impaired or modified during T1:myc or T2:myc expression because the NTD-labelling was unmodified. By probing the samples with NTD, and an anti-tubulin loading control, on western blots we were able to measure the native levels of BILBO1 expression in cells expressing T1:myc or T2:myc truncations for six or 24hours and these were both shown to be 1.4 x higher than wild-type levels. After 24 hours induction these levels remained at 1.4 x higher than wild-type levels (S4 A Fig).

Immunofluorescence on procyclic trypanosome cytoskeletons and western blot analysis of whole cells (WC) or cytoskeletons (CK) demonstrated that T3:myc truncation is insoluble and is associated with the cytoskeleton (Fig. 6A d and 6B d). T3:myc targets primarily to the FPC, but also forms a subset of short fibres that below the FPC (Fig. 6A d). Surprisingly, these fibres were myc positive, but NTD negative, implying that they were formed predominately by T3:myc truncation. In contrast to T1:myc and T2:myc, longer expression of the T3:myc truncation resulted in targeting and binding to the FPC with deleterious effects; endogenous BILBO1 (labelled with anti-NTD) and T3:myc co-localized to a single FPC structure from which both flagella (old and new) emerged (Fig. 6B d).

Moreover, in these T3:myc induced cells, the new flagella were detached from the length of the cell body. This phenotype was characterised by flagellum attachment at the basal body region, but detachment along the length of the cell. For simplicity we have called this a "detached flagellum" phenotype. These cells died within 24 hours of T3:myc induction (Fig. 6D). Interestingly, detached flagella and cell death are phenotypes observed in the induced BILBO1 RNAi cell line [8].

Expression of T4:myc for six hours produced long fibre-like polymers that were observed within the cytoplasm (Fig. 6A, e). This implies that the CC domain, in the absence of the N-terminal domain or the EF-hand domains, is able to form polymers in *T. brucei* as well as in U-2 OS cells. Similarly to T3:myc, expression of >24 hours of T4:myc produced polymer structures that did not contain endogenous BILBO1 signal (Fig. 6B, e). Notably, cells expressing T4:myc died within 24 hours of induction (Fig. 6D) and, as with T3:myc expression, these cells had a detached new flagella phenotype (Fig. 6B e).

As with T1:myc and T2:myc, we probed the T3:myc and T4:myc protein samples by western blot with NTD, anti-myc and anti-tubulin and measured the native levels of BILBO1

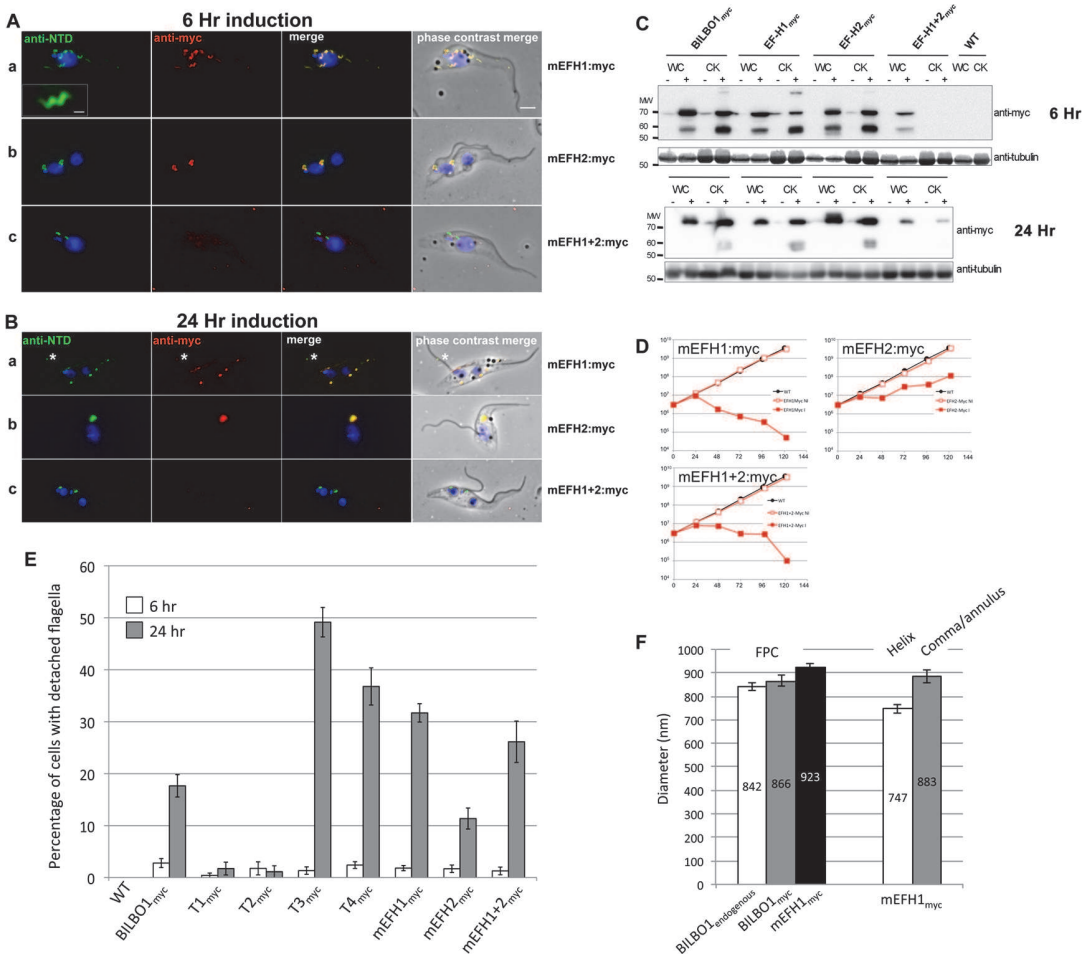

Fig 7. The EF-hand domains modulate the morphology of polymers formed by BILBO1. (A) Immunofluorescence labelling of cytoskeletons from cells expressing mEFH1:myc, mEFH2:myc, mEFH1+2:myc using anti-NTD (green) and anti-myc (red) after six hours of induction. Scale bar in the magnified inset represent 1 μm. Scale bar for all other images represents 5μm. (B) Immunofluorescence labelling of cytoskeleton extracted cells expressing mEFH1:myc, mEFH2:myc, mEFH1+2:myc using anti-NTD (green) and anti-myc (red) after 24 hours of induction. The asterisks indicate a dot in the new detached flagellum. (C) Western-blot of corresponding cells. 2.10^6 cells (WC) or cytoskeletons (CK) non-induced (-) and induced (+) for six hours, were loaded on a 10% SDS-PAGE, transferred and immuno-probed with anti-myc and anti-tubulin as loading control. WT is the non-transfected parental cell line. All expressed proteins except mEFH1+2:myc are insoluble. (D) Growth curves of the parental cell line (WT, black) compared to the cell lines non-induced (NI, red open squares) or induced (I, red closed square) for the expression of mEFH1, mEFH2, mEFH1+2 myc-tagged proteins. (E) Overexpression of BILBO1 coiled-coil truncations or EF-hand domain mutations induces detached flagellum phenotypes. The percentage of cells with a detached flagellum was determined using phase contrast microscopy after six or 24 hours of protein expression. (F) WT cells or cells expressing recombinant proteins (induced for six hours), were fixed and immunolabelled with anti-myc and anti-NTD. The graph represents the measurements of the FPC diameter in WT cells, in BILBO1:myc, mEFH1:myc, mEFH2:myc and mEFH1+2:myc expressing cell lines. The graph also shows the diameter of the helix and comma/annulus shaped polymers formed by mEFH1:myc.

doi:10.1371/journal.ppat.1004654.g007

expression. After 6 hours of induction, endogenous level of BILBO1 appeared to be 6.6 x fold and 5.1 x fold higher in T3:myc and T4:myc truncation expressing cells respectively. After 24 hours of expression these levels were shown to be 6.3 x and 4.2 x fold higher respectively compared to wild-type levels, (S4 B Fig.).

Given that the expression of T3:myc or T4:myc truncations in trypanosomes is lethal and induced detached flagellum phenotypes we counted the percentage of cells exhibited this phenotype after six or 24 hours of expression and compared this to T1:myc, T2:myc and BILBO1:myc expression. Fig. 7E shows that wild-type cells do not have a detached flagella phenotype, and cells expressing T1:myc and T2:myc truncations produced less than 2% detachment.

Table 4. T1:myc—T4:myc and BILBO1:myc detached flagellum phenotypes after expression *T. brucei* cells.

Time of induction	T1:myc detached flagella	T2:myc detached flagella	T3:myc detached flagella	T4:myc detached flagella	BILBO1:myc detached flagella
6h	**0.43%** (SE±, 043) *n* = 183	**1.77%** (SE± 1.25) *n* = 111	**1.35%** (SE± 0.72) *n* = 412	**2.41%** (SE± 0.65) *n* = 556	**2.8%** (SE± 0.87) *n* = 529
24h	**1.74%** (SE± 1.23) *n* = 125	**1.14%** (SE± 1.14) *n* = 97	**49.17%** (SE± 2.84) *n* = 228	**36.79%** (SE± 3.57) *n* = 406	**17.66%** (SE ±2.15) *n* = 495

Quantification of the percentage of cells exhibiting detached flagella phenotypes after six and 24 hours expression of T1:myc—T4:myc tagged proteins or BILBO1:myc tagged protein in procyclic *T. brucei* cells. T3:myc, T4:myc and BILBO1:myc induced detached flagella phenotypes whereas T1:myc and T2:myc did not.

doi:10.1371/journal.ppat.1004654.t004

However, after a 24 hour induction T3 cells showed a 36 x fold increase in detached flagella phenotypes, T4 cells showed 15.2 x fold increase and BILBO1:myc showed a 6.3 x fold increase (please refer to Table 4).

This data suggest that the high number of detached flagella phenotypes induced by BILBO1:myc, T3:myc and T4:myc expression is likely to be a dominant negative effect and the secondary effects of this have influenced the formation or function of the flagella attachment zone (FAZ) [6] resulting in detached flagella. The results obtained by Y2H analysis for T1-T4 correspond with the results obtained using the same truncations expressed in U-2 OS cells and in trypanosomes. Essentially, For T1 and T2 there is no BILBO1 interaction by Y2H, also no polymer formation was observed when these truncations were expressed, but positive protein-protein interaction and polymer formation was observed with expression of full-length BILBO1 or T3 or T4 truncations. These data indicate that the CC domain is required for polymerization and targeting/binding to the FPC. It also illustrates that over-expression (24 hours) of the CC domain alone (T4:myc) is sufficient to induce the detached flagellum phenotypes.

EF-hand 1 domain influences BILBO1 polymer shape in *T. brucei*

To analyse in detail the role of the BILBO1 EF-hand domains in trypanosomes we expressed mEFH1:myc, mEFH2:myc, and mEFH1+2:myc in *T. brucei* procyclic cells (Fig. 7). Expression of mEFH1:myc for six hours demonstrated targeting to the FPC, but in addition we observed the formation of several helical structures independent of the FPC (Fig. 7A a). The diameter of the helices and comma/annuli structures after six hours of expression was 747 nm (*n* = 67, SE± 20nm) and 883 nm (*n* = 39, SE± 27nm) respectively (Fig. 7F).

As with T1—T4 experiments, we probed the proteins from cells expressing BILBO1:myc and mutated EF-hand:myc by western blot and compared them to the native levels of BILBO1. Notably, we observed degradation bands at ∼ 60kDa, which is probably due to the same degradation related reasons we have specified earlier for the expression of BILBO1:myc (Fig. 6A a). Nevertheless, after six hours of expressing BILBO1:myc, mEFH1:myc, mEFH2:myc, or mEFH1+2:myc, wild-type BILBO1 protein levels were shown to be 1.1 x, 0.9 x 1.3 x and 0.9 x fold higher or lower respectively than the expressed myc tagged levels, (S4, C Fig.). After 24 hours of expression these levels were 2.5 x, 1.3 x, 2.9 x, and 1.0 x higher respectively than myc tagged protein levels.

Because mEFH1:myc formed helices when expressed in trypanosomes, we wanted to compare helix dimensions with that of the FPC. We therefore measured the diameter of the FPC (major axis diameter) in wild-type (endogenous BILBO1), BILBO1:myc and mEFH1-myc expressing cells (Fig. 7F). We measured the FPC diameter of wild type G1 procyclic cells after immunolabelling with anti-NTD antibody and the FPC of BILBO1:myc and mEFH1-Myc

expressing cells, for six hours, using anti-myc antibody. The diameter of wild-type FPC was 842 nm (as noted in Table 3) whilst in the BILBO1:myc expressing cells the diameter was measured as 866 nm (n = 48, SE± 20nm) and was 923 nm (n = 88, SE± 20nm) in mEFH1:myc expressing cells (Fig. 7F).

The fact that mEFH1:myc structures were helical indicates that mutation of EF-hand domain 1 influences the type of polymer formed, in the context of the trypanosome (Fig. 7A a). Expression of mEFH1:myc (>24 hours) induced the formation of myc and NTD positive, globular, insoluble structures followed by cell death occurring between 24–48 hours of induction (Fig. 7B, D). Noticeably, as previously observed in T3 and T4 expressing cells, and in BILBO1 RNAi knockdown cells [4,8], expression of mEFH1:myc induced detached flagella phenotypes (Fig. 7B a) (see below for quantification). We observed the formation of a single insoluble BILBO1 positive structure within the length of the new detached flagellum. The presence of this structure along the flagellum suggests the mis-targeting of this mEFH1:myc form of BILBO1 (Fig. 7B a, asterisk).

Similar to observations made with BILBO1:myc, the mEFH2:myc targets to the FPC after a six hour induction, suggesting that EF-hand domain 2 function is not required for targeting to the FPC (Fig. 7A b). Expression >24 hours resulted in cells with new flagella detached phenotypes (see below for counts) and the formation of large insoluble structures that were not associated with the old or new flagella. Cell death occurred between 24 and 48 hours (Fig. 7B b and 7 D).

The majority of mEFH1+2:myc protein when expressed in trypanosomes for six hours was soluble, as observed by WB (Fig. 7C). As in the expression of mEFH1+2 in U-2 OS cells we cannot rule out the possibility of rapid degradation since degradation bands were observed after six hours, and to a much lesser extent 24 hours, of expression. Indeed mEFH1+2:myc expressing cells treated with MG132 had 2.2 x fold higher protein levels when compared to non-treated cells suggesting mEFH1+2:myc degradation *via* the proteasome (S4D Fig.). A weak mEFH1+2:myc signal could be detected on cytoskeletons probed by immunofluorescence and western-blot (Fig. 7A, B, C) and extensive expression of mEFH1+2:myc (>24 hours) resulted in a very weak mEFH1+2:myc immunofluorescence signal close to both old and new FPC structures. When probed by WB a weak signal was also observed in cytoskeleton samples that had been expressing mEFH1+2:myc for 24 hours (Fig. 7 C). Cells died after >24 hours expression of mEFH1+2:myc (Fig. 7B, D). Long induction also induced the production detached flagella phenotypes (see Table 5 for quantification). In all cases where mutated mEF-hand proteins were expressed we noticed that after 24 hours of expression little or no anti-BILBO1 signal (endogenous or myc-tagged) was detected at the base of the new flagellum suggesting sequestration or degradation of wild-type BILBO1 (Fig. 7B a-c).

Since the expression of mEFH1:myc, mEFH2:myc or mEFH1+2:myc in trypanosomes induced detached flagella phenotypes, we investigated the extent of their appearance. We observed a significant difference between a six hour expression and 24h expression of mEFH1:

Table 5. mEFH:myc induced detached flagellum phenotypes after expression in *T. brucei* cells.

Time of induction	mEFH1:myc detached flagella	mEFH2:myc detached flagella	mEFH1+2:myc detached flagella
6h	**1.83%** (SE± 0.49) n = 852	**1.7%** (SE± 0.71 n = 489	**1.29%** (SE± 0.74) n = 181
24h	**31.7%** (SE± 1.76) n = 502	**11.37%** (SE± 2.02 n = 338	**26.14%** (SE± 3.98) n = 148

Quantification of the percentage of cells exhibiting detached flagella phenotypes after six and 24 h expression of mEFH1:myc, mEFH2:myc and mEFH1+2:myc tagged proteins in procyclic *T. brucei* cells. Expression of all EF-hand mutations induced detached flagella phenotypes.

doi:10.1371/journal.ppat.1004654.t005

myc because the number of detached flagella phenotypes increased by 17 x fold. For mEFH2:myc expression we observed a 6 x fold increase in detached flagella and for mEFH1+2:myc there was a 20 x fold increase in detached flagella phenotypes, (please refer to Table 5 and Fig. 7E).

Discussion

The results in this study support the concept that BILBO1 has self-assembly properties that are dependent on the CC region of the protein, and that can be influenced by the EF-hand domains at its N-terminus. We hypothesize that BILBO1 is well suited to play a role in the formation of the FPC annulus. The results reported here establish that BILBO1 can, autonomously, support the formation of various polymers including helical polymers. We suggest that these polymer-forming properties are important in building a FPC.

We demonstrate here that the two tandem EF-hand domains of BILBO1 bind calcium *in vitro* and that mutation of these domains either together or independently prevented calcium binding. The observation that mutation of one EF-hand domain prevented the second from binding calcium is not unprecedented. In fact, the basic unit for a functional EF-hand protein is a pair of EF-hand domains that stably form a four-helix bundle [28,29,30]. Previous studies have also shown that the four-helix bundle should be treated as a single global structure because the two EF-hand domains bind calcium cooperatively [30]. Indeed, our ITC titration fit curve for wild-type *Tb*BILBO1-EF-hand domains indicate that the molar ratio between Ca^{2+} and the protein was approximately 2 (Fig. 2E), suggesting that both EF-hand domains bind calcium. The expression in mammalian cells or trypanosomes of full-length BILBO1 with mutations on either or both EF-hand domains produced different types of polymers (see below), which would also suggest that both hands bind calcium.

The data obtained from Y2H analysis, U-2 OS and trypanosome studies strongly indicate that BILBO1 x BILBO1 interactions exist, and in many cases, are targeted to the FPC of trypanosomes. We have shown that long-term over-expression of full-length BILBO1:myc in *T. brucei* procyclic cells is lethal.

When expressed in *T. brucei* procyclic cells the T1 and T2 truncated forms of BILBO1 are soluble, but neither can interact with full-length BILBO1 nor with the CC domain, and do not form polymers. We can thus consider that the N-terminal domain of BILBO1 is not directly involved in BILBO1 polymerization. On the other hand, the N-terminal domain can regulate the shape of the polymer.

Expression of mutated EF-hand proteins in trypanosomes did not prevent targeting to the FPC indicating that they bind to native BILBO1. mEF-hand 1+2 location to the FPC was very weak when detected by immunofluorescence, but it was also mostly degraded under these conditions. Further, we carried out yeast two-hybrid analysis to test whether full-length BILBO1 interacts with full-length BILBO1, or deltaEF-H1+2 (a deleted EF-hand form of BILBO1 where the N-terminal domain is retained) and full-length BILBO1 versus mEF-hand1+2. We also tested mEF-hand1+2 versus T4 truncation, or mEF-hand1+2 versus T3 truncation. In all cases BILBO1 interacted with these modified proteins indicating that the EF-hand domains are not required for this interaction. Interestingly, the double EF-hand mutant mEF-hand1+2 also bound to BILBO1 indicating that neither lack of calcium binding nor the conformational change induced by calcium binding prevents BILBO1-BILBO1 interactions (S5 A Fig.).

Recently, nuclear magnetic resonance (NMR) and X-ray crystallographic techniques were used to solve the 3D structure of the N-terminal domain of BILBO1. That work involved experiments demonstrating that the N-terminal domain has an exposed surface patch within an ubiquitin-like fold. Expression in trypanosomes of full-length-BILBO1 mutated on this patch is

lethal suggesting that this region has important functional roles which may include interaction with other FPC proteins [14]. Additionally, the authors also showed that EF-hand domains of BILBO1 changes its conformation upon calcium binding, and the CC domain forms anti-parallel dimers and linear polymers and these filaments can condense into fibres through lateral interactions [15].

When expressed in *T. brucei* procyclic cells, T3:myc and T4:myc fragments localised to the FPC, and produced lethal effects. It is also possible that they induced dominant negative effects because detached flagella phenotypes were observed after expression of these proteins, indicating a probable interruption of flagellum attachment zone (FAZ) function or biogenesis.

When expressed in U-2 OS cells, T1 and T2 truncation were soluble, and T3 and T4 truncations formed polymers. Interestingly, expression of the T4 truncation formed exclusively linear spindle-like polymers in these cells. From these results we conclude that the CC domain of BILBO1 can spontaneously form homo-polymers *in vivo* and these are linear due to the absence of the N-terminus, which functions to modulate the type of polymer formed. It is not clear how BILBO1 polymers are formed in U-2 OS cells and although trypanosome FPC proteins are absent there may be other proteins interacting with BILBO1 contributing to the formation of polymers.

Since the FPC has been established in earlier published studies to be an annulus/horseshoe *in vivo* we suggest that, in the parasite, BILBO1 could form the template for the FPC, which then associates with other FPC proteins perhaps under the modulation of calcium to form the final annulus/horseshoe [4,8]. Further evidence for BILBO1 calcium binding and polymer forming properties was provided by Vidilaseris *et al.*, 2014 [15]. Using *in vitro* structural dissections of BILBO1 they showed that the EF-hand domains change conformation upon calcium binding, and the central CC can form anti-parallel dimers. They demonstrated that a C-terminal leucine zipper is present and appears to contain targeting information so that inter-dimer interactions can form between adjacent leucine zippers of the CC domain, which allow BILBO1 to form extended filaments. Finally, they showed that these filaments could condense into fibers through lateral interactions [15]. From these observations it is suggested that two BILBO1 molecules can form an anti-parallel dimer *via* their CC domains, which assemble into a filament through the interactions between the C-terminal leucine zippers. BILBO1 forms polymers spontaneously *in vitro* with no apparent need for nucleotide hydrolysis [15], but spontaneous polymerization is not unprecedented for cytoskeleton proteins and has been observed for intermediate filaments and bacterial flagellins [31,32,33,34].

Within the parasite BILBO1 is unlikely to function alone and must interact with other proteins to form the scaffold of the FPC. Based on Y2H analysis we have identified numerous BILBO1 binding proteins, two of which bind to the N-terminus of BILBO1. One of these proteins, FPC5, is kinetoplastid specific, but it is feasible that other BILBO1 binders are structural and may influence BILBO1 conformation *in vivo*. Indeed it is also possible there is interplay between calcium and protein binding to BILBO1 and this may regulate how BILBO1 functions or perhaps even form polymers. Data to support this in presented in S5B Fig. where we use Y2H assays to illustrate that the BILBO1 binding domain of FPC5 interacts with full-length BILBO1 as bait or prey, but does not interact with BILBO1 if the EF-hand domains have been deleted or mutated to prevent calcium binding.

In order to test the effects of calcium chelation on polymers we treated U-2 OS cells, which have expressed untagged BILBO1 for six or 24 hours, with the membrane permeable calcium chelator BAPTA-AM. We did not observe any difference between treated and untreated cells (S6A Fig.) suggesting that once polymerization occurs the protein is somewhat stable to calcium chelation. We also treated cytoskeletons derived from cells that had expressed BILBO1myc or the EF-hand mutants, with 50mM EGTA, but the chelation treatment did not disrupt the

FPC nor solubilize the polymers formed by mEF-hand 1 domains under these conditions (S6B Fig.). The former results suggests that these polymers may have very strong and/or irreversible inter-molecule interactions, and the latter result is probably due to both strong interactions and the stabilizing properties of other FPC proteins that prevent depolymerisation. Such stabilization is not unprecedented and a good example of this is alphaB-crystallin, which has been demonstrated to stabilize microtubules against calcium depolymerization [35,36].

The results observed from the ITC studies and the effects of the mutation of the EF-hand domains in BILBO1 on polymer assembly *in vivo* demonstrates that BILBO1 does binds calcium. The expression of mEFH1 in U-2 OS cells produced small aggregates, whereas expression of mEFH2 in these cells induced the formation of helical polymers. When expressed in trypanosomes mEFH1 formed helical polymers whereas mEFH2 did not. We do not have a clear explanation for this difference between mammalian cells and trypanosomes, but one can speculate that it may reflect a change in three-dimensional structure when the protein in question interacts with, or binds to, parasite specific proteins. It is apparent from our studies and confirmed by other work that mutating calcium-binding domains can also influence BILBO1 structure and this may influence if and how polymers are formed [15]. The fact that BILBO1 can form different shapes such a linear or annular/comma shaped polymers is especially interesting when we consider the helices formed when either EF-hand domain was mutated. Therefore it is possible that these mutations prevent calcium binding and could stop the domain folding correctly, which could result in alternative BILBO1 polymerization.

In trypanosome procyclic cells mEFH1:myc targeted to the FPC, but also within the new detached flagellum of these cells. It is unclear why these mis-targeted mEFH1 "spots" are present within the length of the flagellum, but it may be due to the limited ability to bind to partners for FPC retention or may be due to modified access to the intraflagellar transport system. Mutated EFH1+2:myc was apparently predominantly soluble when expressed in trypanosomes, but in this context it is not unusual, because the mutation of a single amino acid has been noted in some cases to modify protein solubility such as maltose binding protein and haemoglobin [37,38,39]. We also show that EFH1+2:myc is mostly soluble, but can form some small punctate or aggregates in U-2 OS cells and is predominantly degraded when expressed. Longer expression of EFH1+2:myc in trypanosomes induced flagella detachment phenoptypes suggesting perturbation of the FAZ. Low levels appear to be very toxic to cells perhaps by recruiting inappropriate proteins or preventing the correct binding of partner proteins such as FPC5.

In the trypanosome expression experiments the mutant mEF-hand 1 and 2 proteins are only recognized by the anti-myc antibody and show that they do target to the FPC. This provides some evidence to suggest that in a six-hour induction they do not sequester all native BILBO1 from targeting to the collar. After 24 hours of expression this is not the case and native BILBO1 does appear to be degraded, not targeted to, and/or sequestered from the FPC as seen in Fig. 7, B a and b. The sequestering of wild-type BILBO1 may also be the cause of flagella detachment and cell death.

The diameter of mEFH2-induced helices in U-2 OS cells was 730 nm and comma diameter was 787 nm whilst annuli diameter was 771 nm. The diameter of the helices formed by procyclic cells expressing mEFH1:myc is 750nm, whilst the diameter of the wild-type FPC was 842 nm. The similarity between the diameters of these polymers compared to the FPC is probably not coincidental and could be envisaged to be associated with the intrinsic properties of BILBO1. Based on our observations, we propose a model in which BILBO1 is a structural scaffold of the FPC and assembles into polymers *via* the CC domain and leucine zipper as proposed by Vidilaseris, *et al.*, 2014 [15]. This polymer forms an elliptical or annular structure, the exact state depending on the calcium-binding functionality of the EF-hand domain and the presence or absence of partner proteins. In this model the role of the EF-hand domain is vital and is involved

in the plasticity of the structure, but clearly in the trypanosome there must be other proteins that bind to or regulate the structure of the FPC. If we consider a hypothesis where the FPC changes dimensions to accommodate a new flagellum during the cell cycle then one hypothetical interpretation could be that the interplay with binding partners is important during the parasite cell cycle, wherein an annular/horseshoe shaped FPC is required in early cell cycle stages, whilst a more elliptical FPC is required during emergence of the new flagellum during S/G2 or later. Nevertheless, it is unclear how precisely a new FPC is formed. If a new FPC is formed *de novo* then we would expect much less need for dramatic changes in its shape and this interpretation provides a role for BILBO1 whereby it forms a FPC as the new flagellum exits the FP.

The primary and motile cilia and the flagella of differentiating spermatids have a ciliary pocket (CP) [40,41,42], which is physically associated with clathrin-coated endocytotic vesicles [40,41] and shares a conspicuously similar structure to the FP. Surprisingly, it is not known if the equivalent of the FPC, the CP collar (CPC) actually exists. Therefore it is unknown if the CP indeed requires a BILBO1-like protein or if the CP is constructed differently to the FP.

The importance of a precisely constructed primary cilia cytoskeleton is revealed by studies on ciliopathies; defective primary cilia in humans lead to polycystic kidney disease and a variety of other illnesses [43,44,45,46,47]. Clearly, a thorough understanding of how the FP and/or the CP are formed will provide important insights into both parasite biology and human ciliopathies. The data we have reported here have elucidated *in vivo*, and in a tractable system, some interesting properties of BILBO1 and these have advanced our understanding of how the FP is constructed. The ongoing search for the identification and characterization of additional FPC proteins will add to our understanding of the ways in which the FPC is organized and maintained. We anticipate that this data will be useful to obtain a more general understanding of the assembly of kinetoplastid FPC complexes and provide important clues on how to inhibit FPC biogenesis.

Materials and Methods

Cell lines, cell culture and cell transfection

U-2 OS cells (human bone osteosarcoma epithelial cells, ATCC Number: HTB-96 [48] were grown in D-MEM Glutamax (Gibco) supplemented with final concentrations of 10% fetal calf serum (Invitrogen), 100 units.mL^{-1} of Penicillin (Invitrogen), and 100 μg.mL^{-1} of Streptomycin (Invitrogen) at 37°C plus 5% CO_2. Exponentially growing U-2 OS cells in 24 well plate with glass coverslips were lipotransfected as in Dacheux et al., [49] with 0.5–2 μg DNA using Lipofectamine 2000 in OPTIMEM (Invitrogen) according to the manufacturer's instructions and processed for IF six to 24 hours post-transfection.

The *BILBO1* ORF and truncations were amplified by PCR from *T. brucei* TREU927/4 GUTat10.1 genomic DNA [50]. The work described in this study uses the parental procyclic form (PCF) *T. brucei* 427 29–13 cell-line, co-expressing the T7 RNA polymerase and tetracycline repressor, named for the purposes of this study as wild-type (WT) [51]. WT cells were transfected with NotI linearized plasmids as in [52] and cloned. Expression of recombinant proteins was induced with 1 μg.mL^{-1} tetracycline. Growth curves were done by using a mallassez cell counter every 24 hours and by diluting the cells back to 3.10^6 cells/ml. Growth curves in Figs. 6 and 7 represent the cumulative cell number.

Vectors

Mammalian expression vectors. The *BILBO1* ORF and truncations were cloned into the pcDNA3 between HindIII-XbaI sites for *BILBO1* full length and EcoRI-XhoI for the truncations or into pcDNA3.1 CT-GFP TOPO (Invitrogen). Mutations of the EF-hand domain 1

(D194A (GAT/GcT); N198A (AAC/gcC); D202A (GAC/GcC); D205A (GAC/GcC), the EF-hand domain 2 (D230A (GAC/GcC); N232A (AAC/gcC); E241A (GAA/GcA), and the serine 163 mutations (S163D (TCG/gat) and S163A (TCG/gCG) were done by site-directed mutagenesis following the instructions from the Agilent QuickChange Site-directed Mutagenesis kit.

Trypanosome expression vector. The pLew100X-3myc has been modified in the laboratory from pLew100 [49]. BILBO1 and truncations 1, 2, 3, 4, and mutated EF-hands versions of BILBO1 were cloned into pLew100X-3myc between the *HindIII-XbaI* sites.

Yeast two-hybrid vectors. Open reading frames were amplified by PCR from *T. brucei* PCF genomic DNA and cloned in the prey (pGADT7-AD, Clontech) and bait (pGBKT7, Clontech) vectors between the *EcoRI-BamHI* sites.

Immunofluorescence

In trypanosomes. For cytoskeleton preparations, cells were washed in PBS, loaded on poly-l-lysine coated glass slides, and extracted with 1% or 0.25% NP40 in Pipes buffer (100 mM Pipes pH6.9, 1 mM $MgCl_2$) for 5 minutes then washed twice in Pipes buffer. Cytoskeletons were fixed in -20°C methanol or 3% paraformaldehyde (PFA) in PBS. After PFA fixation, cells were neutralized 10 min in glycine (100 mM in PBS). After 3 washes in PBS, samples were incubated with the primary antibodies for 1 hour at room temperature in a moist chamber: anti-BILBO1 (mouse monoclonal 5F2B3, which recognizes the CC domain [8], 1:10 dilution) or rabbit anti-NTD (which recognises the first 110 aa of BILBO1, [9]) diluted 1:50 in PBS. After two PBS washes, cells were incubated for 1 hour with the secondary antibodies anti-mouse-IgG (H+L) conjugated to Alexa 594 (Molecular Probes A21201, 1:400 dilution) or FITC (Sigma F-2012, 1:100 dilution), or anti-rabbit IgG (H+L) from goat conjugated to FITC (Sigma #F-9887, 1:100 dilution). The nuclei and kinetoplasts were labeled with DAPI (10 $\mu g.mL^{-1}$ in PBS for 5 minutes), washed twice in PBS for 5 minutes. Slides were mounted with Slowfade Gold (Molecular Probes S-36936).

In U-2 OS cells. For observation of whole cells, transfected U-2 OS cells were fixed in 3% PFA in PBS for 15 minutes (at RT or at 37°C). When indicated, transfected cells were incubated with the membrane permeable calcium chelator BAPTA-AM (Sigma A1076, 25μg/ml final concentration) for three hours or with the proteasome inhibitor MG132 (Sigma C2211, 20–50 μM final concentration) for six hours before fixation. To remove soluble proteins, cells were briefly extracted for 2 min with 30 μl of EMT, TX-100 0.5%, glycerol 10% then fixed in PFA 3% (at 37° C, 15 min). After fixation, cells were neutralized 10 min in glycine (100 mM in PBS). After two washes in PBS, cells were incubated in permeabilization buffer PB (PBS, 10% foetal calf serum, 0.1% saponin) for 10–30 minutes. Primary antibodies anti-BILBO1 (mouse monoclonal 5F2B3), [8] 1:10 dilution, anti-NTD BILBO1 (which binds to aa 1–110, rabbit polyclonal, 1:50 dilution, [9]), anti-alpha-tubulin DM1A (Sigma T9026, 1:500 dilution) or TAT1 (1:100 dilution, [53]), anti-calnexin (rabbit polyclonal, 1:500 dilution), anti-giantin (rabbit polyclonal, 1:750 dilution), anti-Vimentin V9 (Interchim NB200-622, 1:250 dilution) were added and the slides were incubated for 1 hour in a dark, moist chamber. After two PBS washes, cells were incubated for 1 hour with the secondary antibodies anti-mouse-IgG (H+L) conjugated to Alexa-594 (Molecular Probes A21201, 1:400 dilution), or to FITC (Sigma F-2012, 1:100–1:400 dilution), or to anti-rabbit Texas-Red-conjugated (Molecular Probes T-6391, 1:400 dilution), or to anti-rabbit FITC-conjugated (Sigma F-9887, 1:100–1:400 dilution). For the F-actin labelling, Texas-red-conjugated phalloidin (Molecular Probes A12380, 1:160 dilution) was incubated with the secondary antibody. The nuclei were stained with DAPI (0.25 $\mu g.mL^{-1}$ in PBS for 5 minutes) and cells were washed and mounted with Prolong (Molecular Probes S-36930).

Images were acquired on a Zeiss Axioplan2 or a Zeiss Imager Z1 microscope, using a Photometrics Coolsnap HQ2 camera, with Zeiss 100x or 63x objectives (NA 1.4) using Metamorph software (Molecular Devices), and processed with ImageJ. Polymer dimensions were measured using ImageJ. Total fluorescence intensities in U-2 OS cells were quantified from Z-stack acquisitions and using ImageJ on SUM intensity Z project, after background subtraction, and selection of each cell as region of interest. The measurement of polymers was done using fluorescence or immunofluorescence based images. The dimensions were measured from at least three separate experiments and were measured by hand using Image J software.

Protein expression and purification. *Tb*BILBO1 wild-type and mutated EF-hands proteins (residues 177–250; WT, mEFH1, mEFH2, and mEFH1+2), were cloned into the custom vector MalpET as described previously [15]. All recombinant proteins, each carrying an N-terminal MBP-His_{10} tag, were expressed in *E. coli* BL21 (DE3). Bacteria transformed with the cloned constructs were grown at 37°C to an A_{600} of ∼0.6–0.8 and then subjected to cold shock (ice, 30 min). Protein expression was induced by addition of 0.25 mM isopropylthio-β-D-galactoside, and protein production was continued for 20–22 hours at 16°C.

Cells were harvested by centrifugation (4,000×g, 20 min) and resuspended in cold lysis buffer (20 mM Tris-HCl pH 8.0, 300 mM NaCl, 20 mM imidazole, 5% (v/v) glycerol). The cells were broken open with an EmulsiFlex-C3 homogenizer (Avestin) and the lysate was cleared by centrifugation (16,000×g, 45 min; 4°C) to remove cell debris. The supernatant was filtered (0.45-μm pore size) and loaded onto a Ni-HiTrap column (GE Healthcare) pre-equilibrated with the same lysis buffer in order to capture the expressed proteins. The column was washed with 5 × column volume of lysis buffer, and bound protein was eluted by a linear gradient concentration of imidazole (20–600 mM, 10× column volume) in the lysis buffer. Target proteins were further purified on a Superdex S-200 16/60 column (GE Healthcare) pre-equilibrated with 20 mM Tris-HCl pH 8.0, 100 mM NaCl, 5mM DTT and 5% (v/v) glycerol. Fractions containing target proteins were pooled and concentrated according to requirements for subsequent experiments.

Isothermal titration calorimetry (ITC). For all ITC experiments, ultrapure water (milli-Q apparatus, Millipore) was used. All plastic materials were washed with 1 mM EDTA (pH 8.0) and then rinsed with milli-Q water to minimize Ca^{2+} contamination. ITC measurements were carried out using an iTC200 microcalorimeter (MicroCal) at 25°C in ITC buffer (20 mM Tris-HCl pH 8.0, 100 mM NaCl). Potentially pre-bound calcium was removed from the *Tb*BILBO1-EFh by incubating the protein with 50 mM EDTA (pH 8.0) for 1 hour at RT. EDTA was subsequently removed by dialyzing the protein sample against 3L of ITC buffer 5 times over 36 hours at 4°C. Before each ITC experiment, the sample cell of the microcalorimeter was washed several times with 1 mM EDTA (pH 8.0) and then rinsed with milli-Q water.

The sample cell was loaded with 200 μl of 30μM protein in ITC buffer. The reference cell contained only milli-Q water. Titration was carried out using a 40-μl syringe filled with 600μM $CaCl_2$ prepared in ITC buffer under continuous stirring at 1,000 × rpm. Injections were started after baseline stabilization. Each titration experiment consisted of an initial 0.4-μl injection followed by 19 consecutive injections of 2 μl each with duration of 0.8 s. The interval between each two injections was 150 seconds. The heat of dilution was measured by injecting $CaCl_2$ into the sample buffer without protein. The enthalpy change for each injection was calculated by integrating the area under the peaks for the recorded time course of power change, and then subtracting the control titration. Data were analyzed using the MicroCal Origin software and fitted to obtain thermodynamic parameters of calcium binding to the protein using a model with one set of sites.

Electron microscopy. Transfected U-2OS cells were harvested by scraping and then pelleted at 800 x g for 10 min at room temperature. They were then resuspended in 250μL PBS

(plus protease inhibitors), for 30 min at 4°C to depolymerize the sub-pellicular microtubules. 10μL of cell suspension was placed on freshly charged formvar/carbon coated G200 nickel electron EM grids at (4°C). After the cells had adhered the grids were inverted onto extraction buffer (500μL PBS, 1% Nonidet P40 plus benzonase and protease inhibitors) and extracted for 15 minutes in at R/T. Grids were then washed (1 x 5 minutes) by floating on 500μL PBS and fixed 5 minutes in 500μL of 2.5% glutaraldehyde in PBS. Grids were then washed in 500μL water, 1 x 5 minutes and negatively stained with a 10μL drop/grid of 50:50 mix of NanoVan:NanoW. For striation measurements, digital images were taken from grids of at least three different experiments. Filaments were measured and striations were counted by hand on all filaments identified using Image J software.

Yeast two-hybrid interaction assays

The pGADT7-AD (prey) and pGBKT7 (bait) based plasmid constructs were transformed in the yeast cell lines Y187 and Y2HGold respectively. After production of diploids cells, interaction tests were done using the drop test technique according to the manufacturer's instructions (Matchmaker Gold Yeast Two-Hybrid System, Clontech). Haploid and diploid strains were grown in SC medium (YNB (w/o ammonium sulfate 1.7 $g.L^{-1}$ (BD, #233520), Ammonium sulfate 5 $g.L^{-1}$ (Euromedex, #2019), CSM (-Leu, -His, -Trp, -Ade, -Ura) 0.59 $g.L^{-1}$ (MP, #4550–122), Dextrose (D+Glucose) 0.59 $g.L^{-1}$ (Euromedex, #UG3050), Uracil (0.02 $g.L^{-1}$) and complemented with Leucine (1 $g.L^{-1}$), Tryptophan (0.05 $g.L^{-1}$), Histidine (0.02 $g.L^{-1}$), or Adenine (0.04 $g.L^{-1}$) as required. Absence of auto-activation for each pGBKT7 bait construct was tested on SC-Tryptophan-Histidine medium. Absence of toxicity for each pGADT7-AD and pGBKT7 construct was tested on SC-Leucine and SC-Tryptophan respectively. Diploid yeasts were selected on SC-Leucine-Tryptophan medium (SC-L-W). Interaction tests were done on SC-L-W-Histidine media. All interactions were tested in both prey and bait configuration. Interaction using T2 as bait could not be tested because of auto-activation on SC-W-H medium.

Bioinformatics

The two EF-hand domains were predicted by InterProScan [54] and Smart [55] software, and the CC domain by the Coils software [56].

Sample preparation and western blots

Trypanosome cells. $2.5.10^7$ non-induced and induced cells (six or 24 hours) PCF were split in two flasks for whole cells (WC) and cytoskeleton (CK) samples. For WC samples, cells were spun at 1,000 x g for 10 minutes, washed once and resuspended at 1.10^6 cells/μL^{-1} in PBS. An equivalent volume of 2x sample buffer and 25U of benzonase (Sigma, E1014) was added before boiling 3 minutes. For CK samples, cells were spun at 1,000 g for 10 minutes and washed once in PBS, EDTA 10mM and resuspended at 1.10^6 cells/μL^{-1} in 100 mM PIPES pH6.8, 2 mM $MgCl_2$, 0.25% NP-40, Protease inhibitor (Calbiochem, 1:10,000 dilution) and 25U of benzonase. After 10 minutes incubation on ice, cytoskeletons were pelleted at 1,000 x g for 30 minutes then washed in 1 mL 100 mM PIPES pH6.8, 2 mM $MgCl_2$ and resuspended in the same buffer (1.10^6 cells/μL^{-1} final). An equivalent volume of 2x sample buffer was added before boiling for 3 minutes. 2.10^6 cells (or cytoskeleton) were loaded on 10 or 12% SDS-PAGE, semi-dry transferred on PVDF membrane or nitrocellulose membrane.

U-2 OS cells. Exponentially growing U-2 OS cells in T-25 flask were lipotransfected with 12.5 μg DNA using Lipofectamine 2000 in OPTIMEM (Invitrogen) according to the manufacturer's instructions and processed for western-blot for 6 hours post-transfection (or 24 hours post-transfection for the mEFH1+2 sample). Cells were collected by; scraping the bottom of

the respective culture flasks and transferring the detached cells into ice cold PBS. Cells were then centrifuged 5 min, 1,000 x g and resuspended in 125μL of buffer (PIPES 60 mM, HEPES 25 mM, EGTA 10 mM, $MgCl_2$ 10 mM adjusted to pH6.9 with KOH, glycerol 10%, protease inhibitors (Calbiochem Cocktail set III, 1:10,000 dilution and 1mM PMSF) then lysed by adding 125μL of buffer supplemented with 0.2% TX-100. The supernatant was collected after a 5 minute centrifugation at 1,500 x g and 62.5μL of sample buffer 4x was added. Boiling 5 for minutes denatured the sample and then benzonase (5U) was added. The pellet was resuspended in 250 μL of buffer with 0.1% TX-100, 62.5μL sample buffer 4x was added and the sample was denatured by boiling for 5 minute before adding 7.5U of benzonase. Protein concentrations were assayed using the Pierce 660 nm Protein Assay (#22660) with the ionic detergent compatibility reagent (#22663) kit according to the manufacturer's instructions. 13–20μg of protein from supernatant samples, and a corresponding volume of pellet samples, were separated by SDS-PAGE (10%) and semi-dry transferred onto PVDF membrane. Membranes were blocked in Tris-buffered saline (TBS), 0.2% Tween-20, 5% skimmed milk powder for 1 hour then incubated overnight at 4°C with the primary antibodies diluted in blocking solution: rabbit polyclonal anti-NTD diluted at 1:200, mouse monoclonal 5F2B3 undiluted, anti-myc monoclonal 9E10 (A kind gift from K. Ersfeld, University of Bayreuth, Germany) at 1:200, anti-alpha-Tubulin TAT1 monoclonal antibody (a kind gift from K. Gull, Sir William Dunn School of Pathology, University of Oxford, England, U.K) at 1:500. After 3 washes (10 min) in TBS, 0.2% Tween-20, 1M NaCl, the membranes were incubated for 1 hour at room temperature with secondary antibodies diluted in blocking solution: anti-mouse HRP conjugated antibody (Jackson 115-055-068, 1:10,000), ECL Plex anti-mouse Cy3 conjugated (GE Healthcare #PA43009V, 1:2,500), ECL Plex anti-rabbit Cy5 conjugated (GE Healthcare #PA45011V, 1:2,500). After washes in blocking solution, in TBS, 0.2% Tween-20 then TBS, membranes were revealed by ECL (Clarity Biorad chemiluminescence kit # 170–5061) according to the manufacturer's instructions) or direct fluorescence detection on a LAS4010 (GE Healthcare #28-9558-11) with R670 Cy5 filter, 575DF20 Cy3 filter, according to the manufacturer's instructions.

LC MS/MS and phosphorylation analysis

T. brucei brucei PCF 427 29–13 whole cell extracts was run on a 12% SDS-PAGE and stained with colloidal blue. After several H_2O washes, a 60–80KDa band was excised and trypsin digested before LC-MS/MS analysis. Using Discoverer 1.3 (PhosphoRS module), one phosphorylation was identified on serine 163 (HAsFHGSTSNALVPR).

Supporting Information

S1 Fig. BILBO1 forms helical polymers when expressed in a heterologous system. Heterologous expression of un-tagged BILBO1 in mammalian U-2 OS cells demonstrates that BILBO1 has self-polymerizing properties. Un-tagged full-length BILBO1 protein was immuno-labelled with anti-BILBO1 monoclonal antibody 24 hours after transfection. In this image long helical polymers are formed within the cell. (A) DAPI (blue) and immunofluorescence (red) merged image of full-length BILBO1 polymers. (B) Enlarged immunofluorescence image of full-length BILBO1 polymers. (C) Phase contrast image of the same polymers observed in B. (D). Phase contrast and fluorescence-merged images B and C. Scale bars represent 10 μm in A and 1 μm in B.
(TIF)

S2 Fig. BILBO1 polymers are formed independently of the Golgi, ER, or the cytoskeleton when expressed in U-2 OS cells. U-2 OS cells expressing BILBO1-GFP for six hours were

probed or immuno-labelled with cellular markers. F-Actin was probed with Texas red-coupled phalloidin (A-C), intermediate filaments were labelled with anti-vimentin (D-F), microtubules were labelled with anti-tubulin (G-I), the Golgi apparatus was labelled with anti-giantin (J-L), and the endoplasmic reticulum was labelled with anti-calnexin (M-O). Scale bar represents 10 μm. No apparent co-localization of BILBO1-GFP with any of these structures was observed.
(TIF)

S3 Fig. mEFH1+2 protein is degraded in U-2 OS cells. (A) U-2 OS cells expressing mEFH1+2 for six hours were treated with 50μM of the proteasome inhibitor MG132 for six hours, then extracted, fixed and processed for immunofluorescence using anti-NTD. (B) The graph shows the percentage of cells in the MG132 experiment that retained anti-NTD signal. (C) U-2 OS whole cells (WC) that were expressing mEFH1+2 were MG132 treated (+) or mock treated (-) and subject to western blotting using anti-BILBO1 5F3B3. Quantification of the western-blot and tubulin normalization indicates and increase in protein level in MG132 treated cells.
(TIF)

S4 Fig. Impact on the overexpression of myc tagged recombinant forms of BILBO1 on endogenous BILBO1 levels in *T. brucei*, and effect of the proteasome inhibitor on mEFH1+2:myc protein levels. Western blot analysis of overexpression of myc tagged recombinant forms of BILBO1 on endogenous BILBO1 levels in *T. brucei*. Endogenous BILBO1 levels was quantified in *T. brucei* cytoskeletons derived from cell lines expressing recombinant T1:myc, T2:myc (A), T3:myc, T4:myc (B), BILBO1:myc, mEFH1:myc, mEFH2:myc, and mEFH1+2:myc (C). All samples were tested for six or 24 hours. In (C) the NTD antibody was able to define the difference between wild-type and myc tagged protein due to the higher molecular mass of the myc tagged form. Therefore in the upper panel of (C) wild-type protein is present as the lower band and myc tagged protein is the upper band. (D) *T. brucei* mEFH1+2:myc expressing cells were mock treated (-) or treated with 42 μM MG132 (+). Quantification analyses were done using tubulin as loading control (probed with TAT1). Anti-NTD labels endogenous BILBO1, BILBO1:myc, T1:my, T2:myc, mEFH1:myc, mEFH2:myc, and mEFH1+2:myc.
(TIF)

S5 Fig. Yeast two-hybrid analysis of FPC5-BILBO1 EF-hand mediated interaction. (A) Yeast two-hybrid analysis indicates that full-length BILBO1 interacts with full-length BILBO1, and a deleted EF-hand form of BILBO1 where the N-terminal domain is retained ΔEFH1+2). We also tested mutant forms of both EF-hands (mEFhand1+2) versus the coiled-coil domain of BILBO1 (T4), or the N-terminal deleted form of BILBO1 (T3). (B) Full-length BILBO1 interacts with the binding domain of FPC5 ($FPC5_{binding\ domain}$), whilst deletion of both EF-Hands (ΔEFH1+2) or mutation of both EF-Hands (mEHH1+2) prevents this interaction. BILBO1 and $FPC5_{binding\ domain}$, were tested both as bait (AD) or prey (BD) and demonstrate that EF-hands are required for BILBO1-$FPC5_{binding\ domain}$. Yeast transformants expressing the combinations of constructs indicated in the figure were spotted onto plates without or with histidine (-His and +His, respectively). Bait and prey interactions were tested by drop test (10^5cells) and incubated at 30°C for 3 days before analysis.
(TIF)

S6 Fig. (A) Determination of the percentage of simple or complex fibres in BILBO1 U-2 OS cells after six or 24 hours post-transfection with or without BAPTA-AM treatment (25ug/ml, for three hours). No significant difference was observed between treated and untreated cells. (B) Immunofluorescence labelling of cytoskeletons from cells expressing mEFH1:myc for six hours and then treated with 5mM EGTA for 10 minutes before fixation and processing. Cytoskeletons were probed using anti-myc (red) and anti-NTD (green) antibodies and

show that the polymers were not extracted by EGTA treatment. Scale bars represent 5 μm. (TIF)

Acknowledgments

We thank K. Gull for the anti-tubulin TAT1 antibody, K. Ersfeld fotr the anti-myc antibody, E. Chevet (INSERM 1053, France) for the anti-Giantin and anti-Calnexin antibodies, F. Soulet (INSERM U1029, France) for the anti-Vimentin antibody, G. Cross (The Rockefeller University, U.S.A.) for the *T. brucei* parental cell lines and pLew100 vector, Ms N. Chalard, J. Marcos and G. Cougnet-Houlery (UMR5234) for the continued lab infrastructure.

Author Contributions

Conceived and designed the experiments: NL DD AA DRR MB EHB. Performed the experiments: CF AS KV GD NL DD AA EHB MB DRR. Analyzed the data: CF AS KV GD NL DD AA EHB MB DRR. Contributed reagents/materials/analysis tools: CF AS KV GD NL DD AA EHB MB DRR. Wrote the paper: CF EHB AS NL DD MB DRR.

References

1. Malvy D, Chappuis F (2011) Sleeping sickness. Clin Microbiol Infect 17: 986–995. doi: 10.1111/j.1469-0691.2011.03536.x PMID: 21722252
2. Rassi A, Rezende JM, Rassi A Jr (2012) Advanced megaesophagus (Group III) secondary to vector-borne Chagas disease in a 20-month-old infant. Rev Soc Bras Med Trop 45: 266–268. PMID: 22535006
3. Kedzierski L (2011) Leishmaniasis. Hum Vaccin 7: 1204–1214. doi: 10.4161/hv.7.11.17752 PMID: 22048116
4. Sherwin T, Gull K (1989) The cell division cycle of Trypanosoma brucei brucei: timing of event markers and cytoskeletal modulations. Philos Trans R Soc Lond B Biol Sci 323: 573–588. PMID: 2568647
5. Field MC, Carrington M (2009) The trypanosome flagellar pocket. Nat Rev Microbiol 7: 775–786. doi: 10.1038/nrmicro2221 PMID: 19806154
6. Lacomble S, Vaughan S, Gadelha C, Morphew MK, Shaw MK, et al. (2009) Three-dimensional cellular architecture of the flagellar pocket and associated cytoskeleton in trypanosomes revealed by electron microscope tomography. J Cell Sci 122: 1081–1090. doi: 10.1242/jcs.045740 PMID: 19299460
7. Gadelha C, Rothery S, Morphew M, McIntosh JR, Severs NJ, et al. (2009) Membrane domains and flagellar pocket boundaries are influenced by the cytoskeleton in African trypanosomes. Proc Natl Acad Sci U S A 106: 17425–17430. doi: 10.1073/pnas.0909289106 PMID: 19805090
8. Bonhivers M, Nowacki S, Landrein N, Robinson DR (2008) Biogenesis of the trypanosome endo-exocytotic organelle is cytoskeleton mediated. PLoS Biol 6: e105. doi: 10.1371/journal.pbio.0060105 PMID: 18462016
9. Esson HJ, Morriswood B, Yavuz S, Vidilaseris K, Dong G, et al. (2012) Morphology of the trypanosome bilobe, a novel cytoskeletal structure. Eukaryot Cell 11: 761–772. doi: 10.1128/EC.05287-11 PMID: 22327007
10. Morriswood B, He CY, Sealey-Cardona M, Yelinek J, Pypaert M, et al. (2009) The bilobe structure of Trypanosoma brucei contains a MORN-repeat protein. Mol Biochem Parasitol 167: 95–103. doi: 10.1016/j.molbiopara.2009.05.001 PMID: 19445968
11. Morriswood B, Havlicek K, Demmel L, Yavuz S, Sealey-Cardona M, et al. (2013) Novel bilobe components in Trypanosoma brucei identified using proximity-dependent biotinylation. Eukaryot Cell 12: 356–367. doi: 10.1128/EC.00326-12 PMID: 23264645
12. Bangs JD (2011) Replication of the ERES:Golgi junction in bloodstream-form African trypanosomes. Mol Microbiol 82: 1433–1443. doi: 10.1111/j.1365-2958.2011.07900.x PMID: 22026408
13. Vidilaseris K, Dong G (2014) Expression, purification and preliminary crystallographic analysis of the N-terminal domain of Trypanosoma brucei BILBO1. Acta Crystallogr F Struct Biol Commun 70: 628–631. doi: 10.1107/S2053230X14005743 PMID: 24817725
14. Vidilaseris K, Morriswood B, Kontaxis G, Dong G (2013) Structure of the TbBILBO1 N-terminal domain from Trypanosoma brucei reveals an essential requirement for a conserved surface patch. J Biol Chem 289: 3724–3735. doi: 10.1074/jbc.M113.529032 PMID: 24362019

15. Vidilaseris K, Shimanovskaya E, Esson HJ, Morriswood B, Dong G (2014) Assembly mechanism of Trypanosoma brucei BILBO1, a multidomain cytoskeletal protein. J Biol Chem 289: 23870–23881. doi: 10.1074/jbc.M114.554659 PMID: 25031322

16. Lacomble S, Portman N, Gull K (2009) A protein-protein interaction map of the Trypanosoma brucei paraflagellar rod. PLoS One 4: e7685. doi: 10.1371/journal.pone.0007685 PMID: 19888464

17. del Castillo FJ, Cohen-Salmon M, Charollais A, Caille D, Lampe PD, et al. (2010) Consortin, a trans-Golgi network cargo receptor for the plasma membrane targeting and recycling of connexins. Hum Mol Genet 19: 262–275. doi: 10.1093/hmg/ddp490 PMID: 19864490

18. Alaoui-Ismaili MH, Richardson CD (1998) Insect virus proteins (FALPE and p10) self-associate to form filaments in infected cells. J Virol 72: 2213–2223. PMID: 9499079

19. Gifford JL, Walsh MP, Vogel HJ (2007) Structures and metal-ion-binding properties of the Ca2+-binding helix-loop-helix EF-hand motifs. Biochem J 405: 199–221. PMID: 17590154

20. Zhou Y, Yang W, Kirberger M, Lee HW, Ayalasomayajula G, et al. (2006) Prediction of EF-hand calcium-binding proteins and analysis of bacterial EF-hand proteins. Proteins 65: 643–655. PMID: 16981205

21. Grabarek Z (2006) Structural basis for diversity of the EF-hand calcium-binding proteins. J Mol Biol 359: 509–525. PMID: 16678204

22. Freyer MW, Lewis EA (2008) Isothermal titration calorimetry: experimental design, data analysis, and probing macromolecule/ligand binding and kinetic interactions. Methods Cell Biol 84: 79–113. PMID: 17964929

23. Han BG, Han M, Sui H, Yaswen P, Walian PJ, et al. (2002) Crystal structure of human calmodulin-like protein: insights into its functional role. FEBS Lett 521: 24–30. PMID: 12067719

24. de Godoy LM, Marchini FK, Pavoni DP, Rampazzo Rde C, Probst CM, et al. (2012) Quantitative proteomics of Trypanosoma cruzi during metacyclogenesis. Proteomics 12: 2694–2703. doi: 10.1002/pmic.201200078 PMID: 22761176

25. Marchini FK, de Godoy LM, Rampazzo RC, Pavoni DP, Probst CM, et al. (2011) Profiling the Trypanosoma cruzi phosphoproteome. PLoS One 6: e25381. doi: 10.1371/journal.pone.0025381 PMID: 21966514

26. Rock KL, Gramm C, Rothstein L, Clark K, Stein R, et al. (1994) Inhibitors of the proteasome block the degradation of most cell proteins and the generation of peptides presented on MHC class I molecules. Cell 78: 761–771. PMID: 8087844

27. Wirtz E, Clayton C (1995) Inducible gene expression in trypanosomes mediated by a prokaryotic repressor. Science 268: 1179–1183. PMID: 7761835

28. Nelson MR, Chazin WJ (1998) Structures of EF-hand Ca(2+)-binding proteins: diversity in the organization, packing and response to Ca2+ binding. Biometals 11: 297–318. PMID: 10191495

29. Strynadka NC, James MN (1989) Crystal structures of the helix-loop-helix calcium-binding proteins. Annu Rev Biochem 58: 951–998. PMID: 2673026

30. Nelson MR, Thulin E, Fagan PA, Forsen S, Chazin WJ (2002) The EF-hand domain: a globally cooperative structural unit. Protein Sci 11: 198–205. PMID: 11790829

31. Wilson AK, Coulombe PA, Fuchs E (1992) The roles of K5 and K14 head, tail, and R/K L L E G E domains in keratin filament assembly in vitro. J Cell Biol 119: 401–414. PMID: 1383231

32. Lee CH, Coulombe PA (2009) Self-organization of keratin intermediate filaments into cross-linked networks. J Cell Biol 186: 409–421. doi: 10.1083/jcb.200810196 PMID: 19651890

33. Iino T (1974) Assembly of Salmonella flagellin in vitro and in vivo. J Supramol Struct 2: 372–384. PMID: 4612254

34. Minamino T, Namba K (2004) Self-assembly and type III protein export of the bacterial flagellum. J Mol Microbiol Biotechnol 7: 5–17. PMID: 15170399

35. Fujita Y, Ohto E, Katayama E, Atomi Y (2004) alphaB-Crystallin-coated MAP microtubule resists nocodazole and calcium-induced disassembly. J Cell Sci 117: 1719–1726. PMID: 15075233

36. Boelens WC (2014) Cell biological roles of alphaB-crystallin. Prog Biophys Mol Biol 115: 3–10. doi: 10.1016/j.pbiomolbio.2014.02.005 PMID: 24576798

37. Izard J, Parker MW, Chartier M, Duche D, Baty D (1994) A single amino acid substitution can restore the solubility of aggregated colicin A mutants in Escherichia coli. Protein Eng 7: 1495–1500. PMID: 7716161

38. Fox JD, Kapust RB, Waugh DS (2001) Single amino acid substitutions on the surface of Escherichia coli maltose-binding protein can have a profound impact on the solubility of fusion proteins. Protein Sci 10: 622–630. PMID: 11344330

39. Vekilov PG (2007) Sickle-cell haemoglobin polymerization: is it the primary pathogenic event of sickle-cell anaemia? Br J Haematol 139: 173–184. PMID: 17897293

40. Ghossoub R, Molla-Herman A, Bastin P, Benmerah A (2011) The ciliary pocket: a once-forgotten membrane domain at the base of cilia. Biol Cell 103: 131–144. doi: 10.1042/BC20100128 PMID: 21275905

41. Molla-Herman A, Ghossoub R, Blisnick T, Meunier A, Serres C, et al. (2010) The ciliary pocket: an endocytic membrane domain at the base of primary and motile cilia. J Cell Sci 123: 1785–1795. doi: 10.1242/jcs.059519 PMID: 20427320

42. Fawcett DW (1970) A comparative view of sperm ultrastructure. Biol Reprod 2: Suppl 2:90–127. PMID: 5521054

43. Veland IR, Awan A, Pedersen LB, Yoder BK, Christensen ST (2009) Primary cilia and signaling pathways in mammalian development, health and disease. Nephron Physiol 111: p39–53. doi: 10.1159/000208212 PMID: 19276629

44. Pazour GJ, Dickert BL, Vucica Y, Seeley ES, Rosenbaum JL, et al. (2000) Chlamydomonas IFT88 and its mouse homologue, polycystic kidney disease gene tg737, are required for assembly of cilia and flagella. J Cell Biol 151: 709–718. PMID: 11062270

45. Hu Q, Nelson WJ (2011) Ciliary diffusion barrier: the gatekeeper for the primary cilium compartment. Cytoskeleton (Hoboken) 68: 313–324. doi: 10.1002/cm.20514 PMID: 21634025

46. Chih B, Liu P, Chinn Y, Chalouni C, Komuves LG, et al. (2012) A ciliopathy complex at the transition zone protects the cilia as a privileged membrane domain. Nat Cell Biol 14: 61–72. doi: 10.1038/ncb2410 PMID: 22179047

47. Vincensini L, Blisnick T, Bastin P (2011) 1001 model organisms to study cilia and flagella. Biol Cell 103: 109–130. doi: 10.1042/BC20100104 PMID: 21275904

48. Heldin CH, Johnsson A, Wennergren S, Wernstedt C, Betsholtz C, et al. (1986) A human osteosarcoma cell line secretes a growth factor structurally related to a homodimer of PDGF A-chains. Nature 319: 511–514. PMID: 3456080

49. Dacheux D, Landrein N, Thonnus M, Gilbert G, Sahin A, et al. (2012) A MAP6-Related Protein Is Present in Protozoa and Is Involved in Flagellum Motility. PLoS One 7: e31344. doi: 10.1371/journal.pone.0031344 PMID: 22355359

50. Berriman M, Ghedin E, Hertz-Fowler C, Blandin G, Renauld H, et al. (2005) The genome of the African trypanosome Trypanosoma brucei. Science 309: 416–422. PMID: 16020726

51. Wirtz E, Leal S, Ochatt C, Cross GA (1999) A tightly regulated inducible expression system for conditional gene knock-outs and dominant-negative genetics in Trypanosoma brucei. Mol Biochem Parasitol 99: 89–101. PMID: 10215027

52. Pradel LC, Bonhivers M, Landrein N, Robinson DR (2006) NIMA-related kinase TbNRKC is involved in basal body separation in Trypanosoma brucei. J Cell Sci 119: 1852–1863. PMID: 16608878

53. Woods A, Sherwin T, Sasse R, MacRae TH, Baines AJ, et al. (1989) Definition of individual components within the cytoskeleton of Trypanosoma brucei by a library of monoclonal antibodies. J Cell Sci 93 (Pt 3): 491–500.

54. Zdobnov EM, Apweiler R (2001) InterProScan—an integration platform for the signature-recognition methods in InterPro. Bioinformatics 17: 847–848. PMID: 11590104

55. Schultz J, Milpetz F, Bork P, Ponting CP (1998) SMART, a simple modular architecture research tool: identification of signaling domains. Proc Natl Acad Sci U S A 95: 5857–5864. PMID: 9600884

56. Lupas A, Van Dyke M, Stock J (1991) Predicting coiled coils from protein sequences. Science 252: 1162–1164. PMID: 2031185

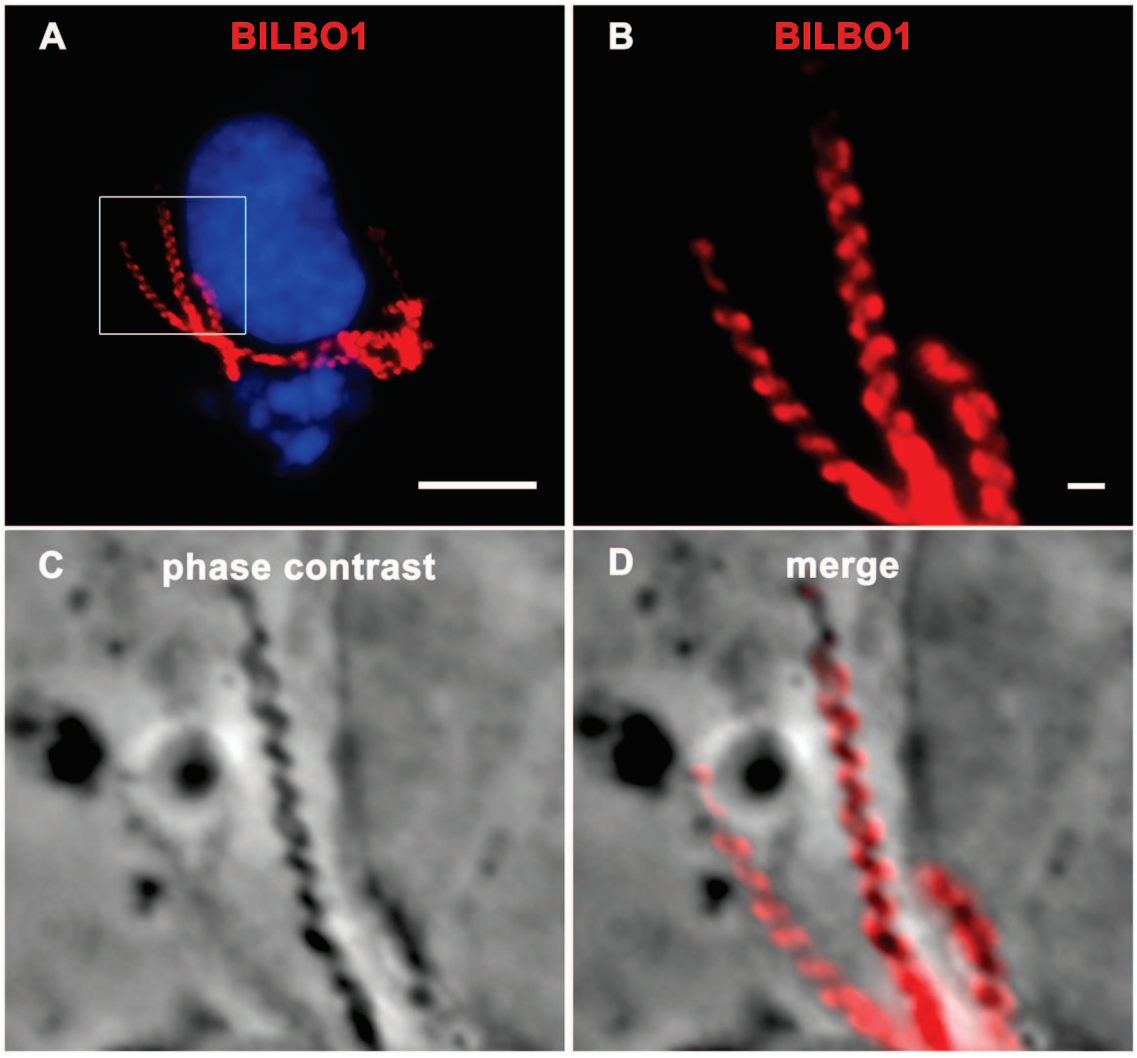
A
BILBO1
B
BILBO1
C
phase contrast
D
merge

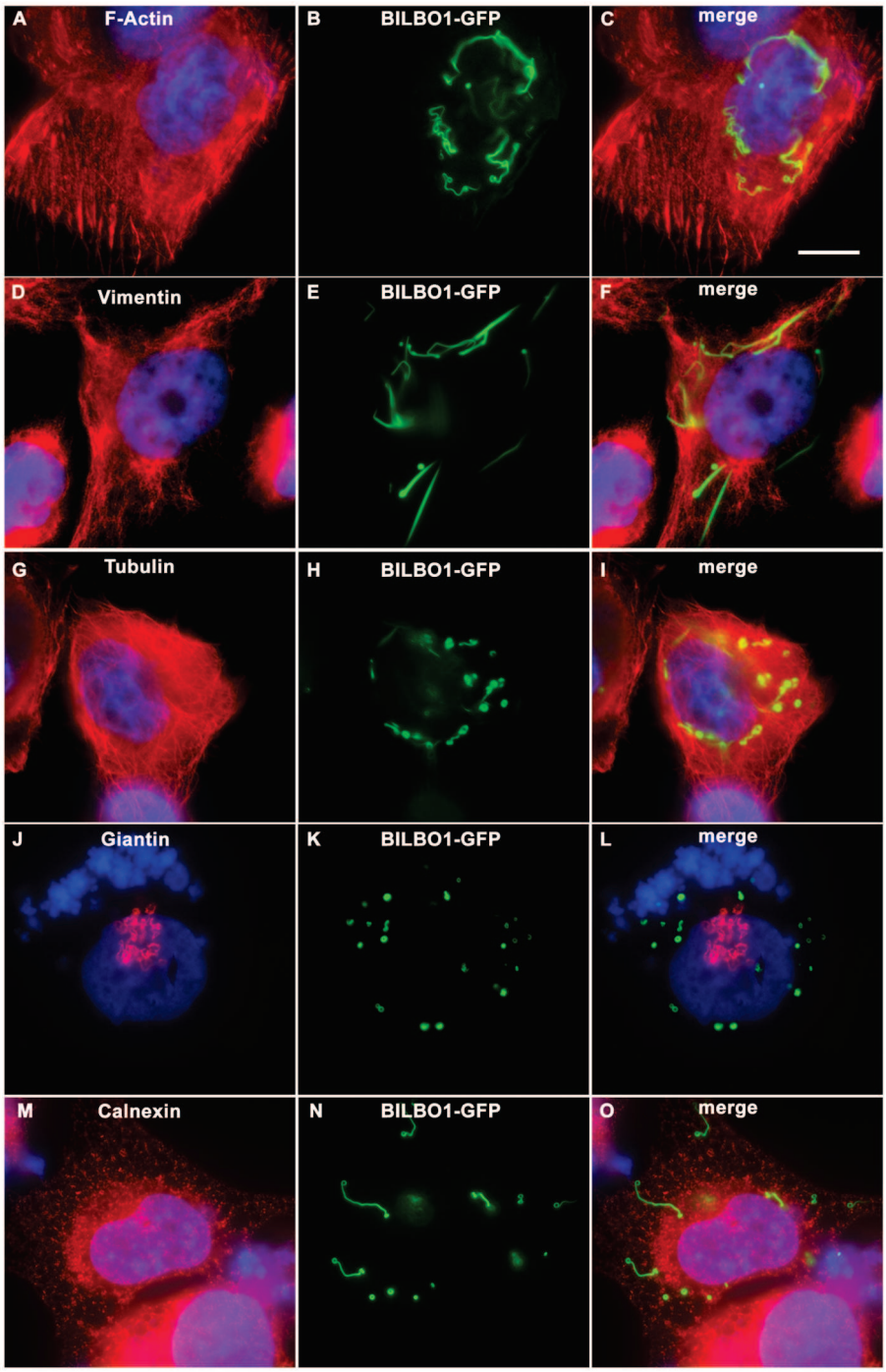
A
F-Actin
B
BILBO1-GFP
C
merge
D
Vimentin
E
BILBO1-GFP
F
merge
G
Tubulin
H
BILBO1-GFP
I
merge
J
Giantin
K
BILBO1-GFP
L
merge
M
Calnexin
N
BILBO1-GFP
O
merge

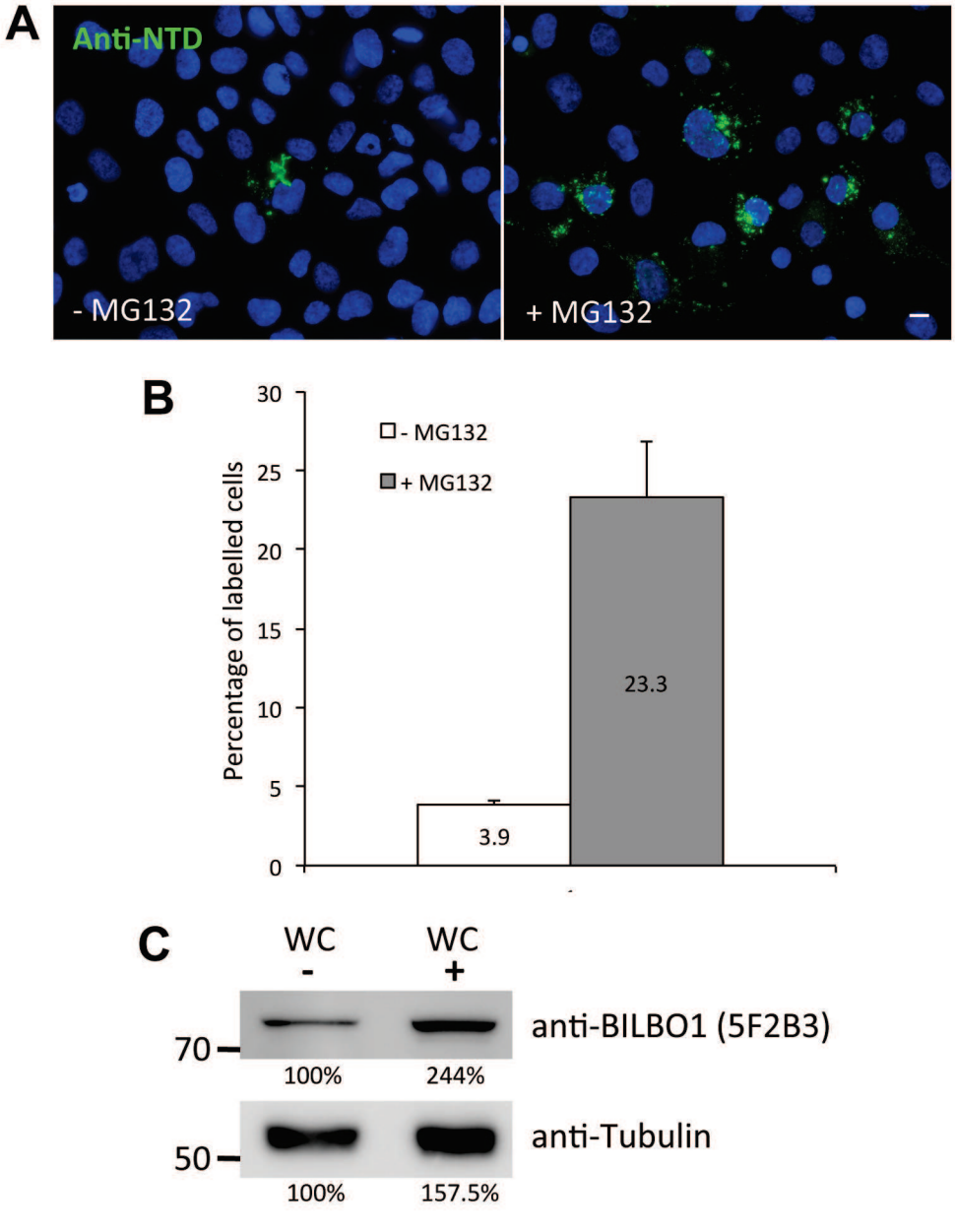
A
Anti-NTD
- MG132
+ MG132
B
Percentage of labelled cells
30
25
20
15
10
5
0
- MG132
+ MG132
23.3
3.9
C
WC
-
WC
+
70
anti-BILBO1 (5F2B3)
100%
244%
50
anti-Tubulin
100%
157.5%

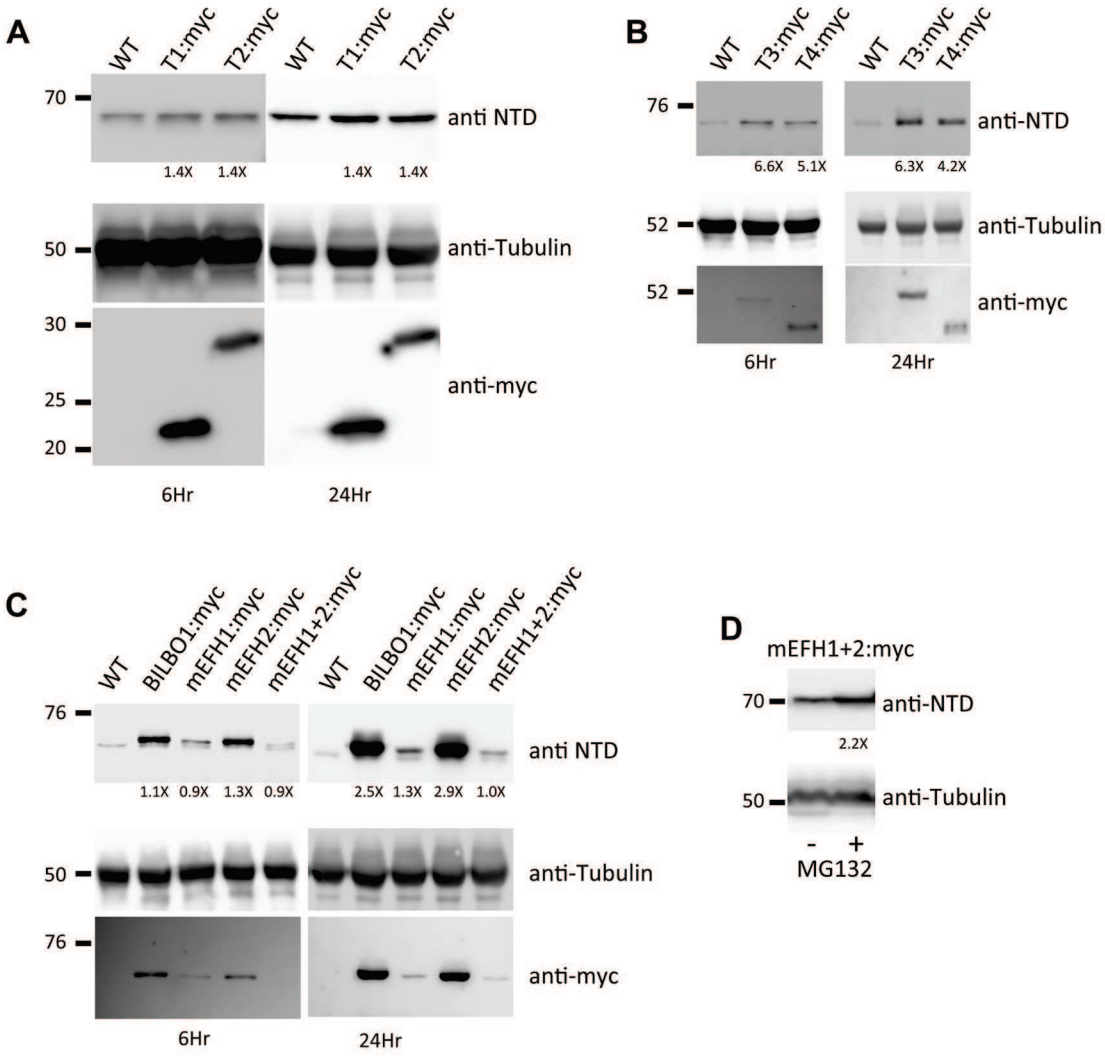
A
WT
T1:myc
T2:myc
WT
T1:myc
T2:myc
70
anti NTD
1.4X
1.4X
1.4X
1.4X
50
anti-Tubulin
30
25
20
anti-myc
6Hr
24Hr
B
WT
T3:myc
T4:myc
WT
T3:myc
T4:myc
76
anti-NTD
6.6X
5.1X
6.3X
4.2X
52
anti-Tubulin
52
anti-myc
6Hr
24Hr
C
WT
BILBO1:myc
mEFH1:myc
mEFH2:myc
mEFH1+2:myc
WT
BILBO1:myc
mEFH1:myc
mEFH2:myc
mEFH1+2:myc
76
anti NTD
1.1X
0.9X
1.3X
0.9X
2.5X
1.3X
2.9X
1.0X
50
anti-Tubulin
76
anti-myc
6Hr
24Hr
D
mEFH1+2:myc
70
anti-NTD
2.2X
50
anti-Tubulin
-
+
MG132

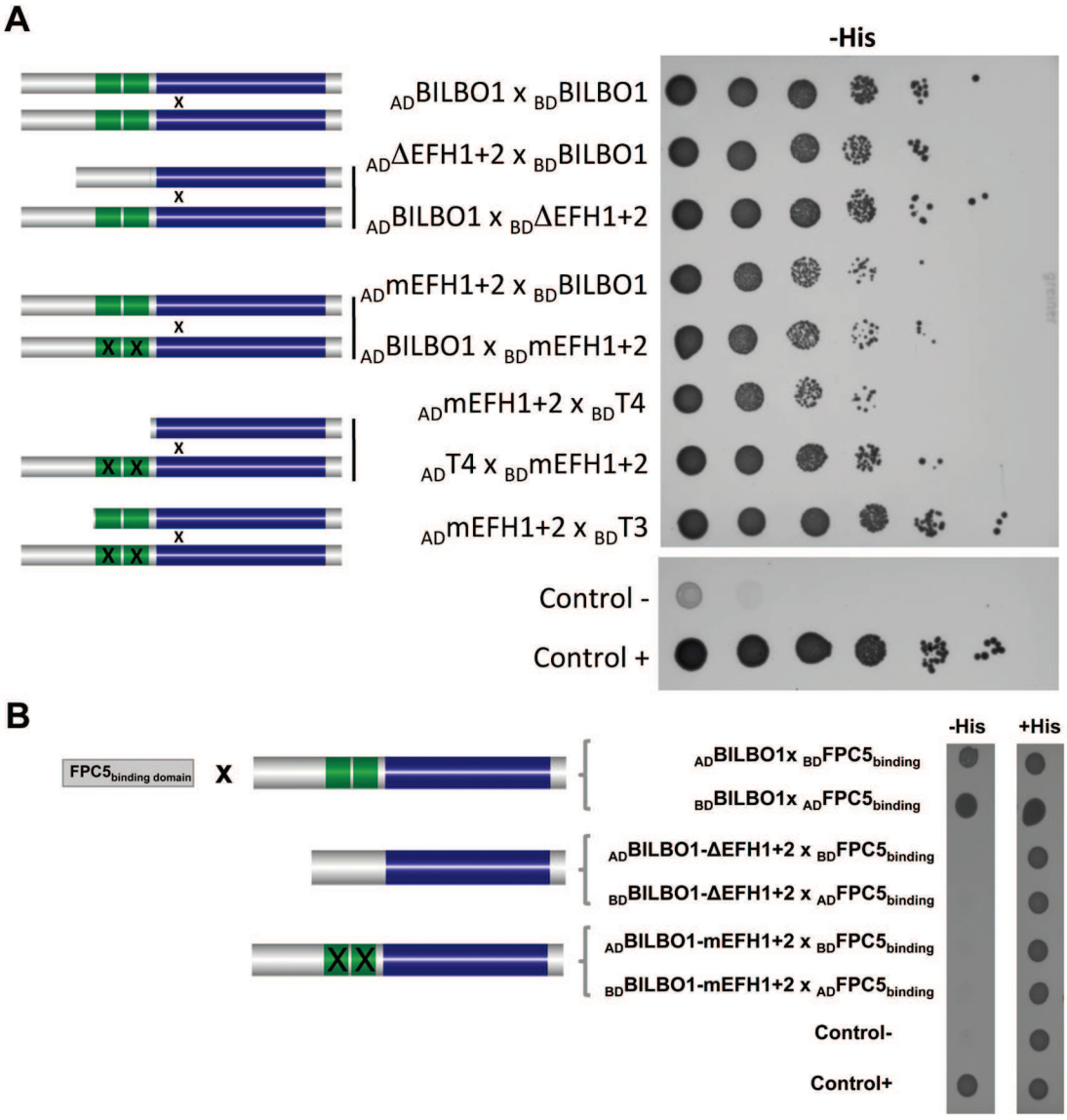
A
-His
$_{AD}$BILBO1 x $_{BD}$BILBO1
$_{AD}$ΔEFH1+2 x $_{BD}$BILBO1
$_{AD}$BILBO1 x $_{BD}$ΔEFH1+2
$_{AD}$mEFH1+2 x $_{BD}$BILBO1
$_{AD}$BILBO1 x $_{BD}$mEFH1+2
$_{AD}$mEFH1+2 x $_{BD}$T4
$_{AD}$T4 x $_{BD}$mEFH1+2
$_{AD}$mEFH1+2 x $_{BD}$T3
Control -
Control +
B
FPC5$_{binding\ domain}$
X
-His
+His
$_{AD}$BILBO1x $_{BD}$FPC5$_{binding}$
$_{BD}$BILBO1x $_{AD}$FPC5$_{binding}$
$_{AD}$BILBO1-ΔEFH1+2 x $_{BD}$FPC5$_{binding}$
$_{BD}$BILBO1-ΔEFH1+2 x $_{AD}$FPC5$_{binding}$
$_{AD}$BILBO1-mEFH1+2 x $_{BD}$FPC5$_{binding}$
$_{BD}$BILBO1-mEFH1+2 x $_{AD}$FPC5$_{binding}$
Control-
Control+

A

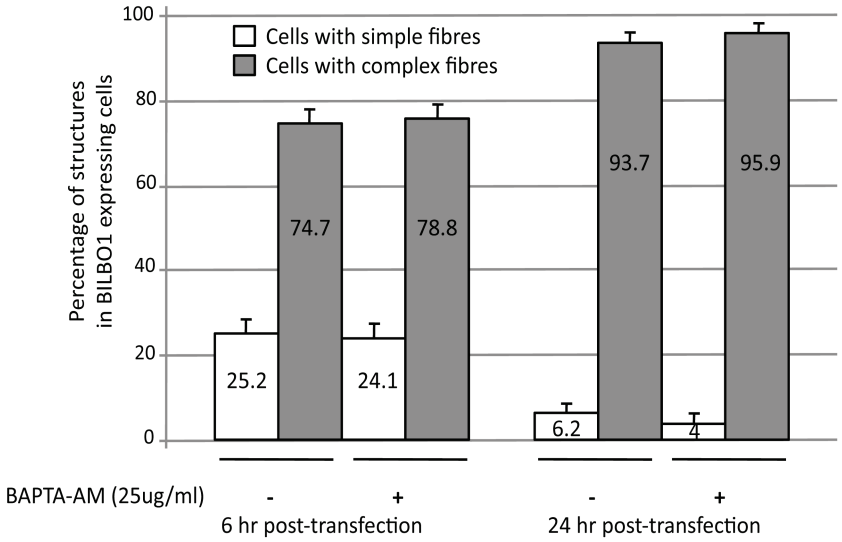
Cells with simple fibres
Cells with complex fibres
Percentage of structures in BILBO1 expressing cells
100
80
60
40
20
0
25.2
74.7
24.1
78.8
6.2
93.7
4
95.9
BAPTA-AM (25ug/ml)
-
+
-
+
6 hr post-transfection
24 hr post-transfection

B

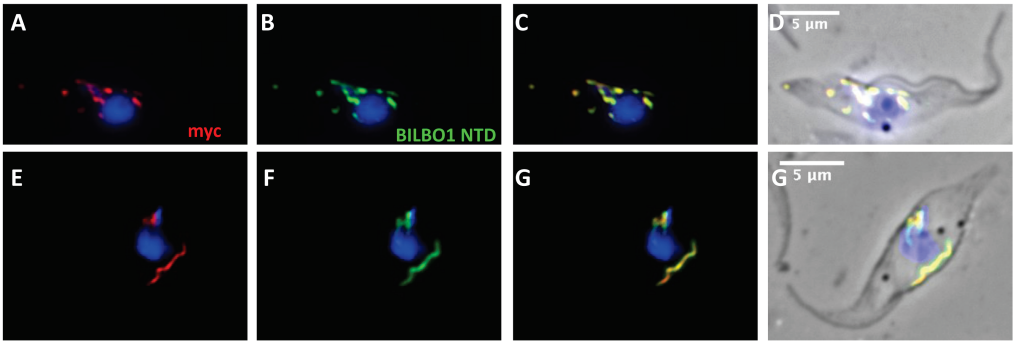
A
myc
B
BILBO1 NTD
C
D
5 µm
E
F
G
G
5 µm

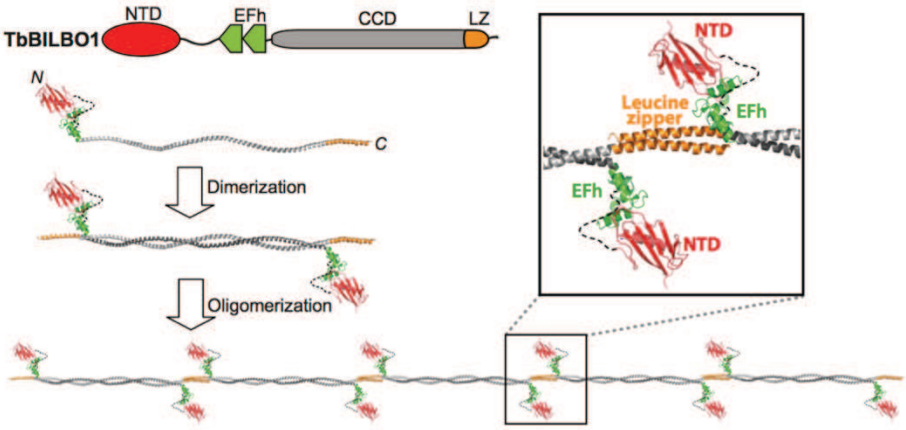

Fig. 3.1 *Proposed assembly mechanism of BILBO1 (Vidilaseris et al., 2014b)*
Two BILBO1 molecules form an antiparallel dimer *via* their CC-domains (grey) and can then assemble into filaments *via* the LZ (orange). The NTD (red) and the EF-Hands (green) are projected outward from the filament in opposite directions.

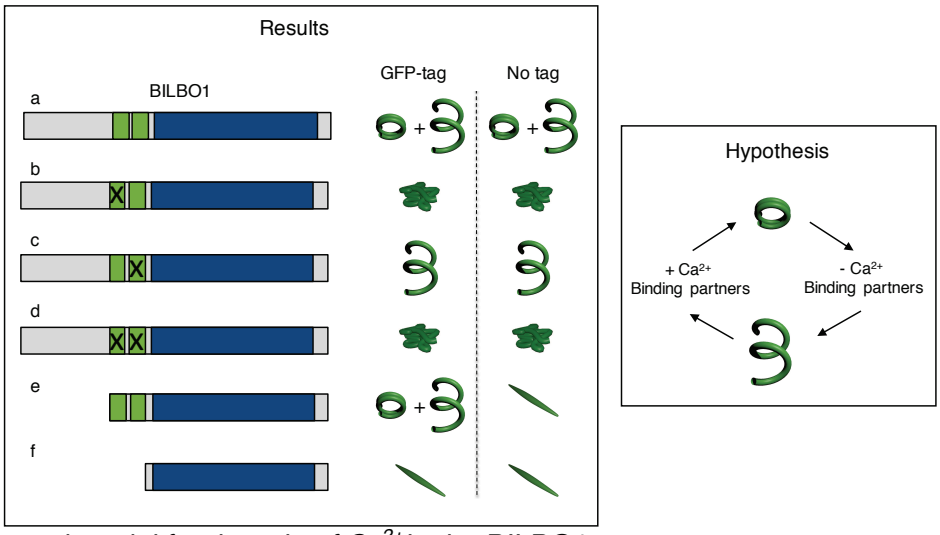

Fig. 3.2 *Proposed model for the role of Ca^{2+} in the BILBO1 structure*
A schematic diagram that describes the structures formed by BILBO1 and mutants when expressed in U-2 OS cells and the hypothesis of the role of calcium and/or binding partners in the shape of the structure. Part of the BILBO1-GFP data is unpublished.
(Results panel) Whilst presence of the coiled-coil domain (in blue) is required for BILBO1 polymerization, the calcium binding sites (in green) play a role in the shape of the structure formed. Both functional EF-Hand domains induce the formation of rings and corkscrew-like structures (a, e). Mutated EF-hand1 induces the formation of aggregates only (b). Mutation of EF-Hand2 induces the formation of corkscrew-like structures only (c). Mutation of both EF-Hands also induces aggregates (d). Absence of the N-terminal domain does not impair the formation of rings and corkscrew-like structures (e). However, absence of the N-terminal and of both EF-Hands leads to the formation of shuttle-like structures only (f). This suggests strongly that the N-terminal domain associated to the calcium-loaded/unloaded EF-Hands play a major role in the shape of the structures formed even though the N-terminal domain is not required for polymerization.
(Hypothesis panel) Based on our data, we propose the hypothesis where BILBO1 is a scaffold for the FPC structure. All domains of BILBO1 (the N-terminal domain, the EF-Hand domains, and the coiled-coil domain) are involved in the formation of the ring/corkscrew-like structures with a regulation based on the calcium-loaded state of the EF-Hands, and most probably on the interaction with protein partners of BILBO1.

c) Discussion: BILBO1 function and assembly in light of complementary data

To date, not much is known about the FPC. This cytoskeletal structure visible by TEM, encloses the flagellum at its exit site. The unique protein characterized so far in the FPC is BILBO1 (Bonhivers et al., 2008b).

Concomitantly to our study, the group of Gang Dong analysed *in vitro* the BILBO1 polymerizing properties (Vidilaseris et al., 2014b). Their *in vitro* analysis shows that BILBO1 is able to self-interact *via* its CC domain into anti-parallel homodimers and can form polymers *via* the interaction of the leucine zipper (LZ) at the end of the long CC domain. They thus proposed a model where the BILBO1-BILBO1 interaction let the N-terminus and the EF-Hands “freely” exposed on the outside of the polymer (Fig.3.1) (Vidilaseris et al., 2014b).

Both studies (Florimond et al., 2015; Vidilaseris et al., 2014b) show that both EF-Hand domains of BILBO1 are able to bind Ca^{2+} and that the absence of Ca^{2+} has an impact on protein folding.

All together, these data suggest that BILBO1 forms a scaffold that can adopt different conformations depending on the calcium binding status as described in the hypothesis Figure 3.2.

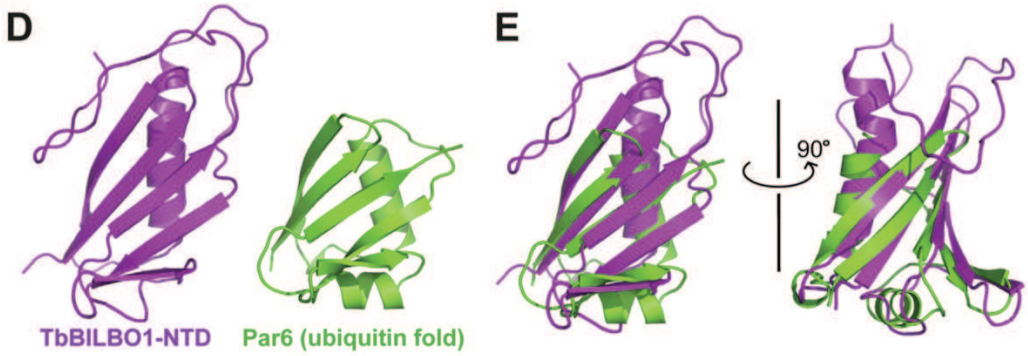

Fig. 3.3 *NMR structure of BILBO1-NTD reveals a ubiquitin-like fold*
Structural comparison (D) and superimposition (E) of BILBO1-NTD and the PB1 domain of Par6, which shows a ubiquitin-like fold (Vidilaseris et al., 2014a).

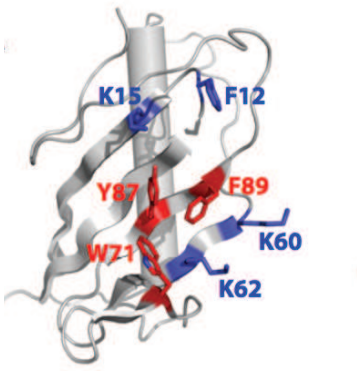

Fig. 3.4 *The conserved surface patch in the NTD of BILBO1 (Vidilaseris et al., 2014b).*
The seven conserved residues are highlighted. Three aromatic residues are found at the bottom of the crater-like structure (red) and the four residues at the rim are shown in blue.

d) Results – 2nd part

d1) Introduction: on the right track to understand BILBO1

Recently, the Dong laboratory solved the 3D structure of the N-terminal domain (NTD, aa 1 to 110) of BILBO1 and showed that it adopts a ubiquitin-like fold, similar to the PB1 domain of Par6 involved in protein-protein interaction (Vidilaseris et al., 2014a) (Fig.3.3). Moreover, this exposed N-terminal region shows a conserved surface patch, containing four aromatic residues (Phe-12, Trp-71, Tyr-87 and Phe-89) and three basic ones (Lys-15, Lys-60 and Lys-62). This patch forms a crater-like structure (Fig.3.4), with Trp-71, Tyr-87 and Phe-89 lying at the bottom of the crater and the other four residues exposed on the surface.

In *T. brucei*, the over-expressed N-terminal Ty1-tagged BILBO1 with a complete deletion of the NTD or over-expressed proteins containing mutations of specific residues of the conserved surface patch (mut1: F12A, K15A, K60A and K62A; and mut2: W71A, Y87A and F89A) were correctly targeted to the FPC and lead to morphological phenotypes, such as a detached new flagellum at the posterior end of the cell, and ultimately to cell growth arrest, as a dominant negative effect (Vidilaseris et al., 2014a). Comparable phenotypes were seen in the BILBO1 RNAi cell line (Bonhivers et al., 2008b). This demonstrates that the NTD of BILBO1 is essential for the parasite survival, but it is not involved in the targeting to the FPC.

It has been shown that the LZ is required but not sufficient for BILBO1 targeting to the FPC, whereas the NTD is not involved in targeting (Vidilaseris et al., 2014b; Florimond et al., 2015). The NTD might therefore play a structural role. The fact that single residues mutations (mut1 and mut2) in the NTD lead to dramatic phenotypes allowed us to think that the free NTD, and consequently also the EF-Hands, can act as binding sites for other FPC proteins.
Moreover, the fact that Ca^{2+} can influence the polymer structure (Vidilaseris et al., 2014b; Florimond et al., 2015b) renders Ca^{2+} an additional player in the FPC formation and function.

d2) Complementary analysis: are there other essential residues in the NTD of BILBO1?

In this context, and in collaboration with the Dong laboratory, we have initiated the analysis of novel residue mutations in the conserved surface patch (mut2b: Y87A, F89A and mut3: K60A, K62A) (Fig.3.5) within *T. brucei*, but also in U-2 OS cells.
The objectives are to identify key residues in the function of BILBO1, in particular residues involved in binding to putative protein partners.

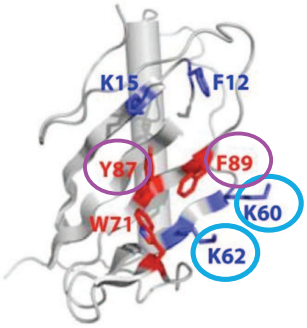

Fig. 3.5 *Mut2b and mut3 in the NTD of BILBO1.*
Two additional sets of mutations have been generated: mut2b in violet (Y87A and F89A) and mut3 in light blue (K60A and K62A).

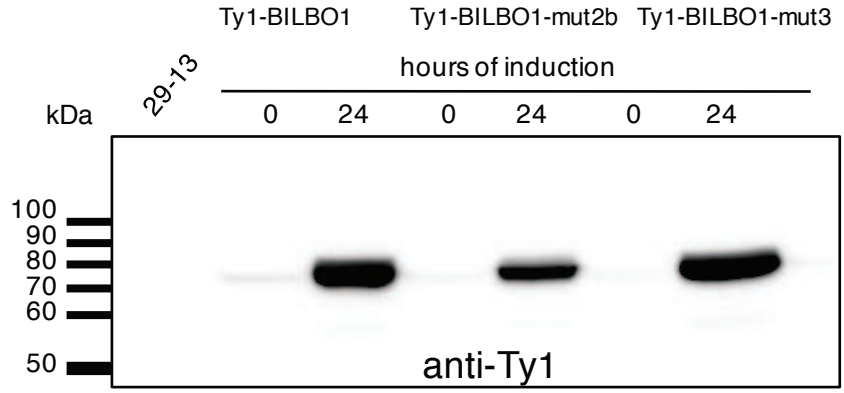

Fig. 3.6 *Ty1-BILBO1, mut2b and mut3 over-expression in T. brucei*
The three cell lines were induced for 24 h with 10 µg/mL tetracycline and $5x10^6$ whole cells/well were loaded. The immuno-blot was probed with anti-Ty1 antibody and confirmed the over-expression of the three constructs. Expected size: 69 kDa.

We over-expressed BILBO1, mut2b and mut3 with an N-terminal Ty1 tag in PCF *T. brucei* and looked at the protein expression, cellular growth rate and phenotypes.
Each construct was indeed expressed as detected by western-blotting with anti-Ty1 antibody on WC extract (Fig.3.6).
A mild growth defect was observed for BILBO1 and mut3 cell-lines induced with 10 µg/mL tetracycline, suggesting that the mut3 does not affect cellular functions (Fig.3.7 A, C). However, over-expression of mut2b was lethal after 48 h of induction (Fig.3.7 B). Preliminary data by light microscopy analyses showed a curious phenotype for the mut2b mutation. The cells rounded-up as soon as 24 h post induction and the resulting flagellum was partially or completely detached (Fig.3.8), resembling the tubulin RNAi phenotype (Ngô et al., 1998).
We probed these round cells with anti-BILBO1 and anti-tubulin by IF. Even if the sub-pellicular MT corset was clearly not in the correct elongated shape, tubulin stained the entire cell body. On the contrary, it was difficult to assess the correct position of BILBO1 (Fig.3.8). The DAPI staining helped us to visualize the genetic material. The duplicated nuclei were relatively easy to see, whereas the individual kDNAs were more difficult to identify.
To understand more clearly the phenotypes, more work needs to be done, particularly at shorter induction times and with lower tetracycline concentrations.

We additionally tested the role of these mutations in U-2 OS cells. Preliminary observation by IF showed that the annular or ball-shaped polymers formed by BILBO1 expression in this heterologous system (Florimond et al., 2015) were no longer present in either of the two sets of mutations mut2b or mut3 (Fig.3.9). No specific differences were observed between mut2b and mut3 in U-2 OS cells.
These preliminary data suggest that the Y89-F89 and K60-K62 NTD plays a role in the formation of these polymers.

d3) Conclusion:

The exact role of BILBO1 and how the FPC is formed, replicated and segregated remains elusive. We think that BILBO1 is the scaffold protein of the FPC, which interacts with itself and with other FPC proteins in a very dynamic way to form the annular/horse-shoe shaped FPC. The interaction with Ca^{2+} might confer dynamicity in compacting the structure and relaxing it when Ca^{2+} dissociates. A less compact and more loose spiral-like structure for the FPC could allow a semi-conservative biogenesis of a new FPC by laterally inserting new

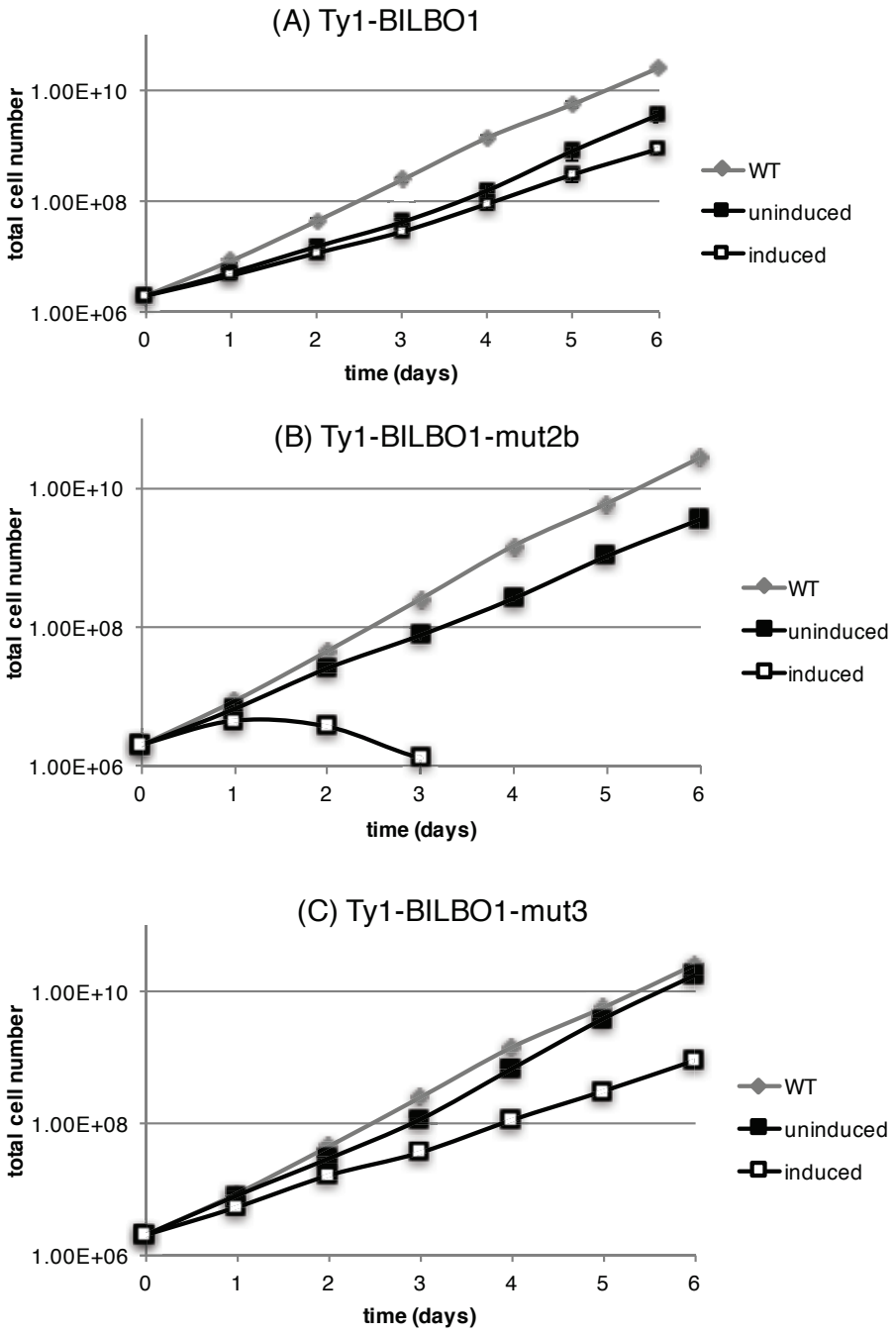

Fig. 3.7 *Growth curves of Ty1-BILBO1, mut2b and mut3 in T. brucei*
(A) No major growth difference between uninduced and induced Ty1-BILBO1-FL was observed (10 µg/mL tetracycline). However, both grew more slowly than the parental cell line. (B) The over-expression of the Ty1-BILBO1-mut2b construct was lethal and cell death occurred as soon as 2-3 days post-induction. (C) A reduced growth rate is observed when Ty1-BILBO1-mut3 was overexpressed, without, however, leading to cell death. Error bars are present, but often smaller than the data point mark and represent standard error of the mean (SEM) N=3.

BILBO1 molecules and interaction partners that could, in a second step, pull the newly formed FPC apart.

We can additionally say that the mutation of Y87 and F89 (mut2b) in the NTD of BILBO1 is indeed disadvantageous for the *T. brucei* parasites and its over-expression leads to severe morphological phenotypes and cell death within a few days post-induction. Furthermore, mutations of key residues (mut2b and mut3) of BILBO1 expressed in U-2 OS cells affect the formation of the globular or comma-shaped structure, but not the formation of long polymers. Since the 3D structure of the NTD of BILBO1 shows similarities with a protein-protein interaction domain, the mutation of key residues can abolish the interaction with some BILBO1 partners. I will therefore come back to these key residues in the section b2) "The proof: FPC4 is a real BILBO1 partner protein".

More work is needed to elucidate how exactly BILBO1 is formed and segregated, but the FPC remain a fascinating field of study, because BILBO1 is essential in FP and FPC biogenesis and is therefore a potential drug target.

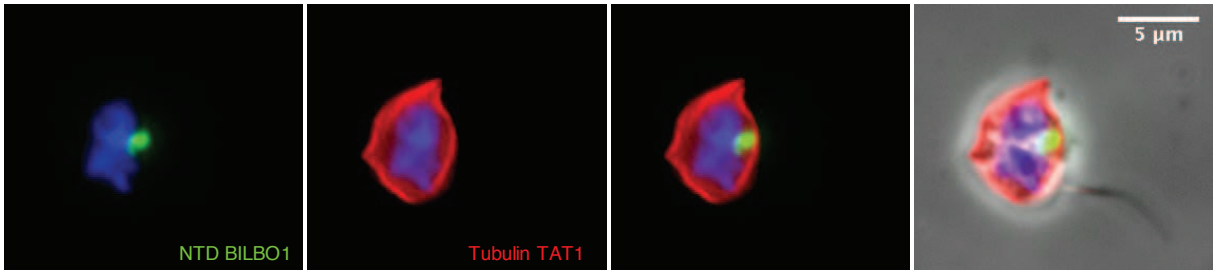

Fig. 3.8 *Immuno-fluorescence analysis of Ty1-BILBO1-mut2b*
The Ty1-BILBO1-mut2b cell line induced 24-48 h (10 µg/mL tetracycline) showing cells that rounded up, assuming a very unusual shape. The MT corset stained with anti-tubulin is intact but morphologically different and the flagellum is detached.

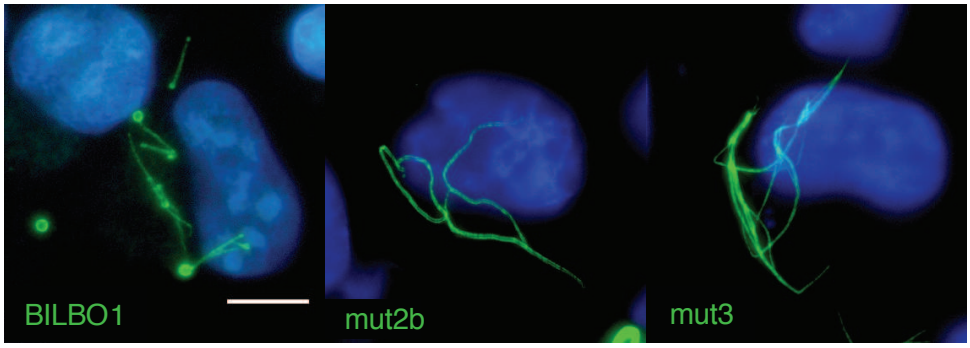

Fig. 3.9 *Immuno-fluorescence analysis of BILBO1-mut2b and mut3 in U-2 OS*
The expression of BILBO1-mut2b and mut3 in U-2 OS cells resulted in a different polymer organization of BILBO1. The annular or ball-shaped termini of BILBO1 are no longer present in mut2b nor mut3. Therefore, the mutations have an impact on polymer shape. Scale bar 10 µm.

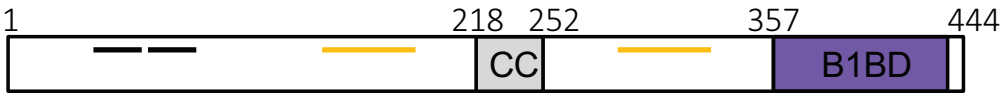

Fig. 3.10 *Schematic representation of the FPC4.*
In the FPC4 protein, a small coiled-coil domain (218-252 aa) has been identified by bioinformatics analysis. The BILBO1 Binding Domain (B1BD) in the C-terminal part of FPC4 has been identified by a Yeast-Two-Hybrid genomic screen (Hybrigenics). Repeats are marked in black (27-50 and 53-79) and orange (106-150 and 290-340).

Fig. 3.11 *Prediction of intrinsically unstructured domains of FPC4*
Analysis performed with IUPred (http://iupred.enzim.hu) (Dosztányi et al., 2005) identifies the CC domain, and the B1-BD domain as non-disordered regions of FPC4 (< 0.5: non-disordered).

II. Identification and functional characterization of FPC4, a BILBO1 partner, in *T. brucei*

a) Introduction and preliminary data

BLAST analysis of the DNA sequence, identified by the Y2H during the genomic library screen for BILBO1 partners (Hybrigenics), identified a DNA sequence (BILBO1 binding sequence or B1-BD) that we use for BLAST analysis using the TriTryp database (Aslett et al., 2010). The result identified *Tb*927.8.6370 encoding a 444 amino acids protein that we named FPC4 for Flagellar Pocket Collar protein 4 with the B1-BD between aa 357 to 440. FPC4 is a 49 kDa basic protein (pI 10.61) (Fig.3.10).
Except for a predicted coiled-coil domain (CC, aa 218 - 252) (COILS, Lupas et al., 1991) and two couples of repeated sequences (repeat 1: aa 27-50 and aa 53-79 aa, repeat 2: aa 106-150 and aa 290-340) (RADAR, Heger and Holm, 2000), bioinformatics analysis of FPC4 did not identify any particular feature related to its possible function. Folding predictions using IUPred (Dosztányi et al., 2005) indicated that FPC4 is globally unfolded except for the CC domain and a region in the C-terminus (approximately from aa 390 to 444) (Fig.3.11).

FPC4 has not been identified in the two flagellar proteome analyses (Broadhead et al., 2006; Oberholzer et al., 2011), suggesting that FPC4 is not a flagellar protein *per se*. Recently, FPC4 was identified in a BioID analysis as a putative partner of SAS-4, a protein located at the FAZ distal tip (Hu et al., 2015). Depletion of SAS-4 generates epimastigote-like cells, disrupts the elongation of the new FAZ and consequently leads to asymmetrical cell division. The authors indicated a cytoskeleton localization for FPC4, however the function of FPC4 was not assessed in this study. We will discuss later this cytoskeleton localisation.

Orthologues of FPC4 can be found in *T. b. gambiense*, *T. cruzi* and other kinetoplastids. The *FPC4* gene is syntenic, except for *Leishmania* ssp.

Objectives of the work:
FPC4 has been fished out by the Y2H screen with BILBO1 as bait and might therefore be a new BILBO1 partner.
The main goal of my thesis was to characterize FPC4 at the molecular and functional level and to confirm that FPC4 is a real BILBO1 interacting partner.

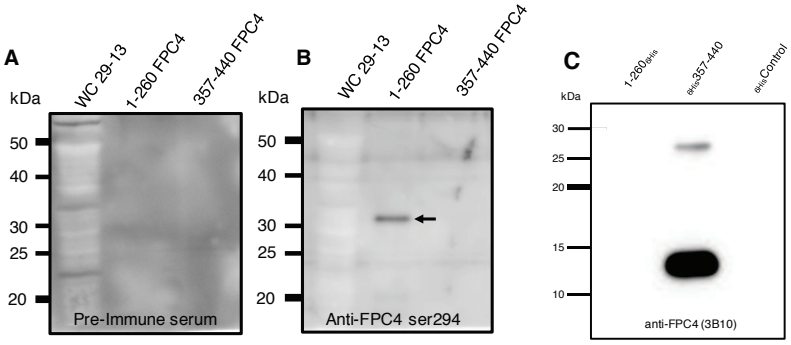

Fig. 3.12 *Western Blot to test FPC4 antibodies specificity (rat polyclonal ser294 and mouse monoclonal 3B10).*
(A) Rat pre-immune serum neither labels any protein in WC of *T. brucei,* nor recognizes the purified fragments of FPC4.
(B) The FPC4-specific serum ser294 recognizes the FPC4 1-260 amino acids purified fragment (31 kDa), but not the purified BILBO1 binding domain (aa 357-440).
(C) The mouse monoclonal FPC4 3B10 antibody specifically recognizes the truncation used to immunize the mice (357-440) at 14 kDa. An additional weak band is detected at around 28 kDa and we cannot exclude that it is a dimer of this FPC4 truncation. The absence of specificity to the histidine tag was tested with another histidine-tagged protein purified from bacteria ($_{6His}$Control).
Lanes were loaded with either 5 x 10^6 cells or 20 ng purified protein.

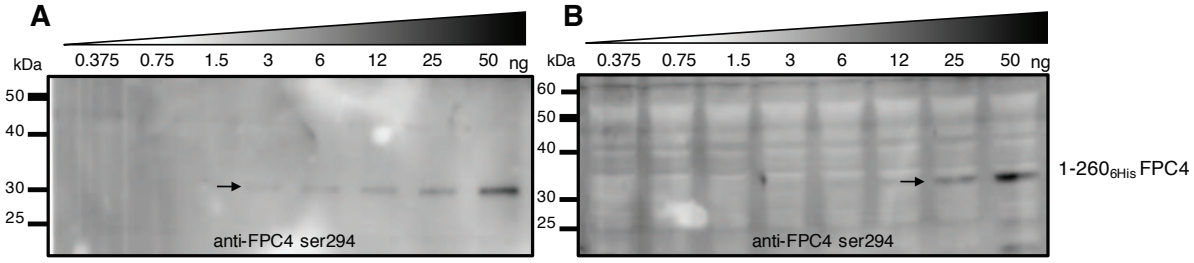

Fig. 3.13 *Western Blot to test the detection limit of anti-FPC4 ser294*
(A) Increasing amounts of purified 1-260_{6His} FPC4 protein and (B) increasing amounts of purified 1-260_{6His} FPC4 protein mixed with *T. brucei* WC extract were probed with rat polyclonal FPC4 ser294 antibody. The detection limit is around 3 ng (A, arrow) in the case of the purified protein alone, and increases up to 25 ng (B, arrow) in the presence of the WC lysate (5x10^6 cells/well) of *T. brucei*.

b) Results

b1) Development of tools to study FPC4 in vivo and in vitro; difficulties and successes

In the first two sections we present the tools we developed in order to study FPC4. These include the production of monoclonal and polyclonal antibodies raised against FPC4, as well as endogenously tagged and over-expressing FPC4 cell lines.

i) Production of FPC4 specific antibodies

- Rat polyclonal serum ser294: FPC4 specificity analysis

A polyclonal antibody against FPC4 was produced in the rat by Eurogentec preliminary to my arrival in the laboratory. To do this, recombinant $_{6His}$FPC4$_{6His}$ was purified on Ni-NTA column from IPTG induced BL21(*DE3*) *E. coli* bacteria, and eluted in urea, due to its poor solubility. Two sera were obtained (ser293 and ser294) and tested by WB on wild-type (WT) *T. brucei* cells and on purified protein. Pre-immune and immune sera were tested to control the specificity of the antibodies (Fig.3.12A). Ser293 was negative on both *T. brucei* and purified protein (data not shown), whereas ser294 antibody could label specifically the purified amino acids 1-260 of FPC4 (Fig.3.12B). However, it did not detect the expected band at 49 kDa on *T. brucei* whole cells lysate (WC) (Fig.3.12 B).
Increasing amounts of purified 1-260 FPC4$_{6His}$ without or with *T. brucei* WC lysate (5 x 10^6 cells/well) were probed by WB (Fig.3.13). Interestingly, 3ng (6.22 x 10^{10} molecules) of purified protein alone was detectable, whereas the purified protein mixed with 5x10^6 WC shifted the detection limit to 25 ng (5 x 10^{11} molecules). This means that 1 x 10^5 molecules/cell are needed to allow FPC4 detection by WB.
The fact that we cannot detect a band in the WC extract of WT *T. brucei* means that the endogenous amount of FPC4 protein is under the detection limit (fewer than 1x 10^5 molecules/cell) and that the presence of the entire protein lysate renders this detection even harder.

Mouse monoclonal 3B10: immunisation, fusion and FPC4 specificity analysis

In the laboratory, we also tried to produce monoclonal antibodies against the N-terminal (1-260 aa) and the C-terminal (357-440 aa) domains of FPC4. We immunized mice with purified 1-260$_{6His}$ and $_{6His}$357-440 recombinant proteins, respectively (see material and methods).

After the fusion between antibody-producing B-cells and myeloma cells, we screened for hybridoma secreting immunoglobulins specific for FPC4. To do so, the supernatants of hybridoma culture medium (>100 samples per recombinant protein) were tested by IF on *T. brucei* CK. Unfortunately, the few (3) hybridomas for the 1-260 truncation giving a positive labelling by IF, died within few days. Therefore, no monoclonal antibody against the N-terminal of FPC4 was obtained.

For the C-terminal truncation (aa 357-440) we were able to isolate a single positive monoclonal antibody: 3B10.

The monoclonal antibody was tested on WB (Fig.3.12 C). As expected, 3B10 recognizes specifically the aa 357-440 purified protein, but not the aa 1-260 protein or another histidine-tagged protein. Similarly to ser294, 3B10 did not detect FPC4 in *T. brucei* WC extract (data not shown).

Both, polyclonal and monoclonal antibodies raised against FPC4 were likewise tested by IF, and the results are shown in the section below b2) iv) FPC4 is a FPC- Hook complex protein.

To conclude, the antibodies produced to detect FPC4 are specific for this protein but do not detect the endogenous FPC4 by WB.

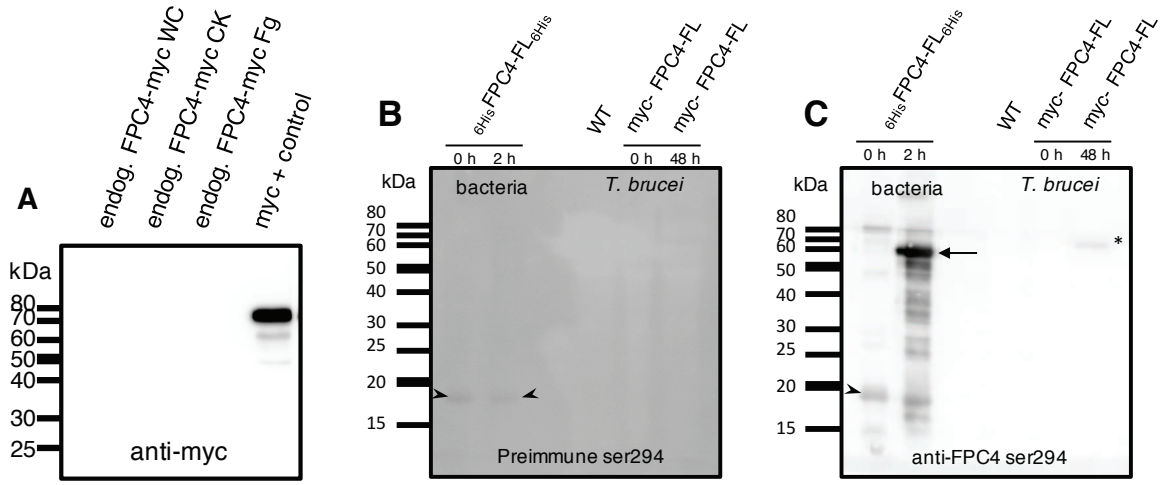

Fig. 3.14 *Western Blot of endogenously tagged FPC4-myc and*
(A) Endogenous FPC4-myc cannot be detected by WB in Whole Cells (WC), Cytoskeleton (CK) or Flagella (Fg) preparations ($5x10^6$ WC/CK/Fg per well). Myc positive (+) control serves as a test for myc dilution and detection.
(B) Pre-immune ser294 (1:500) does not detect $_{6His}$FPC4-FL$_{6His}$. (expected 52 kDa) in induced bacteria. No specific bands are detected on *T. brucei* extracts (WT, uninduced and induced myc-FPC4-FL). Only a weak band at 18 kDa is detected and is unspecific.
(C) The polyclonal antibody anti-FPC4 ser294 (1:500) detects a band at 18 kDa in the non-induced bacteria (arrow-head), as for the pre-immune serum, and a strong band at around 55 kDa (arrow) in the induced bacteria. This band corresponds to the $_{6His}$FPC4-FL$_{6His}$ construct. Moreover, anti-FPC4 ser294 detects the over-expression of myc-FPC4-FL in *T. brucei* but no bands are recognized in the WT. FPC4 ser294 is therefore able to detect the over-expression of FPC4, only.
($5x10^6$.bacteria/well and $5x10^6$ *T. brucei* WC/well)

ii) Cell lines: Endogenous and over-expression of myc tagged FPC4

- endogenous C-terminal myc-tag

We decided to generate a cell line with an endogenous 3'-end triple myc tag *FPC4*, in order to detect the protein on WB without the need of an antibody raised against FPC4. The triple myc-tag (≈ 5 kDa) is considered a small tag, which should not disturb the protein.

To produce the endogenous *FPC4-myc* tagged cell line, we took advantage of the pMOTag23M plasmid (modified from (Oberholzer et al., 2006) as a template for a PCR with long primers. These specific primers contained the recombination sites that allowed the insertion of the triple myc tag coding sequence and a resistance gene between the end of the *FPC*4 gene (before the stop codon) and the beginning of the 3' UTR. The PCR product, after purification, was directly transfected into *T. brucei* PCF 427 29-13. The choice to use the *T. brucei* PCF 427 29-13 instead of the original WT as the parental strain was made in prevision of an additional transfection in the same cell line, which could require the inducible system.

Following transfection, several resistant clones were selected. Unfortunately, the endogenous expression of FPC4-myc was not detectable by WB (Fig.3.14). Neither high loads of whole cells (WC), cytoskeleton (CK), nor flagella (Fg) were detectable suggesting either that the expression level was too low for WB detection or that the C-terminal myc tag was cleaved off and thus not detectable. The hypothesis of low level of expression was supported by the positive anti-myc immunofluorescence labelling results (see below in section b2) iv) FPC4 is a FPC- Hook complex protein".

Since the detection of endogenous levels of myc-tagged FPC4 by WB was not possible we thus developed *T. brucei* tetracycline inducible cell lines that expressed higher amounts of FPC4. The inducible over-expression consisted of transfecting an ectopic copy of the gene of interest and "forcing" its transcription by the addition of tetracycline. In our case, we additionally added a tag to be able to detect the corresponding protein acknowledging that the size of the tag and its position, N- or C-terminal, might disturb protein folding and interfere with post-translational modifications (PTMs) or protein-protein interactions.

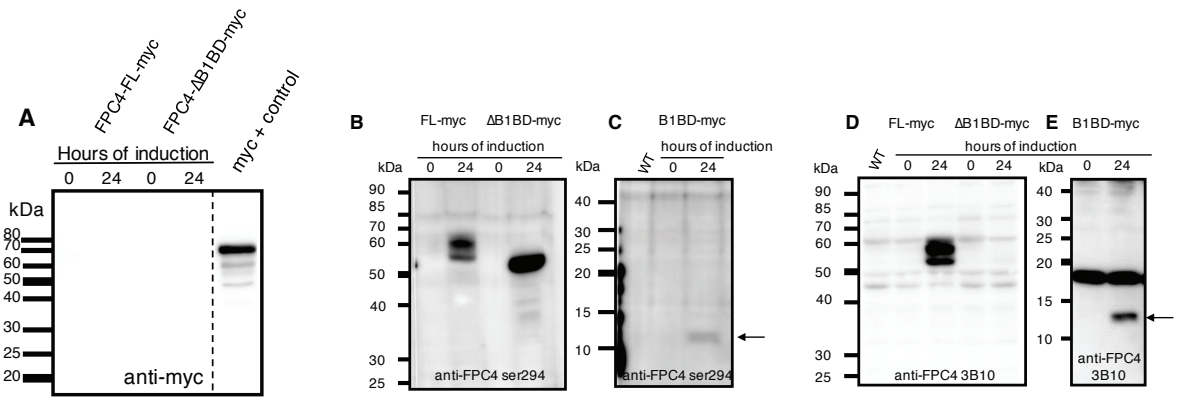

Fig .3.15 *Over-expression of C-terminal myc-tagged FPC4 analysed by WB*
(A) No bands were detected by anti-myc labelling in the cell lines expressing C-terminally myc tagged FPC4-FL and FPC4-ΔB1BD-myc. Specificity of the anti-myc antibody was controlled on an unrelated myc-tagged protein (myc+ control lane).
(B) and (C)The expression of the constructs was tested with anti-FPC4 ser294 (1:300) (arrow in C).
(D) and (E) The expression of the constructs was tested with the 3B10 monoclonal antibody (arrow in E). An unspecific band at 18 kDa was detected when the blots were probed with 3B10 (1:5).
These results confirmed that the constructs were indeed expressed but the myc-tag was most likely cleaved.
Expected size of the constructs: FPC4-FL-myc 54 kDa, FPC4-ΔB1BD-myc 44 kDa and FPC4-B1BD-myc 14 kDa. (A, B, D) 12% SDS-page gel (C, E) 15% SDS-page gel. 5 x 10^6 cells/lane were loaded.

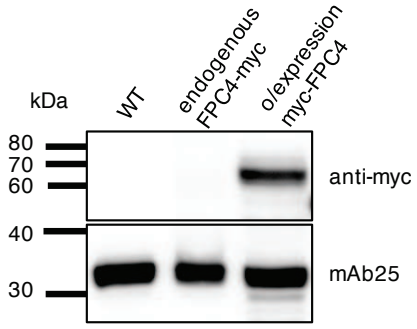

Fig. 3.16 *Western Blot comparing endogenous C-ter myc-tagged and over-expressing N-ter myc-FPC4 cell lines*
We proved that the detection problem by WB was due to FPC4 protein level of expression and over-expressing a tagged copy of FPC4 can obviate this. A monoclonal antibody (mAb25) raised againt *Tb*SAXO (an axonemal protein) was used as loading control (Dacheux et al., 2012). 5 x 10^6 cells/lane.

- C-terminal myc-tag

Endogenous expression of FPC4 myc-tagged at its C-terminus could be detected by IF (see section below b2) iv) FPC4 is a FPC- Hook complex protein.

Therefore, we generated three different PCF inducible cell lines: FPC4-FL-myc, FPC4-ΔB1BD-myc and FPC4-B1BD-myc. By WB analyses (and IF, data not shown), we have not been able to detect the anti-myc labelling for any of the induced cell lines (10 µg/mL tetracycline induction, 24h) (Fig.3.15 A). We therefore repeated the WB analyses with the polyclonal antibody specific to FPC4 ser294 and we could detect FPC4-myc as a double band at around 60 kDa (predicted 54 kDa), FPC4-ΔB1BD-myc as a 50 kDa band (predicted 44 kDa), and FPC4-B1BD-myc as a 12 kDa band (predicted 14 kDa). The recombinant protein was thus expressed (Fig.3.15 B, C). Moreover, we probed the blot with the monoclonal anti-FPC4 antibody 3B10, which is specific to the FPC4-B1BD. As expected and shown in the WB, 3B10 recognizes the FPC4-FL-myc and FPC4-B1BD-myc but not the FPC4-ΔB1BD-myc construct (Fig.3.15 D, E). Note: an unspecific band at 18 kDa is always present when a blot is probed with 3B10 (Fig.3.15 E), and is not present with ser294.

These results confirmed that the C-terminal tagged proteins were over-expressed but the myc-tag was most probably cleaved off. We thus decided to tag FPC4 at its N-terminus.

- N-terminal tag

The over-expression (10 µg/mL tetracycline induction, 24h) of the myc-FPC4-FL was tested by WB and compared to the endogenous expression of FPC4-myc (Fig.3.16). We proved that the detection problem by WB was due to 1) the low level of FPC4 protein and 2) cleavage of the c-ter myc tag, and could be obviated by over-expressing a tagged copy of N-terminal myc FPC4. Moreover, the specificity of FPC4 ser294 antibody was confirmed by WB, comparing the preimmune serum with the ser294 tested on bacterial extract and trypanosome extracts (Fig.3.14 B, C).

Also, Célia Florimond (previous PhD student) generated data using a GFP-FPC4 overexpressing cell line that I will present in section b3), iii) over-expression of GFP-FPC4.

To pursue the characterization of FPC4 we could therefore use several tools: a polyclonal antibody (ser294), a monoclonal antibody (3B10) and several cells lines either expressing an endogenously myc tagged version of FPC4 or over-expressing a N-terminal myc tagged version of FPC4 and its truncations.

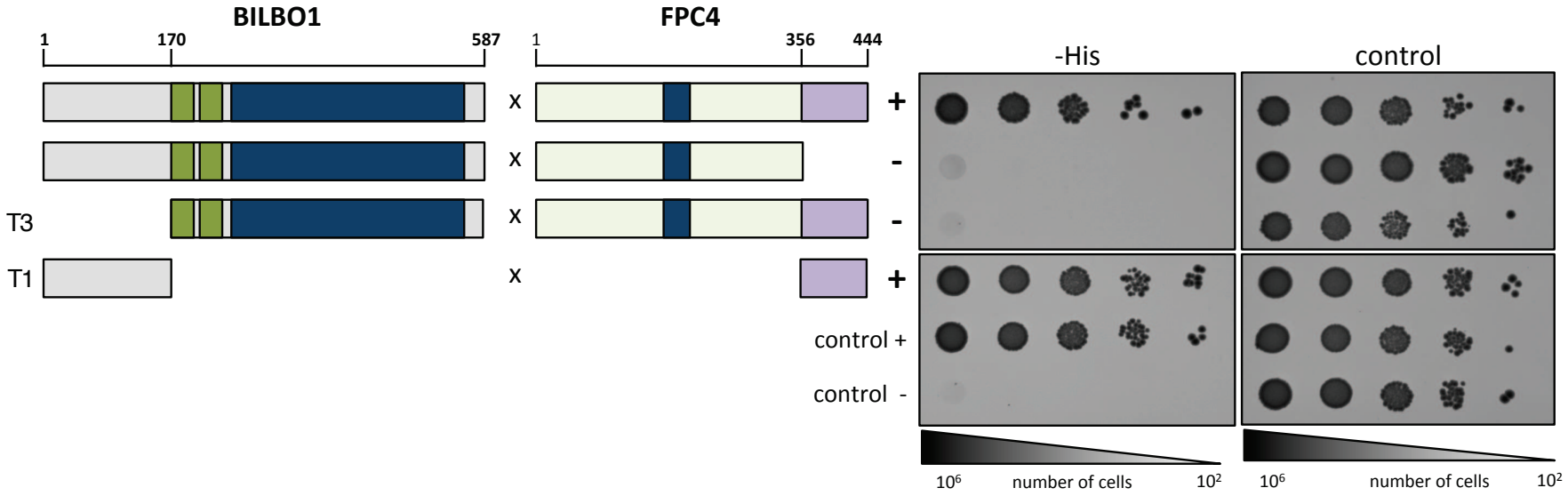

Fig. 3.17 *Yeast-Two-Hybrid interaction test between BILBO1 and FPC4*
Left panel: scheme of the constructs cloned for the tests; FL-BILBO1 (aa 1-587), T1-BILBO1 (aa 1-170) and T3-BILBO1 (aa 171-587) have been tested with FL-FPC4 (aa 1-444), FPC4-ΔB1BD (aa 1-356) and FPC4-B1BD (357-444 aa). Green regions of BILBO1 correspond to the EF-Hands. Blue regions correspond to CC domains. FPC4-B1BD is highlighted in violet.
Right panel: the interactions were tested on a medium without Histidine (-His) and on a control medium, to monitor yeast growth.
The Y2H interaction test allowed us to conclude that the N-terminal domain of BILBO1 (T1) interacts with the C-terminal domain of FPC4 (B1BD aa 357-444).
Note: The interactions were tested in one configuration only (all the FPC4 constructs were fused to the activation domain of *Gal4*, whereas the BILBO1 constructs were fused to the DNA binding domain of *Gal4*) because *FPC4* fused to the BD gave us a positive result in any diploid yeast tested, even with the “empty” activation-domain vector as a control.

b2) The proof: FPC4 is a real BILBO1 partner protein

i) BILBO1-FPC4 interaction tested by Y2H

Because a domain of FPC4 was identified in the Y2H genomic screen, we wanted to confirm the interaction between BILBO1 and FPC4 using full-length sequences and the Y2H system from Clonetech as described in (Florimond et al., 2015). Indeed, full length FPC4 interacts with BILBO1 (Fig.3.17).

Once the interaction between BILBO1 and FPC4 was confirmed, we started looking for the specific domains of both proteins involved in this interaction. We used two truncations of BILBO1: T1 (aa 1-170) corresponding to the N-terminal domain, and T3 (aa 171-578) corresponding to the EF-Hands and the coiled-coil domain (Florimond et al., 2015). FPC4 was truncated in two domains: the BILBO1 Binding Domain (B1BD, aa 357-444) and the long N-terminus (aa 1-356) called delta BILBO1 Binding Domain (ΔB1BD).
As expected, the deletion of the B1BD domain of FPC4 abolished the interaction with BILBO1. The interaction was abolished as well when the N-terminus of BILBO1 was removed (T3 construct). Finally, BILBO1-T1 and FPC4-B1BD were able to interact demonstrating the specificity of the interaction between these two domains (Fig.3.17).

Taken together these results confirmed that FPC4 and BILBO1 are able to interact and allowed the identification of the N-terminal domain of BILBO1 as the interacting with the C-terminal domain of FPC4.
This last result encouraged us to pursue the analysis in the U-2 OS system to further characterize this interaction.

ii) BILBO1-FPC4 interaction tested in the heterologous system U-2 OS

Since FPC4 does not show any particular features by bioinformatics analysis, we wanted to investigate the behaviour of FPC4 in U-2 OS cells, and whether it can bind to BILBO1 in this system. To do so, we cloned *FPC4* (and truncations) into the pcDNA3.1-GFP vector and we transfected them into U-2 OS cells. Twenty-four to 48 h after transfection, cells were extracted with Triton-X100 and fixed, then processed for immunofluorescence using anti-BILBO1 and anti-GFP antibodies (Fig.3.18). FPC4-FL-GFP expressed for 24 h or 48h localized within the nucleus and on filamentous structures, which might be MTs (Fig.3.18 B).

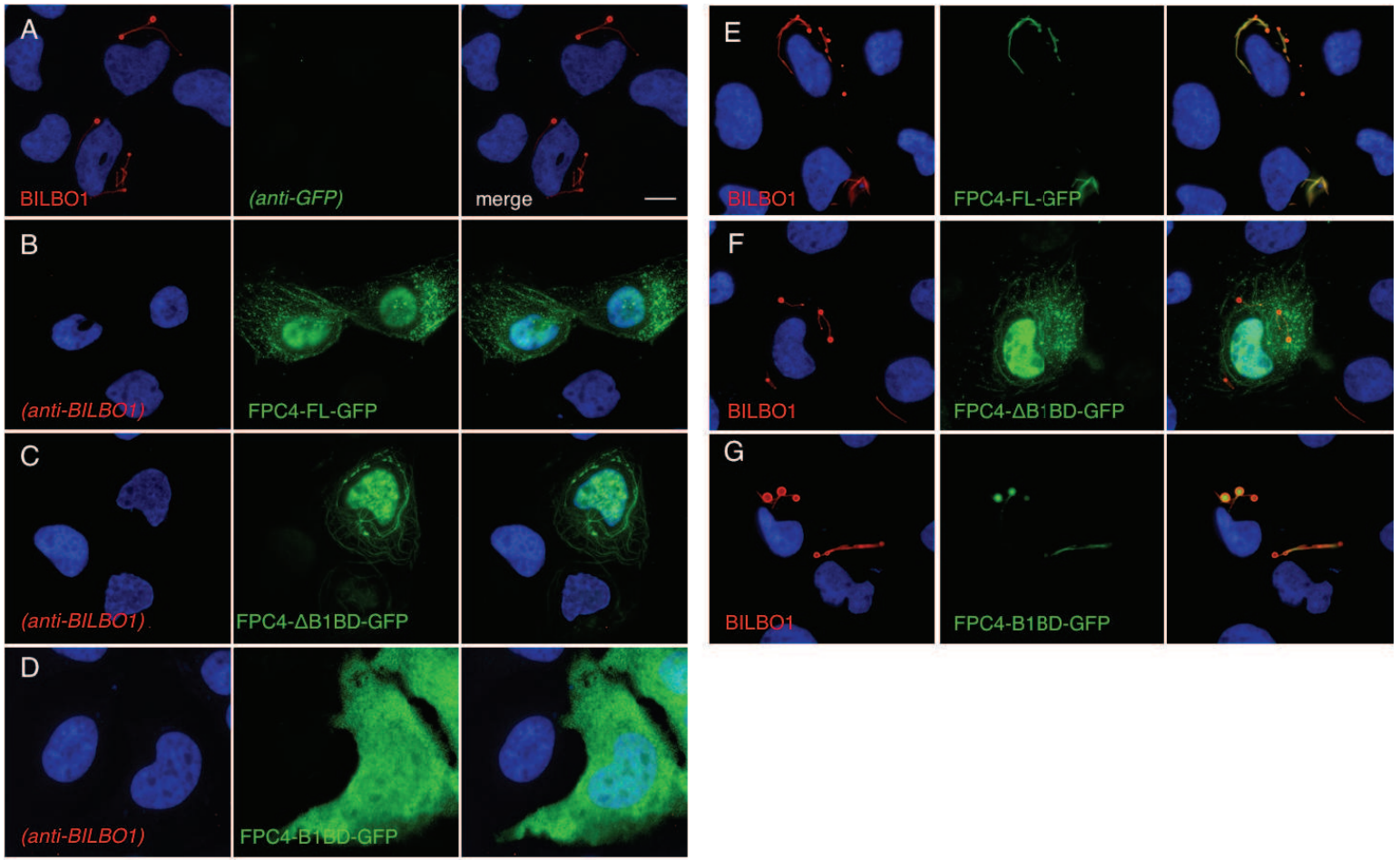

Fig. 3.18 *Co-expression of BILBO1 and FPC4 in a heterologous system (U-2 OS cells) demonstrates that the C-terminus of FPC4 interacts with BILBO1*

Cells were labelled with anti-BILBO1 (red) and anti-GFP (green) to label the FPC4-GFP constructs.
(A) Single expression of BILBO1 shows self-polymerization properties as described previously in (Florimond et al., 2015a). (B) Single expression of FPC4-GFP. (C) Single expression of FPC4-ΔB1BD-GFP. (D) Single expression of FPC4-B1BD-GFP (on WC). (E) Co-expression of BILBO1 and FPC4-GFP. (F) Co-expression of BILBO1 and FPC4-ΔB1BD. (G) Co-expression of BILBO1 and FPC4-B1BD-GFP.
Nuclei are stained with DAPI (blue). Scale bar 10 µm.

The nuclear localization could be due to a weak bipartite NLS sequence between the aa 120-154 that is predicted by NLS mapper (Kosugi et al., 2009). Since in the trypanosomes we had never localized FPC4 to the nucleus (see section below b2) iv) FPC4 is a FPC-Hook complex protein), we did not address the nuclear localization in the U-2 OS cells and we focused on the cytoplasmic side labelling. Whilst ΔB1BD-GFP also localized on filamentous structures (Fig.3.18 C), FPC4-B1BD-GFP was observed as cytosolic on whole cells (Fig.3.18 D), whereas no signal was visible on extracted cells (data not shown).

We then co-expressed BILBO1 with the three FPC4 constructs to test their interaction. We could observe that, as in the Y2H test, BILBO1 and FPC4 FL proteins interact, inducing the relocalization of FPC4 onto BILBO1 structures (Fig.3.18 E). This relocalization was not observed for the FPC4-ΔB1BD construct that remained labelled on filamentous structures without BILBO1 co-labelling and thus did not bind BILBO1 (Fig.3.18 F). The role of B1BD in binding was confirmed by its labelling on BILBO1 polymers and not in the cytoplasm (Fig.3.18G).

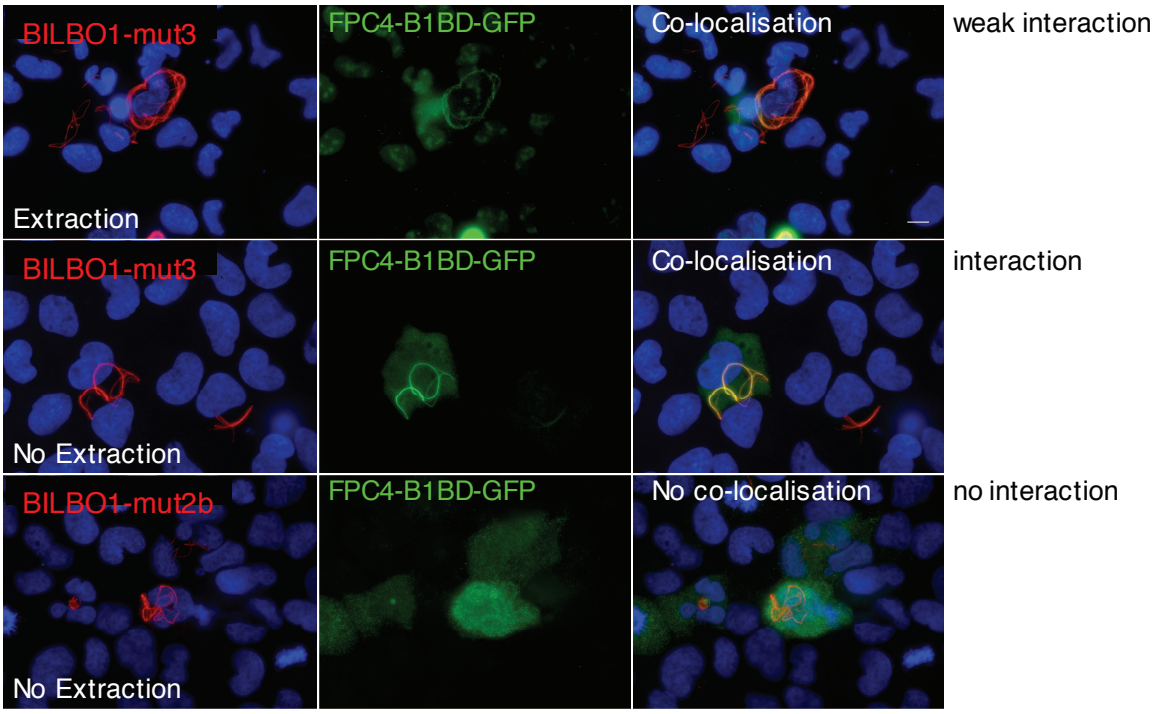

Fig. 3.19 *Key residues in the N-terminal domain of BILBO1 are essential for FPC4 – BILBO1 interaction*

Co-expression of BILBO1-mut3 with FPC4-B1BD resulted in a weak interaction on extracted cells (first panel) and in a stronger interaction on whole cells (second panel).
On the contrary, BILBO1-mut2b completely abolished the interaction with FPC4 (third panel).
These results suggest that mut2b contains residues involved in BILBO1-FPC4 interaction, whereas mut3 only marginally affects BILBO1-FPC4 interaction.
Nuclei are stained with DAPI (blue), scale bar 10 µm.

iii) Key residues in the N-terminal domain of BILBO1 are essential for FPC4-BILBO1 interaction

We assessed the role of the N-terminal domain of BILBO1 in the FPC4 – BILBO1 binding by localizing FPC4, in U-2 OS cells, when co-expressed with BILBO1 mut2b (Y87A and F89A) and mut3 (K60A and K62A) (Fig.3.5).
When expressed alone FPC4-B1BD-GFP was soluble, but co-localizing with BILBO1 when co-expressed (Fig.3.18 G). When FPC4-B1BD-GFP was co-expressed with BILBO1-mut3 the interaction was weak on extracted cells, but clear on whole cells (Fig.3.19). On the contrary, BILBO1-mut2b completely abolished the interaction with FPC4-B1BD-GFP.
This confirms that the NTD is involved in the interaction with FPC4 and moreover, two specific residues (Y87 and F89) present in the conserved surface patch (Vidilaseris et al., 2014a) are required for the interaction.

These data confirmed that the C-terminal domain of FPC4 is the real BILBO1 Binding Domain and that FPC4 is thus a *bona fide* BILBO1 partner.
Moreover, the identification of key residues in the NTD of BILBO1 can be used in drug design.

iv) FPC4 is a FPC – Hook complex protein

The localization of FPC4 in *T. brucei* was studied using the anti-FPC4 monoclonal 3B10 antibody, the anti-FPC4 polyclonal ser294 antibody and the endogenous myc-tagged FPC4 cell line.

Knowing that FPC4 is able to interact with BILBO1, we expected the immuno-labelling in close proximity with the FPC and we consequently used a rabbit anti-BILBO1 polyclonal antibody, raised against the NTD (1-110 aa) of BILBO1 (Gang Dong Lab (NTD) or Robinson Lab. (1-110)), as FPC marker (see Fig.3.20 Fig.3.21). The IF analysis was performed on NP40/Igepal extracted cells, that we called cytoskeleton (CK). WT cells probed with 3B10 showed that FPC4 is located in very close vicinity to BILBO1 during the entire cell cycle progression from 1K1N (1 kinetoplast and 1 nucleus) to 2K2N (2 kinetoplasts and 2 nuclei) cells (Fig 3.20). Additionally, WT cells probed with ser294 showed FPC4 with a short “tail” that elongates towards the anterior end of the cell. This little tail was more clearly visible in 2K1N cells (Fig.3.21). This elongated structure resembled the Hook complex and localized in a similar position. We therefore tested the Hook structure marker rabbit polyclonal anti-

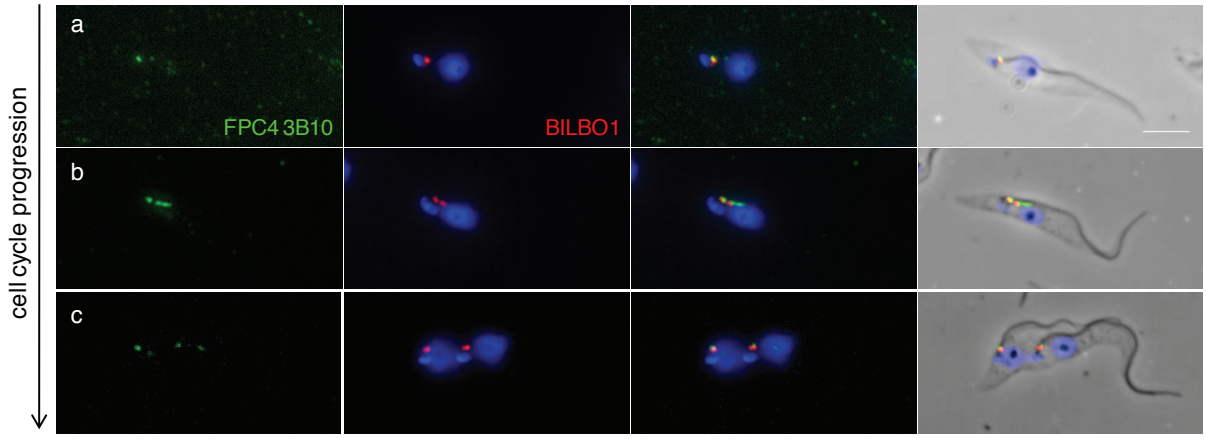

Fig. 3.20 *Immunofluorescence analysis on PCF WT using monoclonal FPC4 antibody (3B10) and polyclonal anti-BILBO1 antibody (NTD)*
FPC4 (green) is present throughout the entire cell cycle and localizes on and close to BILBO1 (red) (scale bar 5 µm).

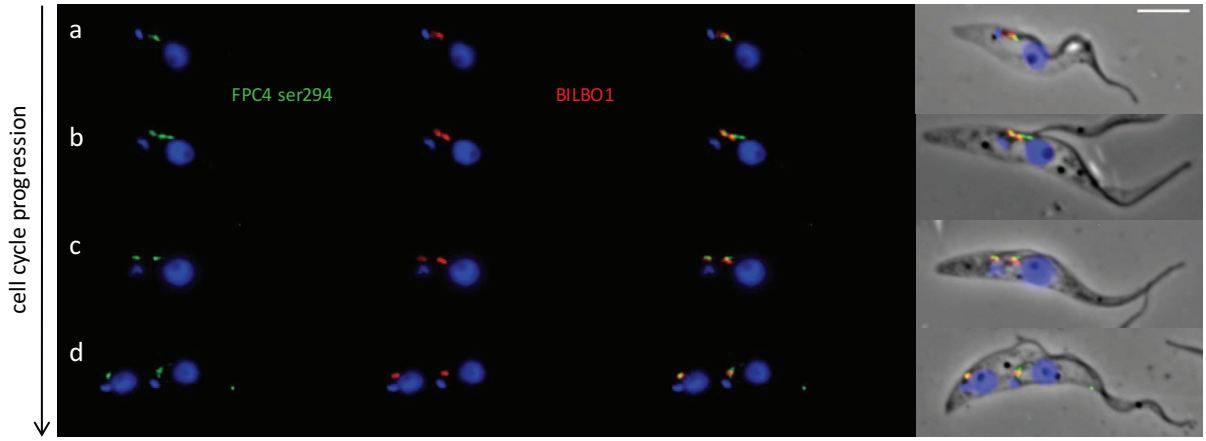

Fig. 3.21 *Immunofluorescence analysis on PCF WT using polyclonal FPC4 antibody (ser294) and anti-BILBO1 (1-110).*
FPC4 (green) is present throughout the entire cell cycle and localizes on and close to BILBO1 (red), the sole FPC marker currently available. (a) represents 1K1N cells, in (b) the kDNA is duplicating and a longer FPC4 structure is visible. (c) shows a cell in the 2K1N stage and with two distinct FPC structures, and (d) a 2K2N cell. (scale bar 5 µm).

MORN1, a kind gift from B. Morriswood (Morriswood and Schmidt, 2015) and compared it with FPC4 localization (see Fig.3.22). The FPC4 localization resulted almost identical to MORN1.

The localization of FPC4 was compared between CK WT, endogenous tagged FPC4 and the myc-overexpressing cell line. FPC4 is detected in all the cell lines at the FPC together with BILBO1 (Fig.3.23). However, when FPC4 is over-expressed (24 h with 10 µg/mL tetracycline), its hook-shaped structure is clearly visible (Fig.3.23 c) as well as its co-localization with MORN1 at the hook complex (Fig.3.23 d). The induction of this cell line with a lower amount of tetracycline did not modify the FPC4 hook-shape (not shown).
The same cell lines were also probed by IF on WC, but we obtained some unspecific labelling on the cell body. We performed the IF analyses on CK.

We concluded that FPC4 is a cytoskeleton-associated protein localizing at the FPC and that it might also be part of the Hook complex.

In order to obtain more insight into the localization of FPC4, immuno-electron microscopy (iEM) analyses were performed on isolated flagella. We used the over-expressing myc-FPC4 cell line (Fig.3.24 A-D) (24 h induction 10 µg/mL tetracycline), because no labelling was observed on either WT cells probed with 3B10 or ser294, or on the cell line expressing endogenous FPC4-myc with anti-myc by iEM (not shown).

The myc antibody labelled a ring-shape structure at the FPC extending towards the tip of the flagellum that resembles the hook structure described by Esson and colleagues (Esson et al., 2012) (Fig.3.24 C, D). Surprisingly, myc labelling was also observed on a filament-like structure that elongated from the FPC toward the BB (Fig.3.24 B). Whilst this labelling was not observed by IF on PCF (neither with ser294, 3B10 nor anti-myc), a similar pattern was observed on BSF CK probed with ser294 (Fig.3.24 E). This suggests that the amount of FPC4 present towards the BB is not detectable by IF in PCF. Unfortunately, because of the impossibility to detect the endogenous FPC4 by WB, we cannot compare the protein expression level in PCF and BSF to see whether this influences the detection of FPC4.

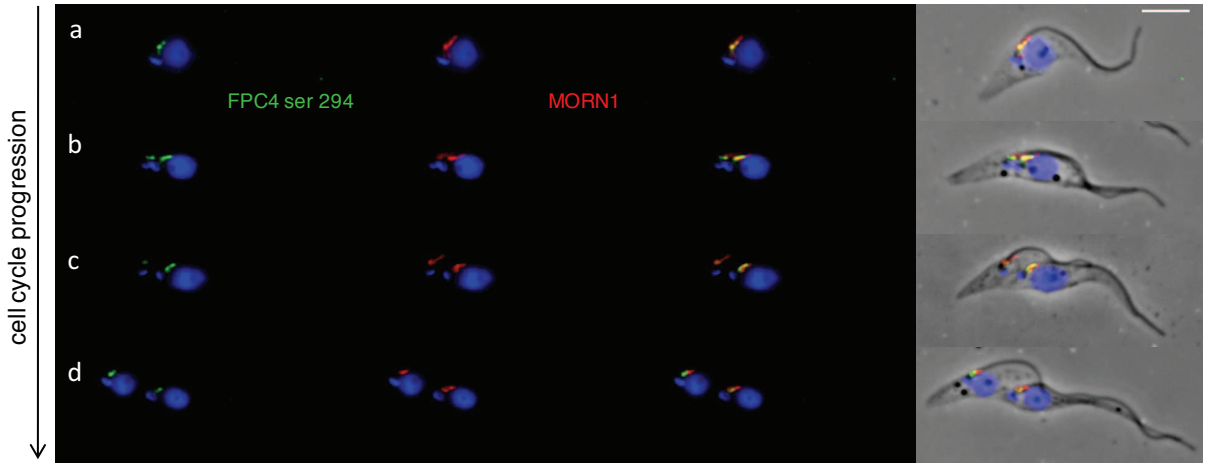

Fig. 3.22 *Immunofluorescence analysis on PCF WT CK using polyclonal anti-FPC4 antibody (ser294) and anti-TbMORN1*
FPC4 (green) is present throughout the entire cell cycle and localizes very close to MORN1, a hook-complex marker. (a) represents 1K1N cells, in (b) the kDNA is duplicating and a longer FPC4 structure is visible. (c) shows cells in a 2K1N conformation, with already two separated FPC4 and MORN1 structures, and in (d) a 2K2N cell is visible. (scale bar 5 µm)

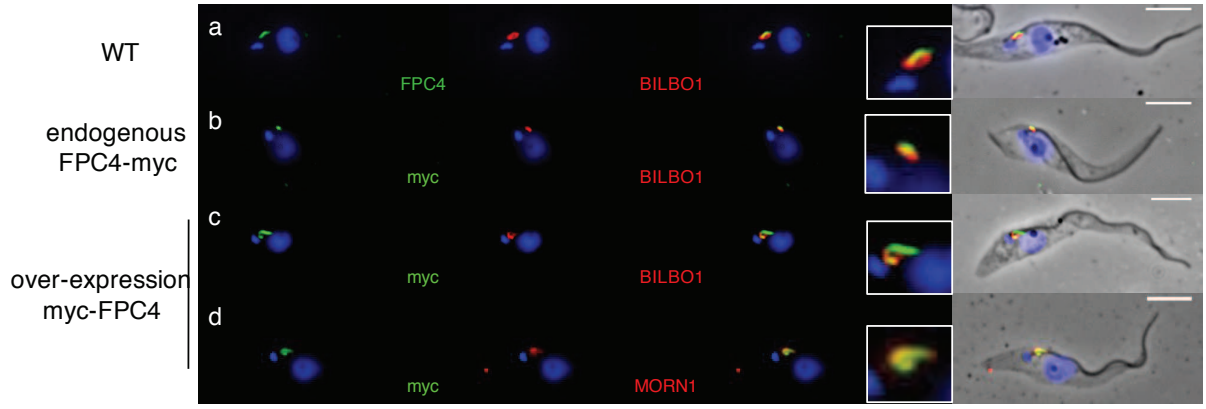

Fig. 3.23 *Immunofluorescence analysis to compare FPC4 signal on WT, endogenously myc-tagged FPC4 cell line, or myc-over-expressing FPC4 cell line.*
(a) FPC4 is detected on WT cells with the polyclonal anti-FPC4 ser294 antibody and partially co-localizes with BILBO1 at the FPC. (b) anti-myc localized the endogenously tagged FPC4-myc at the FPC together with BILBO1. (c) The cell line over-expressing myc-FPC4-FL (24 h induction 10 µg/mL tetracycline) shows FPC4 as a hook-shaped structure, which is located at the FPC together with BILBO1 at the hook, but with an additional elongation toward the anterior end the cell. (d) The hook-shaped FPC4 co-localizes with MORN1 at the hook-complex (24 h induction 10 µg/mL tetracycline). Scale bar 5 µm.

Conclusion:

Immunofluorescence analyses allowed us to localize FPC4 at the FPC, together with BILBO1, and at the hook complex, with MORN1. FPC4 is a cytoskeletal protein, which remains attached to the flagellum after flagella preparation.

Additionally, immuno-gold EM confirmed the observation made by IF and allowed us to have a better resolution, which led to the detection of a myc signal between the BB and the FPC.

Could, therefore, FPC4 be a shared partner between the FPC and the hook complex? We thus decided to investigate more in this direction.

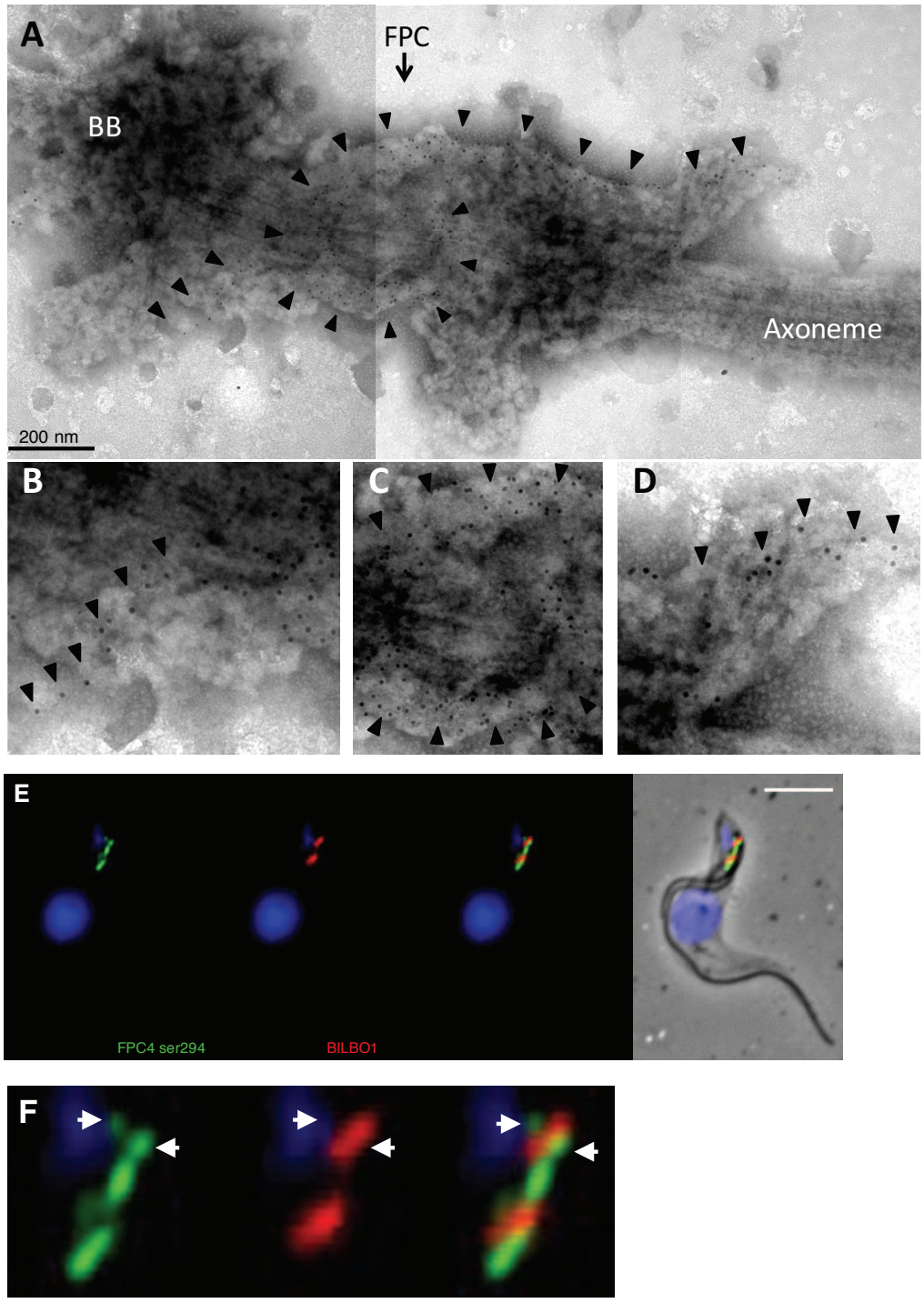

Fig. 3.24 *Immuno-localization of myc-FPC4 on PCF isolated flagella, and of endogenous FPC4 in BSF CK.*
(A) Immuno-gold labelling and electron microscopy on isolated flagella from cells overexpressing myc-FPC4 induced (24h induction, 10 µg/mL tetracycline). Flagella were isolated and probed with anti-myc (10 nm gold particles). Myc-FPC4 localizes at a hook-shaped structure indicated by the arrowheads. (B), (C) and (D) are enlargements of (A).
(E) WT BSF cytoskeletons were probed with anti-FPC4 ser294. The elongated shape of FPC4 is visible anterior and posterior to the FPC, as seen in PCF iEM (B, D). (F) is an enlargement of (E) and arrows show the presence of FPC4 anterior and posterior to the FPC. Scale bar represents 5 µm.

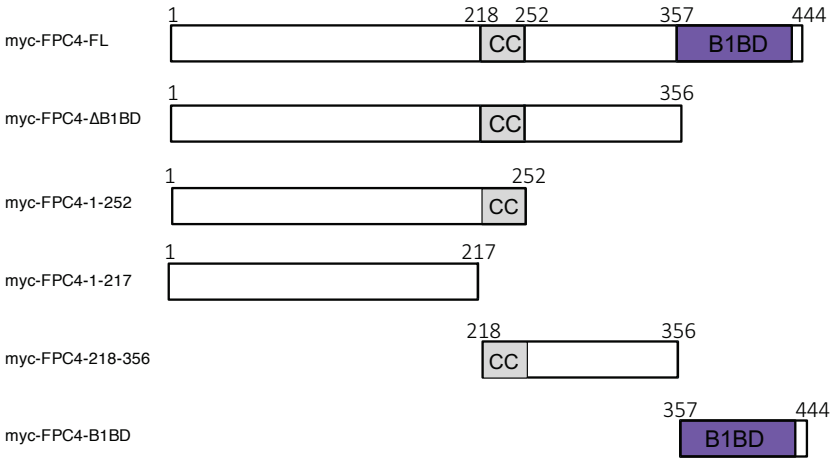

Fig. 3.25 *Schematic representation of the FPC4 truncations used in this study*
Different truncations of FPC4 were N-terminally myc-tagged and over-expressed in PCF *T. brucei*. FPC4-FL (aa 1-444), FPC4-ΔB1BD (aa 1-356), FPC4 aa 1-252, FPC4 aa 1-217, FPC4 aa 218-356 and FPC4-B1BD (aa 357-444).

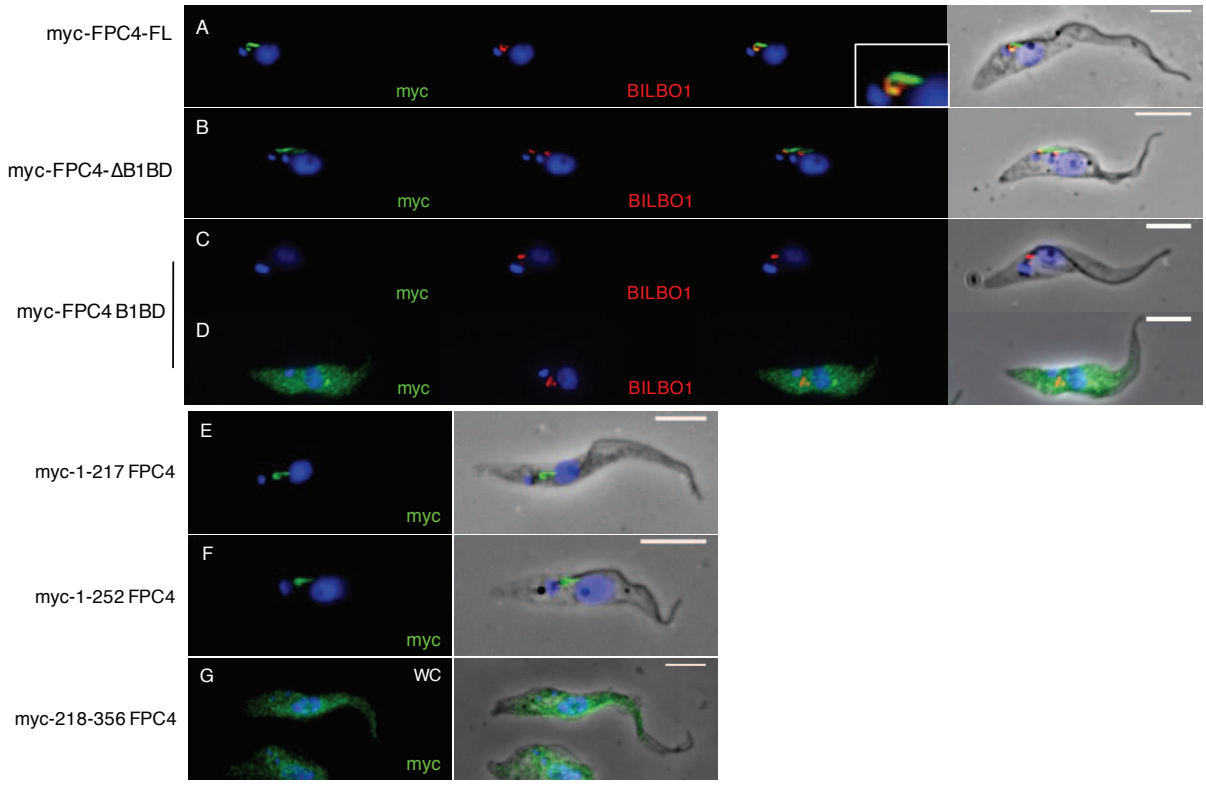

Fig. 3.26 *Immuno-localization by IF of the FPC4 truncations*
Overexpressing cells (24 hours, 10 µg/mL tetracycline) were probed with anti-myc (green) (A-G) and anti-BILBO1 (red) (A-D).
Myc-FPC4-FL (A) and myc-FPC4-ΔB1BD (B) localize at the FPC/Hook complex. Myc-FPC4-B1BD is soluble (whole cell in D) and therefore not detectable on CK (C).
Two shorter truncations of FPC4, myc-FPC4-1-217 (E) and myc-FPC4-1-252 (F), are correctly targeted to the FPC, whereas the truncation myc-FPC4-218-356 (G), lacking the N-terminal domain and the B1BD were soluble (D), and therefore detectable on whole cells only. Scale bar 5 µm.

v) The FPC4 BILBO1 binding domain is not required for FPC – Hook complex targeting

To date, no targeting motif to the FPC or to the Hook complex has been identified for FPC4. The only identified domain of FPC4 is the B1BD and therefore we decided to truncate the protein in two domains, ΔB1BD (aa 1-356) and B1BD (aa 357-444), to search for the FPC targeting motif. Both truncations were over-expressed with a triple myc N-terminal tag (Fig.3.25). The cells were induced for 24h with 10 µg/mL tetracycline and CK were probed with the anti-myc antibody and anti-BILBO1 (Fig.3.26). Similar to myc-FPC4-FL (Fig.3.26 A), myc-FPC4-ΔB1BD showed an elongated-shaped structure, which co-localized with BILBO1, on the collar part, with the elongated tail extending towards the anterior end of the cell body (Fig.3.26 B). Interestingly, myc-FPC4-B1BD was cytoplasmic and extracted during CK preparation suggesting that the B1BD is dispensable for the targeting to the FPC (Fig.3.26 C, D) and that the FPC targeting domain is present within the ΔB1BD of FPC4.

We therefore decided to study in more detail the long N-terminal domain of FPC4 in order to narrow down the targeting sequence to the FPC. Three additional truncations were tested: myc-FPC4-1-217 (truncated before the CC domain), myc-FPC4-1-252 (truncated at the end of the CC domain), myc-FPC4-218-356 FPC4 (CC domain up to B1BD) (Fig. 3.25).
The first two constructs were targeted to the FPC and assumed the same hook-shaped structure (Fig.3.26 E, F), whereas the central part of the protein was soluble (on WC) as was the B1BD (Fig.3.26 G).
We can thus conclude that the aa 1-217 domain in of FPC4 is involved in targeting to the FPC4 and that the B1BD is dispensable for this task.

Conclusion:

Taken together these data clearly show that FPC4 is present on a cytoskeletal structure, which resists detergent extraction. FPC4 is present at the FPC with BILBO1 and additionally localizes at the hook complex together with MORN1.
Moreover, the targeting of FPC4 to the FPC is not mediated by the B1BD but by its N-terminal domain (aa 1-217).

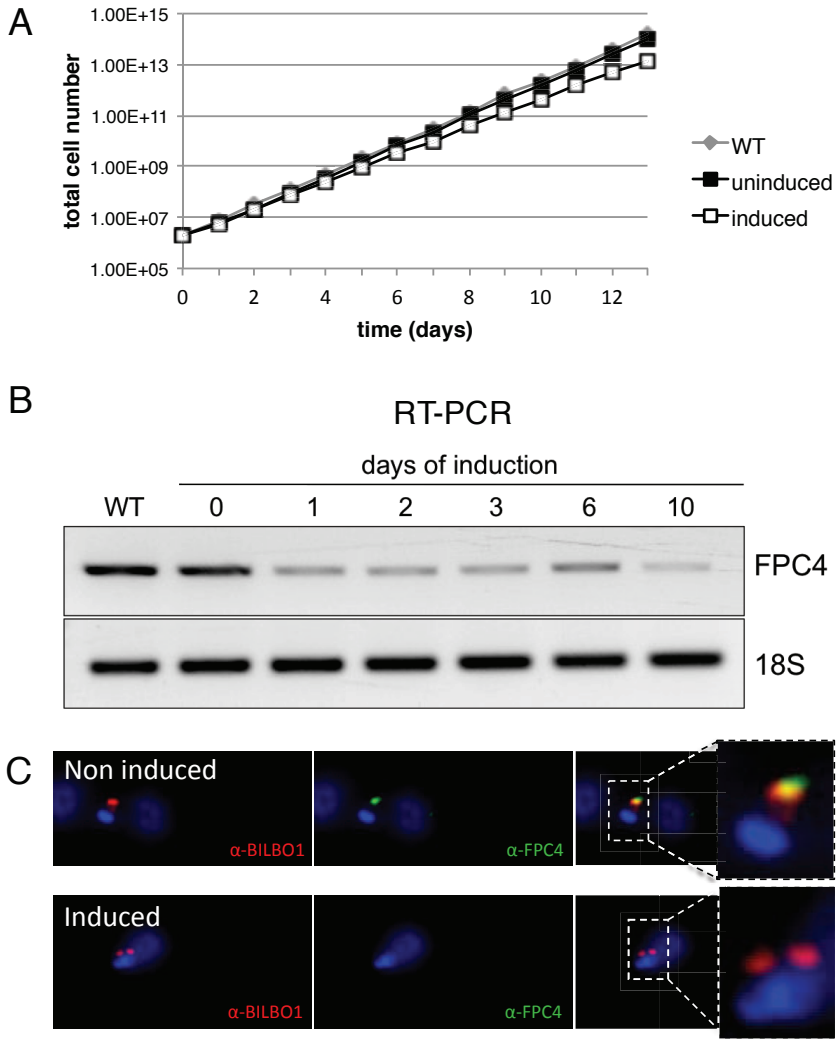

Fig. 3.27 *FPC4 RNAi knockdown in PCF*
The RNAi^{FPC4} cell line was tested upon tetracycline induction (10 µg/mL). The induced cell line did not show any growth defect (A). The efficiency of the RNAi system was controlled by semi quantitative RT-PCR (B), showing a decrease in the level of *FPC4 mRNA*; however, *FPC4 mRNA* was still detected after 10 days of induction. FPC4 protein was not detected by immunofluorescence after 48h post-induction (C) on CK.
Error bars in (A) represent the SEM but are often smaller than the data point mark.

b3) Functional analysis of FPC4

i) FPC4 knockdown by RNA interference

In order to study the function of a protein, a very commonly used method is RNA interference (RNAi) (Fig. 2.4 in the material and method section). With this technique, the mRNA transcript corresponding to the *FPC4* gene of interest is degraded upon tetracycline induction, thus impeding its translation. This down-regulation on transcript level can shed some light on the essentialness of the protein of interest or the functional role that it assumes in normal conditions. To analyse these two aspects of FPC4, the growth rate and the morphological aspect of FPC4 RNAi (RNAi^{FPC4}) PCF and BSF cells were monitored over time.

Because no clear evidence is provided in the literature to prove that one construct is more efficient than the other in this knockdown system, we used a pLew100 based sense-antisense constructs and a p2T7-based double promoter construct in PCF (Fig.2.4 in the material and methods section). Transfected cell lines were induced with 10 µg/mL of tetracycline to follow the growth rate.

Both PCF cell lines (transfected either with the stem-loop construct or the double promoter construct) behaved similarly, therefore I present here the data concerning the stem-loop construct only (Fig.3.27 A). No major differences were observed between WT, non-induced and induced cells up to 25 days of induction (data shown up to 13 days). Therefore, the efficiency of the knockdown was tested by IF and by semi quantitative RT-PCR. Two days post-induction, the FPC4 protein was no longer detectable by IF (Fig.3.27 C). However, mRNA was not fully depleted even after 10 days of induction, suggesting that minute amount of FPC4 might still be produced and eventually be sufficient for cell growth (Fig.3.27 B).

Another technique to test the efficiency of the RNAi is to control the amount of the protein by WB analysis. Sadly, our antibodies against FPC4 do not work on WB and therefore we cannot take advantage of this technique.

From this analysis we can conclude either that FPC4 does not seem to be essential for parasite survival and its down regulation does not lead to morphological phenotypes, or that low level of expression of FPC4 is sufficient for cell survival.

We also transfected BSF parasites with the stem-loop construct. Unfortunately, upon induction with 10 µg/mL tetracycline only a slight delay in growth was observed (Fig.3.28 A). We controlled by IF analyses FPC4 expression, and we noticed that the FPC4 signal was still present (Fig.3.28). This means that the RNAi was not efficient enough to deplete FPC4 or that we selected parasites able to by-pass the RNAi knockdown to survive, suggesting that

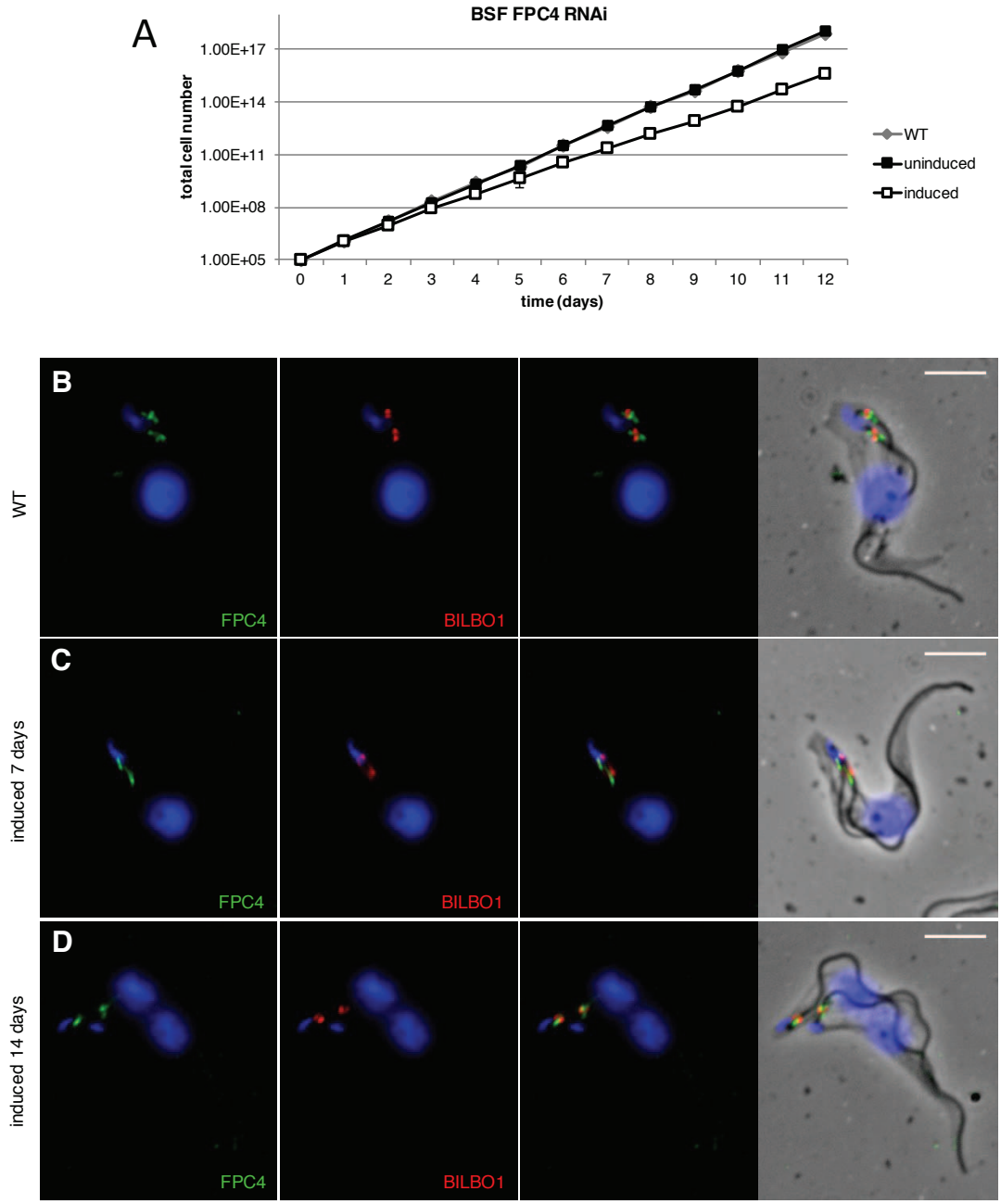

Fig. 3.28 *FPC4 RNAi knockdown in BSF*
The RNAi^{FPC4} cell line was tested upon tetracycline induction (10 µg/mL). The growth curve showed a mild growth defect for the induced cells (A). The efficiency of the RNAi system was controlled by IF. (B) shows the WT BSF probed with anti-FPC4 (ser294). Unfortunately, we noticed that the RNAi system was not efficient because FPC4 (ser294) was still detectable after 7 (C) and 14 days (D) post-induction without any observable phenotype. Error bars in (A) represent the SEM but are often smaller than the data point mark. Scale bar (B, C, D) 5 µm.

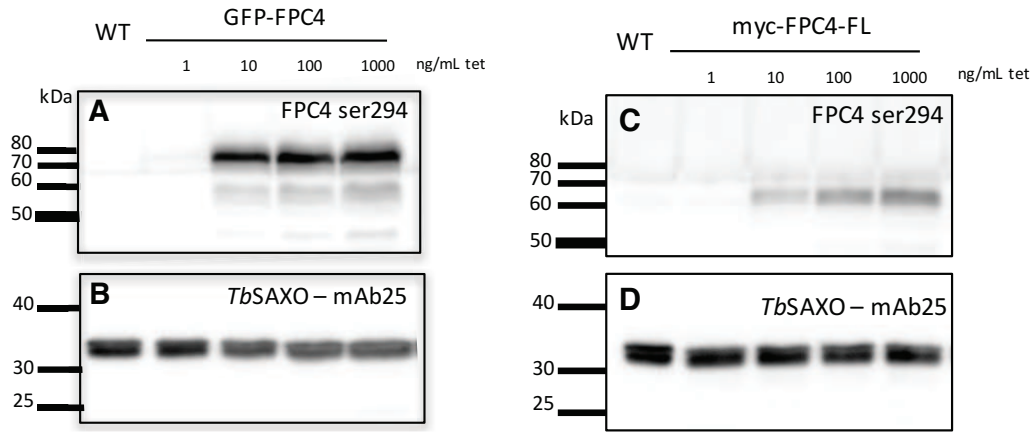

Fig. 3.29 *Over-expression of N-terminal GFP-FPC4*
Immuno-labelling with ser294 showed that (A) GFP-FPC4 construct (76 kDa) and the (C) myc-FPC4-FL (54 kDa) were correctly over-expressed in PCF *T. brucei* after 48 hours of induction and were detectable when induced with at least 10 ng/mL of tetracycline. (B, D) mAb25 was used as loading control (30 kDa). Quantification relative to *Tb*SAXO loading control showed that the GFP-FPC4 is 4-fold more expressed than the myc-FPC4-FL.

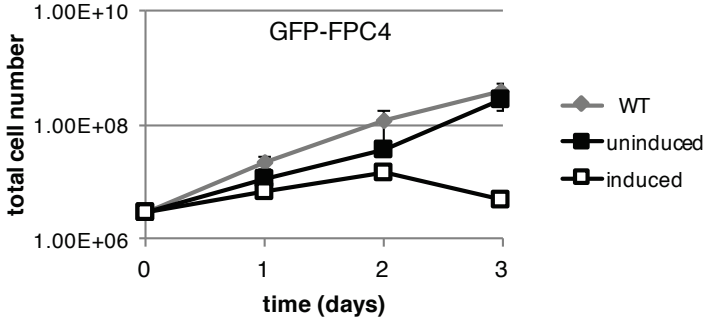

Fig. 3.30 *Growth curve of the GFP-FPC4 PCF cell line*
The growth of cells over-expressing GFP-FPC4 was reduced after 1 day of induction (10 µg/mL tetracycline), and the cells eventually died after 2-3 days of induction. Error bars representing the SEM are present but often smaller than the data point mark.

FPC4 might be essential in PCF and BSF. We thus tried several attempts to generate a *FPC4* knockout cell line in both PCF and BSF. Unfortunately, we were never able to knock-out both alleles of the *FPC4* gene. These data could suggest an important role of FPC4.

ii) Functional analysis of FPC4 by over-expression: a dominant-negative phenotype analysis

Another way to analyse the function of a protein is to over-express it and see if this leads to a dominant negative phenotype.
We generated in PCF a GFP-FPC4 (Célia Florimond) and a myc-FPC4 overexpressing cell lines to further characterise FPC4 in the trypanosome cellular context. Both plasmids used were pLew-based and therefore inducible by the addition of tetracycline.

In order to avoid the C-terminal cleavage, FPC4 was tagged at its N-terminus with a large Green Fluorescent Protein (GFP) tag (27 kDa) and the small triple myc-tag (5 kDa total).

The overexpression was controlled by WB with the anti-FPC4 ser294 antibody (see Fig. 3.29). Different concentrations of tetracycline were used to control the level of expression of GFP-FPC4. We observed a difference in expression between 1 ng/mL and the other concentrations, whereas no major differences were noticed between 10, 100 and 1000 ng/mL of tetracycline. Interestingly, after quantification using mAb25 as loading reference, we noticed that the GFP-FPC4 construct resulted in 4-fold higher expression than the myc-FPC4-FL. This might suggest that the expression of the myc-FPC4-FL is somehow controlled by the parasites and that the phenotypes occur when the over-expression level is higher than the myc-FPC4-FL.

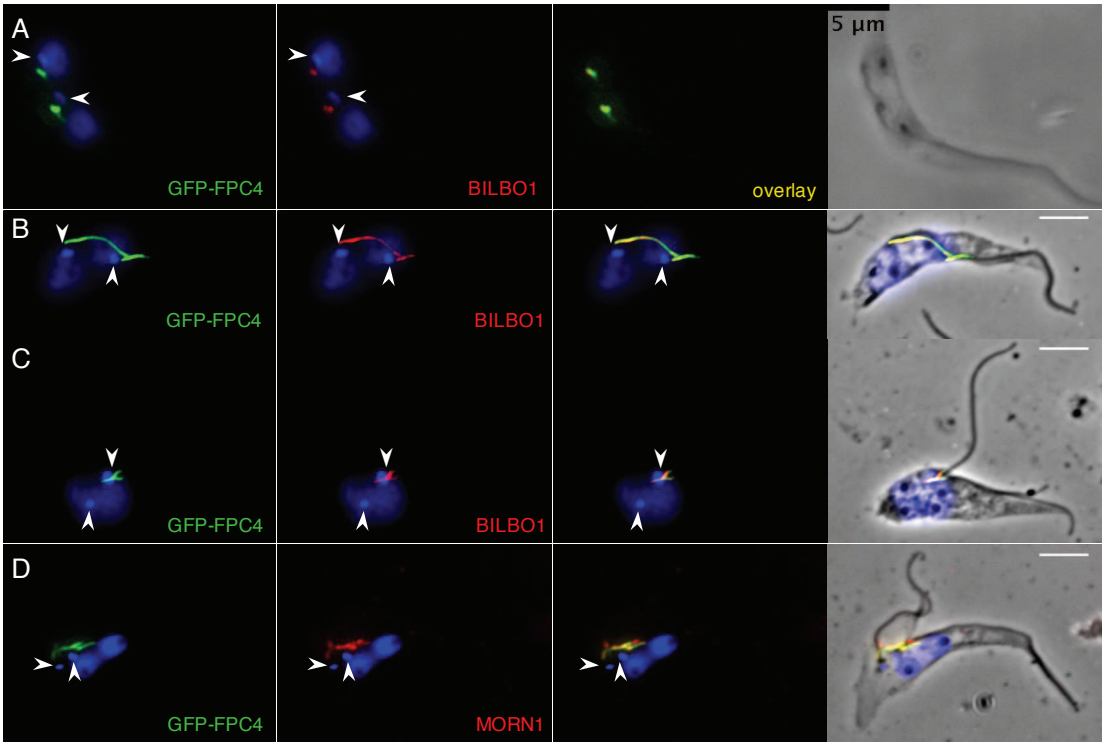

Fig. 3.31 *Immuno-fluorescence analysis on GFP-FPC4 overexpressing cells (CK).*
(A) CK of GFP-FPC4 expressing cells induced for 6 h and probed with anti-GFP showing the correct localization of the fusion protein. (B, C, D) CK of GFP-FPC4 expressing cells (48 h, 10 µg/mL tetracycline) probed with anti-GFP. (B) shows a long GFP-FPC4 filament connecting two FPCs with BILBO1 relocated on it. (C) Detached flagella and mispositioned/not properly segregated kDNAs are also visible. (D) MORN1 localization is also affected by the GFP-FPC4 over-expression. Arrowheads indicate the kDNAs. Scale bars represent 5 µm.

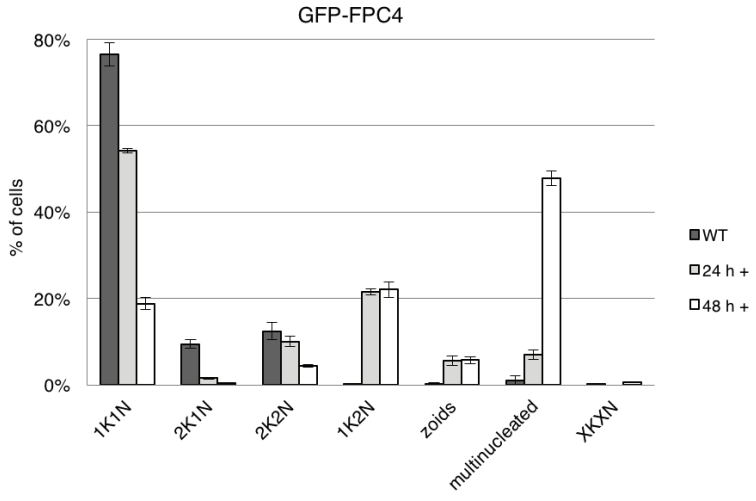

Fig. 3.32 *Phenotypes observed upon GFP-FPC4 overexpression in PCF cells*
Upon induction (24h or 48h) with 10 µg/mL of tetracycline, GFP-FPC4 over-expressing cells showed an increase of different morphological phenotypes, such as multinucleated cells, zoids and 1K2N cells. The percentage of normal cells (1K1N, 2K1N, 2K2N), compared to WT, dropped dramatically as early as 24h post induction. (Error bars SEM).

iii) Overexpression of GFP-FPC4 induces defect in kinetoplast segregation and in cytokinesis

A culture of GFP-FPC4 overexpressing cells was induced with 10 µg/mL tetracycline and cells were counted every day. Cell death happened after two days of induction demonstrating that the over-expression of GFP-FPC4 is lethal for the parasites (Fig.3.30).

We analysed further the phenotypes induced during the GFP-FPC4 overexpression by immunofluorescence and electron microscopy.
After a short induction (6h)), GFP-FPC4 was labelled at the FPC with anti-GFP and assumed a shape similar to the hook obtained with the polyclonal antibody against FPC4 (Fig.3.31 A).
At longer induction times (48h), we observed GFP-FPC4 at the FPC, but also along fibrous structures extending from the FPC area (Fig.3.31 B, C, D). In (Fig.3.31 B) The fibre induced by GFP-FPC4 seems to connect two FPCs. Surprisingly, BILBO1 labelling co-localised with GFP-FPC4-induced fibres suggesting that GFP-FPC4 induces some perturbation in the FPC structure (Fig.3.31 B, C). Furthermore, MORN1 localisation was also disturbed since it had lost its hook-structure to follow the GPF signal (Fig.3.31 D).

We could conclude that the GFP tag did not impair FPC4 targeting, but the over-expression disturbed the FPC and the hook complex organization, as highlighted by the BILBO1 and MORN1 localization respectively. The most straightforward hypothesis is that this happens because FPC4 can interact with BILBO1, and maybe with MORN1, as well.
On the other hand, GFP is a large tag and is notorious for dimerization and could therefore be the cause of these phenotypes. Nevertheless, this potential artefactual dimerization induced interesting phenotypes, demonstrating that disturbing FPC4, also affects, directly or indirectly, BILBO1 and MORN1.

Since the parasites were monitored for their growth rate and they died within three days, their morphology was also examined. Cells were fixed and nuclei (N) and kDNAs (K) were labelled with DAPI for quantification of the different morphological phenotypes (Fig.3.26). Multinucleated cells were the major phenotype after 48h of induction with an increase in 1K2N cells (20% at 24 and 48h of induction). Unusual 1K2N cells could either come from a 2K2N cell that had lost a kDNA (thus producing a zoid), or a cell in which the kinetoplast was duplicated but not segregated. This hypothesis was supported by the defect in kinetoplast segregation and positioning that was observed (Fig. 3.31 B, C, D).

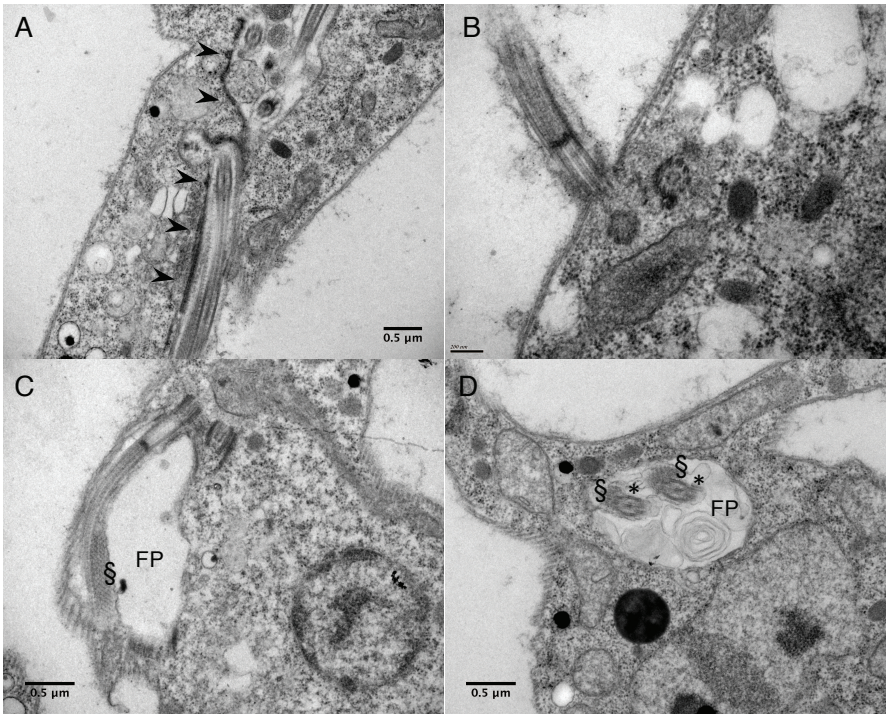

Fig. 3.33 *TEM on thin sections on GFP-FPC4 expressing cells.*
(A) An electron dense filament (arrowheads) is visible upon GFP-FPC4 over-expression, for 72 h with 10 µg/mL tetracycline. (B) Detached flagella, not associated to a FP, are visible as well. (C) The FP became enlarged and the PFR (§) was located within the Flagellar Pocket (FP). (D) A transversal section of the pocket shows the presence of material within the FP.

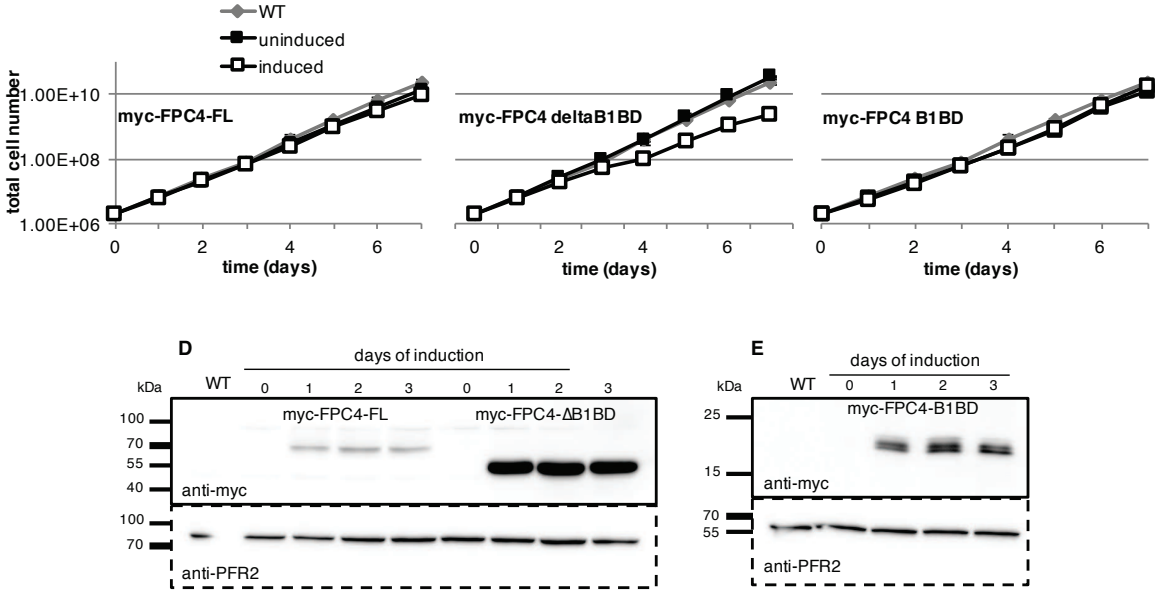

Fig. 3.34 *Growth curves of myc-FPC4-FL over-expressing cell lines and protein over-expression controlled by WB*
The over-expression was induced with 10 µg/mL tetracycline.
The over-expression of myc-FPC4-FL (A) and myc-FPC4-B1BD (C) does not induce any growth defect, whereas the myc-FPC4-ΔB1BD (B) cell line shows a reduced growth rate upon tetracycline induction. Error bars (SEM) are present but often smaller than the data point mark. To control and compare the expression level by WB, 5 x 10^6 cells/lane were loaded on SDS-PAGE, transferred onto PVDF membrane that was were probed with anti-myc antibody and with anti-PFR2 as a loading control. (D) It is clearly visible that the myc-FPC4-FL construct was less over-expressed than the myc-FPC4-ΔB1BD and (E) FPC4-B1BD. (D) 12% SDS-PAGE and (E) 15% SDS-PAGE.

The K and N numbers per cell were counted and compared with those of WT cells. The position of K and N were also taken into account. Abnormal cells, such as 1K2N, 1K0N (zoids) or multinucleated cells were observed as early as day one of induction (Fig.3.32). Some cells also showed detached flagella (Fig.3.31C). The increase in multinucleated cells suggested a cytokinesis defect (Fig.3.31 D) that would lead to 1K0N and 1K2N cells and cell death.

To obtain more information about the FP and FPC structure after over-expression of GFP-FPC4, the cells were induced for 72 h and analysed by transmission electron microscopy (TEM). The cells were fixed, embedded in a resin-block and ultrathin sections were analysed by negative staining (data generated by Derrick Robinson).
Similar to the IF labelling, we could observe some long uncharacterised fibre-like electron-dense material extending from the FP and the FPC and along the FAZ (Fig.3.33 A). Interestingly, the detached new flagella, that we could observe by IF, were not associated with an FP whilst still associated with a kinetoplast. This phenotype is reminiscent of the BILBO1 RNAi phenotype (see Introduction Fig. 1.28 Fig. 1.29). Furthermore, we were able to observe a disorganized FP, where flagella with the PFR were located within the FP and uncharacterized material was present as well within the pocket (Fig.3.33 C, D).

Conclusion:
Taken together these observations can give a first clue about the reason why this over-expression is lethal. First of all, the long GFP-FPC4 fibre observed by IF and by EM, led to a mis-localization of BILBO1 and MORN1. Secondly, the mis-positioning of the kDNAs, as possible consequence of a defect in segregation, might have caused problems in the cytokinesis process and induced the production of multinucleated cells and zoids. Moreover, the enlarged FP or absence of FP might have led to cell death.

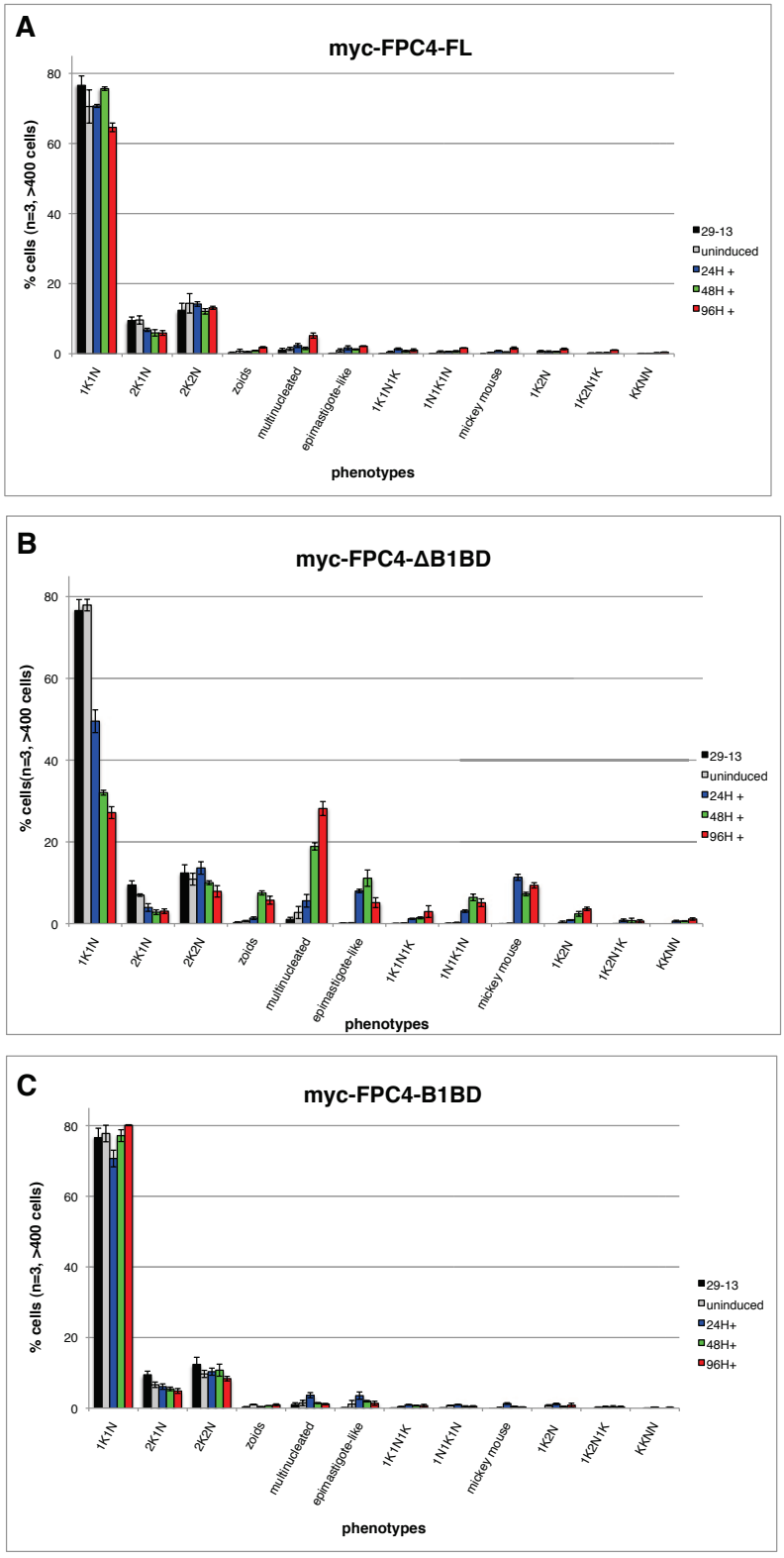

Fig. 3.35 *Phenotypes observed upon induction of the expression of myc-FPC4-FL,* myc-FPC4-B1BD *and* myc-FPC4-ΔB1BD

Upon induction with 10 µg/mL tetracycline, myc-FPC4-FL (A) and myc-FPC4-B1BD (C) over-expressing cells did not show any morphological difference compared to WT cells. Contrarily, myc-FPC4-ΔB1BD (B), showed a decrease in normal cells (1K1N, 2K1N and 2K2N) and an increase in multinucleated cells, zoids and “mickey mouse” cells (meaning 2K2N cells, with the 2 kDNAs positioned in between the 2 nuclei). An interesting phenotype observed was the presence of epimastigote-like cells.

iv) Overexpression of myc-FPC4-ΔB1BD: effect on the kinetoplast segregation

To circumvent the phenotypes that might have been induced by the GFP, we decided to monitor the growth rate of the three cell lines overexpressing myc-FPC4-FL, myc-FPC4-ΔB1BD and myc-FPC4-B1BD.
No differences were noticed between the growth of WT, uninduced and induced cells (10 µg/mL tetracycline) of myc-FPC4-FL and myc-FPC4-B1BD cells (Fig.3.34 A, C).
On the contrary, the growth rate of myc-FPC4-ΔB1BD induced cells was slower than WT and uninduced cells (Fig.3.34 B). Consequently, the over-expression of myc-FPC4-ΔB1BD is able to slow down the growth, without, however, inhibiting it.

The fact that the over-expression of myc-FPC4-FL does not impair the cell growth is in opposition to the result obtained during the over-expression of GFP-FPC4, which was lethal within 3 days of induction. However, the higher level of expression of GFP-FPC4 compared to myc-FPC4-FL might participate to the induction of dominant negative phenotypes (Fig. 3.29). Moreover, the myc-FPC4-ΔB1BD construct is approximately 9-fold more over-expressed than the myc-FPC4-FL (Fig.3.34 D).
The amount of the protein, rather than the truncation, might therefore play a role in the occurrence of the phenotypes.

Even without major growth defects, we looked at morphological phenotypes to eventually find out which part of the cell was affected by this dominant negative effect.
The number and position of kDNAs and nuclei were monitored by DAPI staining on CK.
The myc-FPC4-FL and the myc-FPC4-B1BD expressing cells lines remained similar to the WT and did not show particular phenotypes (Fig.3.35 A, C). Contrarily, we observed a wider range of phenotypes in the myc-FPC4-ΔB1BD cell line (Fig.3.35 B) that we analysed further.
After 24-48h of induction, the percentage of cells with normal morphology, referring to 1K1N – 2K1N – 2K2N in the correct position within the cell, decreased dramatically. The most striking effect was seen with 1K1N cells. Generally, in a WT population in exponential phase, around 75% of the cells are in G1 phase, corresponding to 1K1N, and the remaining 25% is distributed between 2K1N or 2K2N cells.
In the myc-FPC4-ΔB1BD induced cells only about 30% of 1K1N cells were observed 48 h post-induction (Fig.3.35B). Interestingly, a considerable percentage of multinucleated cells and zoids appeared, as previously seen with the overexpression of GFP-FPC4. Two particular phenotypes were quantified; we observed almost 10% of cells with an epimastigote-like conformation – i.e. the kDNA is anterior to the nucleus –, and 10% of cells

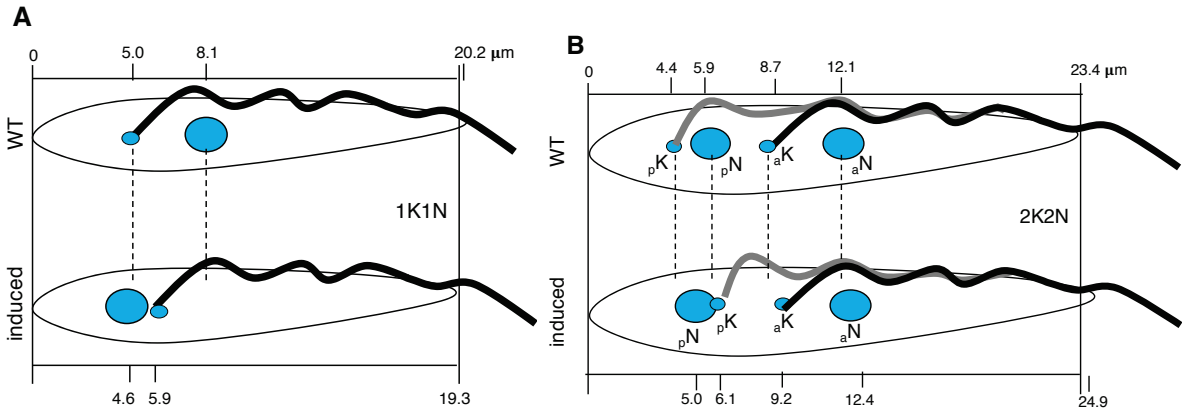

C	WT	epimastigote-like
	distance (µm) ± SEM	distance (µm) ± SEM
1K1N		
cell body length	20.2 ± 0.3	19.3 ± 0.5
posterior end to K	5 ± 0.2	5.9 ± 0.2
posterior end to N	8.1 ± 0.2	4.6 ± 0.2
	WT	**mickey mouse**
	distance (µm) ± SEM	distance (µm) ± SEM
2K2N		
cell body length	23.4 ± 0.6	24.9 ± 1.0
posterior end to anterior N	12.1 ± 0.3	12.4 ± 0.5
posterior end to anterior K	8.7 ± 0.2	9.2 ± 0.5
posterior end to posterior N	5.9 ± 0.2	5.0 ± 0.4
posterior end to posterior K	4.4 ± 0.1	6.1 ± 0.5
K-K distance	4.5 ± 0.2	3.2 ± 0.3
N-N distance	6.1 ± 0.2	7.5 ± 0.5

Fig. 3.36 *Position of kinetoplasts and nuclei in WT versus induced myc-FPC4-ΔB1BD cells*
One of the observed phenotypes upon induction of myc-FPC4-ΔB1BD was epimastigote-like cells. (A, B) This scheme represents the distances between the posterior end of the cell and the kinetoplasts and the nuclei in 1K1N and 2K2N WT (A) and epimastigote-like cells (B) (n=3, 50 cells, 10 µg/mL tetracycline for 48 h). (C). These schemes summarize the distances between the posterior end of the cells and the kinetoplasts and nuclei with two nuclei and one kinetoplast or two kinetoplasts between the nuclei – i.e. 1N1K1N, 1N2K1N– also called a “mickey mouse” phenotype.

with two nuclei and one kinetoplast or two kinetoplasts between the nuclei – i.e. 1N1K1N, 1N2K1N– also called “mickey mouse” phenotype.

Altogether these data show that the over-expression of myc-FPC4-ΔB1BD in PCF leads to the production of cells with a disturbed kinetoplast-nucleus position. Moreover, the duplication of the kDNA does not seem to be affected, whereas its segregation does.
We therefore decided to measure, in the epimastigote-like cells, the distances between the kinetoplasts and nuclei, and their distance relative to the posterior end of the cell. The aim of this experiment was to try to figure out whether there was a kDNA segregation problem. We summarized the measurements in Fig.3.36. We could observe that in 1K1N cells, the kinetoplast remained almost in the same position as in WT cells, but the nucleus had moved toward the posterior end of the cell. In 2K2N, the new kinetoplast and the old kinetoplast were closer to each other than in WT and this can be a sign of an impaired BB/kDNA segregation.

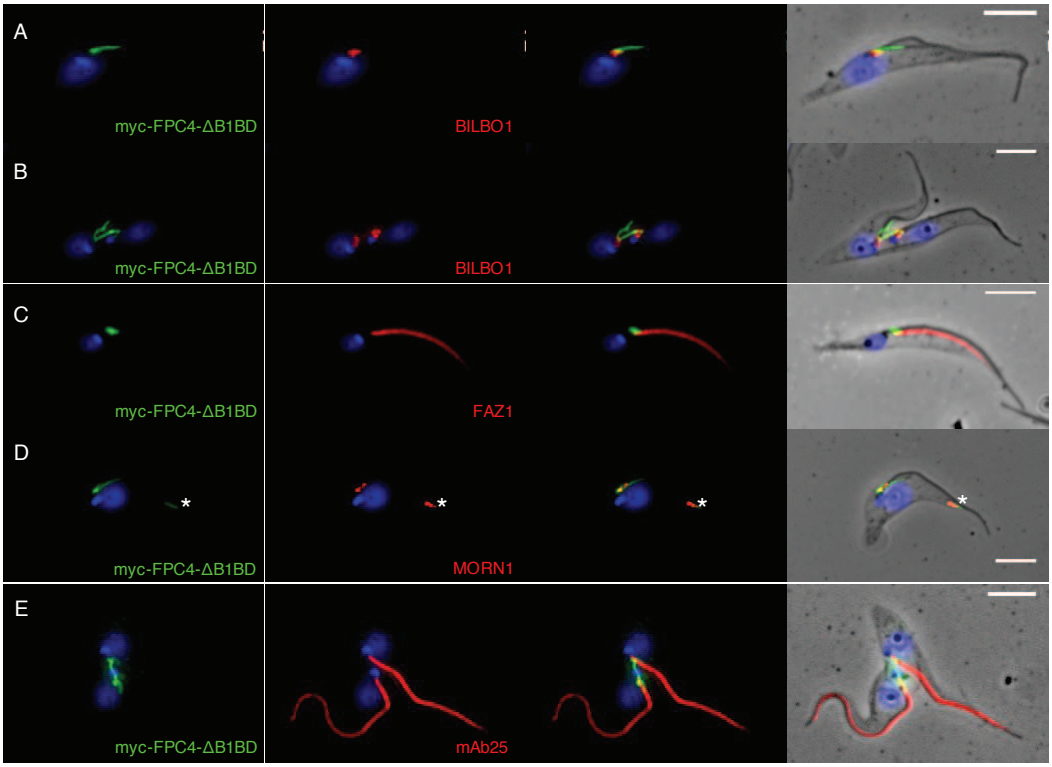

Fig.3.37 *Immuno-fluorescence analysis on myc-FPC4-ΔB1BD with BILBO1, a FAZ marker, MORN1 and an axonemal marker*

Myc-FPC4-ΔB1BD (anti-myc, green) expressing cells induced for 48 h with 10 µg/mL tetracycline were probed with anti-BILBO1 (A and B), anti-FAZ1 (C), anti-MORN1 (D) and mAb25 (E).

Morphological phenotypes such as epimastigote-like cells (A and C) and mickey mouse cells (B and E) were observed, with no apparent effect on BILBO1, FAZ or axoneme (mAb25) formation and localization.

In mickey mouse cells, the myc signal connects the two FPCs (B, E).

A myc-positive dot is often visible at the anterior end of the cell body where the flagellum detaches from the cell body (D, *), and MORN1 signal is present on it.

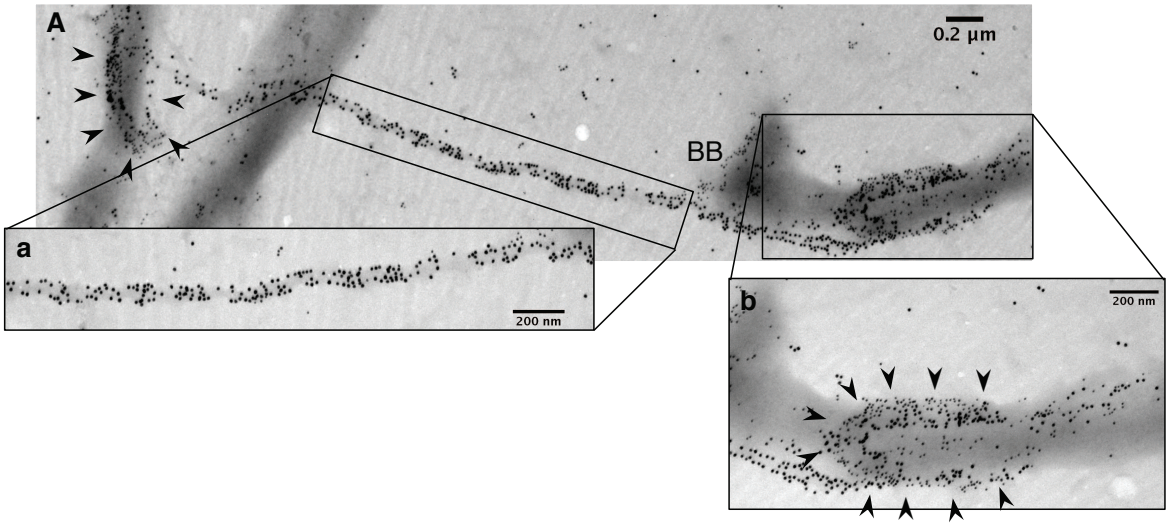

Fig. 3.38 *Immuno-electron microscopy on flagella probed with anti-BILBO1 and anti-myc.*

(A) On isolated flagella from myc-FPC4-ΔB1BD expressing cells (48 h induced, 10 µg/mL tetracycline), a connection between two FPC (arrowheads) (a) is labelled with the anti-myc (15 nm gold particles). BILBO1 (10 nm gold particles) was located at the FPC (b - arrowheads), but not on this filamentous connection (a).

v) Overexpression of myc-FPC4-ΔB1BD: effect on cytoskeleton structures

We proved that the FPC4 is targeted, thanks to its N-terminus, to the FPC and to the hook complex. For that reason, we wanted to determine what happens to these two cytoskeletal structures during FPC4 over-expression. Immuno-fluorescence analyses were performed at 48 h post-induction and this time point was chosen according to the results of the phenotype counting (Fig.3.37).
Different markers have been tested together with the myc antibody to determine the effect of the over-expression on different cytoskeletal structures. BILBO1 was used as an FPC marker, MORN1 as a Hook complex marker, FAZ1 (L3B2) as FAZ maker, mAb25 as an axonemal marker and DAPI was used to stain K and N DNA (Fig.3.37).

Over-expression of myc-FPC4-FL did not affect any of the cytoskeletal structures as the labelling was the same as in WT cells (not shown). Despite the morphological phenotypes, BILBO1 localization, FAZ formation and the flagellum did not seem to be affected by the over-expression of myc-FPC4-ΔB1BD (Fig.3.37 B, C, E).
Interestingly, in 2K2N cells the myc-FPC4-ΔB1BD overexpression induced a connection between the two FPCs (Fig.3.37 B, E). The same connection between two FPCs was visible on iEM on extracted flagella by iEM (Fig.3.38). The myc-FPC4-ΔB1BD were induced for 48 h with 10 µg/mL tetracycline and probed with anti-myc (15 nm gold-beads) and anti-BILBO1 (10nm gold-beads). The myc signal present at the FPC was extended on a filament-structure and connected to a second FPC. No BILBO1 signal was observed on this FPCs-connection (Fig.3.38).

Furthermore, in the myc-FPC4-ΔB1BD overexpressing cells, the Hook structure appeared to be affected, as shown with the anti-myc and anti-MORN1 labelling (Fig.3.37 D). We noticed that, often, a myc positive dot was visible at the anterior end of the cell, where the flagellum loses its connection with the cell body (Fig.3.37 D, *), and MORN1is also present on it.
This additional FPC4 signal will be considered in the discussion.

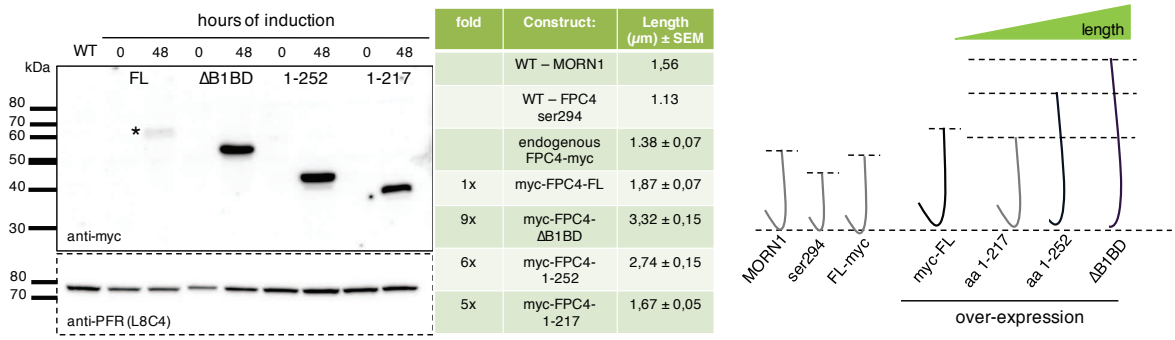

fold	Construct:	Length (μm) ± SEM
	WT – MORN1	1,56
	WT – FPC4 ser294	1.13
	endogenous FPC4-myc	1.38 ± 0,07
1x	myc-FPC4-FL	1,87 ± 0,07
9x	myc-FPC4-ΔB1BD	3,32 ± 0,15
6x	myc-FPC4-1-252	2,74 ± 0,15
5x	myc-FPC4-1-217	1,67 ± 0,05

Fig. 3.39 *The length of the FPC4-hook*

Additionally to the myc-FPC4 and myc-FPC4-ΔB1BD constructs, we generated cell lines expressing myc-FPC4-1-252 and myc-FPC41-217. Expression of the constructs was controlled by WB with anti-myc anti-body and anti-PFR as loading control, and quantified. Except for the FL (*), which showed a lower expression level, the other three constructs were respectively 9- 6- and 5-fold more expressed than the FL.

The length of the myc labelled hook structure was measured for the different myc-FPC4 constructs after 48 h of induction with 10 µg/mL tetracycline by immunofluorescence.

The length measurements of the hook are summarized in the table, as well as the fold of over-expression compared to myc-FPC4-FL. The myc-FPC4-ΔB1BD construct was almost twice the length of the normal size of myc-FPC4-FL. (n=3, 60 cells, measured on 1K1N or 2K2K cells, where the two structures were completely separated).

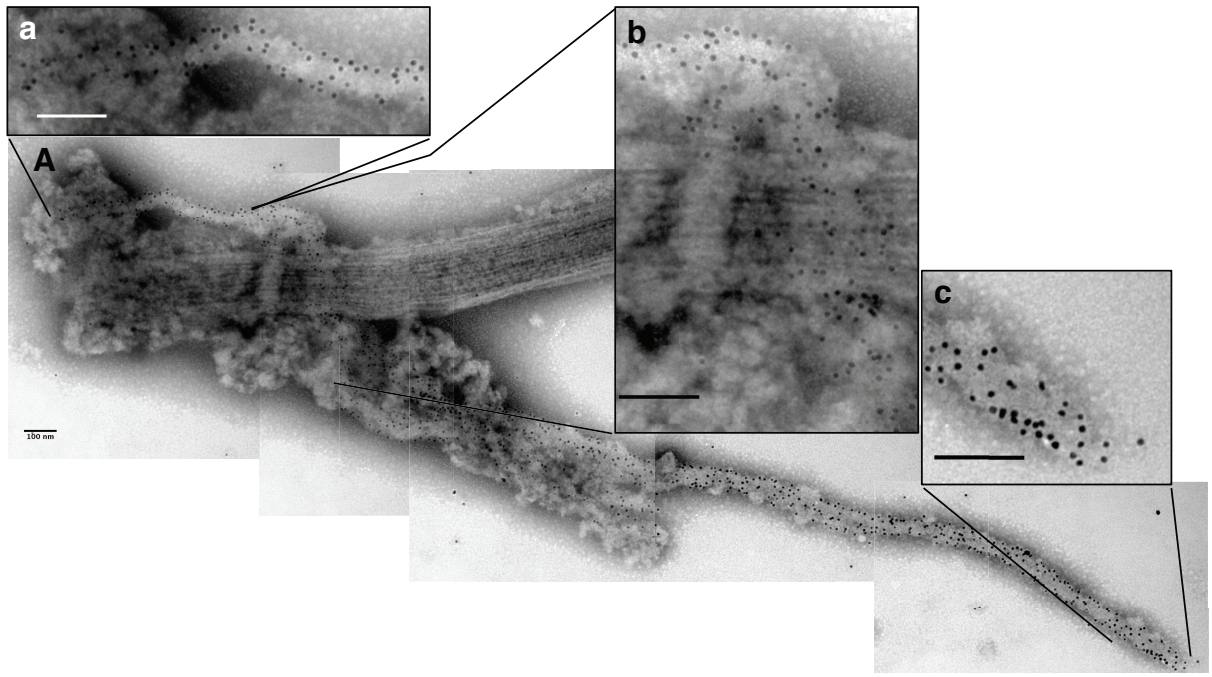

Fig. 3.40 *Immuno-electron microscopy labelling of isolated flagella from myc-FPC4-ΔB1BD overexpressing cells.*

(A). Isolated flagella were probed with anti-myc antibody (10 nm gold particles) that was decorating a fibre-like structure from the BB (a) passing the FPC (b) and extending downstream the FPC (c). Cells were induced 48 h with 10 µg/mL tetracycline.

vi) Overexpression of myc-FPC4-ΔB1BD affects the Hook complex

Since we noticed that the myc signal in myc-FPC4-ΔB1BD expressing cells appeared extended in length, we decided to measure the size of the hook structure in 1K1N or 2K2N cells, when the two structures were well separated. Additionally to the myc-FPC4 and myc-FPC4-ΔB1BD constructs, we generated cell lines expressing myc-FPC4-1-252 and myc-FPC41-217. The expression levels of the different constructs were compared by WB (Fig. 3.39). The myc-FPC4-FL construct was clearly less expressed than the other constructs. The constructs ΔB1BD, 1-252 and 1-217 were respectively 9-fold, 6-fold and 5-fold more expressed than myc-FPC4-FL, showing again a cellular control over the expression level of the recombinant proteins.

Immunofluorescence using anti-FPC4 and anti-MORN1 on WT cells, and anti-myc on overexpressing myc-FPC4 constructs cell lines and on FPC4-myc endogenous cell line, allowed us to measure the length of the hook structure (summarized in Fig.3.33). In WT cells, the Hook structure labelled with anti-MORN1 measured 1.56 µm (n=1, 37 cells), a length slightly shorter than measured by Morriswood (Morriswood, 2015); this length was even shorter with anti-FPC4 ser294 (1.13 µm). In myc-FPC4-FL expressing cells the structure measured 1.87± 0.07 µm, showing a direct effect of the overexpression on the structure length.

The myc-FPC4-ΔB1BD, that was 9-fold more expressed than myc-FPC4-FL, resulted in a hook almost twice as long: 3.32 ± 0.15 µm. We additionally measured the size of myc-FPC4-1-217 and myc-FPC4-1-252 FPC4 constructs, in order to compare the hook length of the constructs in absence or presence of the CC domain. The myc-FPC4-1-217 construct, which lacks the CC domain, resulted in a slightly shorter hook (1.67 ± 0.05 µm) than with myc-FPC4-FL, whereas the myc-1-252-FPC4 construct, carrying the CC domain, resulted in a longer hook than with myc-FPC4-FL (2,74 ± 0.15 µm) but shorter than the myc-FPC4-ΔB1BD (3.32 ± 0.15 µm) (Fig.3.33).

We do not know whether the myc-FPC4-ΔB1BD signal was larger due to the efficiency of the over-expression and therefore a larger amount of protein producing a longer fiber, or the fact that lacking B1BD allowed FPC4 to elongate.

Hypothetical explanations will be discussed in the discussion chapter.

The myc-FPC4-ΔB1BD localization was analysed by iEM on isolated flagella (Fig.3.40) (induced 48 h with 10 µg/mL tet). The myc-FPC4-ΔB1BD signal was found on a fibre-like structure visible from the BB, passing by the FPC and extending toward the flagellar tip. Myc-FPC4-ΔB1BD was co-labelled with BILBO1 (Fig.3.41 A). We could observe that BILBO1

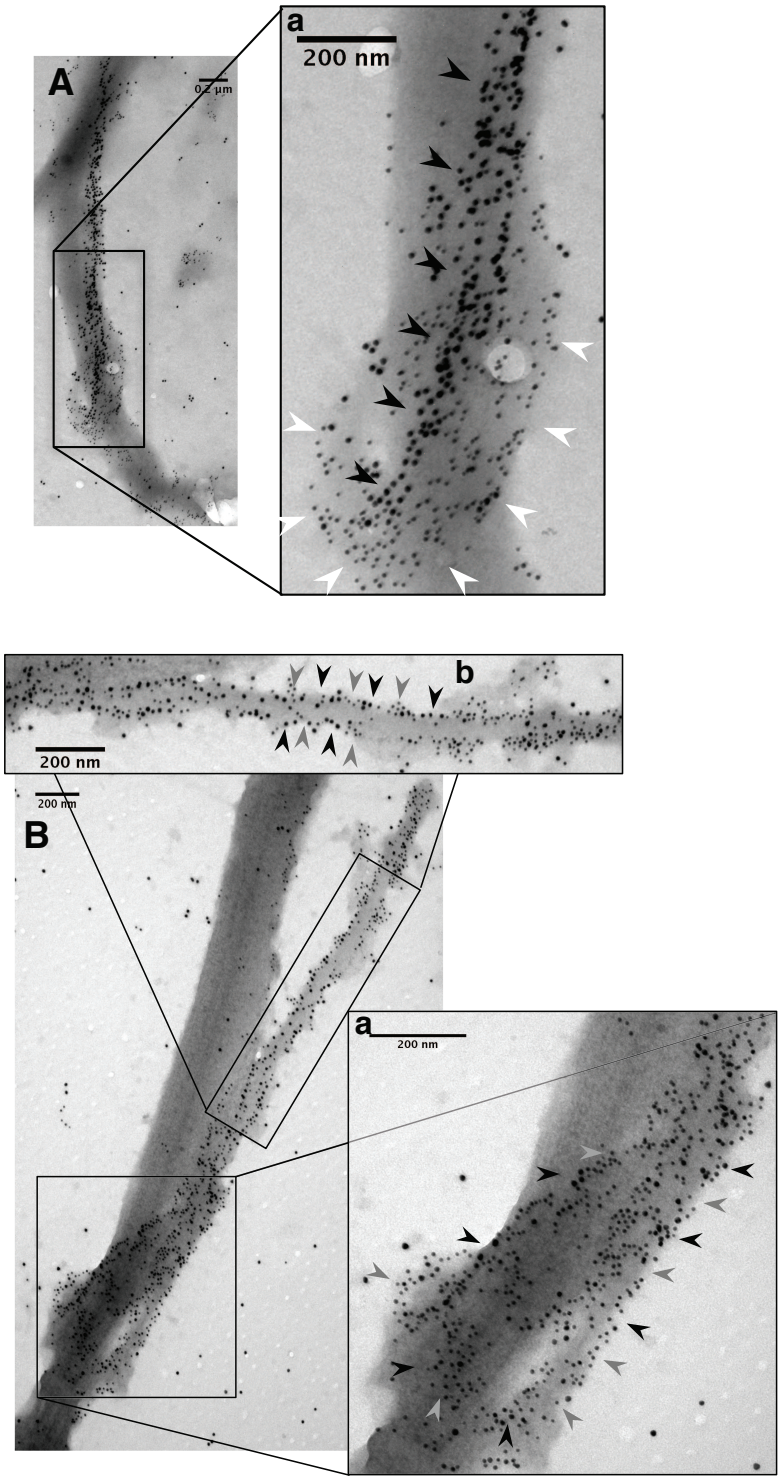

Fig.3.41 *BILBO1 or MORN1 and myc-FPC4-ΔB1BD co-immuno-gold labelling.*
(A). Isolated flagella were probed with anti-myc antibody (15 nm gold particles – black arrow-heads) and anti-BILBO1 (10 nm gold particles- white arrow-heads) (a) is an enlargement of (A) which shows that myc-FPC4-ΔB1BD sits on top of BILBO1 on the FPC (distal to the BB compared to BILBO1) and elongates along the flagellum toward the flagellum tip.
(B). Isolated flagella were probed with anti-myc antibody (15 nm gold particles – black arrow-heads) and anti-MORN1 (10 nm gold particles – grey arrow-heads). (a) and (b) are an enlargement of (B). The myc-FPC4-ΔB1BD signal is found together with MORN1 at the FPC (b) and on an elongated structure toward the flagellum tip (a). Cells were induced 48 h with 10 µg/mL tetracycline.

was present at the FPC, assuming a collar-shape, and that myc-FPC4-ΔB1BD was observed on top of it (distal to the BB compared to BILBO1) as well as was extended along the flagellum (Fig.3.41 A). The flagella were also probed with anti-myc and anti-MORN1 (Fig.3.41 B). In this case, the two signals (15 nm gold for the myc antibody, 10 nm gold particles for MORN1), localised on the same structure, confirming that FPC4 and MORN1 are both at the hook complex (Fig.3.41 B).

To obtain more information and have a more precise overview of the phenotypes produced by the over-expression of the myc-FPC4-ΔB1BD cell line, thin sections were analysed by TEM (Fig.3.42). Epimastigote-like cells, visible on fluorescence microscopy, were identified on EM as well. The typical epimastigote conformation is clearly visible in Fig.3.42 A, with the nucleus positioned posterior to the kDNA. Additionally, peculiar phenotypes were discovered (Fig.3.42). By IF analyses we could observe that BILBO1 was not particularly disturbed, but by EM we could see that the FP sometimes appeared “open”, allowing the release of its content (Fig.3.42 B). The flagellum and the FAZ seemed correctly formed, although the PFR, which is normally located within the flagellum on the cell body side close to the FAZ, was located on the opposite side of the flagellum, facing toward the outside (Fig.3.42 B).

General conclusion:
The over-expression of myc-FPC4-ΔB1BD induced severe morphological defects without greatly affecting the cell growth. If the ability to precisely accomplish the cytokinesis process is lost, the scission might occur more randomly resulting in some cells able to properly divide and some cells that need more time to properly divide.
We observed a drastic reduction in normal phenotypes (1K1N, 2K1N, 2K2N) one and two days post-induction and an increase in multinucleated cells, zoids, epimastigote-like cells and mickey mouse cells, where the two kDNAs were found in between the two nuclei.
The same phenotypes were observed by TEM on thin sections. Additionally, a myc signal connecting two FPCs has been observed by iEM on extracted flagella, as well.
These results confirmed, as for the GFP-FPC4-FL, a defect in cytokinesis and suggested an additional impairment of the proper BB/kDNA segregation.

A clearer view of the FPC area was obtained by iEM on myc-FPC4-ΔB1BD flagella.
Myc-FPC4-ΔB1BD signal was detected situated on top of BILBO1, whereas myc-FPC4 and MORN1 were located within the same structure. These observations strengthened the fact that FPC4 is located at both, the FPC and the hook-complex.

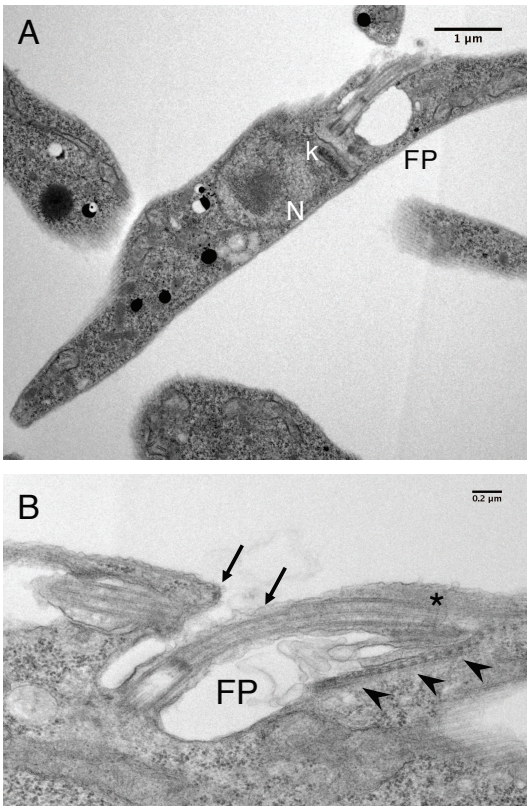

Fig. 3.42 *Thin sections of myc-ΔB1BD FPC4 expressing cells*
Epimastigote-like cells (A) in which the nucleus (N) is located posterior to the kDNA (k).
(B) The FAZ was correctly formed (arrowheads), but the PFR (*), normally found on the cell body side of the flagellum, was found facing toward the outside of the cell. An additional observed phenotype was the unusual opening of the flagellar pocket (FP). Most likely a loose FPC, or no FPC at all in this region (arrows), would allow the dissociation between the plasma and the flagellar membrane, and the release of the FP content.

Our data showed that FPC4 is a FPC and Hook complex protein and that its B1BD is not required for targeting. Essentiality of FPC4 was not demonstrated by RNAi, however overexpression of mutant FPC4 induces defect in kinetoplast segregation, most probably due to a connexion that is maintained between the old and the new FPC as observed by IF and immuno-EM. It also affects the localization of MORN1, a Hook complex protein. Altogether these results identified FPC4 as a physical link between the FPC and the Hook complex.

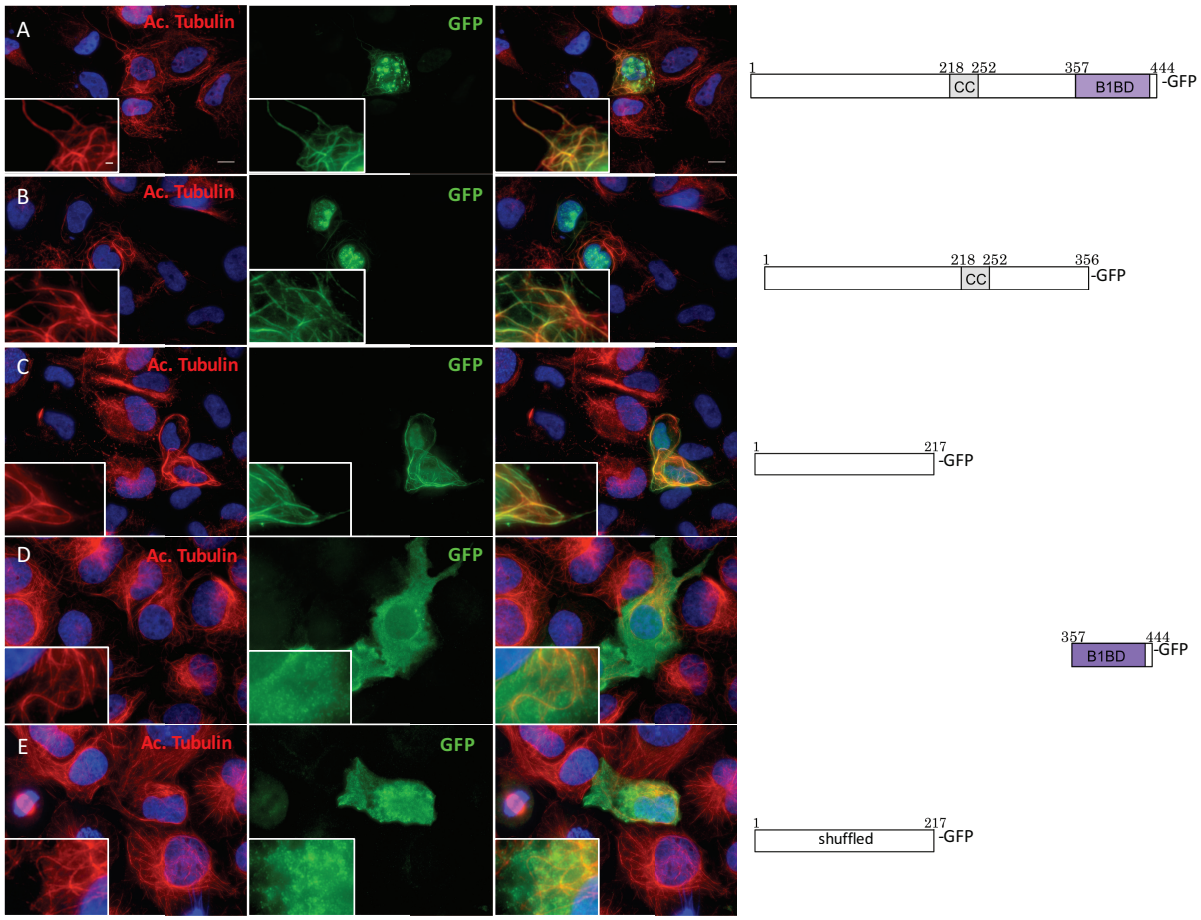

Fig. 3.43 *Immunofluorescence analysis on U-2 OS cells expressing FPC4 and FPC4 domains.*

Different FPC4-GFP truncations were expressed in U-2 OS cells and probed with anti-GFP (green) and anti-tubulin (red). We noticed that when the N-terminal part of FPC4 was present (A, B, C), the recombinant proteins were located on MTs. On the contrary the B1BD-FPC4-GFP construct (D) was soluble, as previously shown in U-2 OS cells (Fig. 3.18 D). Shuffling the first 217 aa of FPC4 allowed us to test the specificity of this MT-interaction. The basic pI (11.05) of this truncation was maintained as well as the aa composition but not the order of the residues; this shuffling abolished the MT interaction (E).

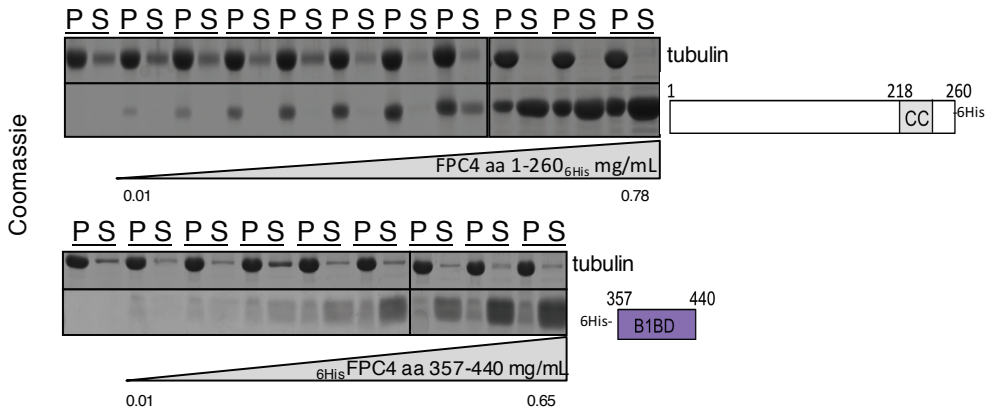

Fig. 3.44 *FPC4 is a microtubule binding protein.*

Microtubule-co-sedimentation assay. Increasing amounts of purified FPC4 aa 1-260$_{6His}$ (upper panel) and $_{6His}$-FPC4 aa 357-440 (lower panel) were incubated with 0.4 mg/ml polymerized microtubules (tubulin), then centrifuged to collect the MTs and the MT-binding proteins in the pellet (P), whilst non MT-binding proteins remain in the supernatant (S). Samples were loaded on SDS-PAGE and proteins were stain with Instant Blue^{TM}.

b4) FPC4 is a microtubule binding protein

By bioinformatics analyses, FPC4 did not show any functional domain, except for a CC domain. However, FPC4 has an overall basic pI (10.61) and shows two couples of repeated sequences (Fig. 3.10), that are typical features of microtubule associated proteins (MAPs).

i) FPC4 binds to microtubules in mammalian cells

We decided to have a closer look at FPC4 behaviour in U-2 OS to find out its intrinsic properties. To do this, we tagged FPC4 and other four truncations with a C-terminal GFP tag. FPC4-FL-GFP and FPC4-ΔB1BD-GFP localized on MT as shown with an anti-acetylated tubulin antibody labelling (Fig.3.43 A, B). Similar to the cytoplasmic localization in the trypanosome, the FPC4-B1BD-GFP construct localized in the U-2 OS cytoplasm (Fig.3.18 D Fig.3.43 D).
The domain of FPC4 involved in the MT association resides therefore within the FPC4-ΔB1BD construct. Consequently, we tested a shorter domain (1-217 aa), which is involved in the targeting to the FPC in trypanosomes. FPC4-1-217-GFP behaved exactly like FPC4-FL-GFP and FPC4-ΔB1BD-GFP also localizing onto the MTs (Fig.3.43 C).

One of the characteristics of MT-associated proteins (MAPs) is their basic pI (Amos and Schlieper, 2005). FPC4 has an overall pI of 10.61, the first 1-217 aa domain has a pI of 11.05, and the 218-444 aa domain is also basic (pI 8.7). To be sure that the association with MT in U-2 OS is specific to the amino acid sequence of the protein and not to its basic pI, we shuffled the sequence of the first 1-217 residues (FPC4-shuffled-1-217-GFP), i.e. the amino acids composition remained the same, but the residues where randomly mixed (produced by Eurofins MWG). FPC4-shuffled-1-217-GFP expressed in U-2 OS localized in the cytoplasm and not to the MTs (Fig.3.43 E). This result confirms that it is the sequence specificity of FPC4, which determines the MT interaction *in vivo*, and not the basic characteristics of the residues.

ii) FPC4 binds directly to microtubules *in vitro*

The ability of FPC4 to interact directly with MT was additionally tested *in vitro*, with a technique called MT co-sedimentation assay. This method is conceptually very simple: when a soluble protein, able to bind to MTs, is incubated with MTs, the protein-MTs complex can

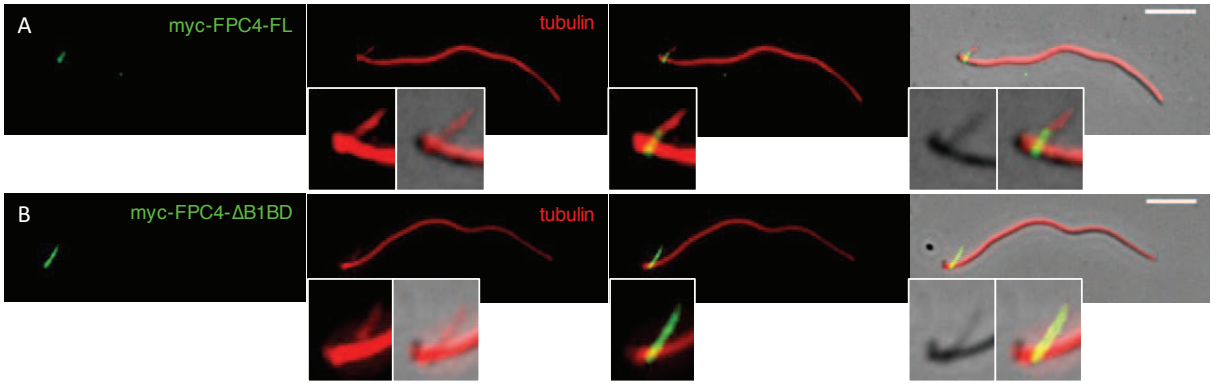

Fig. 3.45 *IF on isolated flagella from myc-FPC4 and* myc-FPC4-ΔB1BD *expressing cells probed with anti-tubulin and anti-myc.*
Isolated flagella of cells expressing myc-FPC4 (A) or myc-FPC4-ΔB1BD (B) (48 h induced with 10 µg/mL tetracycline) were probed with anti-tubulin and anti-myc. In both cases, the myc signal was co-localizing with a tubulin positive structure originating from the BB, visible by phase contrast. Scale bar 5 µm

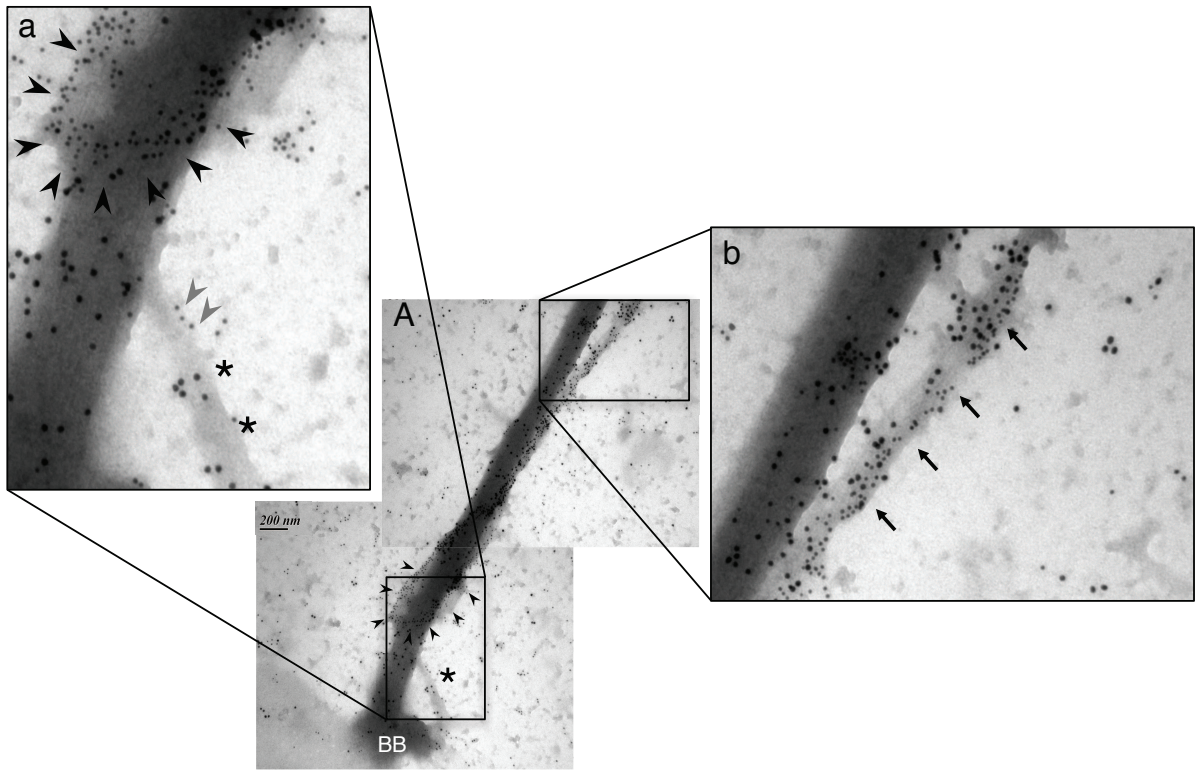

Fig. 3.46 *Immuno-gold electron microscopy of isolated flagella from myc-FPC4-ΔB1BD expressing cells.*
(A) Isolated flagella from myc-FPC4-ΔB1BD expressing cells (induced for 48 h, 10µg/mL tetracycline) were probed with anti-tubulin (15 nm gold particles) and anti-myc (10 nm gold particles). (a) The myc signal was mainly present on the FPC (black arrowheads), with an additional signal toward the BB (grey arrowheads) on a tubulin positive structure. The myc-signal was seen extending towards the flagellum tip, co-localizing with a tubulin positive structure (b, arrows). This tubulin positive structure (*) originating from the BB, crossing the FPC and elongating along the flagellum, most likely represents the MtQ.

be pelleted with a centrifugation step. On the contrary, a soluble protein, without MT-binding properties, remains in the supernatant after the centrifugation step.

The experiment was performed by Marie Eggenspieler, a master student. We purified two recombinant forms of FPC4, aa 1-260 (FPC4-1-260$_{6His}$) and aa 357-440 ($_{6His}$FPC4-357-440), with a 6_{His} tag on the C- and N- terminus, respectively. *In vitro* polymerized MTs were incubated with increasing amount of the purified proteins and then ultra-centrifuged. Supernatant (S) and pellet (P) fractions after centrifugation were loaded on an SDS gel. The gel was stained with Instant Blue^{TM} and revealed a band at 50 kDa, which corresponded to tubulin, and a band at 30 kDa and 10 kDa for FPC4-1-260$_{6His}$ and $_{6His}$FPC4-357-440, respectively (Fig.3.44). We found FPC4-1-260$_{6His}$ in the pellet fraction together with the MTs (Fig.3.44 upper panel) and $_{6His}$FPC4-357-440 mostly in the supernatant fraction (Fig.3.44 lower panel). At high concentrations of the purified proteins, the system can be saturated, and therefore the proteins might be found in both fractions. Very little amount of $_{6His}$FPC4-357-440 was found in the pellet fraction even at high concentration due to little precipitation of the protein (data not shown).
We confirmed thus that the N-terminal part of FPC4 is involved in the interaction with MT. Preliminary experiments estimated the dissociation constant (K_d) – which represents the protein concentration at which 50% of the available MT binding sites are occupied – to be 120 nM for FPC4-1-260$_{6His}$, and this value is comparable with other MAPs (Roger et al., 2004).

iii) FPC4 binds to the MtQ in trypanosome

Knowing that FPC4 is able to interact with MT and that, by IF, FPC4 localizes to a specific region of the cell and not on the entire MT corset, we started thinking that FPC4 binds to a specific sub-set of MTs. Close to the FPC, there are the neck MT and the MtQ (Lacomble et al., 2009).
We observed, by IF analysis on isolated flagella that the myc signal of myc-FPC4-FL and myc-FPC4-ΔB1BD expressing cells localized on a tubulin-positive structure emerging from the base of the flagellum (see Fig.3.45). Similar samples were analysed by iEM demonstrating that the myc signal was present on the FPC (Fig. 3.46 a) and was elongating towards the anterior end of the flagellum. On this elongated part the myc signal was co-localizing with a tubulin positive structure (Fig 3.46 b). This structure originated from the BB and pBB region (Fig.3.46 A) and resembled the MtQ.
We therefore concluded that FPC4 is a new MAP, able to bind to the MtQ anterior to the FPC. Currently, only SpefI (Gheiratmand et al., 2013) has been identified as MAP uniquely

located on the MtQ. However, this protein binds exclusively to the first part of the MtQ, from the BB to the FPC.

In many immuno-EM pictures, we could observe some labelling of FPC4-FL (or FPC4-ΔB1BD) on the MtQ between the BB and the FPC. We, however, never saw this signal by IF on PCF. This, most probably, is due to the detection level of the protein or due to differences in the protocol for the preparation of the samples. A slight, but clear, FPC4 signal towards the BB has been seen, however, on BSF by IF (Fig.3.24 E, F). More work needs to be done on BSF in order to define whether FPC4 is located only from the FPC toward the flagellum tip or if it also partially co-localizes with SpefI.

c) Conclusion: FPC4 a new MAP linking the FPC, the Hook complex and the MtQ

We were able to demonstrate that FPC4 is a new MAP of *T. brucei*. Its localization at the FPC, at the hook complex and also on the MtQ renders FPC4 a multi-partner protein.
In U-2 OS cells FPC4 was located together with acetylated tubulin, a marker for stable MTs. This suggests that FPC4 plays a role in the stabilization of MTs. Moreover, the fact that, by over-expressing FPC4, we see an impairment in the proper BB/kDNA segregation, can be explained by the fact that the MtQ originates from the BB, and an excess of FPC4 on this structure might stabilize the MtQ and block or slow down the proper segregation of the BBs. An alternative explanation can be that the new MtQ originates close to the old MtQ and a connection between the two MtQs, mediated by the excess of FPC4, might limit their separation and consequently the BB/kDNA segregation.

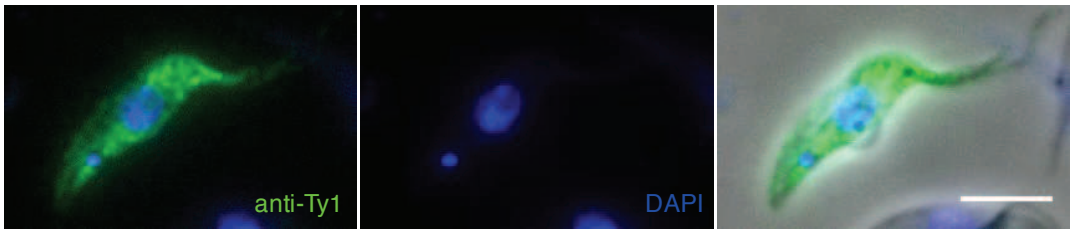

Fig. 3.47 *BioID attempt for N-terminal Ty1-BirA*-FPC4*
Cells overexpressing Ty1-BirA*-FPC4 (induced 24 h with 10 µg/mL tetracycline) were probed with anti-Ty1. The construct Ty1-BirA*-FPC4 was not targeted to the FPC/Hook complex position, but was soluble (WC). This cell line was therefore not suitable for the BioID experiment (scale bar 5 µm).

III. FPC4, one of the missing links?

Introduction:

After the localization of the novel MT-associated protein FPC4 at the FPC and at the Hook complex, and the confirmation of its interaction with BILBO1, we wanted to insert these discoveries into a more general context.
The fact that the FPC and the hook complex are two very close but distinct structures and the fact that FPC4 localizes above BILBO1, might suggest that FPC4 could be the linker between these two structures.

Objectives:

A series of experiments have been performed in order to obtain a more general picture of the FPC/Hook complex area, to identify additional proteins located in this area and to figure out their interactions. The results presented here are preliminary.

Results:

a) BioID: a screen to identify additional FPC4 interaction partners

After BILBO1, FPC4 is now the second protein identified to belong to the FPC. Moreover, FPC4 is also part of the Hook complex. This suggests that FPC4 is a multi-partner protein.
Recently, the BioID technique was used to identify proximity partners of the MORN1 protein in the Hook complex structure (Roux et al., 2012; Morriswood et al., 2013). However, FPC4 was not identified among the Hook complex protein candidates.
In order to identify FPC4 partners, we decided to try the same experiment using FPC4.
Because the C-terminal myc-tag of FPC4 was cleaved when overexpressed, a PCF cell line over-expressing the N-terminally tagged fusion protein Ty1-BirA*-FPC4 was generated. Unfortunately, this fusion protein was not targeted to the FPC and remained in the cytoplasm as shown by IF (Fig.3.47). We consequently did not pursue this experiment.

b) The FPC4 - MORN1 interaction

Given that MORN1 and FPC4 are located in the same structure, or in close proximity, we decided to test their interaction by Y2H and in the heterologous system (U-2 OS).

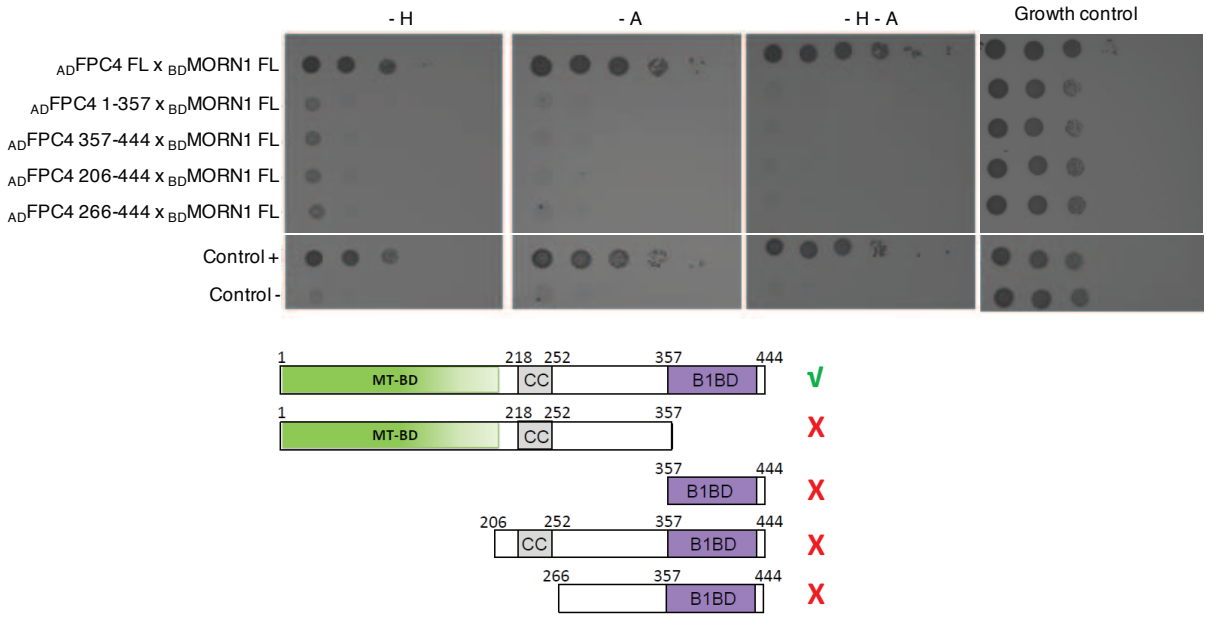

Fig. 3.48 *Y2H interaction test between FPC4 and MORN1*
The interactions between MORN1 and FPC4 were tested on three different media: - Histidine (1st panel), - Adenine (2nd panel) and –Histidine and – Adenine (3rd panel). A growth control was also performed (4th panel).
In the lower panel, a summarizing scheme of the truncations of FPC4 tested by Y2H with MORN1. Only the two full-length proteins were able to interact (√). We were not able to define the specific domain involved in the interaction (X).

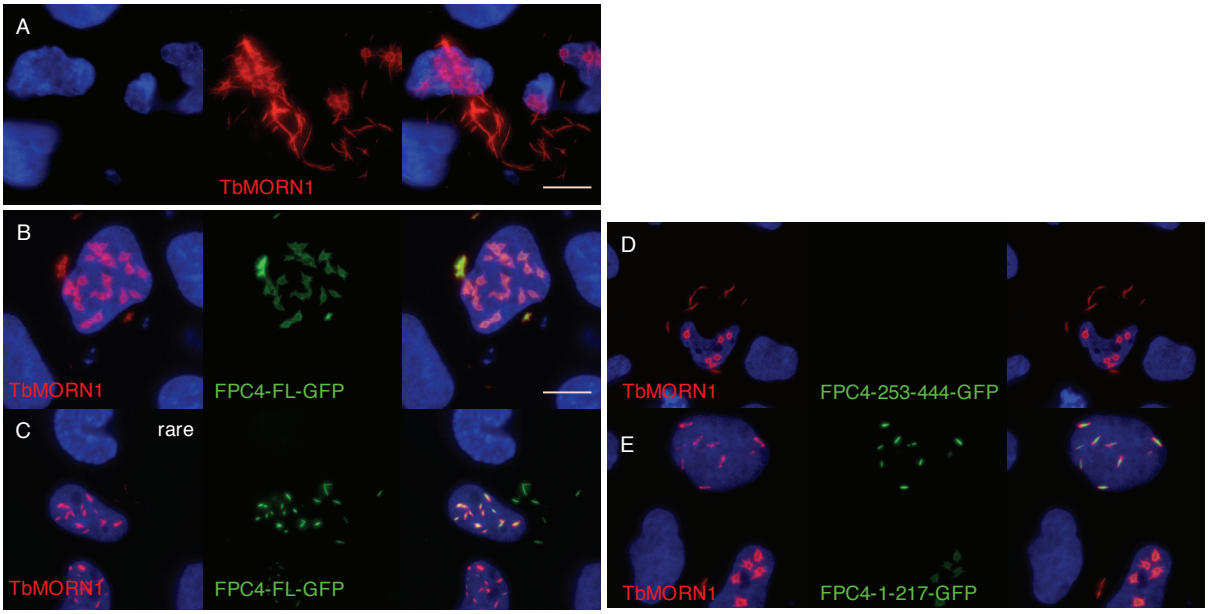

Fig. 3.49 *MORN1 and FPC4-GFP co-localize in the heterologous system U-2 OS cells*
MORN1 expressed in U-2 OS cells (A) assumes a smarties-like shape with spikes or forms a filament. When MORN1 is co-expressed with FPC4-FL-GFP (B, C) FPC4-FL-GFP localizes on the MORN1-structures. The interaction between the two proteins is abolished when the first 252 amino acids of FPC4 are absent (D). FPC4-1-217 is sufficient to promote the FPC4-MORN1 interaction (E).

MORN1 was cloned into the Y2H prey and bait vectors and its interaction with the FPC4 was tested (experiment performed by Johanna Cormenier, a bachelor student).
The full-length FPC4 and MORN1 proteins indeed interacted as shown in Fig.3.48. Deletion of the FPC4 B1BD abolished this interaction but this domain alone was not sufficient to promote the interaction.
Unfortunately, we were not able to determine which domain of FPC4 interacts with MORN1 because every other interaction tested was negative. This suggests that the folding of the full length FPC4 might be affected when the B1BD is deleted, consequently affecting the interaction with MORN1. For this reason, we used the U-2 OS heterologous system to confirm the FPC4 – MORN1 interaction and identify the domains involved.

In U-2 OS cells, when MORN1 was expressed alone it assumed a “smarties”-like shape with spikes in the cytoplasm and also within the nucleus (Fig.3.49 A). This is the first evidence that MORN1 is able to form atypical structures. This aspect of the work will be analysed further in collaboration with Brooke Morriswood (Wurzburg university)
When MORN1 was co-expressed together with FPC4-FL, the two proteins co-localized on these “smarties with spikes” shape and, rarely, on tiny sticks (Fig.3.49 B C).
Different truncations of FPC4 have been tested with MORN1-FL. Interestingly, the truncations FPC4-253-444, which lacked the aa 2-252 (Fig.3.49 D), was not able to interact with MORN1. However, the FPC4-1-217 protein also co-localized with MORN1 (Fig.3.49 E, G).

These results confirm the interaction between MORN1 and FPC4, mediated by the N-terminal domain of FPC4 (aa 1-217). More work needs to be done to identify the MORN1 interaction domain, and characterise further this complex.

FPC4 is therefore a multi-partner protein, which is able to interact with MORN1, BILBO1 and the MtQ. It can now be described as one of the missing links connecting the three structures: the FPC, the Hook complex and the MtQ.

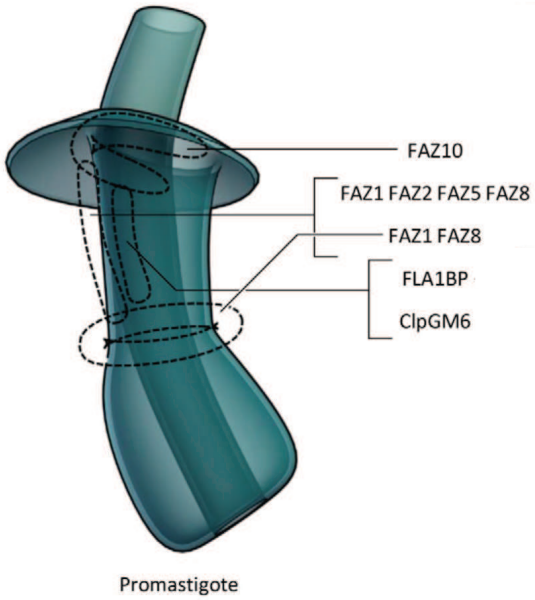

Fig. 3.50 *Three-dimensional model of the FP and FAZ proteins in promastigote L. mexicana from (Wheeler et al., 2016).*
The FP is enclosed at its proximal end via a ring-shaped structure formed by FAZ1 and FAZ8. FLA1BP and ClpGM6 are located at the FP neck (between the ring formed by FAZ1 and the flagellum exit site), together with FAZ1, FAZ2, FAZ5 and FAZ8. FAZ10 is located at the flagellum exit site and assumes a horseshoe-shaped structure.

Tab. 3.1 *Episomal gene expression cell lines in Leishmania major*
This table summarizes the different *L. major* cell lines generated for the study.

cell line	protein + tag	resistance	protein + tag	resistance
M756	*Lm* BILBO1-GFP	Hygro		
M818	*Lm* MORN-GFP	Hygro		
M819	myc-*Lm* FPC4	Hygro		
M822	*Lm* BILBO1-mRED	Blast	*Lm* MORN1-GFP	Hygro

IV. FPC4, the FPC and the Hook complex in *Leishmania*; preliminary study.

a) Introduction

Leishmania promastigote parasites, differently from *T. brucei* trypomastigote, possess a 9+2 flagellum which protrudes from the FP in the anterior part of the cell body. Amastigote parasites, instead, possess a short 9+0 flagellum, which does not exit the cell body. Since the FP is an essential structure in *T. brucei*, the FP in *Leishmania* is likely to be important as well.

In a recent study on the FAZ organization in *Leishmania*, Wheeler and colleagues have localized 7 FAZ orthologues, myc-*Lm*BILBO1 and eYFP-*Lm*LRRP1 in *L. mexicana* (Wheeler et al., 2016). All the proteins localized to structures in the FP region and the architecture of the FP in promastigote parasites is shown in Fig. 3.50.

In *L. major* the FPC/Hook complex region has never been studied, although the orthologue genes (such as FPC4 and MORN1) are present in the genome.

Objectives:

In a collaborative project within the ParaFrap network with the Bastien Laboratory (UMR5290, Laboratory of Parasitology and Mycology) in Montpellier, we decided to localize, and if possible co-localize, *Lm*BILBO1, *Lm*MORN1 and *Lm*FPC4 in order to understand the FPC and Hook complex organization in promastigote *Leishmania major* and potentially find a common therapeutic target for both parasites, *T. brucei* and *L. major*.

b) Results

b1) Orthologues identification

Bioinformatic (BLASTp) searches in the *Lm* Friedlin genome allowed us to identify *Lm* orthologues of BILBO1, MORN1 and FPC4. *Lm*BILBO1 (LmjF.09.0100 – 582 aa) and *Lm*MORN1 (LmjF.30.3310 – 358 aa) were found by BLASTp and were 58% and 76% identical at the protein level respectively. Compared to the *T. brucei* BILBO1, *Lm*BILBO1 is 5 aa shorter, whereas *Lm*MORN1 is a 358 aa protein in both species. The identity between *Lm*FPC4 (LmjF.24.1860 – 535 aa), and *Tb*FPC4 is of 37%, but only over a 75 aa region in the middle of the protein, corresponding to the CC domain (protein alignments in the Annex 5.1, 5.2, 5.3). The aa sequence of *Lm*FPC4 (535 aa) is longer than the *Tb* orthologue (444 aa). Except for the CC, no predicted domain could be identified for *Lm*FPC4.

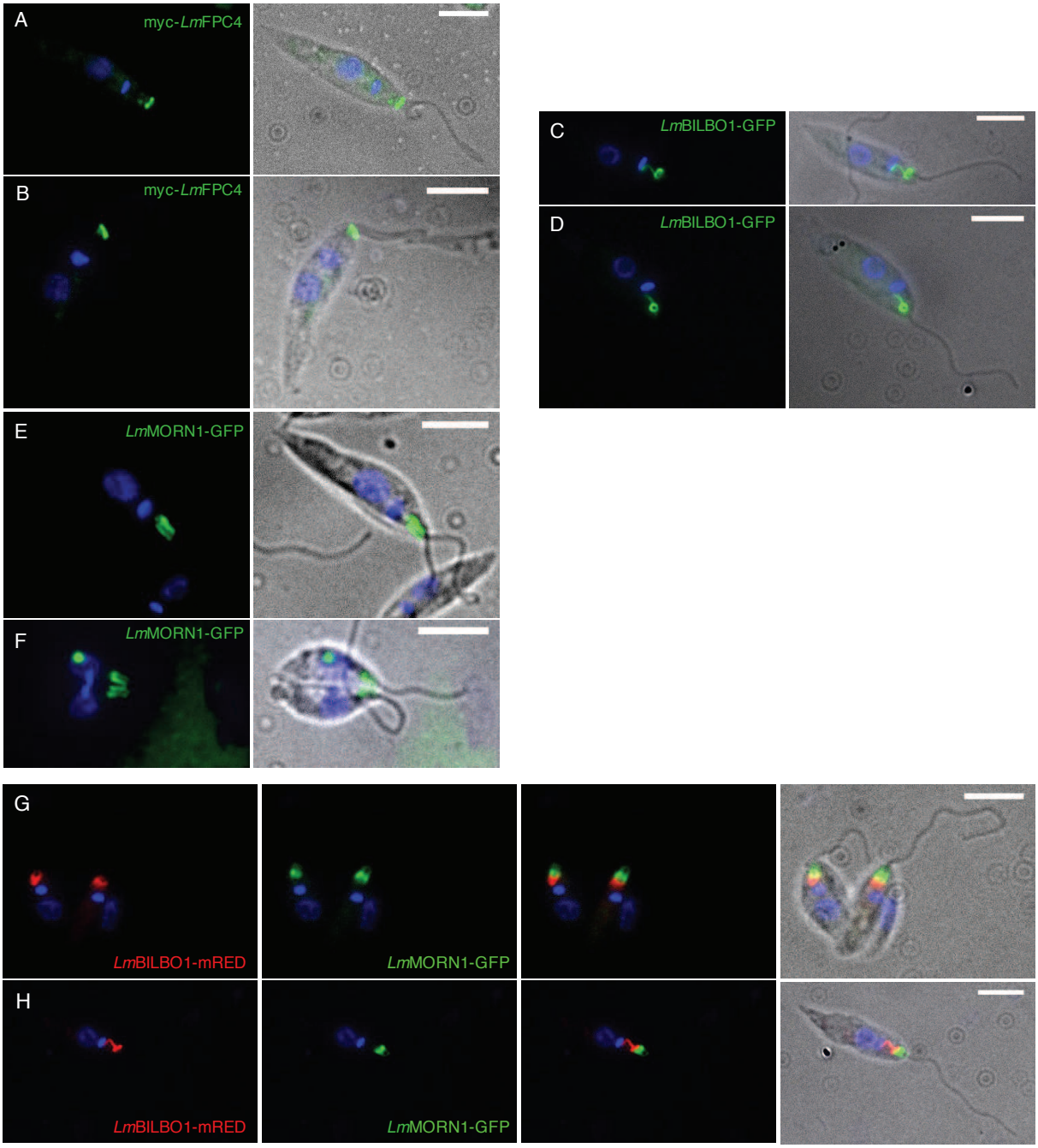

Fig. 3.51 *Immunofluorescence of L. major cell lines expressing tagged versions of* *Lm*BILBO1-mRed, *Lm*MORN1-GFP and myc-*Lm*FPC4.
(A, B) show the localization of myc-*Lm*FPC4, (C, D) *Lm*BILBO1-GFP and (E, F) *Lm*MORN1-GFP. Cell line, co-expressing *Lm*BILBO1-mRED and *Lm*MORN1-GFP are shown in (G, H). (scale bar 5 µm).

b2) Cellular localization

An advantage of *L. major* parasites compared with *T. brucei* is that they can maintain an exogenous DNA sequence as an episomal plasmid and can replicate and transmit them to the daughter cells. We therefore used this easy technique to produce cell lines carrying episomal plasmids, allowing the constitutive expression of tagged versions of *Lm*BILBO1, *Lm*MORN1 and *Lm*FPC4, as tag-fusion proteins (see table 3.1).

Immunofluorescence on detergent extracted cells showed that the three proteins localized in the same area of the parasite, between the kDNA and the flagellum exit site (Fig. 3.51).

Myc-*Lm*FPC4, localized in very close proximity to the flagellum exit site (Fig. 3.51 A, B). The shape of the labelling looked like a “plate” / “disc”, close to the anterior end of the cell, resembling FAZ10 localization in Fig. 3.44.

*Lm*BILBO1-mRED or GFP assumed a horse-shoe/ring-shaped structure. Interestingly, we observed that the horse-shoe/ring structure was extending towards the kDNA (Fig. 3.51 C, D). This extension was also visible in the case of myc-BILBO1 in the work of Wheeler and co-workers (Wheeler et al., 2016). We have recently observed a similar signal on *T. brucei* labelled with a novel anti-BILBO1 antibody (Robinson lab), suggesting that this is a conserved feature. We will pursue the analysis of this novel BILBO1 localization as it might shed some light on the processes involved in the segregation of the FPC.

*Lm*MORN1-GFP looked like a tubular or bi-lobed structure between the kDNA and the flagellum exit site (Fig. 3.51 E, F), similar to eYFP-LRRP1 signal in *L. mexicana*. The cell line co-expressing *Lm*BILBO1 and *Lm*MORN1 gave us a clearer idea of the relative position of both proteins. *Lm*BILBO1 labelling localized between the kinetoplast and the *Lm*MORN1 labelling (Fig. 3.51 G, H). Unfortunately, we did not succed yet in generating cell-lines co-expressing myc-*Lm*FPC4 and *Lm*BILBO1 or *Lm*MORN1, and co-expressing the three proteins.

It is interesting to see that in *L. mexicana* there is a ring-shaped structure enclosing the FP, distal to the flagellum exit site where FAZ1 and FAZ8 localize, similar to what we observed for *Lm*BILBO1 in *L. major*. We observed a similar bi-lobed structure with our *Lm*MORN1 labelling that is similar to the localisation of FLA1BP, ClpGM6, FAZ1, FAZ2, FAZ5 and FAZ8 in the FP neck of *L. mexicana*. This can suggest that MORN1 localizes at the neck of *L. major*. Proximal to the flagellum exit site, Wheeler and colleagues (Wheeler et al., 2016) observed an open ring (FAZ10) where we localized *Lm*FPC4.

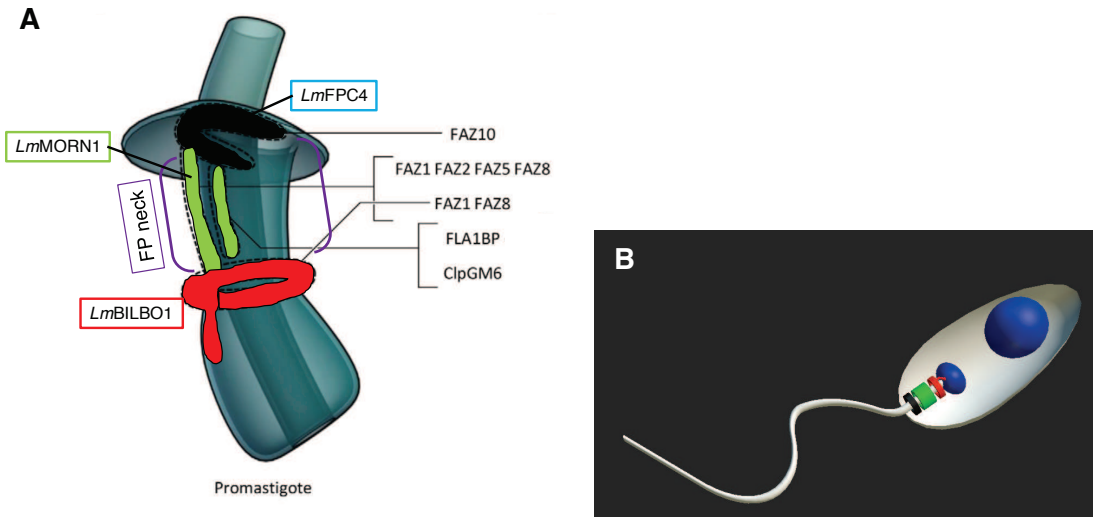

Fig. 3.52 *The probable localization of LmFPC4 and LmMORN1 in a modified three-dimensional model of the FP and FAZ proteins in promastigote L. mexicana* (modified from (Wheeler et al., 2016).
(A)*Lm*FPC4 (black) might localize at the flagellum exit site together with FAZ10, whereas *Lm*MORN1 (green) can be located at the FP neck together with FLA1BP and ClpGM6 and/or with FAZ1, FAZ2, FAZ5 and FAZ8. *Lm*BILBO1 (red) is located together with FAZ1 and FAZ8 and possesses an elongated tail toward the kDNA. (B) The 3D model in *L. major*, with *Lm*FPC4 (black), *Lm*MORN1 (green) and *Lm*BILBO1 (red).

Using these data, we could, on the previous scheme, superimpose *Lm*FPC4 and *Lm*MORN1 as the first evidence of a Hook structure in *Leishmania* (Fig.3.52).

These preliminary data suggest that the organization of the FP-neck region of promastigote *L. major* and promastigote *L. mexicana* seem to be conserved. However, the arrangement of the different proteins in this region, compared to *T. brucei,* might differ. Furthermore, the situation in amastigote *L. major* parasite has not been investigated.

Perspective:

The next step into this study is to label the flagellum to see whether *Lm*MORN1 is located around it, as a tubular structure, or if it is close to it, as ClpGM6.

Moreover, we will have to localize other Hook-complex orthologous proteins, such as Centrin-2 and Centrin-4. Furthermore, the localization of *Lm*SpefI, protein that in *T. brucei* is located on the MtQ between the BB and the FPC, might shed some light on the MtQ organization in *L. major.* In fact, the *Lm*SpefI localization might help the understanding of the functioning of the FP/FP-neck region in these parasites.

4. DISCUSSION AND PERSPECTIVES

4. Discussion and Perspectives

I. BILBO1, an essential scaffold protein

T. brucei parasites are the causative agents of the human African trypanosomiasis and Nagana disease in cattle. These parasites are one of the major factors, which have an impact on the economy and the life standards in sub-Saharan Africa.
The fact that a vaccine is not available, due to antigenic variation, and the fact that the current treatments are highly toxic, renders the research in this field of major interest in order to find potential therapeutic targets to combat this neglected disease.

The laboratory focuses its interest on the biogenesis of the Flagellar Pocket, and the Flagellar Pocket Collar, a cytoskeletal structure.
The cytoskeleton is indeed important for the parasite morphology, since the cell body shape is constituted and maintained by a sub-pellicular MT array. Moreover, the cell shape is modified during the life cycle to adapt to the vector and to the mammalian host. Furthermore, the cytoskeleton plays an important role in organelles positioning and in the flagellum biogenesis, an essential organelle with motility and pathogenicity role. Cytoskeletal elements are therefore promising drug targets.

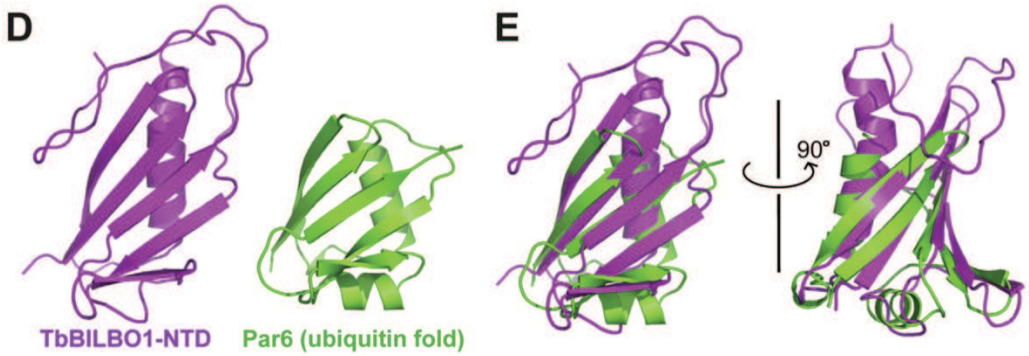

Fig. 4.1 *NMR structure of BILBO1-NTD reveals an ubiquitin-like fold*
Comparison (D) and superimposition (E) of BILBO1-NTD (violet) and the PB1 domain of Par6 (green) (Vidilaseris et al., 2014a).

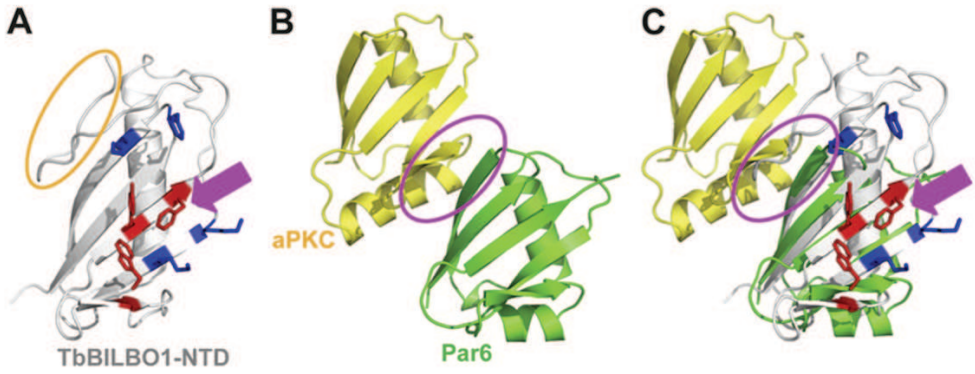

Fig. 4.2 *Comparison of BILBO1-NTD with the PB1 domain of Par6 in the Par-complex.*
Red and blue residues show the conserved surface patch of the NTD (A). The interaction surface between aPKC and Par6 in the Par complex is shown in (B) and the superimposition with BILBO1NTD (C) shows the C-terminal loop of the NTD (encircled) that blocks the aPKC binding site of Par6 (Vidilaseris et al., 2014a).

a) BILBO1 is a cytoskeletal ring scaffold protein in *T. brucei*

The results obtained in this study allowed us to define the self-assembly properties of BILBO1. In fact, this protein is able to interact with itself *via* its CC-domain, and can autonomously form polymers, including helical-shaped ones. The shape of these polymers can be influenced by the EF-Hands domains, depending on their association with calcium, which has been proved in this study and by Vidilaseris and colleagues (Vidilaseris et al., 2014b).
The intrinsic polymer forming properties of BILBO1 might therefore be important for the building of a FPC.
It is unlikely that BILBO1 acts on its own to create and make the FPC function, so it must interact with other proteins and might serve as template for the FPC structure. For this reason, in this study, we were able to demonstrate the interaction of BILBO1 with a kinetoplastid-specific protein, FPC5.

With these results, we suggest that BILBO1 is indeed a structural scaffold protein with self-assembly properties, which is probably one of the main components of the FPC and is essential for the FPC and FP biogenesis.

b) The 3D structure of the BILBO1 N-terminal domain: a hint for its function?

The three-dimensional structure of the N-terminal domain (NTD) of BILBO1 has been solved recently (Vidilaseris et al., 2014a) (Fig.4.1) and shows similarities with the PB1 domain of Par6. The PB1 (Phox and Bem1) domain is a protein-binding domain involved in heteromerization or oligomerization and has a ubiquitin-like fold (Terasawa, 2001).
Par6 is part of a larger complex of polarity proteins constituted primarily by Par3, Par6 and aPKC (atypical Protein Kinase C), which regulates, for example, cell polarization or tight junction's formation in epithelial cells (Gopalakrishnan et al., 2007; Chen et al., 2013).

The structure of Par6-PB1 domain in the Par-complex has been solved and has been compared with that of BILBO1-NTD (Fig.4.2). Interestingly, substituting Par6-PB1 domain with BILBO1-NTD in the model with aPKC, revealed that the aPKC-interacting interface is blocked by the long loop of the C-terminal domain of the NTD. This long loop can therefore be a domain used in protein-protein interaction, maybe involving other FPC components.

The similarities with Par6 and BILBO1, and between FPC4 and Par3 are multiple. Both Par3 and Par6 are multi-modular scaffold proteins, able to interact with each other, as well as with other proteins. They are located at junctional complexes, where two different membranes come closer and interact. Moreover, the ubiquitin-like fold of BILBO1 and of Par6 is in both cases located at the N-terminal part of the proteins (Chen et al., 2013).
Par3 is composed of a multimerisation domain including a MT-binding domain, both located at the N-terminus of the protein, and a C-terminal domain involved in aPKC binding (Chen et al., 2013). FPC4, as well, possesses a MT binding domain in its N-terminus and the BILBO1 binding domain at its C-terminus.

The third component of the Par complex is aPKC, a kinase, which phosphorylates Par3 and induces its release from the Par6-aPKC complex (Chen et al., 2013).
T. cruzi FPC4 orthologue possesses multiple putative phosphorylation sites, and two of the residues are conserved in the *Tb*FPC4 protein (Marchini et al., 2011): a serine residue (S83) in the N-terminus and a threonine residues (T334). Additionally, a recent phosphoproteome of *T. brucei* identified 6 putative phosphorylation sites in FPC4, with two of them, S394 and S396 located within the B1BD (Urbaniak et al., 2013). Their phosphorylation status might be involved in regulatory processes. It would therefore be of major interest to mutate these residues and test the constructs in U-2 OS cells for MT binding and BILBO1 interaction.
We can hypothesize that the FPC, the complex containing BILBO1 and its partners, shows similarities with the Par3/Par6/aPKC complex and might play a role in polarity, for example by determining or influencing cytokinesis-related tasks, or organelle positioning.

A second hypothesis about BILBO1 and, more in general, the FPC function could be related to its morphological similarities to septin rings. In fact, septin rings in yeast act as diffusion barriers or are involved in cytokinesis (Hu and Nelson, 2011). Septin-rings in yeasts and the annulus in sperm cells represent a junction between two or more membranes.
Could thus the FPC be a sort of diffusion barrier between the flagellar, the plasma and the FP membrane? This question was already raised in 2008 (Bonhivers et al., 2008b), but no clear answer has been found yet.

II. BILBO1 and FPC4 interaction

We demonstrated that BILBO1 and FPC4 are authentic interacting partners, involving their N-terminal and C-terminal domain respectively. Thanks to the collaboration with Dr..G. Dong

and its PhD student Keni Vidilaseris, an in vitro analysis using gel filtration chromatography showed that this interaction occurs in a 1:1 ratio (unpublished data).
The BILBO1 NTD is required neither for targeting to the FPC nor for the polymerisation (Vidilaseris et al., 2014b; Florimond et al., 2015) but has, more likely through its conserved surface patch, a role in protein interaction. The conserved surface patch appears as a crater-like structure, and seven residues in this patch are important for the correct function of BILBO1. Mutations in this surface patch (mut1 or mut2) led to morphological phenotypes, similar to those of BILBO1 RNAi, and ultimately to cell death (Vidilaseris et al., 2014a).
We have tested two additional sets of mutations, mut2b (Y87A and F89) and mut3 (K60A and K62A). Mut2b completely abolishes the interaction with FPC4 *in vivo* in the heterologous system U-2 OS cells and its over-expression in *T. brucei* leads rapidly to cell death. The overexpression of mut3 shows a milder phenotype in *T. brucei* and the interaction with FPC4 is not completely abolished in U-2 OS cells.
In light of these data, it is clear that FPC4 and BILBO1 are real interacting partners. However, my hypothesis is that the FPC4-BILBO1 interaction is mediated by the proximity of the two proteins, but the retention of FPC4 at the collar is mediated by the interaction with other proteins or structures close to the FPC, such as the MtQ or the hook-complex. This hypothesis is supported by the fact that the FPC4 does not need the B1BD to be targeted to the FPC and, moreover, the B1BD alone results in a cytosolic localization.
The hypothesis could be tested in *T. brucei* with RNAi cell lines depleting MORN1 or SpefI to see whether the absence of one of the main components of the hook-complex or the absence of the new MtQ, respectively, leads to the misplacing of FPC4.
Could thus FPC4 be principally a Hook-complex protein, which additionally interacts with the FPC?

a) Which role does FPC4 play?

We progressed in the characterization of FPC4 as BILBO1 partner and as a member of the hook-complex.

a1) GPF-FPC4 and myc-FPC4-ΔB1BD induced phenotypes: Real or artefactual?

We know that GFP tag is a large molecule and, due to its dimerization ability, might induce undesirable phenotypes, which are not forcedly related to the expressed fusion protein. Indeed, the GFP used to create the construct possesses a single mutation S65T (Leica webpage) to enhance the brightness of the signal, but does not carry the

three mutations (A206K, L221K, F223R) that reduce the ability of GFP to form dimers. Therefore, at high concentration GFP can form dimers (Zacharias et al., 2002; LaCount et al., 2002). The phenotypes observed with the over-expression of GFP-FPC4 might be due to the excess of FPC4 in the cell, but we cannot exclude that the GFP itself influenced the formation of the long fibres. However, the dominant negative phenotypes can still be analysed.

The over-expression of GFP-FPC4 leads to the production of cells with a detached flagellum, multinucleated cells and zoids formation and, ultimately, to rapid cell death. Interestingly, cytokinesis defects are often associated with the absence of the FAZ, which therefore induces a detachment of the flagellum. In the literature it is documented that the lack of the FAZ proteins can impair the correct cleavage furrow ingression and consequently results in an incorrect cytokinesis (zoids for example) or in the cytokinesis block (multinucleated cells) (LaCount et al., 2002; Sunter et al., 2015). The over-expression of GFP-FPC4 could thus impacts the FAZ.

The over-expression of myc-FPC4-ΔB1BD leads, as well, to morphological phenotypes. In this case, we strongly doubt that the myc tag provokes these phenotypes, since it is smaller than GFP.

An interesting phenotype observed in this cell line, additionally to multinucleated cells and zoids, are the epimastigote-like cells (> 10%). In these cells the nucleus is positioned posterior to the kDNA. Moreover, we observed cells with the two kinetoplasts in between the two nuclei (> 10%). It might seem surprising that the growth rate was not so strongly affected by these phenotypes, but, this has already been observed with the RNAi of ClpGM6 (a calpain-like protein) that induced epimastigote-like cells without affecting proliferation (Hayes et al., 2014).

The fact that the myc-FPC4-FL does not lead to any morphological or growth defect, whereas the myc-FPC4-ΔB1BD does, can have two explanations. First, modification of the expression level of a protein (reduction or increase) might induce some phenotypes. The myc-FPC4-FL construct is less expressed than the myc-FPC4-ΔB1BD construct, suggesting that the level of expression is responsible for the phenotype. Myc-FPC4-ΔB1BD is more overexpressed than GFP-FPC4 but showed a less potent phenotype suggesting that deletion of the B1BD does affect the function of the protein. Second, deletion of the B1BD leaves the FPC4 with its MT binding domain and without any interaction with BILBO1. Overexpression of the MT binding domain might therefore disturb the equilibrium of the binding between the FPC, the Hook complex and the MtQ affecting the segregation of the FPC, and in consequence the segregation of the kDNAs.

a2) FPC4: a FAZ-interacting protein?

In the literature it was reported that transition to epimastigote-like cells can be the results of the knock down of FAZ proteins proliferation (Hayes et al., 2014; Sunter et al., 2015). I personally do not think that FPC4 belongs to the FAZ complex *per se*. However, the origin of the FAZ structure is close to the FPC, then it runs along the MtQ. Therefore, FPC4 might also interact with some FAZ proteins due to their vicinity. In a recent publication, FPC4 has been identified by BioID as a *Tb*SAS-4 neighbour partner (Hu et al., 2015). *Tb*SAS-4 is concentrated at the distal tip of the FAZ filament and is involved in regulating the length of the FAZ. FPC4 and *Tb*SAS-4 more likely come in close proximity when the FAZ starts its elongation. Interestingly, when overexpressed, FPC4 is occasionally observed as a dot at the end of the cell body together with MORN1.

a3) FPC4: a new MT-associated protein of *T. brucei*

Our data demonstrate that FPC4 is a new MAP of *T. brucei* that binds to the MtQ.
IF analysis in PCF showed that FPC4 is located on the MtQ, anterior to the FPC, and iEM labelling suggests that FPC4 is also present on the MtQ posterior to the FPC. The situation for FPC4 is slightly different in BSF; in fact, the FPC4 signal by IF shows a little tail toward the BB, which could be in the same region where SpefI is located. This discrepancy between IF and iEM labelling might be due to a low FPC4 protein level posterior to the FPC that is not labelled by IF. SpefI also binds to the MtQ, between the BBs and the FPC. Interestingly, in Xenopus embryos, SpefI (also named CLAMP) interacts with aPKC and is stabilizing MT (Werner et al., 2014). Further work on the role of FPC4 might help understanding how the FPC is segregated, if it is mediated by the “MtQ separation”.

Preliminary results in BSF show, as in PCF, that BILBO1 and FPC4 are located together at the FPC, and additionally that FPC4 assumes an elongated shape. Differently to PCF, the elongation of FPC4 is visible on both sides of the FPC, toward the BB and the flagellar tip. This is for sure a part of the project, which should be analysed in more details since the kDNA positioning differs between WT PCF and BSF parasites. The fact that WT BSF 2K2N show a KKNN distribution rather than KNKN, as in WT PCF, might be the results of a slightly different kDNA segregation, or the results of a different cytoskeletal organization.

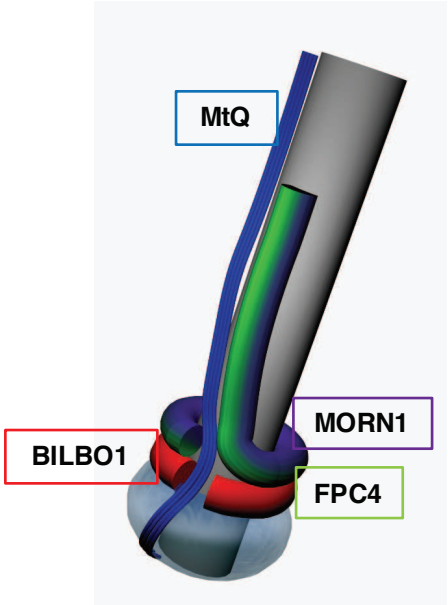

Fig. 4.3 *Three-dimensional model of the FPC area in T. brucei*
A 3D-model of the FP-FPC area. BILBO1 (red) is an open-ring crossed by the MtQ (blue) located proximal to the FP. FPC4 (green), in the hook complex, sits on top of BILBO1 and elongates in between the MtQ and MORN1 (violet).

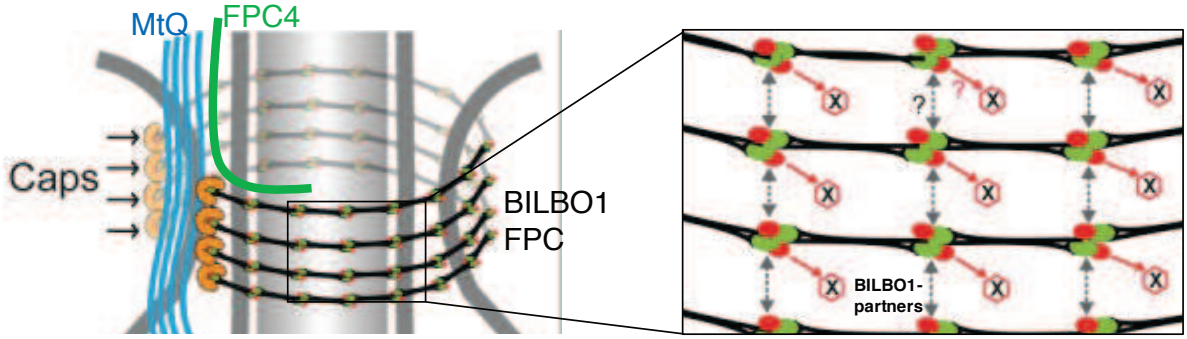

Fig. 4.4 *Model of BILBO1 organization within the collar* (Vidilaseris et al., 2014b)
(right panel) BILBO1 is able to polymerize and laterally assembly with other BILBO1 polymers.
(left panel) The NTD (red) and the EF-hands domains can be represented as “exposed” domains since they do not play a role in BILBO1 polymerization (modified from (Vidilaseris et al., 2014b). BILBO1 partners can therefore bind to these exposed domain (X).

Altogether these results allow me to state that FPC4 is a multi-partner protein, which acts as a linker between different cytoskeletal structures. It is the first identified link between the FPC, the hook-complex and the MtQ and might play a role in FPC segregation and cytokinesis.

We generated a simple 3D model for the physical organization of the FPC area (Fig.4.3). FPC4 is located at the hook-complex together with MORN1 (most probably by a direct interaction), on the MtQ, and is connected to the FPC *via* BILBO1.

A theoretical model about the organization of BILBO1 within the collar is shown in Fig.4.3 (modified from (Vidilaseris et al., 2014b). BILBO1 molecules are able to polymerize and to laterally interact. In the proposed model BILBO1 forms an open ring allowing the MtQ to pass by the structure. In the zoom (Fig.4.4 right panel) the NTD (red) and the EF-Hand domains (green) are represented exposed/"free", since they are not involved in the oligomerization of BILBO1. The fact that these two domains are not necessary for BILBO1 self-assembly, make us hypothesize that they might be involved in the binding of other BILBO1 partners.

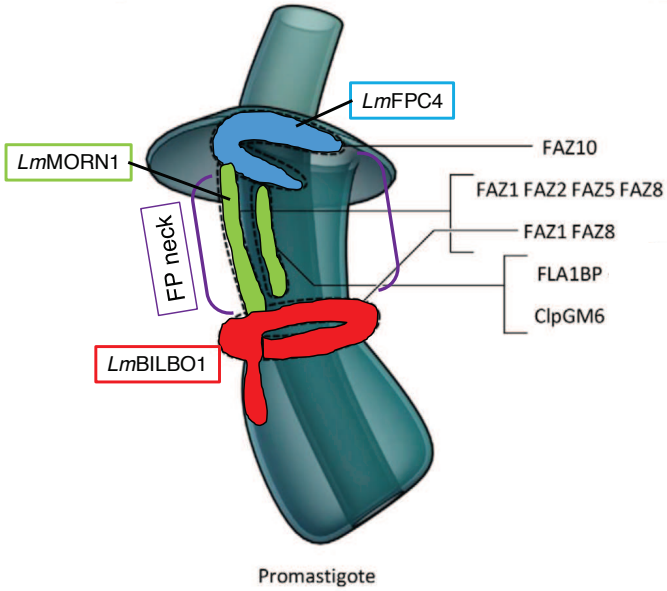

Fig. 4.5 *Three-dimensional model of FP and FAZ proteins in L. mexicana*
The promastigote organization of FAZ proteins in *L. mexicana* (Wheeler et al., 2016). The FP is enclosed, proximal to the FP, via a ring-shaped structure formed by FAZ1 and FAZ8. FLA1BP and ClpGM6 are located at the FP neck, together with FAZ1, FAZ2, FAZ5 and FAZ8. FAZ10 is located at the flagellum exit site and assumes a horseshoe-shaped structure.
*Lm*BILBO1 (red), *Lm*MORN1 (green) and *Lm*FPC4 (blue) are superimposed on the *Lmx* model based on our data in *L. major*.

III. A first view of the FPC/hook-complex region in *L. major*

Recently in *L. mexicana* (*Lmx*) the FP and the FAZ have been studied in more details and *Lmx*BILBO1 was identified and localized (Wheeler et al., 2016). Based on their model and on our data generated (by the localization of BILBO1, MORN1 and FPC4 in *L. major*) we have positioned *Lm*BILBO1, *Lm*MORN1, and *Lm*FPC4 relative to the architecture of the FP in promastigote parasites (Fig. 4.5). BILBO1 position in promastigote *L. mexicana* is comparable to what we observed in promastigote *L. major*. It is interesting to see that Wheeler and colleagues observed a ring-shaped structure distal to the flagellum exit site (resembling FAZ1 and FAZ8 localization), similar to what we observed for *Lm*BILBO1 in *L. major*. They then noticed a bi-lobed structure (with FLA1BP, ClpGM6, FAZ1, FAZ2, FAZ5 and FAZ8) on the FP neck, where we localized *Lm*MORN1. Proximal to the flagellum exit site they observed an open ring (FAZ10) where we localized *Lm*FPC4.

The striking difference with *T. brucei* was the FPC4 localization. Considering the respective localization of *Lm*BILBO1 and *Lm*FPC4 is it difficult to imagine an interaction, whilst *Lm*FPC4 and *Lm*MORN1 could interact. Yet, major rearrangement occurs in amastigote (Wheeler et al., 2016) suggesting that in this life cycle stage *Lm*BILBO1 and *Lm*FPC4 could be in closer proximity.

This field remains mostly undiscovered and requires some additional work in order to shed some light in evolutionary processes within the trypanosomatid family.

IV. Perspectives

Although intense researches in the FP-FPC area are in progress, the precise role of BILBO1 remains elusive. It is clearly involved in FP and FPC biogenesis, but still a lot of details and connections need to be discovered. Here I suggest some experiments that can help to shed some light on it.

First of all, to solve the mystery about of the collar formation (semi-conservative vs *de novo*), cells in early 2K1N stage should be analysed with an antibody against BILBO1 and an inducible expression of a tagged version of BILBO1. If tagged-BILBO1 only localizes at one of the collars, one can conclude that the FPC formation occurs *de novo*. If tagged-BILBO1 localizes at both collars, it is a semi-conservative biogenesis.

It would be interesting to look for BILBO1 partners that show GTPase activity, such as the cdc42 protein, which activates aPKC in the Par3/Par6/aPKC complex. Or it would be of major interest as well to directly look for a kinase, such as aPKC, which would be able to phosphorylate FPC4. As such, the Polo-like kinase (*Tb*PLK) identified and characterized in *T. brucei* (Graham et al., 1998; Kumar and Wang, 2006; Hammarton et al., 2007a) is able to phosphorylate SPPB1, located at the BBs (Hu 2015), and Centrin-2 (de Graffenried et al., 2013; de Graffenried et al., 2008) which is located at the hook-complex. FPC4 could be a substrate as well for this kinase. This could be tested *in vitro* with a kinase assay with WT FPC4 and a mutated version of the predicted phosphorylation sites of FPC4 as substrate.

To prove or falsify the hypothesis that BILBO1 might play the role of a cytokinesis septin-ring, it could be possible to perform a complementation assay in yeast. A mutant yeast strain, lacking the septin genes, but expressing *Tb*BILBO1, could be tested to see whether *Tb*BILBO1 can act as septin. In the laboratory Annelise Sahin expressed *Tb*BILBO1 in yeast (not depleted by septin genes), but no cytokinesis ring was formed by *Tb*BILBO1.

Localization and role of FPC4 in *T. cruzi*?

Epimastigote *T. cruzi* possesses additionally to the FP, a cytostome and a cytopharynx that are involved in the endocytosis and exocytosis processes. Interestingly, additionally to the MtQ around the FP, *T. cruzi* owns two sets of MT around the cytostome: a triplet of MT and another quartet of MT (Alcantara et al., 2014). It would be interesting to localize the *T. cruzi* orthologue of FPC4 and see if this can bind to MT and if it is located specifically to one of these additional MT subsets.

The research on cytoskeleton is, as previously said, of outstanding interest, since it is a source of potential drug targets. More than single proteins, also protein-protein interactions can be used as a target, and destroying those interactions can be the aim of a drug screen. FPC4-BILBO1 interaction has been proved *in vitro* (gel filtration) and *in vivo* (Y2H and U-2 OS). Moreover, the domains involved in this interaction are known, as well as key residues in the NTD of BILBO1. A drug screen (for example, the alpha-screen Amplified Luminescent Proximity Homogenoeous Assay) could be performed to try to block or dissociate this interaction.

Since the domains of FPC4 and BILBO1 responsible for their interaction are known, and since the 3D structure of the BILBO1 NTD has been solved, it would be interesting to co-crystallize these two interacting domains to identify key residues within the B1BD. These residues could be lately tested in *T. brucei* to assess FPC4 functionality. Moreover, the identification of key residues can be very important in drug design.

The essentiality of FPC4 has not been proved and knock down experiments did not lead to any growth defect. Knock out attempts in PCF and BSF have failed and therefore the best solution to solve this “mystery” is to try a conditional knock-out. In a conditional knock out cell, the first FPC4 allele is substituted by a resistance gene, then, an inducible ectopic copy of FPC4 is added. Then, the second allele of FPC4 is knocked out. Removing the tetracycline will stop the ectopic FPC4 expression and might give an idea about the essentiality and the function of the protein.
FPC4 is a multi-partner protein and, additionally to BILBO1 and MORN1, it can eventually have other partners belonging to the FPC or the hook-complex. In the laboratory we have other FPC-candidates. Testing the interaction with these other FPC proteins by Y2H or in U-2 OS might help identify the FPC-members.

A further technique, which is taking hold recently, is CLEM (Correlative Light and Electron Microscopy). This technique allows the analysis of the same sample with a combination of light and electron microscopy. It might therefore be useful to see if FPC4 binds to only one MT of the MtQ, or if FPC4 interacts on a particular region of the FPC only. It is, however, to take into account that the Hook-complex has never been seen by EM or tomography studies.
It would also be interesting to test SpefI-FPC4 interaction in U-2 OS cells, to see whether these two proteins are able to interact and therefore hypothesize a potential connection on the MtQ, too.

In L. major, only preliminary data have been produced. To broaden the knowledge about this area, it would be fruitful to localize *Lm*SpefI, *Lm*Centrin-2 and *Lm*Centrin-4, to obtain a clearer view of the MtQ and the hook-complex, respectively.

To conclude, the ultimate goal of our research remains to find conserved structures or features that can be used as common drug target for the three main kinetoplastids responsible for diseases in humans, i.e *Leishmania sp.*, *T. cruzi*, and *T. brucei*.

5. BIBLIOGRAPHY

5. Bibliography

Acosta-Serrano, A., Vassella, E., Liniger, M., Kunz Renggli, C., Brun, R., Roditi, I. and Englund, P. T. (2001). The surface coat of procyclic Trypanosoma brucei: programmed expression and proteolytic cleavage of procyclin in the tsetse fly. *Proc. Natl. Acad. Sci. U. S. A.* **98**, 1513–1518.

Adl, S. M., Simpson, A. G. B., Farmer, M. A., Andersen, R. A., Anderson, O. R., Barta, J. R., Bowser, S. S., Brugerolle, G., Fensome, R. A., Fredericq, S., et al. (2005). The new higher level classification of eukaryotes with emphasis on the taxonomy of protists. *J. Eukaryot. Microbiol.* **52**, 399–451.

Affolter, M., Hemphill, A., Roditi, I., Müller, N. and Seebeck, T. (1994). The repetitive microtubule-associated proteins MARP-1 and MARP-2 of Trypanosoma brucei. *J. Struct. Biol.* **112**, 241–251.

Agabian, N. (1990). Trans splicing of nuclear pre-mRNAs. *Cell* **61**, 1157–1160.

Agüero, F., Verdún, R. E., Frasch, A. C. and Sánchez, D. O. (2000). A random sequencing approach for the analysis of the Trypanosoma cruzi genome: general structure, large gene and repetitive DNA families, and gene discovery. *Genome Res.* **10**, 1996–2005.

Alcantara, C. L., Vidal, J. C., de Souza, W. and Cunha-e-Silva, N. L. (2014). The three-dimensional structure of the cytostome-cytopharynx complex of Trypanosoma cruzi epimastigotes. *J. Cell Sci.* **127**, 2227–2237.

Alcantara, C. de L., Vidal, J. C., de Souza, W. and Cunha-E-Silva, N. L. (2016). The cytostome-cytopharynx complex of Trypanosoma cruzi epimastigotes disassembles during cell division. *J. Cell Sci.* (ahead of print)

Alexeieff, A. (1917). Mitochondries et corps parabasal chez les flagellés. *Comptes Rendus de la Société de Biologie* **80**, 358–361.

Alibu, V. P., Storm, L., Haile, S., Clayton, C. and Horn, D. (2005). A doubly inducible system for RNA interference and rapid RNAi plasmid construction in Trypanosoma brucei. *Mol. Biochem. Parasitol.* **139**, 75–82.

Alsford, S., Turner, D. J., Obado, S. O., Sanchez-Flores, A., Glover, L., Berriman, M., Hertz-Fowler, C. and Horn, D. (2011). High-throughput phenotyping using parallel sequencing of RNA interference targets in the African trypanosome. *Genome Res.* **21**, 915–924.

Amos, L. A. and Schlieper, D. (2005). Microtubules and Maps. In (ed. Chemistry, B.-A. in P.), pp. 257–298. Academic Press.

Aslett, M., Aurrecoechea, C., Berriman, M., Brestelli, J., Brunk, B. P., Carrington, M., Depledge, D. P., Fischer, S., Gajria, B., Gao, X., et al. (2010). TriTrypDB: a functional genomic resource for the Trypanosomatidae. *Nucleic Acids Res.* **38**, D457-462.

Atyame Nten, C. M., Sommerer, N., Rofidal, V., Hirtz, C., Rossignol, M., Cuny, G., Peltier, J.-B. and Geiger, A. (2010). Excreted/secreted proteins from trypanosome procyclic strains. *J. Biomed. Biotechnol.* **2010**, 212817.

Baines, A. and Gull, K. (2008). WCB is a C2 domain protein defining the plasma membrane - sub-

pellicular microtubule corset of kinetoplastid parasites. *Protist* **159**, 115–125.

Balaban, N., Waithaka, H. K., Njogu, A. R. and Goldman, R. (1989). Isolation of a subpellicular microtubule protein from Trypanosoma brucei that mediates crosslinking of microtubules. *Cell Motil. Cytoskeleton* **14**, 393–400.

Balaban, N., Waithaka, H. K., Njogu, A. R. and Goldman, R. (1995). Intracellular antigens (microtubule-associated protein copurified with glycosomal enzymes)--possible vaccines against trypanosomiasis. *J. Infect. Dis.* **172**, 845–850.

Barnes, R. L., Shi, H., Kolev, N. G., Tschudi, C. and Ullu, E. (2012). Comparative genomics reveals two novel RNAi factors in Trypanosoma brucei and provides insight into the core machinery. *PLoS Pathog.* **8**, e1002678.

Bastin, P., Sherwin, T. and Gull, K. (1998). Paraflagellar rod is vital for trypanosome motility. *Nature* **391**, 548.

Bates, P. A. (2007). Transmission of Leishmania metacyclic promastigotes by phlebotomine sand flies. *Int. J. Parasitol.* **37**, 1097–1106.

Bates, P. A. and Rogers, M. E. (2004). New insights into the developmental biology and transmission mechanisms of Leishmania. *Curr. Mol. Med.* **4**, 601–609.

Bayer-Santos, E., Aguilar-Bonavides, C., Rodrigues, S. P., Cordero, E. M., Marques, A. F., Varela-Ramirez, A., Choi, H., Yoshida, N., da Silveira, J. F. and Almeida, I. C. (2013). Proteomic analysis of Trypanosoma cruzi secretome: characterization of two populations of extracellular vesicles and soluble proteins. *J. Proteome Res.* **12**, 883–897.

Ben Amar, M. F., Pays, A., Tebabi, P., Dero, B., Seebeck, T., Steinert, M. and Pays, E. (1988). Structure and transcription of the actin gene of Trypanosoma brucei. *Mol. Cell. Biol.* **8**, 2166–2176.

Benmerah, A. (2013). The ciliary pocket. *Curr. Opin. Cell Biol.* **25**, 78–84.

Bernstein, E., Caudy, A. A., Hammond, S. M. and Hannon, G. J. (2001). Role for a bidentate ribonuclease in the initiation step of RNA interference. *Nature* **409**, 363–366.

Berriman, M., Ghedin, E., Hertz-Fowler, C., Blandin, G., Renauld, H., Bartholomeu, D. C., Lennard, N. J., Caler, E., Hamlin, N. E., Haas, B., et al. (2005). The genome of the African trypanosome Trypanosoma brucei. *Science* **309**, 416–422.

Besteiro, S., Barrett, M. P., Rivière, L. and Bringaud, F. (2005). Energy generation in insect stages of Trypanosoma brucei: metabolism in flux. *Trends Parasitol.* **21**, 185–191.

Bonhivers, M., Landrein, N., Decossas, M. and Robinson, D. R. (2008a). A monoclonal antibody marker for the exclusion-zone filaments of Trypanosoma brucei. *Parasit. Vectors* **1**, 21.

Bonhivers, M., Nowacki, S., Landrein, N. and Robinson, D. R. (2008b). Biogenesis of the Trypanosome Endo-Exocytotic Organelle Is Cytoskeleton Mediated. *PLOS Biol* **6**, e105.

Borst, P. and Fairlamb, A. H. (1998). Surface receptors and transporters of Trypanosoma brucei. *Annu. Rev. Microbiol.* **52**, 745–778.

Borst, P., Bitter, W., Blundell, P. A., Chaves, I., Cross, M., Gerrits, H., van Leeuwen, F., McCulloch, R., Taylor, M. and Rudenko, G. (1998). Control of VSG gene expression sites in

Trypanosoma brucei. *Mol. Biochem. Parasitol.* **91**, 67–76.

Brasseur, A., Bayat, S., Chua, X. L., Zhang, Y., Zhou, Q., Low, B. C. and He, C. Y. (2014). The bi-lobe-associated LRRP1 regulates Ran activity in Trypanosoma brucei. *J. Cell Sci.* **127**, 4846–4856.

Brenndörfer, M. and Boshart, M. (2010). Selection of reference genes for mRNA quantification in Trypanosoma brucei. *Mol. Biochem. Parasitol.* **172**, 52–55.

Briggs, L. J., McKean, P. G., Baines, A., Moreira-Leite, F., Davidge, J., Vaughan, S. and Gull, K. (2004). The flagella connector of Trypanosoma brucei: an unusual mobile transmembrane junction. *J. Cell Sci.* **117**, 1641–1651.

Broadhead, R., Dawe, H. R., Farr, H., Griffiths, S., Hart, S. R., Portman, N., Shaw, M. K., Ginger, M. L., Gaskell, S. J., McKean, P. G., et al. (2006). Flagellar motility is required for the viability of the bloodstream trypanosome. *Nature* **440**, 224–227.

Brun, R. and Schönenberger, null (1979). Cultivation and in vitro cloning or procyclic culture forms of Trypanosoma brucei in a semi-defined medium. Short communication. *Acta Trop.* **36**, 289–292.

Bütikofer, P., Ruepp, S., Boschung, M. and Roditi, I. (1997). "GPEET" procyclin is the major surface protein of procyclic culture forms of Trypanosoma brucei brucei strain 427. *Biochem. J.* **326 (Pt 2)**, 415–423.

Capewell, P., Clucas, C., DeJesus, E., Kieft, R., Hajduk, S., Veitch, N., Steketee, P. C., Cooper, A., Weir, W. and MacLeod, A. (2013). The TgsGP gene is essential for resistance to human serum in Trypanosoma brucei gambiense. *PLoS Pathog.* **9**, e1003686.

Chan, S. W., Fowler, K. J., Choo, K. H. A. and Kalitsis, P. (2005). Spef1, a conserved novel testis protein found in mouse sperm flagella. *Gene* **353**, 189–199.

Chappuis, F., Stivanello, E., Adams, K., Kidane, S., Pittet, A. and Bovier, P. A. (2004). Card Agglutination Test for Trypanosomiasis (catt) End-Dilution Titer and Cerebrospinal Fluid Cell Count as Predictors of Human African Trypanosomiasis (trypanosoma Brucei Gambiense) Among Serologically Suspected Individuals in Southern Sudan. *Am. J. Trop. Med. Hyg.* **71**, 313–317.

Checchi, F., Filipe, J. A. N., Barrett, M. P. and Chandramohan, D. (2008). The natural progression of Gambiense sleeping sickness: what is the evidence? *PLoS Negl. Trop. Dis.* **2**, e303.

Chen, S., Chen, J., Shi, H., Wei, M., Castaneda-Castellanos, D. R., Bultje, R. S., Pei, X., Kriegstein, A. R., Zhang, M. and Shi, S.-H. (2013). Regulation of microtubule stability and organization by mammalian Par3 in specifying neuronal polarity. *Dev. Cell* **24**, 26–40.

Chomczynski, P. and Sacchi, N. (1987). Single-step method of RNA isolation by acid guanidinium thiocyanate-phenol-chloroform extraction. *Anal. Biochem.* **162**, 156–159.

Conde, C. and Cáceres, A. (2009). Microtubule assembly, organization and dynamics in axons and dendrites. *Nat. Rev. Neurosci.* **10**, 319–332.

Cox, F. E. G. (2002). History of human parasitology. *Clin. Microbiol. Rev.* **15**, 595–612.

Cross, G. A. M., Kim, H.-S. and Wickstead, B. (2014). Capturing the variant surface glycoprotein repertoire (the VSGnome) of Trypanosoma brucei Lister 427. *Mol. Biochem. Parasitol.* **195**, 59–73.

Dacheux, D., Landrein, N., Thonnus, M., Gilbert, G., Sahin, A., Wodrich, H., Robinson, D. R. and Bonhivers, M. (2012). A MAP6-related protein is present in protozoa and is involved in flagellum motility. *PloS One* **7**, e31344.

Dacheux, D., Roger, B., Bosc, C., Landrein, N., Roche, E., Chansel, L., Trian, T., Andrieux, A., Papaxanthos-Roche, A., Marthan, R., et al. (2015). Human FAM154A (SAXO1) is a microtubule-stabilizing protein specific to cilia and related structures. *J. Cell Sci.* **128**, 1294–1307.

DaRocha, W. D., Otsu, K., Teixeira, S. M. R. and Donelson, J. E. (2004). Tests of cytoplasmic RNA interference (RNAi) and construction of a tetracycline-inducible T7 promoter system in Trypanosoma cruzi. *Mol. Biochem. Parasitol.* **133**, 175–186.

Das, A., Banday, M. and Bellofatto, V. (2008). RNA polymerase transcription machinery in trypanosomes. *Eukaryot. Cell* **7**, 429–434.

de Andrade, A. L., Zicker, F., de Oliveira, R. M., Almeida Silva, S., Luquetti, A., Travassos, L. R., Almeida, I. C., de Andrade, S. S., de Andrade, J. G. and Martelli, C. M. (1996). Randomised trial of efficacy of benznidazole in treatment of early Trypanosoma cruzi infection. *Lancet Lond. Engl.* **348**, 1407–1413.

De Gaudenzi, J. G., Noé, G., Campo, V. A., Frasch, A. C. and Cassola, A. (2011). Gene expression regulation in trypanosomatids. *Essays Biochem.* **51**, 31–46.

de Graffenried, C. L., Ho, H. H. and Warren, G. (2008). Polo-like kinase is required for Golgi and bilobe biogenesis in Trypanosoma brucei. *J. Cell Biol.* **181**, 431–438.

de Graffenried, C. L., Anrather, D., Von Raußendorf, F. and Warren, G. (2013). Polo-like kinase phosphorylation of bilobe-resident TbCentrin2 facilitates flagellar inheritance in Trypanosoma brucei. *Mol. Biol. Cell* **24**, 1947–1963.

De Greef, C. and Hamers, R. (1994). The serum resistance-associated (SRA) gene of Trypanosoma brucei rhodesiense encodes a variant surface glycoprotein-like protein. *Mol. Biochem. Parasitol.* **68**, 277–284.

De Kyvon, M.-A. L.-C., Maakaroun-Vermesse, Z., Lanotte, P., Priotto, G., Perez-Simarro, P., Guennoc, A.-M., De Toffol, B., Paris, L., Bernard, L., Goudeau, A., et al. (2016). Congenital Trypanosomiasis in Child Born in France to African Mother. *Emerg. Infect. Dis.* **22**, 935–937.

DeGrasse, J. A., DuBois, K. N., Devos, D., Siegel, T. N., Sali, A., Field, M. C., Rout, M. P. and Chait, B. T. (2009). Evidence for a shared nuclear pore complex architecture that is conserved from the last common eukaryotic ancestor. *Mol. Cell. Proteomics MCP* **8**, 2119–2130.

Demmel, L., Schmidt, K., Lucast, L., Havlicek, K., Zankel, A., Koestler, T., Reithofer, V., Camilli, P. de and Warren, G. (2014). The endocytic activity of the flagellar pocket in Trypanosoma brucei is regulated by an adjacent phosphatidylinositol phosphate kinase. *J Cell Sci* **127**, 2351–2364.

den Boer, M., Argaw, D., Jannin, J. and Alvar, J. (2011). Leishmaniasis impact and treatment access. *Clin. Microbiol. Infect. Off. Publ. Eur. Soc. Clin. Microbiol. Infect. Dis.* **17**, 1471–1477.

Detmer, E., Hemphill, A., Müller, N. and Seebeck, T. (1997). The Trypanosoma brucei autoantigen I/6 is an internally repetitive cytoskeletal protein. *Eur. J. Cell Biol.* **72**, 378–384.

Dosztányi, Z., Csizmok, V., Tompa, P. and Simon, I. (2005). IUPred: web server for the prediction of intrinsically unstructured regions of proteins based on estimated energy content. *Bioinforma. Oxf. Engl.* **21**, 3433–3434.

Dougherty, G. W., Adler, H. J., Rzadzinska, A., Gimona, M., Tomita, Y., Lattig, M. C., Merritt, R. C. and Kachar, B. (2005). CLAMP, a novel microtubule-associated protein with EB-type calponin homology. *Cell Motil. Cytoskeleton* **62**, 141–156.

Durand-Dubief, M. and Bastin, P. (2003). TbAGO1, an argonaute protein required for RNA interference, is involved in mitosis and chromosome segregation in Trypanosoma brucei. *BMC Biol.* **1**, 2.

Elbashir, S. M., Harborth, J., Lendeckel, W., Yalcin, A., Weber, K. and Tuschl, T. (2001). Duplexes of 21-nucleotide RNAs mediate RNA interference in cultured mammalian cells. *Nature* **411**, 494–498.

El-Sayed, N. M., Myler, P. J., Blandin, G., Berriman, M., Crabtree, J., Aggarwal, G., Caler, E., Renauld, H., Worthey, E. A., Hertz-Fowler, C., et al. (2005). Comparative genomics of trypanosomatid parasitic protozoa. *Science* **309**, 404–409.

Engstler, M., Thilo, L., Weise, F., Grünfelder, C. G., Schwarz, H., Boshart, M. and Overath, P. (2004). Kinetics of endocytosis and recycling of the GPI-anchored variant surface glycoprotein in Trypanosoma brucei. *J. Cell Sci.* **117**, 1105–1115.

Engstler, M., Weise, F., Bopp, K., Grünfelder, C. G., Günzel, M., Heddergott, N. and Overath, P. (2005). The membrane-bound histidine acid phosphatase TbMBAP1 is essential for endocytosis and membrane recycling in Trypanosoma brucei. *J. Cell Sci.* **118**, 2105–2118.

Ersfeld, K. (2011). Nuclear architecture, genome and chromatin organisation in Trypanosoma brucei. *Res. Microbiol.* **162**, 626–636.

Ersfeld, K., Melville, S. E. and Gull, K. (1999). Nuclear and genome organization of Trypanosoma brucei. *Parasitol. Today Pers. Ed* **15**, 58–63.

Esson, H. J., Morriswood, B., Yavuz, S., Vidilaseris, K., Dong, G. and Warren, G. (2012). Morphology of the Trypanosome Bilobe, a Novel Cytoskeletal Structure. *Eukaryot. Cell* **11**, 761–772.

Evans, G. On a horse disease in India known as “surra”, probably due to a haematozoon. *The Veterinary Journal and Annals of Comparative Pathology* **13**, 1–10, 82–88, 180–200, 326–333.

Fairlamb, A. H., Smith, K. and Hunter, K. J. (1992). The interaction of arsenical drugs with dihydrolipoamide and dihydrolipoamide dehydrogenase from arsenical resistant and sensitive strains of Trypanosoma brucei brucei. *Mol. Biochem. Parasitol.* **53**, 223–231.

Fantoni, A., Dare, A. O. and Tschudi, C. (1994). RNA polymerase III-mediated transcription of the trypanosome U2 small nuclear RNA gene is controlled by both intragenic and extragenic regulatory elements. *Mol. Cell. Biol.* **14**, 2021–2028.

Fawcett, D. W., Anderson, W. A. and Phillips, D. M. (1971). Morphogenetic factors influencing the shape of the sperm head. *Dev. Biol.* **26**, 220–251.

Ferguson, M. A. (1999). The structure, biosynthesis and functions of glycosylphosphatidylinositol

anchors, and the contributions of trypanosome research. *J. Cell Sci.* **112 (Pt 17)**, 2799–2809.

Field, M. C., Adung'a, V., Obado, S., Chait, B. T. and Rout, M. P. (2012). Proteomics on the rims: insights into the biology of the nuclear envelope and flagellar pocket of trypanosomes. *Parasitology* **139**, 1158–1167.

Florimond, C., Sahin, A., Vidilaseris, K., Dong, G., Landrein, N., Dacheux, D., Albisetti, A., Byard, E. H., Bonhivers, M. and Robinson, D. R. (2015a). BILBO1 Is a Scaffold Protein of the Flagellar Pocket Collar in the Pathogen Trypanosoma brucei. *PLoS Pathog* **11**, e1004654.

Florimond, C., Sahin, A., Vidilaseris, K., Dong, G., Landrein, N., Dacheux, D., Albisetti, A., Byard, E. H., Bonhivers, M. and Robinson, D. R. (2015b). Correction: BILBO1 Is a Scaffold Protein of the Flagellar Pocket Collar in the Pathogen Trypanosoma brucei. *PLoS Pathog* **11**, e1004844.

Franco, J. R., Simarro, P. P., Diarra, A. and Jannin, J. G. (2014). Epidemiology of human African trypanosomiasis. *Clin. Epidemiol.* **6**, 257–275.

Fridberg, A., Buchanan, K. T. and Engman, D. M. (2007). Flagellar membrane trafficking in kinetoplastids. *Parasitol. Res.* **100**, 205–212.

Fujita, O., Sanabria, L., Inchaustti, A., De Arias, A. R., Tomizawa, Y. and Oku, Y. (1994). Animal reservoirs for Trypanosoma cruzi infection in an endemic area in Paraguay. *J. Vet. Med. Sci. Jpn. Soc. Vet. Sci.* **56**, 305–308.

Gadelha, C., Rothery, S., Morphew, M., McIntosh, J. R., Severs, N. J. and Gull, K. (2009). Membrane domains and flagellar pocket boundaries are influenced by the cytoskeleton in African trypanosomes. *Proc. Natl. Acad. Sci. U. S. A.* **106**, 17425–17430.

Gadelha, C., Holden, J. M., Allison, H. C. and Field, M. C. (2011). Specializations in a successful parasite: what makes the bloodstream-form African trypanosome so deadly? *Mol. Biochem. Parasitol.* **179**, 51–58.

Gadelha, C., Zhang, W., Chamberlain, J. W., Chait, B. T., Wickstead, B. and Field, M. C. (2015). Architecture of a Host-Parasite Interface: Complex Targeting Mechanisms Revealed Through Proteomics. *Mol. Cell. Proteomics MCP* **14**, 1911–1926.

Gallo, J. M., Précigout, E. and Schrével, J. (1988). Subcellular sequestration of an antigenically unique beta-tubulin. *Cell Motil. Cytoskeleton* **9**, 175–183.

García-Salcedo, J. A., Pérez-Morga, D., Gijón, P., Dilbeck, V., Pays, E. and Nolan, D. P. (2004). A differential role for actin during the life cycle of Trypanosoma brucei. *EMBO J.* **23**, 780–789.

Geiger, A., Hirtz, C., Bécue, T., Bellard, E., Centeno, D., Gargani, D., Rossignol, M., Cuny, G. and Peltier, J.-B. (2010). Exocytosis and protein secretion in Trypanosoma. *BMC Microbiol.* **10**, 20.

Gheiratmand, L., Brasseur, A., Zhou, Q. and He, C. Y. (2013). Biochemical Characterization of the Bi-lobe Reveals a Continuous Structural Network Linking the Bi-lobe to Other Single-copied Organelles in Trypanosoma brucei. *J. Biol. Chem.* **288**, 3489–3499.

Ghossoub, R., Molla-Herman, A., Bastin, P. and Benmerah, A. (2011). The ciliary pocket: a once-forgotten membrane domain at the base of cilia. *Biol. Cell Auspices Eur. Cell Biol. Organ.* **103**, 131–

144.

Gibson, W., Backhouse, T. and Griffiths, A. (2002). The human serum resistance associated gene is ubiquitous and conserved in Trypanosoma brucei rhodesiense throughout East Africa. *Infect. Genet. Evol. J. Mol. Epidemiol. Evol. Genet. Infect. Dis.* **1**, 207–214.

Gibson, D. G., Young, L., Chuang, R.-Y., Venter, J. C., Hutchison, C. A. and Smith, H. O. (2009). Enzymatic assembly of DNA molecules up to several hundred kilobases. *Nat. Methods* **6**, 343–345.

Gopalakrishnan, S., Hallett, M. A., Atkinson, S. J. and Marrs, J. A. (2007). aPKC-PAR complex dysfunction and tight junction disassembly in renal epithelial cells during ATP depletion. *Am. J. Physiol. Cell Physiol.* **292**, C1094-1102.

Graham, T. M., Tait, A. and Hide, G. (1998). Characterisation of a polo-like protein kinase gene homologue from an evolutionary divergent eukaryote, Trypanosoma brucei. *Gene* **207**, 71–77.

Gruby, M. (1843). Recherches et observations sur une nouvelle espèce d'hématozoaire, Trypanosoma sanguinis. *Comptes rendus hebdomadaire des séances de l'Académie des Sciences* **17**, 1134–1136.

Gu, Z., Wang, J., Li, M., Zhang, J., Ke, X. and Gong, X. (2007). Morphological and genetic differences of Trypanosoma in some Chinese freshwater fishes: difficulties of species identification. *Parasitol. Res.* **101**, 723–730.

Gubbels, M.-J., Vaishnava, S., Boot, N., Dubremetz, J.-F. and Striepen, B. (2006). A MORN-repeat protein is a dynamic component of the Toxoplasma gondii cell division apparatus. *J. Cell Sci.* **119**, 2236–2245.

Gull, K. (1999). The cytoskeleton of trypanosomatid parasites. *Annu. Rev. Microbiol.* **53**, 629–655.

Günzl, A., Bruderer, T., Laufer, G., Schimanski, B., Tu, L.-C., Chung, H.-M., Lee, P.-T. and Lee, M. G.-S. (2003). RNA polymerase I transcribes procyclin genes and variant surface glycoprotein gene expression sites in Trypanosoma brucei. *Eukaryot. Cell* **2**, 542–551.

Günzl, A., Kirkham, J. K., Nguyen, T. N., Badjatia, N. and Park, S. H. (2015). Mono-allelic VSG expression by RNA polymerase I in Trypanosoma brucei: expression site control from both ends? *Gene* **556**, 68–73.

Haanstra, J. R., González-Marcano, E. B., Gualdrón-López, M. and Michels, P. A. M. (2016). Biogenesis, maintenance and dynamics of glycosomes in trypanosomatid parasites. *Biochim. Biophys. Acta* **1863**, 1038–1048.

Hager, K. M. and Hajduk, S. L. (1997). Mechanism of resistance of African trypanosomes to cytotoxic human HDL. *Nature* **385**, 823–826.

Hammarton, T. C., Clark, J., Douglas, F., Boshart, M. and Mottram, J. C. (2003). Stage-specific differences in cell cycle control in Trypanosoma brucei revealed by RNA interference of a mitotic cyclin. *J. Biol. Chem.* **278**, 22877–22886.

Hammarton, T. C., Kramer, S., Tetley, L., Boshart, M. and Mottram, J. C. (2007a). Trypanosoma brucei Polo-like kinase is essential for basal body duplication, kDNA segregation and cytokinesis. *Mol. Microbiol.* **65**, 1229–1248.

Hammarton, T. C., Monnerat, S. and Mottram, J. C. (2007b). Cytokinesis in trypanosomatids. *Curr. Opin. Microbiol.* **10**, 520–527.

Hayes, P., Varga, V., Olego-Fernandez, S., Sunter, J., Ginger, M. L. and Gull, K. (2014). Modulation of a cytoskeletal calpain-like protein induces major transitions in trypanosome morphology. *J. Cell Biol.* **206**, 377–384.

He, C. Y., Pypaert, M. and Warren, G. (2005). Golgi duplication in Trypanosoma brucei requires Centrin2. *Science* **310**, 1196–1198.

Heger, A. and Holm, L. (2000). Rapid automatic detection and alignment of repeats in protein sequences. *Proteins* **41**, 224–237.

Hellemond, J. J. van, Bakker, B. M. and Tielens, A. G. M. (2005). Energy metabolism and its compartmentation in Trypanosoma brucei. *Adv. Microb. Physiol.* **50**, 199–226.

Hemphill, A., Lawson, D. and Seebeck, T. (1991). The cytoskeletal architecture of Trypanosoma brucei. *J. Parasitol.* **77**, 603–612.

Henley, G. L., Lee, C. M. and Takeuchi, A. (1978). Electron microscopy observations on Trypanosoma brucei: freeze-cleaving and thin-sectioning study of the apical part of the flagellar pocket. *Z. Für Parasitenkd. Berl. Ger.* **55**, 181–187.

Hill, K. L. (2010). Parasites in motion: flagellum-driven cell motility in African trypanosomes. *Curr. Opin. Microbiol.* **13**, 459–465.

Hoare, C. A. (1966). The classification of mammalian trypanosomes. *Ergeb. Mikrobiol. Immun. Exp. Ther.* **39**, 43–57.

Hoff, M. J. B. van den, Moorman, A. F. M. and Lamers, W. H. (1992). Electroporation in "intracellular" buffer increases cell survival. *Nucleic Acids Res.* **20**, 2902–2902.

Hoffmann, A., Jakob, M. and Ochsenreiter, T. (2016). A novel component of the mitochondrial genome segregation machinery in trypanosomes. *Microb. Cell* **3**, 352–354.

Hogan, J. C. and Patton, C. L. (1976). Variation in intramembrane components of Trypanosoma brucei from intact and x-irradiated rats: a freeze-cleave study. *J. Protozool.* **23**, 205–215.

Höög, J. L., Lacomble, S., Bouchet-Marquis, C., Briggs, L., Park, K., Hoenger, A. and Gull, K. (2016). 3D Architecture of the Trypanosoma brucei Flagella Connector, a Mobile Transmembrane Junction. *PLoS Negl Trop Dis* **10**, e0004312.

Horn, D. (2014). Antigenic variation in African trypanosomes. *Mol. Biochem. Parasitol.* **195**, 123–129.

Hotez, P. J., Dumonteil, E., Betancourt Cravioto, M., Bottazzi, M. E., Tapia-Conyer, R., Meymandi, S., Karunakara, U., Ribeiro, I., Cohen, R. M. and Pecoul, B. (2013). An unfolding tragedy of Chagas disease in North America. *PLoS Negl. Trop. Dis.* **7**, e2300.

Hu, Q. and Nelson, W. J. (2011). Ciliary diffusion barrier: the gatekeeper for the primary cilium compartment. *Cytoskelet. Hoboken NJ* **68**, 313–324.

Hu, H., Zhou, Q. and Li, Z. (2015). SAS-4 Protein in Trypanosoma brucei Controls Life Cycle Transitions by Modulating the Length of the Flagellum Attachment Zone Filament. *J. Biol. Chem.*

290, 30453–30463.

Hughes, A. L. and Piontkivska, H. (2003). Phylogeny of Trypanosomatidae and Bodonidae (Kinetoplastida) Based on 18S rRNA: Evidence for Paraphyly of Trypanosoma and Six Other Genera. *Mol. Biol. Evol.* **20**, 644–652.

Hughes, L. C., Ralston, K. S., Hill, K. L. and Zhou, Z. H. (2012). Three-dimensional structure of the Trypanosome flagellum suggests that the paraflagellar rod functions as a biomechanical spring. *PloS One* **7**, e25700.

Hughes, L., Towers, K., Starborg, T., Gull, K. and Vaughan, S. (2013). A cell-body groove housing the new flagellum tip suggests an adaptation of cellular morphogenesis for parasitism in the bloodstream form of Trypanosoma brucei. *J. Cell Sci.* **126**, 5748–5757.

Ikeda, K. N. and de Graffenried, C. L. (2012). Polo-like kinase is necessary for flagellum inheritance in Trypanosoma brucei. *J. Cell Sci.* **125**, 3173–3184.

Ilemobade, A. A. (2009). Tsetse and trypanosomosis in Africa: the challenges, the opportunities. *Onderstepoort J. Vet. Res.* **76**, 35–40.

Imhof, S., Fragoso, C., Hemphill, A., von Schubert, C., Li, D., Legant, W., Betzig, E. and Roditi, I. (2016). Flagellar membrane fusion and protein exchange in trypanosomes; a new form of cell-cell communication? *F1000Research* **5**, 682.

Ivens, A. C., Peacock, C. S., Worthey, E. A., Murphy, L., Aggarwal, G., Berriman, M., Sisk, E., Rajandream, M.-A., Adlem, E., Aert, R., et al. (2005). The genome of the kinetoplastid parasite, Leishmania major. *Science* **309**, 436–442.

Jackson, D. G., Owen, M. J. and Voorheis, H. P. (1985). A new method for the rapid purification of both the membrane-bound and released forms of the variant surface glycoprotein from Trypanosoma brucei. *Biochem. J.* **230**, 195–202.

Jacobs, R. T., Nare, B. and Phillips, M. A. (2011a). State of the Art in African Trypanosome Drug Discovery. *Curr. Top. Med. Chem.* **11**, 1255–1274.

Jacobs, R. T., Plattner, J. J., Nare, B., Wring, S. A., Chen, D., Freund, Y., Gaukel, E. G., Orr, M. D., Perales, J. B., Jenks, M., et al. (2011b). Benzoxaboroles: a new class of potential drugs for human African trypanosomiasis. *Future Med. Chem.* **3**, 1259–1278.

Käser, S., Oeljeklaus, S., Týč, J., Vaughan, S., Warscheid, B. and Schneider, A. (2016). Outer membrane protein functions as integrator of protein import and DNA inheritance in mitochondria. *Proc. Natl. Acad. Sci. U. S. A.* **113**, E4467-4475.

Khare, S., Nagle, A. S., Biggart, A., Lai, Y. H., Liang, F., Davis, L. C., Barnes, S. W., Mathison, C. J. N., Myburgh, E., Gao, M.-Y., et al. (2016). Proteasome inhibition for treatment of leishmaniasis, Chagas disease and sleeping sickness. *Nature* **537**, 229–233.

Killick-Kendrick, R. (1990). Phlebotomine vectors of the leishmaniases: a review. *Med. Vet. Entomol.* **4**, 1–24.

Kohl, L. and Gull, K. (1998). Molecular architecture of the trypanosome cytoskeleton. *Mol. Biochem. Parasitol.* **93**, 1–9.

Kohl, L., Sherwin, T. and Gull, K. (1999). Assembly of the paraflagellar rod and the flagellum attachment zone complex during the Trypanosoma brucei cell cycle. *J. Eukaryot. Microbiol.* **46**, 105–109.

Kohl, L., Robinson, D. and Bastin, P. (2003). Novel roles for the flagellum in cell morphogenesis and cytokinesis of trypanosomes. *EMBO J.* **22**, 5336–5346.

Köhler, G. and Milstein, C. (1975). Continuous cultures of fused cells secreting antibody of predefined specificity. *Nature* **256**, 495–497.

Kosugi, S., Hasebe, M., Tomita, M. and Yanagawa, H. (2009). Systematic identification of cell cycle-dependent yeast nucleocytoplasmic shuttling proteins by prediction of composite motifs. *Proc. Natl. Acad. Sci. U. S. A.* **106**, 10171–10176.

Kozminski, K. G., Johnson, K. A., Forscher, P. and Rosenbaum, J. L. (1993). A motility in the eukaryotic flagellum unrelated to flagellar beating. *Proc. Natl. Acad. Sci. U. S. A.* **90**, 5519–5523.

Kumar, P. and Wang, C. C. (2006). Dissociation of cytokinesis initiation from mitotic control in a eukaryote. *Eukaryot. Cell* **5**, 92–102.

Lacomble, S., Vaughan, S., Gadelha, C., Morphew, M. K., Shaw, M. K., McIntosh, J. R. and Gull, K. (2009). Three-dimensional cellular architecture of the flagellar pocket and associated cytoskeleton in trypanosomes revealed by electron microscope tomography. *J. Cell Sci.* **122**, 1081–1090.

Lacomble, S., Vaughan, S., Gadelha, C., Morphew, M. K., Shaw, M. K., McIntosh, J. R. and Gull, K. (2010). Basal body movements orchestrate membrane organelle division and cell morphogenesis in Trypanosoma brucei. *J. Cell Sci.* **123**, 2884–2891.

LaCount, D. J., Bruse, S., Hill, K. L. and Donelson, J. E. (2000). Double-stranded RNA interference in Trypanosoma brucei using head-to-head promoters. *Mol. Biochem. Parasitol.* **111**, 67–76.

LaCount, D. J., Barrett, B. and Donelson, J. E. (2002). Trypanosoma brucei FLA1 is required for flagellum attachment and cytokinesis. *J. Biol. Chem.* **277**, 17580–17588.

Langousis, G. and Hill, K. L. (2014). Motility and more: the flagellum of Trypanosoma brucei. *Nat. Rev. Microbiol.* **12**, 505–518.

Lee, M. G., Bihain, B. E., Russell, D. G., Deckelbaum, R. J. and Van der Ploeg, L. H. (1990). Characterization of a cDNA encoding a cysteine-rich cell surface protein located in the flagellar pocket of the protozoan Trypanosoma brucei. *Mol. Cell. Biol.* **10**, 4506–4517.

Les, E. P., Ph.D. and Scientist, S. S. (2016). A brief history of the two substrains of BALB/c, BALB/cJ, and BALB/cByJ. *Jackson Lab.*

Li, Z. and Wang, C. C. (2003). A PHO80-like cyclin and a B-type cyclin control the cell cycle of the procyclic form of Trypanosoma brucei. *J. Biol. Chem.* **278**, 20652–20658.

Li, Z., Gourguechon, S. and Wang, C. C. (2007). Tousled-like kinase in a microbial eukaryote regulates spindle assembly and S-phase progression by interacting with Aurora kinase and chromatin assembly factors. *J. Cell Sci.* **120**, 3883–3894.

Liang, X., Haritan, A., Uliel, S. and Michaeli, S. (2003). trans and cis splicing in trypanosomatids: mechanism, factors, and regulation. *Eukaryot. Cell* **2**, 830–840.

Lorestani, A., Sheiner, L., Yang, K., Robertson, S. D., Sahoo, N., Brooks, C. F., Ferguson, D. J. P., Striepen, B. and Gubbels, M.-J. (2010). A Toxoplasma MORN1 null mutant undergoes repeated divisions but is defective in basal assembly, apicoplast division and cytokinesis. *PloS One* **5**, e12302.

Lupas, A., Van Dyke, M. and Stock, J. (1991). Predicting coiled coils from protein sequences. *Science* **252**, 1162–1164.

Lye, L.-F., Owens, K., Shi, H., Murta, S. M. F., Vieira, A. C., Turco, S. J., Tschudi, C., Ullu, E. and Beverley, S. M. (2010). Retention and loss of RNA interference pathways in trypanosomatid protozoans. *PLoS Pathog.* **6**, e1001161.

Magnus, E., Vervoort, T. and Van Meirvenne, N. (1978). A card-agglutination test with stained trypanosomes (C.A.T.T.) for the serological diagnosis of T. B. gambiense trypanosomiasis. *Ann. Société Belge Médecine Trop.* **58**, 169–176.

Mair, G., Shi, H., Li, H., Djikeng, A., Aviles, H. O., Bishop, J. R., Falcone, F. H., Gavrilescu, C., Montgomery, J. L., Santori, M. I., et al. (2000). A new twist in trypanosome RNA metabolism: cis-splicing of pre-mRNA. *RNA* **6**, 163–169.

Malvy, D. and Chappuis, F. (2011). Sleeping sickness. *Clin. Microbiol. Infect.* **17**, 986–995.

Marchini, F. K., de Godoy, L. M. F., Rampazzo, R. C. P., Pavoni, D. P., Probst, C. M., Gnad, F., Mann, M. and Krieger, M. A. (2011). Profiling the Trypanosoma cruzi phosphoproteome. *PloS One* **6**, e25381.

Marx, A., Müller, J., Mandelkow, E.-M., Hoenger, A. and Mandelkow, E. (2006). Interaction of kinesin motors, microtubules, and MAPs. *J. Muscle Res. Cell Motil.* **27**, 125–137.

Matthews, K. R. (2005). The developmental cell biology of Trypanosoma brucei. *J. Cell Sci.* **118**, 283–290.

McAllaster, M. R., Ikeda, K. N., Lozano-Núñez, A., Anrather, D., Unterwurzacher, V., Gossenreiter, T., Perry, J. A., Crickley, R., Mercadante, C. J., Vaughan, S., et al. (2015). Proteomic identification of novel cytoskeletal proteins associated with TbPLK, an essential regulator of cell morphogenesis in Trypanosoma brucei. *Mol. Biol. Cell* **26**, 3013–3029.

McInnes, L. M., Gillett, A., Ryan, U. M., Austen, J., Campbell, R. S. F., Hanger, J. and Reid, S. A. (2009). Trypanosoma irwini n. sp (Sarcomastigophora: Trypanosomatidae) from the koala (Phascolarctos cinereus). *Parasitology* **136**, 875–885.

McKean, P. G. (2003). Coordination of cell cycle and cytokinesis in Trypanosoma brucei. *Curr. Opin. Microbiol.* **6**, 600–607.

Medina-Acosta, E. and Cross, G. A. (1993). Rapid isolation of DNA from trypanosomatid protozoa using a simple “mini-prep” procedure. *Mol. Biochem. Parasitol.* **59**, 327–329.

Michels, P. A. (1989). The glycosome of trypanosomes: properties and biogenesis of a microbody. *Exp. Parasitol.* **69**, 310–315.

Milder, R. and Deane, M. P. (1969). The cytostome of Trypanosoma cruzi and T. conorhini. *J.*

Protozool. **16**, 730–737.

Molla-Herman, A., Ghossoub, R., Blisnick, T., Meunier, A., Serres, C., Silbermann, F., Emmerson, C., Romeo, K., Bourdoncle, P., Schmitt, A., et al. (2010). The ciliary pocket: an endocytic membrane domain at the base of primary and motile cilia. *J. Cell Sci.* **123**, 1785–1795.

Moreira, D., López-García, P. and Vickerman, K. (2004). An updated view of kinetoplastid phylogeny using environmental sequences and a closer outgroup: proposal for a new classification of the class Kinetoplastea. *Int. J. Syst. Evol. Microbiol.* **54**, 1861–1875.

Moreira-Leite, F. F., Sherwin, T., Kohl, L. and Gull, K. (2001). A trypanosome structure involved in transmitting cytoplasmic information during cell division. *Science* **294**, 610–612.

Morga, B. and Bastin, P. (2013). Getting to the heart of intraflagellar transport using Trypanosoma and Chlamydomonas models: the strength is in their differences. *Cilia* **2**, 16.

Morrison, L. J., Vezza, L., Rowan, T. and Hope, J. C. (2016). Animal African Trypanosomiasis: Time to Increase Focus on Clinically Relevant Parasite and Host Species. *Trends Parasitol.* **32**, 599–607.

Morriswood, B. (2015). Form, Fabric, and Function of a Flagellum-Associated Cytoskeletal Structure. *Cells* **4**, 726–747.

Morriswood, B. and Schmidt, K. (2015). A MORN Repeat Protein Facilitates Protein Entry into the Flagellar Pocket of Trypanosoma brucei. *Eukaryot. Cell* **14**, 1081–1093.

Morriswood, B., He, C. Y., Sealey-Cardona, M., Yelinek, J., Pypaert, M. and Warren, G. (2009). The bilobe structure of Trypanosoma brucei contains a MORN-repeat protein. *Mol. Biochem. Parasitol.* **167**, 95–103.

Morriswood, B., Havlicek, K., Demmel, L., Yavuz, S., Sealey-Cardona, M., Vidilaseris, K., Anrather, D., Kostan, J., Djinovic-Carugo, K., Roux, K. J., et al. (2013). Novel bilobe components in Trypanosoma brucei identified using proximity-dependent biotinylation. *Eukaryot. Cell* **12**, 356–367.

Mosser, D. M. and Rosenthal, L. A. (1993). Leishmania-macrophage interactions: multiple receptors, multiple ligands and diverse cellular responses. *Semin. Cell Biol.* **4**, 315–322.

Nagajyothi, F., Machado, F. S., Burleigh, B. A., Jelicks, L. A., Scherer, P. E., Mukherjee, S., Lisanti, M. P., Weiss, L. M., Garg, N. J. and Tanowitz, H. B. (2012). Mechanisms of Trypanosoma cruzi persistence in Chagas disease. *Cell. Microbiol.* **14**, 634–643.

Namangala, B. (2011). How the African trypanosomes evade host immune killing. *Parasite Immunol.* **33**, 430–437.

Natesan, S. K. A., Peacock, L., Matthews, K., Gibson, W. and Field, M. C. (2007). Activation of endocytosis as an adaptation to the mammalian host by trypanosomes. *Eukaryot. Cell* **6**, 2029–2037.

Navarro, M. and Gull, K. (2001). A pol I transcriptional body associated with VSG mono-allelic expression in Trypanosoma brucei. *Nature* **414**, 759–763.

Ngô, H., Tschudi, C., Gull, K. and Ullu, E. (1998). Double-stranded RNA induces mRNA degradation in Trypanosoma brucei. *Proc. Natl. Acad. Sci. U. S. A.* **95**, 14687–14692.

Niemann, M., Wiese, S., Mani, J., Chanfon, A., Jackson, C., Meisinger, C., Warscheid, B. and Schneider, A. (2013). Mitochondrial outer membrane proteome of Trypanosoma brucei reveals novel factors required to maintain mitochondrial morphology. *Mol. Cell. Proteomics MCP* **12**, 515–528.

Oberholzer, M., Morand, S., Kunz, S. and Seebeck, T. (2006). A vector series for rapid PCR-mediated C-terminal in situ tagging of Trypanosoma brucei genes. *Mol. Biochem. Parasitol.* **145**, 117–120.

Oberholzer, M., Langousis, G., Nguyen, H. T., Saada, E. A., Shimogawa, M. M., Jonsson, Z. O., Nguyen, S. M., Wohlschlegel, J. A. and Hill, K. L. (2011). Independent analysis of the flagellum surface and matrix proteomes provides insight into flagellum signaling in mammalian-infectious Trypanosoma brucei. *Mol. Cell. Proteomics MCP* **10**, M111.010538.

Ogbadoyi, E., Ersfeld, K., Robinson, D., Sherwin, T. and Gull, K. (2000). Architecture of the Trypanosoma brucei nucleus during interphase and mitosis. *Chromosoma* **108**, 501–513.

Ogbadoyi, E. O., Robinson, D. R. and Gull, K. (2003). A High-Order Trans-Membrane Structural Linkage Is Responsible for Mitochondrial Genome Positioning and Segregation by Flagellar Basal Bodies in Trypanosomes. *Mol. Biol. Cell* **14**, 1769–1779.

Oli, M. W., Cotlin, L. F., Shiflett, A. M. and Hajduk, S. L. (2006). Serum Resistance-Associated Protein Blocks Lysosomal Targeting of Trypanosome Lytic Factor in Trypanosoma brucei. *Eukaryot. Cell* **5**, 132–139.

Overath, P. and Engstler, M. (2004). Endocytosis, membrane recycling and sorting of GPI-anchored proteins: Trypanosoma brucei as a model system. *Mol. Microbiol.* **53**, 735–744.

Patrick, K. L., Shi, H., Kolev, N. G., Ersfeld, K., Tschudi, C. and Ullu, E. (2009). Distinct and overlapping roles for two Dicer-like proteins in the RNA interference pathways of the ancient eukaryote Trypanosoma brucei. *Proc. Natl. Acad. Sci. U. S. A.* **106**, 17933–17938.

Pérez-Morga, D., Vanhollebeke, B., Paturiaux-Hanocq, F., Nolan, D. P., Lins, L., Homblé, F., Vanhamme, L., Tebabi, P., Pays, A., Poelvoorde, P., et al. (2005). Apolipoprotein L-I promotes trypanosome lysis by forming pores in lysosomal membranes. *Science* **309**, 469–472.

Pigott, D. M., Bhatt, S., Golding, N., Duda, K. A., Battle, K. E., Brady, O. J., Messina, J. P., Balard, Y., Bastien, P., Pratlong, F., et al. (2014). Global distribution maps of the leishmaniases. *eLife* **3**,.

Ploubidou, A., Robinson, D. R., Docherty, R. C., Ogbadoyi, E. O. and Gull, K. (1999). Evidence for novel cell cycle checkpoints in trypanosomes: kinetoplast segregation and cytokinesis in the absence of mitosis. *J. Cell Sci.* **112 (Pt 24)**, 4641–4650.

Portman, N., Lacomble, S., Thomas, B., McKean, P. G. and Gull, K. (2009). Combining RNA interference mutants and comparative proteomics to identify protein components and dependences in a eukaryotic flagellum. *J. Biol. Chem.* **284**, 5610–5619.

Preußer, C., Jaé, N. and Bindereif, A. (2012). mRNA splicing in trypanosomes. *Int. J. Med. Microbiol. IJMM* **302**, 221–224.

Priotto, G., Pinoges, L., Fursa, I. B., Burke, B., Nicolay, N., Grillet, G., Hewison, C. and

Balasegaram, M. (2008). Safety and effectiveness of first line eflornithine for Trypanosoma brucei gambiense sleeping sickness in Sudan: cohort study. *BMJ* **336**, 705–708.

Rasooly, R. and Balaban, N. (2002). Structure of p15 trypanosome microtubule associated protein. *Parasitol. Res.* **88**, 1034–1039.

Rassi, A., Rassi, A. and Marin-Neto, J. A. (2010). Chagas disease. *Lancet Lond. Engl.* **375**, 1388–1402.

Rattner, J. B., Sciore, P., Ou, Y., van der Hoorn, F. A. and Lo, I. K. Y. (2010). Primary cilia in fibroblast-like type B synoviocytes lie within a cilium pit: a site of endocytosis. *Histol. Histopathol.* **25**, 865–875.

Ravel, C., Dubessay, P., Bastien, P., Blackwell, J. M. and Ivens, A. C. (1998). The Complete Chromosomal Organization of the Reference Strain of the Leishmania Genome Project, L. major `Friedlin'. *Parasitol. Today* **14**, 301–303.

Rindisbacher, L., Hemphill, A. and Seebeck, T. (1993). A repetitive protein from Trypanosoma brucei which caps the microtubules at the posterior end of the cytoskeleton. *Mol. Biochem. Parasitol.* **58**, 83–96.

Robinson, K. A. and Beverley, S. M. (2003). Improvements in transfection efficiency and tests of RNA interference (RNAi) approaches in the protozoan parasite Leishmania. *Mol. Biochem. Parasitol.* **128**, 217–228.

Robinson, D. R. and Gull, K. (1991). Basal body movements as a mechanism for mitochondrial genome segregation in the trypanosome cell cycle. *Nature* **352**, 731–733.

Robinson, D. R., Sherwin, T., Ploubidou, A., Byard, E. H. and Gull, K. (1995). Microtubule polarity and dynamics in the control of organelle positioning, segregation, and cytokinesis in the trypanosome cell cycle. *J. Cell Biol.* **128**, 1163–1172.

Rodríguez, J. A., Lopez, M. A., Thayer, M. C., Zhao, Y., Oberholzer, M., Chang, D. D., Kisalu, N. K., Penichet, M. L., Helguera, G., Bruinsma, R., et al. (2009). Propulsion of African trypanosomes is driven by bihelical waves with alternating chirality separated by kinks. *Proc. Natl. Acad. Sci. U. S. A.* **106**, 19322–19327.

Roger, B., Al-Bassam, J., Dehmelt, L., Milligan, R. A. and Halpain, S. (2004). MAP2c, but not tau, binds and bundles F-actin via its microtubule binding domain. *Curr. Biol. CB* **14**, 363–371.

Rotureau, B., Blisnick, T., Subota, I., Julkowska, D., Cayet, N., Perrot, S. and Bastin, P. (2014). Flagellar adhesion in Trypanosoma brucei relies on interactions between different skeletal structures in the flagellum and cell body. *J. Cell Sci.* **127**, 204–215.

Roux, K. J., Kim, D. I., Raida, M. and Burke, B. (2012). A promiscuous biotin ligase fusion protein identifies proximal and interacting proteins in mammalian cells. *J. Cell Biol.* **196**, 801–810.

Rudenko, G. (2011). African trypanosomes: the genome and adaptations for immune evasion. *Essays Biochem.* **51**, 47–62.

Ruepp, S., Furger, A., Kurath, U., Renggli, C. K., Hemphill, A., Brun, R. and Roditi, I. (1997). Survival of Trypanosoma brucei in the tsetse fly is enhanced by the expression of specific forms of

procyclin. *J. Cell Biol.* **137**, 1369–1379.

Salmon, D., Geuskens, M., Hanocq, F., Hanocq-Quertier, J., Nolan, D., Ruben, L. and Pays, E. (1994). A novel heterodimeric transferrin receptor encoded by a pair of VSG expression site-associated genes in T. brucei. *Cell* **78**, 75–86.

Saxena, V. K. and Miyata, A. (1993). An unusual morphological type of Trypanosoma (Herpetosoma) lewisi (Kent, 1880) detected in the blood of Rattus norvegicus in India. *J. Commun. Dis.* **25**, 15–17.

Schnarwiler, F., Niemann, M., Doiron, N., Harsman, A., Käser, S., Mani, J., Chanfon, A., Dewar, C. E., Oeljeklaus, S., Jackson, C. B., et al. (2014). Trypanosomal TAC40 constitutes a novel subclass of mitochondrial β-barrel proteins specialized in mitochondrial genome inheritance. *Proc. Natl. Acad. Sci. U. S. A.* **111**, 7624–7629.

Schnaufer, A., Clark-Walker, G. D., Steinberg, A. G. and Stuart, K. (2005). The F1-ATP synthase complex in bloodstream stage trypanosomes has an unusual and essential function. *EMBO J.* **24**, 4029–4040.

Schneider, A., Sherwin, T., Sasse, R., Russell, D. G., Gull, K. and Seebeck, T. (1987). Subpellicular and flagellar microtubules of Trypanosoma brucei brucei contain the same alpha-tubulin isoforms. *J. Cell Biol.* **104**, 431–438.

Schneider, A., Hemphill, A., Wyler, T. and Seebeck, T. (1988). Large microtubule-associated protein of T. brucei has tandemly repeated, near-identical sequences. *Science* **241**, 459–462.

Schneider, A., McNally, K. P. and Agabian, N. (1993). Splicing and 3'-processing of the tyrosine tRNA of Trypanosoma brucei. *J. Biol. Chem.* **268**, 21868–21874.

Schneider, C. A., Rasband, W. S. and Eliceiri, K. W. (2012). NIH Image to ImageJ: 25 years of image analysis. *Nat. Methods* **9**, 671–675.

Schumann Burkard, G., Jutzi, P. and Roditi, I. (2011). Genome-wide RNAi screens in bloodstream form trypanosomes identify drug transporters. *Mol. Biochem. Parasitol.* **175**, 91–94.

Schwede, A., Macleod, O. J. S., MacGregor, P. and Carrington, M. (2015). How Does the VSG Coat of Bloodstream Form African Trypanosomes Interact with External Proteins? *PLoS Pathog.* **11**, e1005259.

Scott, V., Sherwin, T. and Gull, K. (1997). gamma-tubulin in trypanosomes: molecular characterisation and localisation to multiple and diverse microtubule organising centres. *J. Cell Sci.* **110 (Pt 2)**, 157–168.

Seebeck, T., Whittaker, P. A., Imboden, M. A., Hardman, N. and Braun, R. (1983). Tubulin genes of Trypanosoma brucei: a tightly clustered family of alternating genes. *Proc. Natl. Acad. Sci. U. S. A.* **80**, 4634–4638.

Seebeck, T., Küng, V., Wyler, T. and Müller, M. (1988). A 60-kDa cytoskeletal protein from Trypanosoma brucei brucei can interact with membranes and with microtubules. *Proc. Natl. Acad. Sci. U. S. A.* **85**, 1101–1104.

Shapiro, T. A. and Englund, P. T. (1995). The structure and replication of kinetoplast DNA. *Annu.*

Rev. Microbiol. **49**, 117–143.

Sherwin, T. and Gull, K. (1989a). Visualization of detyrosination along single microtubules reveals novel mechanisms of assembly during cytoskeletal duplication in trypanosomes. *Cell* **57**, 211–221.

Sherwin, T. and Gull, K. (1989b). The cell division cycle of Trypanosoma brucei brucei: timing of event markers and cytoskeletal modulations. *Philos. Trans. R. Soc. Lond. B. Biol. Sci.* **323**, 573–588.

Shi, J., Franklin, J. B., Yelinek, J. T., Ebersberger, I., Warren, G. and He, C. Y. (2008). Centrin4 coordinates cell and nuclear division in T. brucei. *J Cell Sci* **121**, 3062–3070.

Shuman, S. (1991). Recombination mediated by vaccinia virus DNA topoisomerase I in Escherichia coli is sequence specific. *Proc. Natl. Acad. Sci. U. S. A.* **88**, 10104–10108.

Shuman, S. (1994). Novel approach to molecular cloning and polynucleotide synthesis using vaccinia DNA topoisomerase. *J. Biol. Chem.* **269**, 32678–32684.

Sievers, F., Wilm, A., Dineen, D., Gibson, T. J., Karplus, K., Li, W., Lopez, R., McWilliam, H., Remmert, M., Söding, J., et al. (2011). Fast, scalable generation of high-quality protein multiple sequence alignments using Clustal Omega. *Mol. Syst. Biol.* **7**, 539.

Simpson, L., Sbicego, S. and Aphasizhev, R. (2003). Uridine insertion/deletion RNA editing in trypanosome mitochondria: a complex business. *RNA N. Y. N* **9**, 265–276.

Simpson, A. G. B., Stevens, J. R. and Lukeš, J. (2006). The evolution and diversity of kinetoplastid flagellates. *Trends Parasitol.* **22**, 168–174.

Singh, N., Kumar, M. and Singh, R. K. (2012). Leishmaniasis: current status of available drugs and new potential drug targets. *Asian Pac. J. Trop. Med.* **5**, 485–497.

Sloof, P., Menke, H. H., Caspers, M. P. and Borst, P. (1983). Size fractionation of Trypanosoma brucei DNA: localization of the 177-bp repeat satellite DNA and a variant surface glycoprotein gene in a mini-chromosomal DNA fraction. *Nucleic Acids Res.* **11**, 3889–3901.

Stafford, J. L., Neumann, N. F. and Belosevic, M. (2002). Macrophage-mediated innate host defense against protozoan parasites. *Crit. Rev. Microbiol.* **28**, 187–248.

Stepanek, L. and Pigino, G. (2016). Microtubule doublets are double-track railways for intraflagellar transport trains. *Science* **352**, 721–724.

Stephens, J. and Fantham, H. (1910). On the peculiar morphology of a trypanosome from a case of sleeping sickness and the possibility of its being a new species (T. rhodesiense). *Proc R Soc Lond [Biol]* **83**, 23–33.

Steverding, D. (2008). The history of African trypanosomiasis. *Parasit. Vectors* **1**, 3.

Steverding, D., Stierhof, Y. D., Fuchs, H., Tauber, R. and Overath, P. (1995). Transferrin-binding protein complex is the receptor for transferrin uptake in Trypanosoma brucei. *J. Cell Biol.* **131**, 1173–1182.

Strickland, C. (1911). THE MECHANISM OF TRANSMISSION OF TRYPANOSOMA LEWISI FROM RAT TO RAT BY THE RAT FLEA. *Br. Med. J.* **1**, 1049.

Stuart, K. and Panigrahi, A. K. (2002). RNA editing: complexity and complications. *Mol. Microbiol.* **45**, 591–596.

Stuart, K. D., Schnaufer, A., Ernst, N. L. and Panigrahi, A. K. (2005). Complex management: RNA editing in trypanosomes. *Trends Biochem. Sci.* **30**, 97–105.

Stuart, K., Brun, R., Croft, S., Fairlamb, A., Gürtler, R. E., McKerrow, J., Reed, S. and Tarleton, R. (2008). Kinetoplastids: related protozoan pathogens, different diseases. *J. Clin. Invest.* **118**, 1301–1310.

Subota, I., Julkowska, D., Vincensini, L., Reeg, N., Buisson, J., Blisnick, T., Huet, D., Perrot, S., Santi-Rocca, J., Duchateau, M., et al. (2014). Proteomic analysis of intact flagella of procyclic Trypanosoma brucei cells identifies novel flagellar proteins with unique sub-localization and dynamics. *Mol. Cell. Proteomics MCP* **13**, 1769–1786.

Sun, S. Y., Wang, C., Yuan, Y. A. and He, C. Y. (2013). An intracellular membrane junction consisting of flagellum adhesion glycoproteins links flagellum biogenesis to cell morphogenesis in Trypanosoma brucei. *J. Cell Sci.* **126**, 520–531.

Sunter, J. D. and Gull, K. (2016). The Flagellum Attachment Zone: "The Cellular Ruler" of Trypanosome Morphology. *Trends Parasitol.* **32**, 309–324.

Sunter, J. D., Benz, C., Andre, J., Whipple, S., McKean, P. G., Gull, K., Ginger, M. L. and Lukeš, J. (2015). Modulation of flagellum attachment zone protein FLAM3 and regulation of the cell shape in Trypanosoma brucei life cycle transitions. *J. Cell Sci.* **128**, 3117–3130.

Szempruch, A. J., Sykes, S. E., Kieft, R., Dennison, L., Becker, A. C., Gartrell, A., Martin, W. J., Nakayasu, E. S., Almeida, I. C., Hajduk, S. L., et al. (2016). Extracellular Vesicles from Trypanosoma brucei Mediate Virulence Factor Transfer and Cause Host Anemia. *Cell* **164**, 246–257.

Taschner, M., Bhogaraju, S. and Lorentzen, E. (2012). Architecture and function of IFT complex proteins in ciliogenesis. *Differ. Res. Biol. Divers.* **83**, S12-22.

Taylor, A. E. and Godfrey, D. G. (1969). A new organelle of bloodstream salivarian trypanosomes. *J. Protozool.* **16**, 466–470.

Taylor, J. E. and Rudenko, G. (2006). Switching trypanosome coats: what's in the wardrobe? *Trends Genet. TIG* **22**, 614–620.

Terasawa, H. (2001). Structure and ligand recognition of the PB1 domain: a novel protein module binding to the PC motif. *EMBO J.* **20**, 3947–3956.

Trikin, R., Doiron, N., Hoffmann, A., Haenni, B., Jakob, M., Schnaufer, A., Schimanski, B., Zuber, B. and Ochsenreiter, T. (2016). TAC102 Is a Novel Component of the Mitochondrial Genome Segregation Machinery in Trypanosomes. *PLoS Pathog.* **12**, no.12,

Trindade, S., Rijo-Ferreira, F., Carvalho, T., Pinto-Neves, D., Guegan, F., Aresta-Branco, F., Bento, F., Young, S. A., Pinto, A., Van Den Abbeele, J., et al. (2016). Trypanosoma brucei Parasites Occupy and Functionally Adapt to the Adipose Tissue in Mice. *Cell Host Microbe* **19**, 837–848.

Tschudi, C., Shi, H., Franklin, J. B. and Ullu, E. (2012). Small interfering RNA-producing loci in the ancient parasitic eukaryote Trypanosoma brucei. *BMC Genomics* **13**, 427.

Urbaniak, M. D., Martin, D. M. A. and Ferguson, M. A. J. (2013). Global Quantitative SILAC Phosphoproteomics Reveals Differential Phosphorylation Is Widespread between the Procyclic and

Bloodstream Form Lifecycle Stages of Trypanosoma brucei. *J. Proteome Res.* **12**, 2233–2244.

Urwyler, S., Studer, E., Renggli, C. K. and Roditi, I. (2007). A family of stage-specific alanine-rich proteins on the surface of epimastigote forms of Trypanosoma brucei. *Mol. Microbiol.* **63**, 218–228.

Uzureau, P., Uzureau, S., Lecordier, L., Fontaine, F., Tebabi, P., Homblé, F., Grélard, A., Zhendre, V., Nolan, D. P., Lins, L., et al. (2013). Mechanism of Trypanosoma brucei gambiense resistance to human serum. *Nature* **501**, 430–434.

Van der Ploeg, L. H., Cornelissen, A. W., Barry, J. D. and Borst, P. (1984). Chromosomes of kinetoplastida. *EMBO J.* **3**, 3109–3115.

Vanhamme, L., Lecordier, L. and Pays, E. (2001). Control and function of the bloodstream variant surface glycoprotein expression sites in Trypanosoma brucei. *Int. J. Parasitol.* **31**, 523–531.

Vaughan, S. (2010). Assembly of the flagellum and its role in cell morphogenesis in Trypanosoma brucei. *Curr. Opin. Microbiol.* **13**, 453–458.

Vaughan, S. and Gull, K. (2003). The trypanosome flagellum. *J. Cell Sci.* **116**, 757–759.

Vaughan, S. and Gull, K. (2016). Basal body structure and cell cycle-dependent biogenesis in Trypanosoma brucei. *Cilia* **5**, 1–7.

Vaughan, S., Kohl, L., Ngai, I., Wheeler, R. J. and Gull, K. (2008). A repetitive protein essential for the flagellum attachment zone filament structure and function in Trypanosoma brucei. *Protist* **159**, 127–136.

Vedrenne, C., Giroud, C., Robinson, D. R., Besteiro, S., Bosc, C., Bringaud, F. and Baltz, T. (2002). Two related subpellicular cytoskeleton-associated proteins in Trypanosoma brucei stabilize microtubules. *Mol. Biol. Cell* **13**, 1058–1070.

Vickerman, K. (1962). The mechanism of cyclical development in trypanosomes of the Trypanosoma brucei sub-group: an hypothesis based on ultrastructural observations. *Trans. R. Soc. Trop. Med. Hyg.* **56**, 487–495.

Vickerman, K. and Preston, T. m. (1976). Comparative cell biology of the kinetoplastid flagellates / Comparative cell biology of the kinetoplastid flagellates Trypanosomes, leishmanias. *Biol. Kinetoplastida*. **1**, 35-130

Vidilaseris, K., Morriswood, B., Kontaxis, G. and Dong, G. (2014a). Structure of the TbBILBO1 Protein N-terminal Domain from Trypanosoma brucei Reveals an Essential Requirement for a Conserved Surface Patch. *J. Biol. Chem.* **289**, 3724–3735.

Vidilaseris, K., Shimanovskaya, E., Esson, H. J., Morriswood, B. and Dong, G. (2014b). Assembly mechanism of Trypanosoma brucei BILBO1, a multidomain cytoskeletal protein. *J. Biol. Chem.* **289**, 23870–23881.

Votýpka, J., Oborník, M., Volf, P., Svobodová, M. and Lukes, J. (2002). Trypanosoma avium of raptors (Falconiformes): phylogeny and identification of vectors. *Parasitology* **125**, 253–263.

Walker, D. M., Oghumu, S., Gupta, G., McGwire, B. S., Drew, M. E. and Satoskar, A. R. (2014). Mechanisms of cellular invasion by intracellular parasites. *Cell. Mol. Life Sci. CMLS* **71**, 1245–1263.

Webster, P., Russo, D. C. and Black, S. J. (1990). The interaction of Trypanosoma brucei with

antibodies to variant surface glycoproteins. *J. Cell Sci.* **96 (Pt 2)**, 249–255.

Werner, M. E., Mitchell, J. W., Putzbach, W., Bacon, E., Kim, S. K. and Mitchell, B. J. (2014). Radial intercalation is regulated by the Par complex and the microtubule-stabilizing protein CLAMP/Spef1. *J. Cell Biol.* **206**, 367–376.

Wheeler, R. J. (2010). The trypanolytic factor-mechanism, impacts and applications. *Trends Parasitol.* **26**, 457–464.

Wheeler, R. J., Scheumann, N., Wickstead, B., Gull, K. and Vaughan, S. (2013). Cytokinesis in Trypanosoma brucei differs between bloodstream and tsetse trypomastigote forms: implications for microtubule-based morphogenesis and mutant analysis. *Mol. Microbiol.* **90**, 1339–1355.

Wheeler, R. J., Sunter, J. D. and Gull, K. (2016). Flagellar pocket restructuring through the Leishmania life cycle involves a discrete flagellum attachment zone. *J. Cell Sci.* **129**, 854–867.

Wickstead, B., Ersfeld, K. and Gull, K. (2002). Targeting of a tetracycline-inducible expression system to the transcriptionally silent minichromosomes of Trypanosoma brucei. *Mol. Biochem. Parasitol.* **125**, 211–216.

Willert, E. K. and Phillips, M. A. (2008). Regulated expression of an essential allosteric activator of polyamine biosynthesis in African trypanosomes. *PLoS Pathog.* **4**, e1000183.

Wirtz, E., Hartmann, C. and Clayton, C. (1994). Gene expression mediated by bacteriophage T3 and T7 RNA polymerases in transgenic trypanosomes. *Nucleic Acids Res.* **22**, 3887–3894.

Wirtz, E., Leal, S., Ochatt, C. and Cross, G. A. (1999). A tightly regulated inducible expression system for conditional gene knock-outs and dominant-negative genetics in Trypanosoma brucei. *Mol. Biochem. Parasitol.* **99**, 89–101.

Woods, A., Sherwin, T., Sasse, R., MacRae, T. H., Baines, A. J. and Gull, K. (1989). Definition of individual components within the cytoskeleton of Trypanosoma brucei by a library of monoclonal antibodies. *J. Cell Sci.* **93**, 491–500.

Woodward, R. and Gull, K. (1990). Timing of nuclear and kinetoplast DNA replication and early morphological events in the cell cycle of Trypanosoma brucei. *J. Cell Sci.* **95 (Pt 1)**, 49–57.

Xong, H. V., Vanhamme, L., Chamekh, M., Chimfwembe, C. E., Van Den Abbeele, J., Pays, A., Van Meirvenne, N., Hamers, R., De Baetselier, P. and Pays, E. (1998). A VSG expression site-associated gene confers resistance to human serum in Trypanosoma rhodesiense. *Cell* **95**, 839–846.

Yorke, W. and Blacklock, B. (1912). A Note on the Morphology of a Strain of Trypanosoma Equiperdum. *Br Med J* **2**, 473–473.

Zacharias, D. A., Violin, J. D., Newton, A. C. and Tsien, R. Y. (2002). Partitioning of lipid-modified monomeric GFPs into membrane microdomains of live cells. *Science* **296**, 913–916.

Zeledón, R. and Rabinovich, J. E. (1981). Chagas' disease: an ecological appraisal with special emphasis on its insect vectors. *Annu. Rev. Entomol.* **26**, 101–133.

Zhao, Z., Lindsay, M. E., Roy Chowdhury, A., Robinson, D. R. and Englund, P. T. (2008). p166, a link between the trypanosome mitochondrial DNA and flagellum, mediates genome segregation. *EMBO J.* **27**, 143–154.

Zheng, B., Yao, H. and Lee, G. S. (1999). Inactivation of the gene encoding the flagellar pocket protein, CRAM, in African trypanosomes. *Mol. Biochem. Parasitol.* **100**, 235–242.

Zhou, Q., Gheiratmand, L., Chen, Y., Lim, T. K., Zhang, J., Li, S., Xia, N., Liu, B., Lin, Q. and He, C. Y. (2010). A Comparative Proteomic Analysis Reveals a New Bi-Lobe Protein Required for Bi-Lobe Duplication and Cell Division in Trypanosoma brucei. *PLoS ONE* **5**, e9660.

Zhou, Q., Liu, B., Sun, Y. and He, C. Y. (2011). A coiled-coil- and C2-domain-containing protein is required for FAZ assembly and cell morphology in Trypanosoma brucei. *J. Cell Sci.* **124**, 3848–3858.

Zhou, Q., Hu, H. and Li, Z. (2014). New insights into the molecular mechanisms of mitosis and cytokinesis in trypanosomes. *Int. Rev. Cell Mol. Biol.* **308**, 127–166.

Zhou, Q., Gu, J., Lun, Z.-R., Ayala, F. J. and Li, Z. (2016). Two distinct cytokinesis pathways drive trypanosome cell division initiation from opposite cell ends. *Proc. Natl. Acad. Sci. U. S. A.* **113**, 3287–3292.

Ziegelbauer, K. and Overath, P. (1992). Identification of invariant surface glycoproteins in the bloodstream stage of Trypanosoma brucei. *J. Biol. Chem.* **267**, 10791–10796.

Ziegelbauer, K., Multhaup, G. and Overath, P. (1992). Molecular characterization of two invariant surface glycoproteins specific for the bloodstream stage of Trypanosoma brucei. *J. Biol. Chem.* **267**, 10797–10803.

Zomerdijk, J. C., Kieft, R. and Borst, P. (1991). Efficient production of functional mRNA mediated by RNA polymerase I in Trypanosoma brucei. *Nature* **353**, 772–775.

6. ANNEX

6. Annex

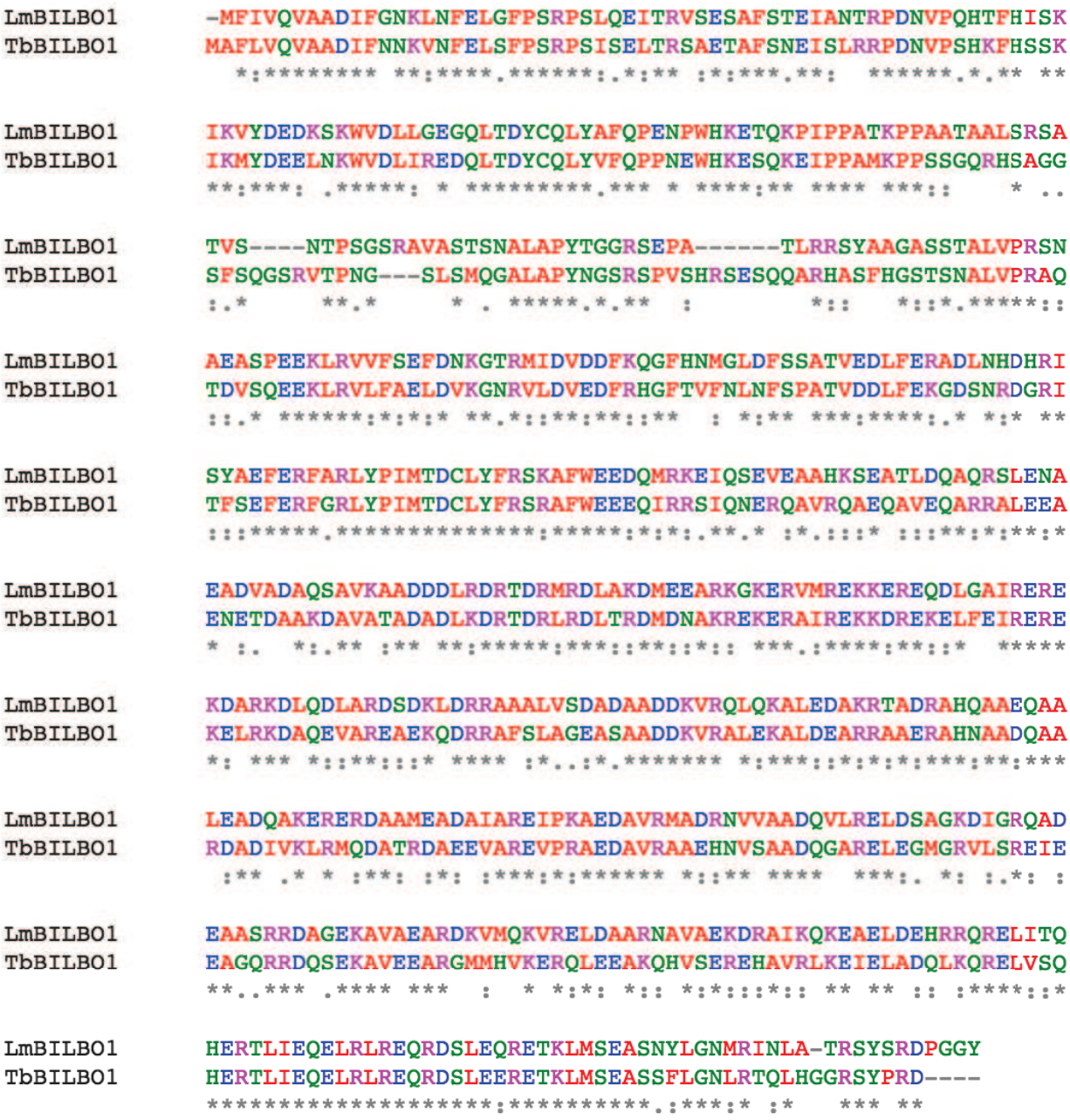

Fig.6.1 *Alignment of LmBILBO1 vs TbBILBO1*
*Lm*BILBO1 (LmjF.09.0100) is composed of 582 aa, whereas *Tb*BILBO1 (Tb927.11.12150) of 587 aa. The two proteins share 58% of identity. (Clustal Omega - (Sievers et al., 2011)

Fig.6.2 *Alignment of LmMORN1 vs TbMORN1*
Both proteins, *Lm*MORN1 (LmjF.30.3310) and *Tb*MORN1 (Tb927.6.4670), are composed of 358 aa and share 76% of identity. (Clustal Omega –(Sievers et al., 2011)

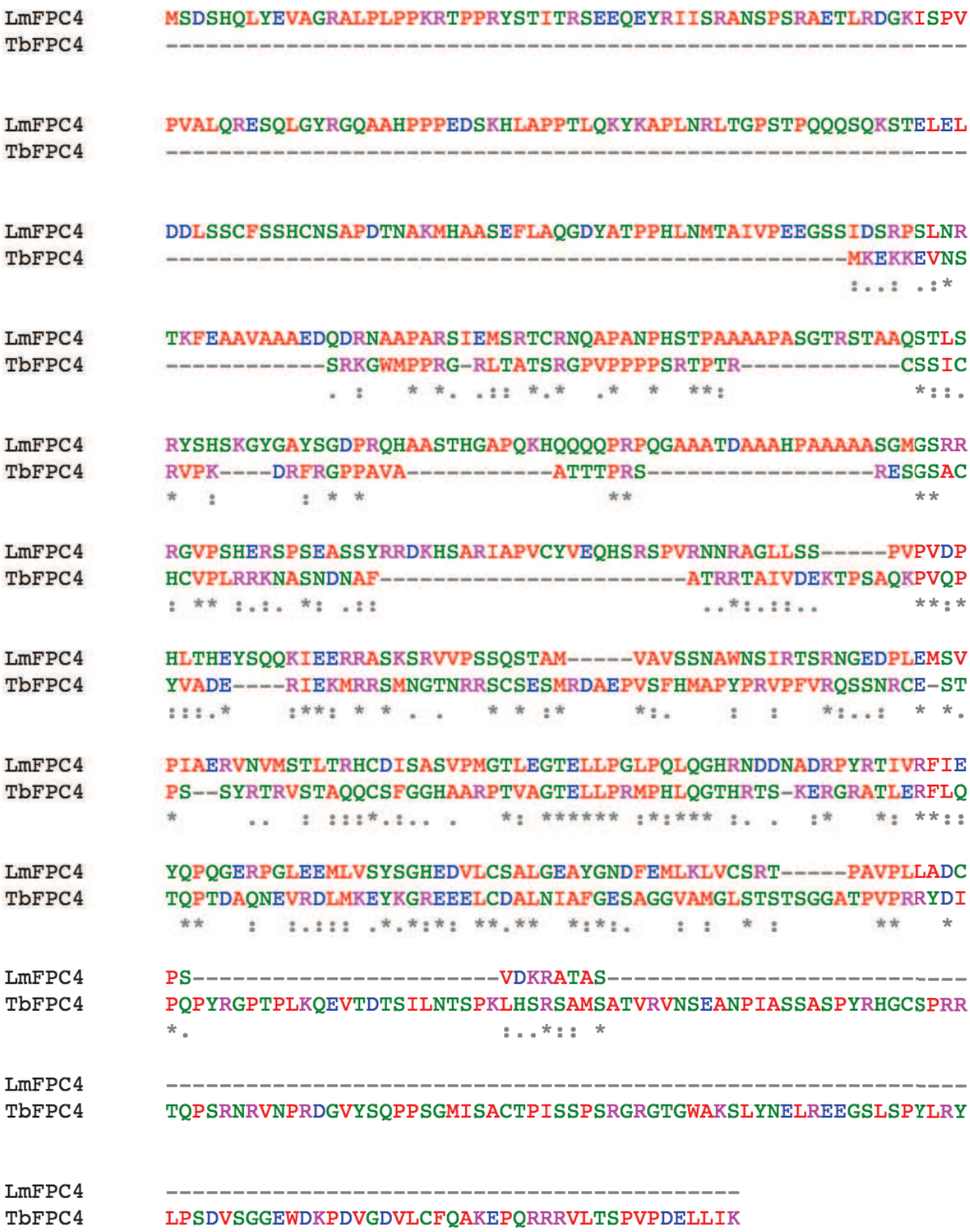

Fig.6.3 *Alignment of LmFPC4 vs TbFPC4*
*Lm*FPC4 (LmjF.24.1860) is composed by 535 aa, whereas *Tb*FPC4 (Tb927.8.6370) is shorter and is composed by 444 aa. These two proteins share 37% of identity over a 75-aa-long stretch, located in the CC domain. (Clustal Omega - (Sievers et al., 2011)